

TECHNISCHE UNIVERSITÄT MÜNCHEN

INSTITUT FÜR ENERGIETECHNIK MW7

LEHRSTUHL FÜR FLUIDMECHANIK

**Functional in-vivo assessment and biofluidmechanical analysis of age-related
and pathological microstructural changes in retinal vessels**

Konstantin Kotliar

Vollständiger Abdruck der von der Fakultät für Maschinenwesen
der Technischen Universität München zur Erlangung des akademischen Grades eines

Doktor-Ingenieurs

genehmigten Dissertation.

Vorsitzender: Univ.-Prof. Dr. rer. nat. Tim C. Lüth

Prüfer der Dissertation: 1. Univ.-Prof. Dr.-Ing., Dr.-Ing. habil. Rudolf Schilling.

2. apl. Prof. Dr. med., Dr. med. habil. Ines Lanzl

Die Dissertation wurde am 03.07.2008 bei der Technischen Universität München
eingereicht und durch die Fakultät für Maschinenwesen am 26.11.2008 angenommen.



Munich University of Technology

Department of Fluid Mechanics
Boltzmannstr. 11 · D-85746 Garching, Germany

Department of Ophthalmology, Klinikum rechts der Isar
Ismaninger Str. 22 · D-81675 Munich, Germany



FUNCTIONAL IN-VIVO ASSESSMENT AND BIOFLUIDMECHANICAL ANALYSIS OF AGE-RELATED AND PATHOLOGICAL MICROSTRUCTURAL CHANGES IN RETINAL VESSELS

Konstantin E. Kotliar

thesis submitted for a doctor's degree: Dr.-Ing. der Medizintechnik

supervisor: Prof. Dr.-Ing. habil. Rudolf Schilling

Department of Fluid Mechanics, Munich University of Technology

consulting supervisor: Prof. Dr.med. habil. Ines M. Lanzl

Department of Ophthalmology, Munich University of Technology

Munich, 2008

Acknowledgements

I would like to express sincere thanks to my supervisor Prof. Dr.-Ing. habil. Rudolf Schilling and to my consulting supervisor and co-examiner Prof. Dr. med. habil. Ines Lanzl for their time, friendly encouragement, and invaluable guidance throughout the period when the work was prepared. Their enthusiastic attitude to research and their truly remarkable personalities have made this experience all the more enjoyable. I am grateful to Prof. Dr. rer. nat. Tim C. Lüth for assuming the presidency of the examination board. I also thank Dr.-Ing. habil. Walthard Vilser from IMEDOS.Ltd in Jena for sharing his vast knowledge and offering invaluable advice throughout my PhD study. I would also like to thank Dr.med. Edgar Nagel from a private eye clinic in Rudolstadt, who kindly provided his raw data for several parts of this research, and offered useful ideas on measurement technique and algorithm development. Many thanks go to Prof. Dr. med. Angelika Shamshinova from Moscow Helmholtz Institute for Eye Diseases for her moral support and her helpful and friendly comments and suggestions.

I thank very much Bruno Mücke for his clinical measurements for an age-dependence study, which have been a valuable resource for this research. Thank you, Seid-Fatima Seidova from Russian R&D Institute for Eye Diseases in Moscow, for your creative help in hypertension study and dimensional reproducibility study.

I would also like to thank the members of the Department of Fluid Mechanics at Munich University of Technology. Many thanks to Danijel Anciger, Johannes Einzinger, Mathias Bogner und Benedikt Flurl for their active and valuable assistance in the development of CFD code and its adaptation to my tasks. I would also like to say thank you to Stefan Herrmann, Florian Kronschnabl and Roland Wunderer for their moral support and valuable advice and Andy Jantzen for his hospitality and readiness to help with computer problems whenever needed.

Special thanks to Prof. Dr.med. habil. Martin Halle from the Department of Preventive and Rehabilitative Sport Medicine at Munich University of Technology for the permission to analyse and to present data on obesity patients I have measured at his Department.

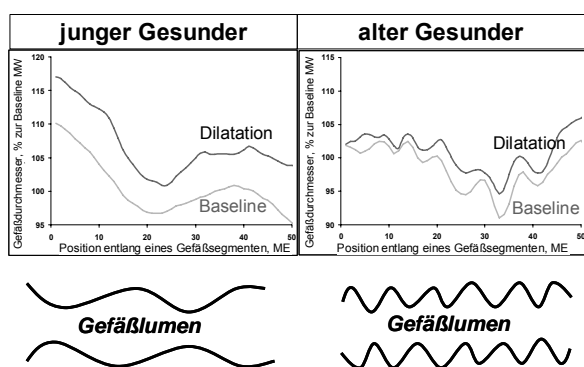
I am really grateful to my first Tutors from St. Petersburg, Russia: Ivan Koshitz (Petercom/MS, Consulting Group), Dr. med. Olga Svetlova (St. Petersburg Medical Academy for Postgraduate Education), Prof. Dr.-Ing. Boris Smolnikov and Prof. Dr.-Ing. Pavel Zhilin (St. Petersburg State Technical University), who brought me into the World of Science and fostered my interest in Biomedical Engineering, Biomechanics and Ophthalmology.

Finally, and most specially, I would like to dedicate my thesis to my parents Efim and Marianna Kotliar and my brother Oleg. For their unlimited love, support and encouragement.

Zusammenfassung

Titel: Funktionelle in-vivo Erfassung und biofluidmechanische Analyse altersbedingter und pathologischer mikrostruktureller Veränderungen retinaler Gefäße

Bei der Arteriosklerose ist das gesamte Gefäßsystem des Menschen in unterschiedlicher Ausprägung betroffen. Meist denkt man an die arteriosklerotischen Läsionen in den großen Arterien, aber auch die Gefäße der Mikrozirkulation sind betroffen. Retinale Gefäße sind ein Teil des mikrovaskulären Gefäßbetts. Sie können nicht invasiv mit relativ einfachen optischen Methoden erfasst werden und sind in ihrem Aufbau und ihrer Funktion zerebralen Gefäßen ähnlich. Retinale Gefäße sind keine geraden Rohre mit einem konstanten Lumen. In ihrem Längsschnitt verfügen sie über enge und breite Stellen, die sich während der Reaktion auf einen metabolischen Reiz verändern können. Das Ziel dieser Arbeit war, funktionelle und morphologische, altersbedingte und pathologische Veränderungen im retinalen Gefäßsystem sowie ihre Auswirkung auf die retinale Perfusion zu untersuchen und quantitative charakteristische Parameter dieser Änderungen zu definieren.



Der Gefäßlängsschnitt retinaler arterieller und venöser Segmente wurden bei gesunden Probanden unterschiedlichen Alters sowie bei Patienten mit systemischem Bluthochdruck, Adipositas und primärem Offenwinkelglaukom mit Hilfe des Retinal Vessel Analyzers der Firma IMEDOS, Jena in vivo untersucht. Das Maß der Mikroirregularität retinaler arterieller und venöser Gefäßinnenwände im Verlauf des Gefäßes nahm bei anamnestisch gesunden Probanden mit zunehmendem Alter signifikant zu. Das Maß der Mikroirregularität retinaler Arterien war bei Glaukompatienten

während der Gefäßdilatation höher als bei altersgematchten gesunden Probanden. Im Gegensatz dazu war das Maß arterieller Mikroirregularität während der Gefäßdilatation bei Patienten mit systemischem Bluthochdruck niedriger als bei altersgematchten Gesunden. Wie bei den altersgematchten Gesunden änderte sich die Mikrostruktur retinaler Gefäßlängsschnittsprofile bei Adipösen nicht während verschiedener Phasen der Gefäßreaktion. Doch waren Gefäßlängsschnittsprofile bei Adipösen signifikant regulärer als bei Gesunden.

Ob diese klinisch untersuchten funktionellen Änderungen in der Gefäßmikrostruktur die hydraulischen Eigenschaften eines Gefäßes beeinflussen können, wurde mit Hilfe der numerischen Biofluidmechanik untersucht. Der hydraulische Widerstand entlang retinaler Gefäßsegmente bei Gefäßwänden unterschiedlicher Irregularität wurde in der Abhängigkeit vom Maß der Irregularität berechnet. Die Finite-Element-Volumen Methode mit den numerischen Biofluidmechanik Code NS3DV43C und NS3DV6C (Institut für Fluidmechanik, Technische Universität München) wurde angewandt. Der Blutfluss wurde als nicht-pulsierend und Newtonisch sowie Nicht-Newtonisch bei den verschiedenen Modellen angenommen. Die Gefäßwände wurden als nicht verformbar angenommen. Bei der Modellformulierung wurde gefunden, dass eine erhöhte Gefäßwandirregularität die hydraulische Leitfähigkeit retinaler Gefäße verschlechtert.

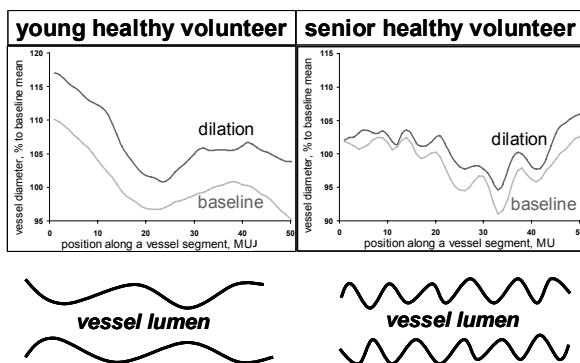
Daraus ergibt sich der Schluss, dass retinale Gefäße im Alter sowie bei den untersuchten systemischen Erkrankungen und Augenerkrankungen signifikante mikrostrukturelle Änderungen ihrer Längsschnittsprofile erleiden, die einen funktionellen und einen irreversiblen Charakter haben. Diese Änderungen können ein Ausdruck der endothelialen Schädigung sowie der biomechanischen Instabilität der Gefäßwand oder für einen partiellen Abbau der Gefäßwandmuskulatur sein.

Üblicherweise beginnt die Pathologie im Herz-Kreislauf-System in den Gefäßen der Mikrozirkulation. Erst später werden größere Gefäße befallen. Deswegen können Veränderungen der Längsschnittsprofile retinaler Gefäße einen Indikator darstellen, der das echte biologische Alter einer Person widerspiegelt und ein zusätzlicher klinischer Marker in der Frühdiagnostik der untersuchten systemischen- und Augenerkrankungen sein. Die Ergebnisse der mathematischen Modellierung weisen darauf hin, dass Änderungen der Mikrostruktur retinaler Gefäße eine wichtige Ursache der veränderten retinalen Perfusion im Alter und bei den untersuchten Pathologien sein können. Die Zunahme des Gefäßwiderstandes bei der Änderung der Mikrostruktur der retinalen Gefäßinnenwand bedeutet einen zusätzlichen fluidmechanischen Mechanismus in der Pathogenese des Alterungsprozesses sowie der untersuchten Erkrankungen.

Summary

Title: Functional in-vivo assessment and biofluidmechanical analysis of age-related and pathological microstructural changes in retinal vessels

Arteriosclerosis involves the whole human vascular system with a somewhat patchy appearance. Although typical arteriosclerotic lesions are confined to major arteries, vessels of microcirculation are affected as well. Retinal vessels are part of the microvascular bed. They can be assessed in non invasive ways by rather simple optical methods and are similar to cerebral vessels in their structure and function. Retinal vessels are not straight tubes with a constant lumen, but rather possess narrower and wider diameters in different segments which are changing in response to a metabolic demand. The aim of the present work was to study functional and morphological age-related and pathological alterations in retinal vasculature and their influence to retinal blood flow as well as to determine quantitative parameters which could characterize these changes.



Changes in longitudinal vessel section of retinal arterial and venous segments in healthy persons of different age and in patients with arterial hypertension, obesity and open angle glaucoma were investigated clinically using the Retinal Vessel Analyzer (IMEDOS, Jena). The rate of microirregularity of retinal arterial and venous inner walls along a vessel increased significantly in anamnestically healthy volunteers with increasing age. The rate of microirregularity was higher in arteries of glaucoma patients than in age-matched healthy volunteers during vessel dilation. On the contrary, the rate of arterial

microirregularity was lower in patients with arterial hypertension than in age-matched healthy volunteers during vessel dilation. The microstructure of longitudinal arterial profiles in obese persons did not change in different phases of the vessel reaction similar to the age-matched healthy volunteers. Longitudinal arterial profiles in obese persons were more regular than in healthy volunteers.

Whether these changes can influence hemodynamic parameters of a vessel was investigated using methods of computational biofluid dynamics. Hydraulic resistances along retinal vessel segments with inner walls of different rate of irregularity were calculated depending on the rate of irregularity. Finite Element Volume method with Computational Fluid Dynamic-codes NS3DV43C and NS3DV6C (Institute of Fluid Mechanics, Munich University of Technology) was used. The blood flow was assumed to be non-pulsatile and Newtonian as well as Non-Newtonian in different models. The vessel walls were non-deformable. In this model formulation it was found that increasing vessel wall irregularity worsens hydraulic conductivity of retinal vessels.

It is concluded, that retinal vessels in the elderly and in the examined systemic and ocular pathologies sustain significant microstructural changes of their longitudinal profiles, which might be of either functional or irreversible nature and might be an expression of endothelial damage, the instability of vessel wall or partial degradation of smooth musculature of vessel wall. Commonly pathological alterations in the cardiovascular system begin in vessels of microcirculation invading larger vessels in a later stage. Hence, the microstructure of longitudinal retinal vessel profile can be an indicator determining the true biological age of a person and representing an additional clinical symptom for early diagnosis of the examined systemic and ocular diseases. Results of CFD simulation show that changes in microstructure of retinal vessels can be a reason for altered retinal perfusion in the elderly and in the examined diseases. The increase of vessel resistance with changing microstructure of the vessel inner wall might represent an additional fluid mechanical mechanism in the pathogenesis of aging and the examined diseases.

Key words: retinal vessels, blood flow, arteriosclerosis, aging, glaucoma, systemic hypertension, obesity

Stichworte: retinale GefäÙe, Blutfluss, Arteriosklerose, Alterung, Glaukom, systemische Hypertonie, Adipostas

Abbreviations, notations and non-systemic units

Since the present work is interdisciplinary and lies on the border of medicine, physiology and biofluid mechanics, not only definitions are provided but also brief explanations of abbreviations, notations and measurement units mentioned in the text.

Abbreviations

- 3D – three dimensional
- A. – artery; Aa. - arteries
- abs. – absolute
- ACA – anterior ciliary artery, which supplies the anterior part of the eye
- ARPS – average reduced power spectrum, computed plot, showing distribution of frequencies within an analysing curve
- AV – arterio-venous
- band sq. – area within a certain frequency band, parameter of power spectrum
- BAS – baseline, a phase of vessel state/reaction
- BMI – body mass index, the measure calculated by dividing the subject's weight by the square of his/her height [kg/m^2]
- CCD – Charge Coupled Device, an electronic light sensor used in digital cameras
- CDI – color Doppler Imaging, technique for ultrasound blood flow measurements
- CDS – Central Differencing Scheme, numerical scheme of approximation
- CFD – computational fluid dynamics, a branch of fluid mechanics, uses numerical methods to solve fluid flow problems
- CLDF – Canon laser Doppler flowmetry, method of retinal blood flow measurements in large retinal vessels
- CNS – central nervous system
- CO – the State of Colorado, United States
- CO_2 – gas, evokes vessel dilation
- CON – constriction, a phase of vessel state/reaction
- CRA – central retinal artery, the artery supplying the retina
- CRV – central retinal vein, the vein draining the retina
- DIL – dilation, a phase of vessel state/reaction
- DSA – digitized subtraction angiography, method of retinal vessel diameter measurements and blood flow estimation
- DVA – Dynamic Vessel Analyser, a novel version of RVA
- e.g. – exempli gratia (lat.), for example
- EDHF – endothelium derived hyperpolarizing factor, secreted by the endothelium, evokes vessel relaxation
- EDV – end diastolic velocity, parameter of ultrasound arterial blood flow measurements
- ET – endothelin, vasoconstricting peptide produced primarily in the endothelium
- FFT – Fast Fourier Transform, an efficient mathematical algorithm to compute the discrete Fourier transform and its inverse
- Fig. – figure
- HFW – high frequency waviness, characteristic of retinal longitudinal vessel profile. It is characterised by SEF.
- HLDF – Heidelberg laser Doppler flowmetry, method of retinal and choroidal blood flow measurements
- IMEDOS - Intelligente Optische Systeme der Medizin- und Messtechnik, German company, manufacturer of RVA
- IMT – intima media thickness, parameter of the vessel structure, commonly used in macrocirculation
- IOP – intraocular pressure, a characteristic of eye turgor
- JNC – Joint National Committee on Detection, Evaluation, and Treatment of High Blood Pressure
- K-L –rheological model of blood by Luo and Kuang (Luo & Kuang 1992)
- LCL – Lien-Chen-Leschziner, eddy viscosity fluid dynamics model by Lien et al. (Lien et al. 1996)
- LCL-RD – eddy viscosity fluid dynamics model by Lien et al. (Lien et al. 1996) implemented by Durbin (Durbin 1996)
- LDV – Laser Doppler velocimetry, method of retinal blood flow velocity measurements in large retinal vessels
- LFW – low frequency waviness, a characteristic of retinal longitudinal vessel profile
- M.O.B.I.L.I.S. – German abbreviation for “multicenter organized motion oriented initiative for changing lifestyle in self responsibility”. A health improving program for obese people

- MAP or meanRR – mean arterial pressure, a characteristic of systemic arterial pressure by Riva-Rocci, integrating its systolic and diastolic values
- MATLAB – "Matrix Laboratory", a numerical computing environment and programming language
- maxV/minV – maximal/minimal velocity, parameter of ultrasound venous blood flow measurements
- MF – median frequency, a parameter of power spectrum, which divides the whole spectrum area into two equal parts
- MINMOD – minimal model, a numerical scheme of approximation
- MPI – message passing interface, program libraries used in CFD code.
- MS – Microsoft, an American multinational computer technology corporation
- MUT – Munich University of Technology
- NIH – National Institute of Health, the primary agency of the United States government responsible for biomedical research
- NO – nitric oxide, gas, vasodilating mediator, secreted by the endothelium
- NS – Navier-Stokes, the abbreviation used in the name of a computational code, denoting the Navier-Stokes equations to be solved
- NYHA – New York Heart Association
- O₂ – oxygen, gas, delivered to tissues by erythrocytes. A powerful vasoconstrictor
- OODG – oculo-oscillo-dynamography, a method to assess or to provoke intraocular microcirculation by artificially increasing IOP
- oscill. – oscillations
- PAF – platelet activating factor, a vasoregulating mediator, secreted by the endothelium
- PC – personal computer
- PCA – posterior ciliary artery, a branch of the ophthalmic artery supplying the choroid
- PGI₂ – prostacyclin, a vasodilating mediator secreted by the endothelium
- POAG - primary open-angle glaucoma, an eye disease
- POST – post-processor, a program to display results of a principal program
- PP_{ret}^s – systolic perfusion pressure in the retina used in OODG assessment
- PP_{cil}^s – systolic perfusion pressure in the ciliary body used in OODG assessment
- PP_{oc}^o – diastolic perfusion pressure used in OODG assessment
- pr. peak fr. – frequency of the primary peak, a parameter of power spectrum
- PSV – pulse systolic velocity, a parameter of ultrasound arterial blood flow measurements
- RBC – red blood cell (erythrocyte) – a biconcave disk-shaped blood constituent, responsible for its Non-Newtonian behaviour
- rel. – relative
- RES – restoration, a phase of vessel state/reaction
- RVA – Retinal Vessel Analyser, a device for automatic non-invasive dynamic measurements of vessel diameters
- SEF – spectral edge frequency – a parameter of power spectrum, which divides its whole area into 5% and 95% pieces
- SIMPLE – Semi Implicit Method for Pressure Linked Equations, numerical scheme for pressure-velocity coupling
- SMART – Sharp and Monotonic Algorithm for Realistic Transport, a numerical scheme of approximation
- SPSS – Statistical Analysis in Social Science, a computer program used for statistical analysis
- tid – three times daily, a recommendation in a medical prescription
- tPA – tissue plasminogen activator, a regulator of fibrinolysis secreted by the endothelium
- TPMA – total protein minus the albumin fraction of blood, a parameter of Walburn rheological model (Walburn & Schneck 1976)
- V. – vein
- VA – visual acuity, a characteristic of vision
- VC – coefficient of variation, statistical measure of data scatter
- WBC – white blood cell (leukocyte) – a spherical shaped multitask blood constituent
- WHO – World Health Organization, an agency of the United Nations, a coordinating authority on international public health

Notations and dimensions of parameters

- **A** – dimensionless magnitude of waviness, modeling longitudinal vessel wall configuration
- **A_p** – parameter of Power Law rheological model (Hussain et al. 1994) [s^{-n_p}]
- **A_{hf}** – dimensionless magnitude of the high frequency component of waviness, modeling the longitudinal vessel wall configuration

- A_{lf} – dimensionless magnitude of the low frequency component of waviness, modeling the longitudinal vessel wall configuration
- A_s – area of a vessel cross-section [m^2]
- a – magnitude of waviness, modeling longitudinal vessel wall configuration [m]
- a_{hf} – magnitude of the high frequency component of waviness, modeling longitudinal vessel wall configuration [m]
- a_{lf} – magnitude of the low frequency component of waviness, modeling longitudinal vessel wall configuration [m]
- \bar{c}_{in} – inflow velocity [m/s]
- \bar{c} – mean velocity [m/s]
- C – hydraulic conductivity [$m^3/Pa*s$]
- $C_{\epsilon 1}, C_{\epsilon 2}, C_L, C_\mu$ – turbulence model constant in the CFD code (Skoda et al. 2007)
- d – vessel diameter [m]
- \bar{d} – mean vessel diameter, modeling longitudinal vessel wall configuration [m]
- D_1, D_2 – turbulence model constant in the CFD code (Skoda et al. 2007)
- f – function in the expression: $A = f(B)$
- f – elliptic operator in the CFD code [s^{-1}]
- f / \underline{f} – true/estimated spatial frequencies of an analyzed vessel segment [Hz]
- f_μ – damping function, turbulent kinetic energy in the CFD code (Skoda et al. 2007)
- G – dimensionless modeling harmonic function of longitudinal vessel wall configuration
- g – modeling harmonic function of longitudinal vessel wall configuration [m]
- H – hematocrit in a point of a vessel cross-section [%]
- H_0 – average blood hematocrit of a subject [%]
- H_c – critical value of hematocrit. Yield stress τ_y does not exist for a hematocrit with a value lesser than H_c [%]
- H_m – the maximum volume fraction (hematocrit for blood) physically permissible in the suspension [%]
- $\vec{i}, \vec{j}, \vec{k}$ – unit vectors of coordinate axes in rectangular Cartesian system of coordinates (x,y,z)
- i – number of an operating fluid element in y direction in a block of the finite volume model
- k – parameter of Quemada model, effective intrinsic viscosity (Quemada 1981)
- k_c – parameter of Cross rheological model (Cross 1965) [s]
- k_∞ – parameter of Quemada model, viscosity index (intrinsic viscosity) at high shear rates, is related to RBC deformability
- k_0 – parameter of Quemada model, viscosity index (intrinsic viscosity) at low shear rates, is related to RBC aggregation
- k_t – turbulence value (turbulent kinetic energy) in the CFD-code (Skoda et al. 2007) [m^2/s^2]
- L – dimensionless length of vessel segment, modeling longitudinal vessel wall configuration
- L_s – length scale in the CFD code (Skoda et al. 2007) [m]
- l – the length of the vessel segment [m]
- m – number of fluid elements in y direction in a block of the finite volume model
- m_c – a parameter of Cross rheological model (Cross 1965)
- n – a natural number in an one-parameter expression for the cross-sectional hematocrite distribution by (Lerche & Oelke 1990)
- n_p – a parameter of Power Law rheological model (Hussain et al. 1994)
- N – number of patients in a study
- p_{stat} – static part of the pressure [Pa]
- p_{total} – pressure [Pa]
- Δp – pressure loss along the vessel segment [Pa]
- Q – blood flow (volumetric flow rate) [m^3/s]
- R – coefficient of flow resistance [$Pa*s/m^3$]
- R^2 – statistical measure of precision
- r – reduced radius of a point within the vessel cross-section
- r_{abs} – absolute radius of the vessel lumen [m]
- Re – Reynolds number
- Re_y – turbulent Reynolds number
- RR – systemic arterial blood pressure measured conventionally by Riva-Rocci with a brachium cuff [mmHg]
- S – strain invariant in the CFD code
- S_{ijk} – strain rate tensor [s^{-1}]
- s – statistical standard deviation
- Sr – Strouhal number
- T / \underline{T} – true/estimated spatial periods of an analyzed segment [s]
- T_s – time scale in the CFD code (Skoda et al. 2007) [s]
- t_A, t_D – characteristic times in Bi-exponent rheological model (Zhang & Kuang 2000) [s]
- u, v, w – velocities along axes x,y,z respectively in a rectangular Cartesian system of coordinates [m/s]
- u_t – turbulent velocity scale in the CFD-code (Skoda et al. 2007) [m/s]
- v^2 – the velocity scale in the CFD-code (Skoda et al. 2007) [m^2/s^2]

- \bar{v}_{av} – average blood velocity [m/s]
- \bar{x} – statistical mean
- x – variable of length, position along the vessel segment [m]
- x, y, z – axes and corresponding co-ordinates in rectangular Cartesian system of coordinates [m]
- \mathbf{X} – a reduced coordinate, modeling longitudinal vessel wall configuration
- \mathbf{X}^* – a dimensionless coordinate along the vessel segment, modeling longitudinal vessel wall configuration
- y – wall distance in the CFD-code (Skoda et al. 2007) [m]
- α – the angle of a vessel branch attachment [$^\circ$]
- α_1, α_2 – viscosity indices in K-L rheological model (Luo & Kuang 1992)
- β_1, β_2 – parameters of the Wang rheological model (Wang & Stoltz 1994)
- ε – turbulence value (turbulent dissipation rate) in the CFD code (Skoda et al. 2007) [m^2/s^3]
- Γ – material constant in Generalized Newtonian rheological model, representing degree of shear thinning (Bird et al. 1987) [s]
- $\dot{\gamma}_c$ – parameter of Quemada model, critical shear rate related to the shear stress under which the structure is broken [s^{-1}]
- $\dot{\gamma}$ – shear rate [s^{-1}]
- μ – dynamic blood viscosity in Newtonian model (Fung 1990) [$\text{Pa}\cdot\text{s}$]
- $\eta, \eta_y, \eta_e, \eta_D, \eta_A$ – apparent dynamic blood viscosities [$\text{Pa}\cdot\text{s}$]
- η_0, η_∞ – asymptotic apparent dynamic blood viscosities (Cross 1965; Bird et al. 1987; Pontrelli 1997) [$\text{Pa}\cdot\text{s}$]
- η_{plasma} – blood plasma viscosity [$\text{Pa}\cdot\text{s}$]
- η_r – relative blood viscosity
- Λ_{hf} – dimensionless period of the high frequency component of waviness, modeling longitudinal vessel wall configuration
- Λ_{lf} – dimensionless period of the low frequency component of waviness, modeling longitudinal vessel wall configuration
- Λ – dimensionless period of waviness, modeling longitudinal vessel wall configuration
- λ_c – friction factor
- λ – period of waviness, modeling longitudinal vessel wall configuration [m]
- λ_{hf} – period of the high frequency component of waviness, modeling longitudinal vessel wall configuration [m]
- λ_{lf} – period of the low frequency component of waviness, modeling longitudinal vessel wall configuration [m]
- λ_1, λ_2 – relaxation and retardation constants in Oldroyd B rheological model (Oldroyd 1958)
- ν – apparent cinematic blood viscosity [m^2/s]
- θ – parameter of Quemada model, critical time, which characterizes the evolution of the structure (Quemada 1981) [s]
- ρ_{plasma} – blood plasma density [kg/m^3]
- ρ_{RBC} – density of RBCs [kg/m^3]
- $\rho, \rho_{\text{blood}}$ – blood density [kg/m^3]
- τ – shear stress [Pa]
- τ_y – yield stress [Pa]
- ν_t – eddy viscosity in the CFD code (Skoda et al. 2007) [m^2/s]
- Ω – rotation invariant in the CFD code (Skoda et al. 2007)
- ζ_v – dimensionless coefficient of hydraulic resistance
- ζ_{v0} – dimensionless hydraulic resistance of the vessel segment with no waviness – straight tube with smooth parallel walls
- ∇ – differential operator in rectangular Cartesian system of coordinate
- \div – range of a value
- frequency band [Hz]
- power of power spectra of longitudinal retinal vessel profiles [MU^2]
- power of reduced power spectra of longitudinal retinal vessel profiles [Hz^{-1}]

Fundamental non SI units. *Because of interdisciplinary character of the present work some non SI units and their derivatives were used. Below are their explanations:*

Length

- **nm** – nanometer. 1 nanometer = 10^{-9} m
- **μm** – micrometer. 1 micrometer (micron) = 10^{-6} m
- **mm** – millimeter. 1 millimeter = 10^{-3} m
- **cm** – centimeter. 1 centimeter = 10^{-2} m
- **RU** – relative unit, unit of length in RVA, 1RU = $1\mu\text{m}$ if the eye has the dimensions of the normal Gullstrand eye
- **MU** – measurement unit, unit of length in RVA, 1MU = 12,5RU

Others

- **mmHg** – millimetres of mercury – pressure unit accepted in medicine. 1mmHg = 133,22 Pa
- **D** – diopter, unit of the optical power of a lens and clinical refraction. [D] = m^{-1}
- **l** – liter, unit of volume. 1l = 10^{-3} m^3

- **mg/dl** – unit of density. $1 \text{ mg/dl} = 10^{-2} \text{ kg/m}^3$
- **$\mu\text{l/min}$** – flow rate in small vessels. $1 \mu\text{l/min} = 1,67 \cdot 10^{-10} \text{ m}^3/\text{s}$
- **ml/min** – flow rate in small vessels. $1 \text{ ml/min} = 1,67 \cdot 10^{-7} \text{ m}^3/\text{s}$

Table of contents

ABBREVIATIONS, NOTATIONS AND NON-SYSTEMIC UNITS	6
TABLE OF CONTENTS	11
1 INTRODUCTION	14
1.1 Purpose and problem statement	14
1.2 Ocular circulation and methods of its assessment.....	16
1.2.1 The organization of the eye	16
1.2.2 Blood supply and drainage of the eye	17
1.2.3 Peculiarities of retinal microcirculation	20
1.2.4 Structural organization of retinal vessels	22
1.2.5 Quantitative parameters of ocular circulation	25
1.2.5.1 Blood flow velocity.....	25
1.2.5.2 Vessel diameter	27
1.2.5.3 Blood flow.....	28
1.2.5.4 Blood pressure, perfusion pressure and flow resistance	30
1.2.6 Normal vascular endothelial function	32
1.2.7 Pathological changes of vessel structure and vascular endothelial alterations in select systemic and ocular diseases	34
1.2.7.1 Atherosclerosis.....	34
1.2.7.2 Aging.....	37
1.2.7.3 Primary open-angle glaucoma.....	38
1.2.7.4 Systemic hypertension.....	40
1.2.7.5 Obesity	41
1.2.8 Abnormalities of longitudinal vessel profiles in micro- and macrocirculation.....	42
1.3 Blood Properties and Blood Rheology	44
1.3.1 Blood, its constituents and properties	44
1.3.2 Blood flow in macro- and microcirculation	45
1.3.2.1 Newtonian behaviour of blood. Blood viscosity and viscoelasticity.....	45
1.3.2.2 Non-Newtonian behaviour of blood.....	46
1.3.3 Fluid-structure interaction.....	48
1.3.4 Rheological models and constitutive equations of blood	48
1.3.5 Principles of rheological model by Quemada.....	50
2 METHODS	53
2.1 Functional in-vivo measurements with the Retinal Vessel Analyzer (RVA).....	53
2.1.1 Principles of RVA measurements.....	53
2.1.2 Functional stimulation of retinal vessels (Flickering light, OODG by Ulrich, etc.)	54
2.1.3 Assessment of temporal vessel reaction	57
2.1.4 Assessment of longitudinal vessel profiles	57
2.1.5 Spectral analysis of longitudinal vessel profiles	58
2.2 Study designs.....	60
2.2.1 Age-related study	60
2.2.2 Glaucoma study	61
2.2.2.1 Study 1 with acute suprasystolic IOP-increase	61
2.2.2.2 Study 2 with moderate 100 s IOP-increase	61
2.2.3 Systemic hypertension study	63
2.2.4 Obesity study.....	65
2.2.5 Repeatability and reproducibility of longitudinal vessel profile assessment and analysis	66
2.2.5.1 Short-term repeatability.....	67
2.2.5.2 Long-term reproducibility	68
2.2.5.3 Dimensional and spatial reproducibility.....	68

2.3	Healthy volunteers and patients	71
2.3.1	Anamnestically healthy volunteers of different age (age-dependence study)	71
2.3.2	Glaucoma patients and age-matched healthy volunteers (glaucoma study)	71
2.3.2.1	Study 1 with acute suprasystolic IOP-increase	71
2.3.2.2	Study 2 with moderate 100 s IOP-increase	71
2.3.3	Patients with systemic hypertension and age-matched healthy volunteers (systemic hypertension study)	72
2.3.4	Patients with obesity and age-matched healthy volunteers (obesity study)	73
2.4	Methods of Computational Fluid Dynamics (CFD) for simulation of blood flow in retinal vessels	75
2.4.1	CFD code NS3DV43C (Institute of Fluid Mechanics, MUT) for solving of the Newtonian problem	75
2.4.2	CFD Code N3DV6C and its extension for simulation of Non-Newtonian blood flow behaviour.....	76
2.4.3	Post-processor N3D_POST	76
2.4.4	CFD model of a retinal vessel	77
2.4.4.1	General assumptions	77
2.4.4.2	3D-geometry generic model of a retinal vessel with a possibility to vary parameters of vessel wall configuration.....	78
2.4.4.3	Parameters of CFD model.....	79
2.4.4.4	CFD simulation of the blood flow in the generic model of a retinal vessel segment -Newtonian model.	80
2.4.4.5	CFD simulation of the blood flow in the generic model of a retinal vessel segment. Non-Newtonian model.	81
2.4.4.6	Modeling of real human retinal vessels.....	84
3	RESULTS	85
3.1	Clinical studies on longitudinal retinal vessel profiles. Healthy aging, select systemic and ocular diseases	85
3.1.1	Age-dependence study	85
3.1.2	Glaucoma study	88
3.1.2.1	Study 1 with acute suprasystolic IOP-increase	88
3.1.2.2	Study 2 with moderate 100 s IOP-increase	89
3.1.3	Systemic hypertension study	89
3.1.4	Obesity study	94
3.1.5	Repeatability and reproducibility of longitudinal vessel profile assessment and analysis	97
3.1.5.1	Short-term repeatability.....	97
3.1.5.2	Long-term reproducibility	97
3.1.5.3	Dimensional and spatial reproducibility.....	98
3.2	CFD simulation of the blood flow in retinal vessels with different internal microstructure	101
3.2.1	Newtonian approach	101
3.2.1.1	Color mapping of the results of CFD simulation	101
3.2.1.2	Increase of high frequency vessel profile microirregularity augments the vessel hydraulic resistance	101
3.2.1.3	Comparison of geometric parameter influence to the model. Sensitivity analysis.....	103
3.2.1.4	Pump head-capacity characteristic	104
3.2.1.5	Influence of the blood viscosity	105
3.2.1.6	Color mapping and hydraulic resistance of real longitudinal vessel profiles. Examples.	106
3.2.2	Non-Newtonian approach	110
3.2.2.1	Color mapping and results of CFD simulation.....	110
3.2.2.2	Increase of high frequency vessel profile microirregularity augments the vessel hydraulic resistance	111
4	DISCUSSION	113
4.1	Microstructural changes and increase of high frequency microirregularity of longitudinal vessel profile – clinical symptoms characterizing vascular dysfunction.	113
4.1.1	Age dependence study	113
4.1.2	Glaucoma study	115
4.1.3	Ocular hypertension study.....	119
4.1.4	Obesity study.....	123
4.1.5	Evaluation of retinal longitudinal vessel profiles. Accuracy, repeatability and reproducibility	124
4.1.5.1	Accuracy of longitudinal vessel profile analysis.....	124
4.1.5.2	Repeatability and reproducibility of longitudinal vessel profile assessment and analysis	125
4.2	CFD simulation of the blood flow in retinal vessels – a powerful tool to assess the influence of internal vessel microstructure to the retinal blood flow	130

5	CONCLUSIONS AND SUGGESTIONS	132
5.1	General conclusions.....	132
5.2	Suggestions for future studies	133
5.2.1	Wavelet analysis of longitudinal vessel profiles.	133
5.2.2	Histological analysis of longitudinal sections of retinal vessels.....	133
5.2.3	Experimental measurements of real flow of a synthetic fluid with blood properties in silicone casts.....	134
5.2.4	CFD simulation of Non-Newtonian pulsatile blood flow in real retinal vessels with structure interaction. .	134
5.2.5	CFD simulation of dynamic processes in retinal vessels during a functional provocation.....	134
5.2.6	CFD simulation of the blood flow in a vessel branching	135
	REFERENCES	137
	LIST OF ILLUSTRATIONS	149
	LIST OF TABLES.....	153
	LIST OF OWN PUBLICATIONS ON THE TOPIC.....	154

1 Introduction

1.1 Purpose and problem statement

The eye possesses unique features in the human body. One of them is the transparency of the optic media, which allows for direct observation of the microvascular bed of retinal vessels. Retinal vasculature resembles the one in the central nervous system and possesses some special properties. Besides, retinal vessels are similar to brain vessels in their structure and function. Thus the assessment and analysis of normal and impaired function of retinal vessels and retinal blood flow can be used for the indirect diagnosis of the central microcirculation.

Change in diameter of arteries, capillaries and veins is the main reaction of local retinal autoregulation to any disturbance within the control loop of tissue perfusion. The most interesting sites within the retinal vascular bed to observe changes in diameter would be the arterioles with a diameter less than 20 μm , because these vessels represent the major sites of resistance to flow secondary to the precapillary sphincters. However quantification of changes in vessel diameter of vessels with a diameter less than 70 μm is difficult because of the limited resolution of any of the present techniques. Changes of less than 1% in diameter of the larger retinal vessels are routinely detectable. By image analysis with the Retinal Vessel Analyzer it is possible to perceive vessels in their dynamic state online non-invasively along a given vessel segment. Retinal arteries and veins were found to demonstrate vasoreactivity in response to various physiological stimuli (Polak et al. 2002; Garhofer et al. 2004; Kotliar et al. 2004; Nagel & Vilser 2004; Nagel & Vilser 2004).

Evidence that vascular factors contribute to the pathogenesis and development of various systemic and ocular diseases continues to accumulate (Cioffi et al. 2003). Arteriosclerotic and other pathologic changes occur in blood vessels with age and in systemic diseases. (Dohi et al. 1995; Stork et al. 2006). These changes involve the whole vascular system in a somewhat patchy appearance (Stary et al. 1992). It is also known that small vessels are affected differently from major vessels like the carotid artery (Criqui et al. 1989).

Retinal vessels are not straight tubes. They rather possess narrow and wide segments in their course. It is known that age, obesity, vascular ocular and systemic diseases induce changes in the configuration of arterial and venous walls in macro- and microcirculation. The inner vessel wall might become more or less irregular in longitudinal vessel section. Moreover the configuration of the inner wall might be altered during vessel constriction and dilation. This effect might have several reasons:

- instability of thin vascular walls, which become more rigid with age or a pathology (Jacobsen et al. 2002);
- partial endothelial damage of retinal vessels (Haefliger et al. 1994);
- partial degradation of smooth musculature of retinal vessel walls (Jacobsen et al. 2002; Vilser et al. 2002)

Pathological changes in the longitudinal structure of retinal vasculature in some systemic diseases, like arterial hypertension and diabetes mellitus are optically visible. However nobody has studied such pathological changes in small vessels of microcirculation in-vivo in detail in aging, in glaucoma and also in the mentioned diseases, especially during dynamic vessel reaction. To the best knowledge of the author, neither attempts to quantify microirregular changes in longitudinal inner vessel wall configuration in the human retina nor studies on the influence of these irregularities on the retinal blood flow have ever been performed.

The in-vivo dynamic assessment and analysis of physiological and pathological structural peculiarities of retinal vessels can be a key for early diagnosis of systemic and ocular diseases of vascular origin. Combined with numerical blood flow simulation such investigations might give valuable insights in the origin and course of vascular pathologies. Moreover, various methods of treatment can be tested in-vivo in regard to their influence on the vascular structure.

In the present work the hypothesis was checked that in young persons the longitudinal inner structure of retinal vessels might differ from one in older persons and in systemic or ocular diseases of vascular origin. A method to assess longitudinal structure of inner wall of retinal arteries and veins was developed. Parameters to quantify these structural changes were proposed and evaluated. Whether changes in the longitudinal inner structure of a retinal vessel can influence its hemodynamic parameters was investigated using contemporary models of blood rheology and novel methods of computational fluid dynamics (CFD).

1.2 Ocular circulation and methods of its assessment

1.2.1 The organization of the eye

The human eye represents a perfect and interrelated system of about 40 individual subsystems, including the retina, the pupil, the iris, the cornea, the lens and the optic nerve (Richards 1989) (Fig. 1). The eye allows to see and to interpret shapes, colors, and dimensions of objects in the world by processing the light they reflect or emit. The eye is approximately 2,5 cm wide, 2,5 cm deep and about 2,4 cm high. It weighs 7,5 grams and its volume is roughly 6,5 milliliters. The detailed anatomy and physiology of the eye is intelligibly represented in several handbooks (Forrester et al. 2002; Kaufmann & Alm 2003; Park & Karesh 2007).

Following are the structural and functional peculiarities of the retina and the adjacent choroid. Then it is turned to the detailed description of the ocular microcirculation, which is instrumental for the present research work.

The term retina derives from the Latin word *rete*, meaning “net.” This name was originally used by ancient Greeks, who observed that the retina had the appearance of a fishing net (Roh et al. 2007). The retina is a very thin, delicate, and transparent light-sensitive membrane. It is approximately 0,5 mm thick, has a surface area of approximately 266 mm² and lines the back of the eye (Fig. 1, top) (Park & Karesh 2007). The retina has two functions. The first, performed by the rod and cone photoreceptors, is to transduce information from an optical image first into a biochemical message and then into electrical signals. The second, performed by the neural tissue of the retina, is to process certain features of the visual world from the photoreceptor signals and transmit this information to the brain.

Rod cells enable to see objects that are not directly to the fore, giving a rough idea of what is around. They enable the mobility and getting around. They also enable to see objects in dim light and to see movement. Cone cells are concentrated in the central part of the retina where the light is focused by the cornea and lens. This area is called the macula (Fig. 1, upper panel). Cone cells give the detailed vision which is used when reading and looking at people’s faces. They are also responsible for the color vision. The optic nerve contains axons of the ganglion cells

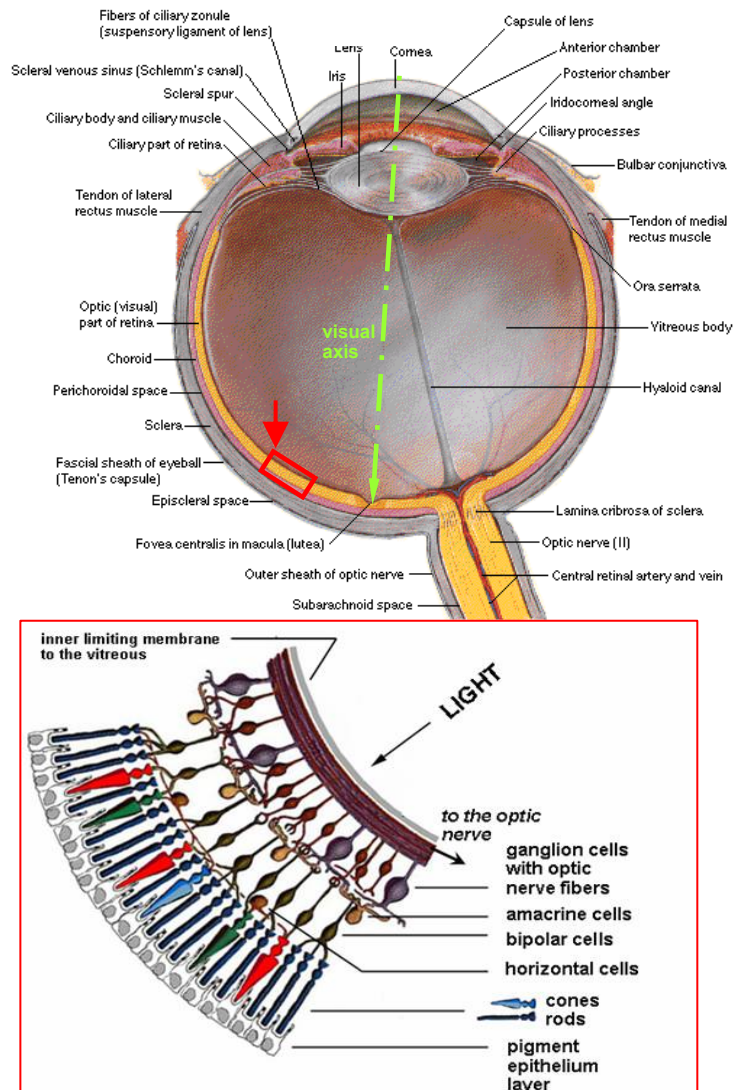


Fig. 1. Top: Detailed diagram of the human eye. Modified from http://www.phys.ufl.edu/~avery/course/3400/gallery/gallery_vision.html. **Bottom:** Morphological organisation of the retina. Scaled up detailed presentation of the area within the red rectangle in the upper panel. Modified from www.dma.ufq.ac.at/assets/16457/intern/retina.jpg.

(the output neurons of the retina) leading to the brain and, additionally, blood vessels that open into the retina to vascularize the retinal layers and drain blood from the retina. The ganglion cells lie innermost in the retina closest to the lens and front of the eye. The rods and cones lie outermost in the retina against the pigment epithelium and choroid. Light must, therefore, travel through the thickness of the retina before striking and activating the rods and cones (Fig. 1, bottom).

The normal avascularity of certain ocular structures such as the cornea, the lens, and the vitreous allows direct light transmission to the retina. Light waves from an object enter the eye first through the cornea. The light then progresses through the pupil, the circular opening in the center of the colored iris (Fig. 1, top). Next, the light passes through the crystalline lens. Initially, the light waves are bent or converged first by the cornea, and then further by the crystalline lens, to a nodal point located immediately behind the back surface of the lens. At that point, the image becomes reversed (turned backwards) and inverted (turned upside-down). The light continues through the vitreous humor, the clear gel that makes up about 80% of the eye's volume, and then, ideally, back to a clear focus on the retina behind the vitreous. Within the layers of the retina (Fig. 1, bottom), light impulses are changed into electrical signals and then sent through the optic nerve, along the visual pathway, to the occipital cortex at the posterior or back of the brain. Here, the electrical signals are interpreted or "seen" by the brain as a visual image.

The choroid is a highly vascularized and pigmented tissue that is the posterior extension of the ciliary body (Fig. 1). The choroid is part of the uveal tract (or uvea) which also includes the iris and the ciliary body. The choroid provides oxygen and nourishment to the outer layers of the retina and the back of the eye. 60 – 80% of oxygen is delivered to the retina from the choroid (Shamshinova & Volkov 1998). Additionally, the choroid is supposed to participate in the temperature control of the eye (Bill et al. 1983), removing the large amount of heat from metabolic processes initiated when photons strike the retina (Parver et al. 1980). The choroid itself probably serves as a mechanical cushion for the internal structures of the eye, participating in the accommodation (Beers & van der Heijde 1996). The choroid extends from the ora serrata anteriorly to the optic nerve posteriorly. It is light to dark brown in color and sponge-like in appearance. The thickness of the choroid is estimated from 0,2 to 0,3 mm at the posterior pole and to 0,1 to 0,15 mm at the ora serrata (Tamm et al. 1992; Park & Karesh 2007). The thickness of the choroid diminishes with age because of a decrease in the size and number of its venous channels. External to the choroid the sclera lies. There is a potential space between these two structures. Posteriorly, this is called the suprachoroidal space, whereas anteriorly it is termed the supraciliary space. The vessels and nerves supplying the choroid traverse this space after penetrating the sclera. The red eye effect on photos and the red color of retinal images like in Fig. 5 are caused by the reflection of light from choroid. It appears red because of the choroid's blood vessels.

1.2.2 Blood supply and drainage of the eye

The human vascular system in general is hidden from direct observation. It lies deep within the body or it is covered by skin. The normal eye provides a unique opportunity to visualize directly the circulatory system in vivo. Systemic vascular pathologies, such as diabetes mellitus and systemic hypertension, can be directly diagnosed by

ophthalmoscopy observing the retina. Some other systemic diseases, such as Fabry disease, can be also diagnosed by examination of the external ocular circulation (Roh et al. 2007).

Interestingly, under normal physiologic circumstances, the large vessels responsible for delivering blood to and draining it from the eye do not have a direct role in the intraocular circulation. Only if, under pathologic conditions such as atherosclerotic cardiovascular disease, the lumen of those vessels becomes critically obstructed, then effects in peripheral ocular vasculature in the form of ocular vascular disease might ensue (Roh et al. 2007).

In humans the ocular vessels are derived from the ophthalmic artery (A. ophthalmica), which is the first branch of the intracranial ramus of internal carotid (A. carotis interna). The ophthalmic artery branches into the central retinal artery (A. centralis retinae) and one to five posterior ciliary arterial trunks (Fig. 2, top). Most of individuals have 2 to 3 posterior ciliary trunks (Cioffi et al. 2003). These trunks branch into the main posterior ciliary arteries (PCA) and muscular arteries. Fig. 3 shows schematically the blood vessels of the human eye. Each of two main PCAs divides further into several short posterior ciliary arteries (10 to 20), before and after entering the sclera. Medial and lateral long PCAs (Aa. ciliaris post. longa) branch from the ciliary trunks, course anteriorly along the outside of the eyeball and penetrate the sclera at the horizontal meridian of the globe near the optic nerve (Fig. 2, top). The two long PCAs travel then anteriorly within the suprachoroidal space, along the horizontal meridians of the globe and typically divide near the *ora serrata* (Fig. 3). The long PCAs supply the iris, the ciliary body and the anterior choroid and a part of the posterior choriocapillaris (Roh et al. 2007). The short posterior ciliary arteries (Aa. ciliaris post. breves) travel anteriorly after branching from the main PCAs (Fig. 2, top) and penetrate the sclera immediately adjacent to the optic nerve, mostly in the nasal and the temporal region (Fig. 3). These arteries supply the posterior choroid and most of the anterior optic nerve. Some short PCAs course, without branching, through the sclera directly into the choroid. Others divide within the sclera giving branches to both the choroid and the anterior optic

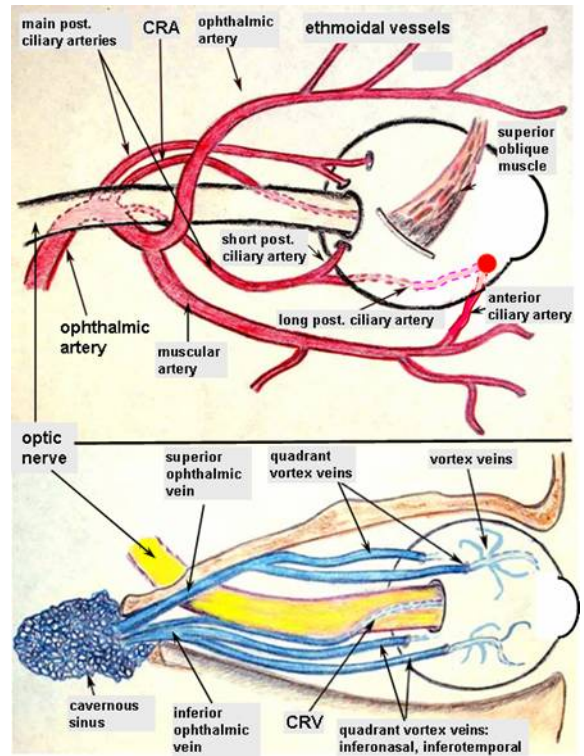


Fig. 2. Macroscopic anatomy of the ocular circulation. **Top:** blood supply to the eye (arterial system). **Bottom:** blood drainage (venous system). Modified from www.missionforvisionusa.org/anatomy/uploaded_images by B. Glasgow, M.D. Los Angeles, CA, USA.

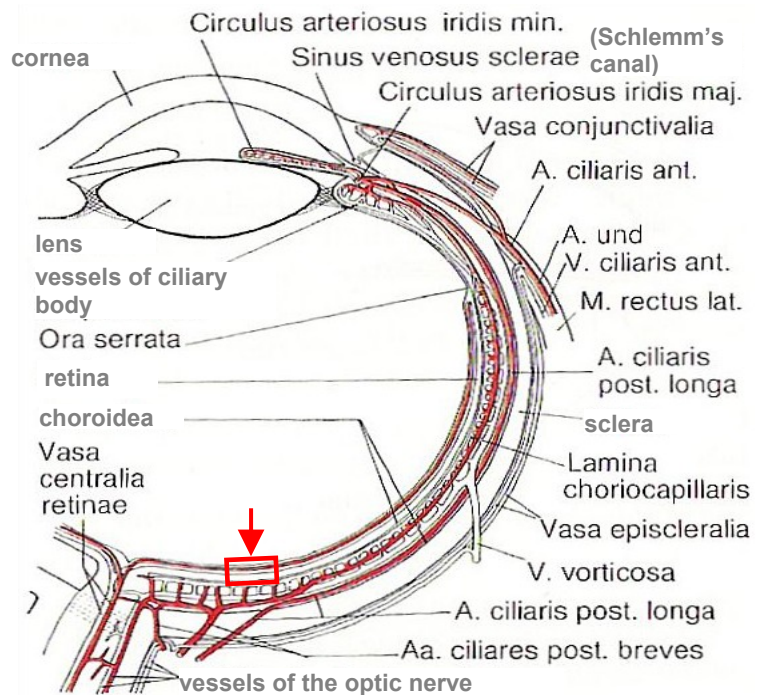


Fig. 3. Blood supply of the human eye. Modified from Schiebler (Schiebler et al. 1999). Detailed presentation of the area within the red rectangle is represented in Fig. 4.

nerve. The short PCAs form the choriocapillaris (Fig. 4), a dense, one layered network adjacent to the Bruch's membrane and the retinal pigment epithelium. Posteriorly, the meshwork of vessels in this layer measures 3 to 18 μm in cross-section, whereas at the equator these vessels measure 6 to 36 μm in cross-section by 36 to 400 μm in length. In the macular region, the diameter of the vessels of choriocapillaris is approximately 20 μm . These capillaries are considerably wider in cross-section than capillaries elsewhere in the body. They have fenestrations measuring 80 nm in diameter (Park & Karesh 2007). In the posterior pole the choriocapillaris is arranged with alternating feeding arterioles and draining venules (Hayreh 1975).

The muscular arteries travel with the outer recti eye muscles (outer muscle responsible for eyeball movement), supplying them. Further they divide into the anterior ciliary arteries (Fig. 2, top). There are generally seven muscular branches. Each ocular rectus muscle has two branches, with the exception of the lateral rectus, which has only one.

The anterior choroid is additionally supplied with anterior ciliary arteries. They course with outer ocular muscles, penetrate the sclera anteriorly and form an intramuscular circle (Fig. 3). Together with the long PCAs they also form the major iridal circle, which is the main supply of the iris and ciliary body. Some branches of anterior ciliary arteries supply peripheral choroid and anterior choriocapillaris.

Two separate vascular systems are involved in the nutrition of the eye: the retinal and the uveal one.

The uveal blood vessels include the vascular beds of the iris, the ciliary body and the choroid (Cioffi et al. 2003). The overall structure of the choroidal circulation is segmental. This segmental distribution of blood begins at the level of the PCA branches and it is reflected in the vortex vein drainage system. The large and medium-sized choroidal arteries act as end arteries. Unlike most other tissues, in the choroid the large vessels do not run parallel to each other. Each terminal choroidal artery supplies an independent segment of choroidal capillaries. Feeding arterioles are usually found in the center of such a segment with draining venules located at its periphery. There is almost no functional communication between adjacent capillary segments (Weiter & Ernest 1974; Hayreh 1975).

Most of the choroid is drained through the vortex venous system, as a rule, one vein in each quadrant of the posterior pole of the eye. Vortex veins empty into the superior and inferior ophthalmic veins. Both vessels drain then into the cavernous sinus (Fig. 2, bottom). Blood from anterior choroid is drained also mainly through the vortex veins. Additionally there are anastomotic communications with anterior episcleral veins. Aqueous humor is drained in these vessels

leaving the anterior chamber through the Schlemm's canal and collector channels, see Fig. 1 and Fig. 3 (Moses 1972; Brubaker 1998). The vasculature of the choroid appears to be under direct adrenergic innervation. Flow in the choroid is more difficult

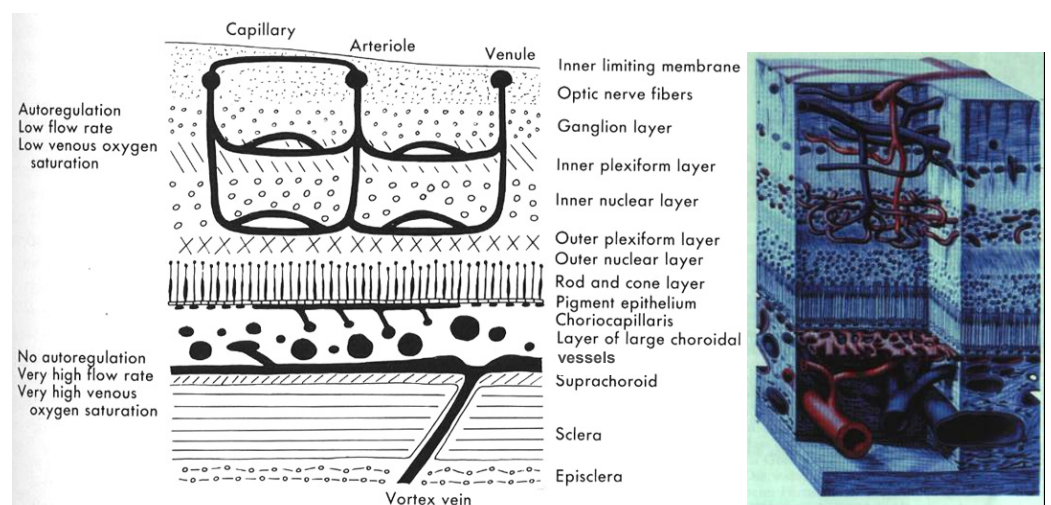


Fig. 4. Blood supply of the retina. Retinal capillaries are densely distributed within inner layers of the retina, ~260 μm thick. The outer layer, ~130 μm thick, has no blood vessels and nourished from the choroid. **a:** Scheme modified from (Alm 1992). **b:** Modified scheme by Bergmann 1962 cited from (Eichhorn 2001).

to describe because of its complex architecture and segmental structure. It is supposed that choroidal blood flow is mostly laminar (Roh et al. 2007).

The complex vascular supply and drainage of the optic nerve, the iris and the ciliary body, including ciliary processes is described in detail elsewhere (Cioffi et al. 2003; Roh et al. 2007).

The retinal system is formed by central retinal artery (CRA), which enters the optic nerve approximately 10 mm behind the eyeball and appears within the eye, at the optic disc (Fig. 2, top). CRA branches into superior and inferior rami (branches) after its entry in the eye at the optic nerve head. Each of the rami branches then into major temporal and minor nasal rami (Fig. 5). Each of these four major retinal arteries supplies one quadrant of the retina. The major retinal arteries and corresponding retinal veins measure 50 ± 250 μm in diameter. They are located under inner limiting membrane within the nerve fiber layer (Fig. 4). Retinal arteries are end arteries without any anastomoses. Their occlusion (closing) may therefore destroy the inner retinal layers. Irreparable damage occurs if such a closing exceeds 1 hour (Fujino & Hamasaki 1967). CRA is the sole circulatory supply for the retinal vasculature, except in the region near the disc where the retina may be supplied by a cilioretinal artery in approximately 20% of eyes. This cilioretinal artery protects the central retina from ischemia (pathologic impairment of blood supply) in cases of retinal artery occlusion (Park 2007).

The venous drainage of the retina and the anterior optic nerve is almost exclusively through the central retinal vein (CRV, V. centralis retinae, Fig. 2, bottom) and its affluents, which subsequently inflow into the superior ophthalmic vein.

In the large part of the retina the retinal system consists of two layers of flat capillary networks. The capillaries are arranged in a laminated fashion. In the central part of the retina at the posterior pole these networks are dense and may have 3 to 4 layers, whereas in the periphery the networks are less dense and are reduced to a single layer. The extreme peripheral inner retina is avascular (Alm 1992). The retinal vessels are distributed within the inner two thirds of the retina, whereas the outer layers, including the photoreceptors are avascular and are supplied from the choroid (Fig. 4). An avascular zone enables light to reach the central photoreceptors. It is located in the fovea with a capillary free zone with an area of 0,5 mm in diameter (Fig. 5).

1.2.3 Peculiarities of retinal microcirculation

The metabolism (the substance exchange) between the blood and tissues, the blood flow and its regulation in blood vessels less than 300 μm in diameter is defined as **microcirculation** (Gaethgens 1980). Hence the whole

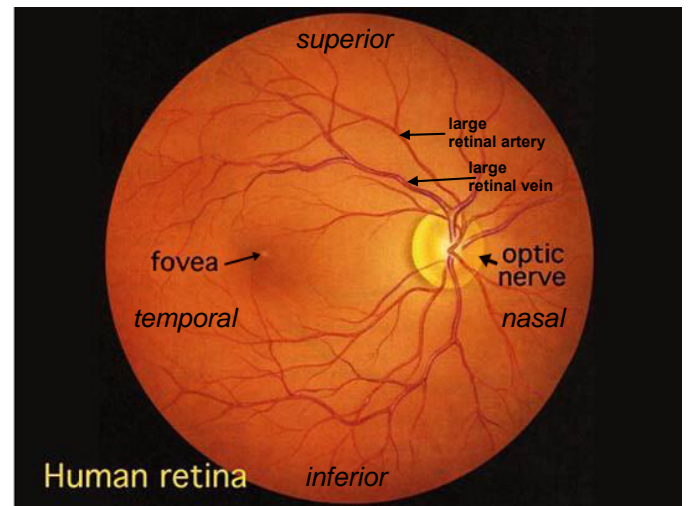


Fig. 5. Normal human retina. A 50° fundus photograph, right eye. The optic nerve: a circular white area ~ 2 x 1.5 mm across. From the center of the optic nerve radiate the major retinal blood vessels. 4,5-5 mm (2,5 half disc diameters) to the left of the disc: slightly oval-shaped, blood vessel-free spot, the fovea, which is at the center of the area known as the macula by ophthalmologists. Modified from: <http://webvision.med.utah.edu/imageswv/huretina.jpeg>.

retinal vessel system including large branches of CRA is a part of the microcirculatory system. The retinal microcirculation maintains the optimal level of oxygen supply and metabolism in the inner retina.

It is generally accepted that there is no functional autonomic innervation to the retinal vessels in humans (Ernest 1977; Alm 1992; Park & Karesh 2007). Instead the retinal circulation is autoregulated. Historically **autoregulation** was first described by Bayliss in 1902 in the sense of local reaction of arterial walls to changes in internal pressure (Bayliss 1902). Guyton assumes, that in order to determine autoregulative capacity in an organ it should best be isolated from the rest of the body to rule out confounding factors such as neural input (Guyton 1977). By the modern definition, autoregulation is the property of a vascular bed to provide constant or nearly constant blood flow throughout a wide range of perfusion pressures (Roh et al. 2007). Autoregulation of the retina is commonly used today in a broader sense. It encompasses the local homeostatic blood flow regulation mechanisms that provide a constant metabolic environment in the retina despite various conditions that tend to disturb this equilibrium. The physiologic basis for the control of retinal blood flow primarily appears to be tissue levels of oxygen, metabolic products, and intraocular and systemic blood pressures (Ernest 1989; Alm 1992).

Retinal autoregulation is a complex physiologic function of its microcirculation. The precise mechanisms of autoregulation are not known at present. Two concepts have been introduced to explain this phenomenon (Roh et al. 2007):

- According to **the myogenic theory** vasodilation and vasoconstriction to maintain blood flow in the presence of changing intravascular pressures are effected by cell-to-cell communication between adjacent smooth muscle cells.
- **The local metabolite theory** proposes that metabolites or other currently unknown substances are produced by the retina itself when it is metabolically stressed. These metabolites might induce local alterations in retinal blood flow in order to maintain a constant retinal environment.

The retinal circulation shows autoregulation within physiologic levels of the intraocular pressure (IOP) in response to perfusion pressure changes. Ocular perfusion pressure is defined as the difference between the blood pressure and the IOP (Riva et al. 1986; Alm 1992). The retinal autoregulation is sensitive to changes in tissue levels of oxygen and carbon dioxide, to local factors, e.g. nitric oxide, prostaglandin, endothelin, and the renin-angiotensin system and to some vasoactive agents and medicaments (see also 2.1.2).

The vascular endothelial cells represent the regulating system within the vessel. They control its basal tone and diameter in reaction to systemic and local demands. Change in retinal vessel diameter is the main reaction of local autoregulation to any disturbance within the control loop of tissue perfusion (Roh et al. 2007). Whether sympathetic or parasympathetic innervation of the retinal arteries exists beyond the level of the optic nerve head is a subject of controversy. Preliminary studies showed that although the ophthalmic artery contains sympathetic nerve fiber endings and is therefore under control of the autonomic nervous system, there is apparently no central regulation of the blood flow in the retina itself (Roh et al. 2007). No nerve fibers could be found in the media or adventitia in human retinal arteries and arterioles (Laties 1967). However, more recent work in human and bovine eyes has shown the presence of adrenergic binding sites in retinal arteries (Forster et al. 1987). In addition, pharmacologic studies reported from several laboratories have shown that retinal blood flow can be altered with the use of adrenergic agonists and antagonists (Ferrari-Dileo et al. 1990; Park 2007).

The tight junctions, closely associated areas of two endothelial cells whose membranes join together forming an impermeable barrier to fluid, in cerebral capillaries are the anatomic counterpart of the blood-brain barrier (Fig. 6, top). The retina, being a part of the brain, has a similar arrangement, called the blood-retinal barrier with continuous capillaries and tight-junctions between the endothelial cells and between the cells of retinal pigment epithelium (Cunha-Vaz et al. 1966). The endothelial cells of larger retinal arteries are arranged circumferentially or obliquely along the long axis of the vessel and also contain these tight junctions. Only liposoluble substances like oxygen and carbon dioxide can pass through the barrier. The blood-retinal barrier is impermeable even to small water-soluble substances, such as glucose and amino acids. Such vital metabolic substrates can be transported through this barrier by means of so-called carrier-mediated transport (Alm et al. 1981). The blood-retinal barrier defends the retina against the penetration of toxins, neuromediators and other active substances from the bloodstream. A defect of the blood-retinal barrier exists at the level of the optic disc (Grayson & Laties 1971). The permeability of the blood-retinal barrier can vary in response to stimuli, including drugs such as histamine and can be altered in several diseases. For example, it increases in diabetes and arterial hypertension (Roh et al. 2007).

1.2.4 Structural organization of retinal vessels

The retinal blood vessels exist to provide nourishment for the inner retinal layers and to dispose of waste products. The major branch retinal arteries are smaller in diameter and straighter in course than their accompanying draining veins. Subsequent division of the arteries results in a decrease in the caliber of the vessel.

The blood column within retinal arteries is visible with a direct ophthalmoscope down to the third-order branches. *Normally, the walls of retinal vessels themselves are transparent to direct observation. It is the blood column that makes the vessels visible on ophthalmoscopy* (Roh et al. 2007).

Overall large blood vessels such as veins and arteries have three layers (Fig. 7):

- **the intima** (innermost layer) consists of macrovascular endothelial cells lining the luminal surface. An endothelial cell is $0,2 \div 0,5 \mu\text{m}$ thick, $10 \div 15 \mu\text{m}$ wide and $20 \div 50 \mu\text{m}$ long (Fung 1990);

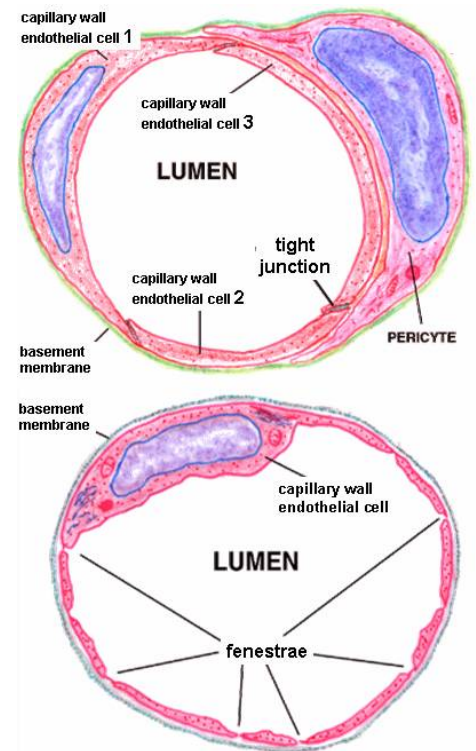


Fig. 6. Structural cross-sectional organization of capillaries. **Top:** closed or continuous capillary. **Bottom:** fenestrated capillary. Modified drawing by Caceci from: <http://education.vetmed.vt.edu/Curriculum/VM8054/Labs/Lab12b/Lab12b.htm>.

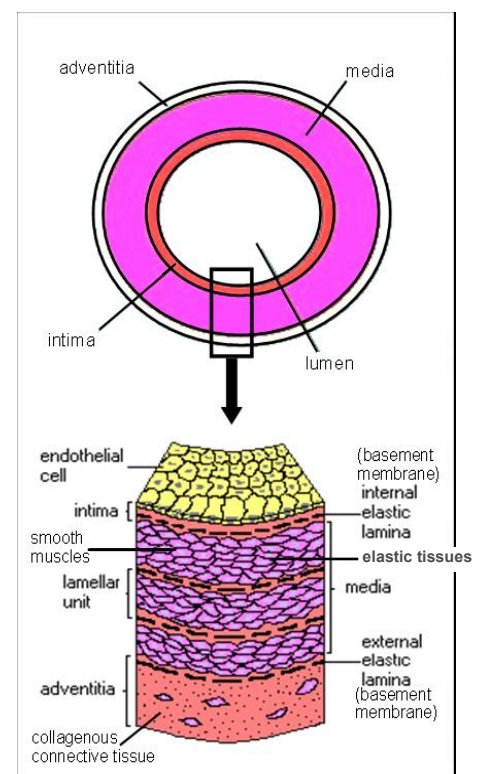


Fig. 7. Structural cross-sectional organization of a small artery. Modified from: www.vascularsurgeon.co.uk/anatomy.htm.

- **the media** is separated from the intima by the basement membrane (0,08 μm thick) and consists of multiple 5 ÷ 15 μm concentric layers of smooth muscle cells. The number of concentric layers and thus media thickness increases with increasing artery diameter. As a rule of thumb it is proposed that the media increases in thickness 50 μm for every 1 mm of artery diameter;
- **the adventitia** is the outermost layer, which contains loose connective tissue with the surrounding tissue stroma and smaller blood vessels and nerves. The adventitia constitutes 10% and 50% of the thickness in elastic and muscular arterial walls correspondingly. It consists primarily of type I collagen fibers with some elastin and fibroblasts.

Small blood vessels such as capillaries, post-capillary venules and arterioles are lined by a single layer of microvascular endothelial cells and are surrounded by a continuous basement membrane composed of several extracellular matrix molecules. Pericytes surround the endothelial layer, which is then encircled by the adventitia.

Retinal arteries

The intima of retinal arteries contains a single layer of endothelial cells surrounded by a basement membrane. Collagen fibrils may be seen in the basement membrane. Elastic fibrils are not present, and there is no internal elastic membrane. The media of the major vessels near the optic disc contains five to seven layers of circularly arranged smooth muscle cells. These cells are surrounded by a thick and often lamellated basement membrane containing collagen fibers. These histological characteristics distinguish retinal arteries from muscular arteries of the same size in other tissues. The unusually developed muscular layers may allow greater constriction of the vessels in response to chemical and pressure changes (Park 2007).

The basement membrane surrounding the innermost layer of the smooth muscle cells is continuous with the basement membrane surrounding the endothelial cells. In some areas this membrane becomes thinner. In these areas the membranes of the endothelial cell and smooth muscle cell are closely apposed. The basement membrane surrounding the outermost layers of smooth muscle cells contains increasing amounts of collagen and tends to become vacuolated (full of membrane bound sacs, vacuoles) and to accumulate debris with aging.

As the major retinal arteries branch and approach the equator of the eye, the media becomes less developed and contains approximately two layers of circularly or obliquely arranged smooth muscle cells. At this point and further peripherally, the retinal vessels should be considered as arterioles. Retinal arterioles are similar to the arteries, but their lumen is smaller measured 8 ÷ 15 μm in diameter.

The arterial adventitia (Fig. 7) consists of collagenous connective tissue that is continuous with the basement membrane surrounding the outer layers of smooth muscle cells of the media. A smooth muscle cell may occasionally be displaced into the adventitia. Glial cells are in direct contact with the adventitia. The arteriolar adventitia is poorly developed and consists of the outermost layer of basement membrane surrounding the smooth muscle cells and small amounts of collagen fibrils.

In the retinal arteries and arterioles there are no precapillary sphincters, which are usual for microcirculation systems. Sphincter-like activity was reported in 90° branchings in the retina (Yu et al. 2005)

Retinal veins

In the normal anatomy CRV is the only outflow channel for the retinal circulation. Potential anastomoses exist between the retinal and choroidal circulations at the disc. In cases of central retinal vein occlusion, anastomoses can enlarge (Park 2007). Throughout the retina, the veins and venules generally follow the course of the arteries and arterioles. When a retinal artery and a vein cross, the artery usually lies anterior (toward the vitreous) to the vein (Duker & Brown 1989). About one third of the time, however, the vein is anterior. At such crossing sites, the two vessels share a common adventitia. Under normal circumstances, the crossing vein's lumen may be decreased by approximately one third as a result of compression from the accompanying artery (Seitz 1964). Arteriovenous crossings represent the most common site of branch retinal vein obstructions. There are many more such crossings temporally than nasally, because the nasal vessels assume a much straighter course (Fig. 5).

The intima of the veins consists of a layer of endothelial cells surrounded by a basement membrane continuous with that of the innermost layer of smooth muscle cells of the media (see Fig. 7). The media of the largest veins in the posterior retina consists of several layers of longitudinally oriented smooth muscle cells. The adventitia makes up the greatest part of the vessel wall and consists of loosely arranged collagen fibers and adventitial cells and is in direct contact with the glial cells of the retina.

Venules are usually less than 20 μm in diameter (Roh et al. 2007). Their media is composed of a single layer of cells resembling pericytes. The pericytes are small cells with long processes that run parallel with the long axis of the vessel and possess shorter processes that encircle the vessel walls (Fig. 6). Elastin is not present in retinal venules. The adventitia contains the basement membrane surrounding the pericyte (Roh et al. 2007).

The three or four layers of smooth muscle cells along the venous wall are quickly lost and replaced by pericytes. These pericytes differ microscopically from smooth muscle cells. They have fewer cytoplasmic filaments and less-dense attachment zones along the plasma membrane. These layers of pericytes lack the contractile and structural strength of smooth muscle cell layers around arteries. Thus, the vessel diameter of veins is flexible and can change with various pathologic processes associated with fluctuations in retinal blood flow. *In diabetes patients or in carotid artery disease, for example, the retinal veins can become sausage-shaped because of the slower flow through these vessels.* In some diseases the retinal veins may expand in response to an increase in venous pressure (Park & Karesh 2007).

The venous system extends peripherally as far as does the arterial system. In this peripheral region and in the junction of the venous and capillary systems in the retina, the walls of the veins become thinner and have the characteristics of venules. In these venules, the endothelial cell cytoplasm and basement membrane are so thin that the nuclei of the endothelial cells are seen bulging into the vessel lumen. Such a venule consists only of a single layer of pericytes containing a poorly developed contractile apparatus. The adventitia also becomes thinner and lose its collagenous support (Park 2007).

A capillary-free zone is present around each of the larger retinal arteries and veins (Fig. 8). It is larger around the arteries, measuring up to 100 μm . The capillary-free zone is a product of the vascular remodeling process, initiated probably by direct

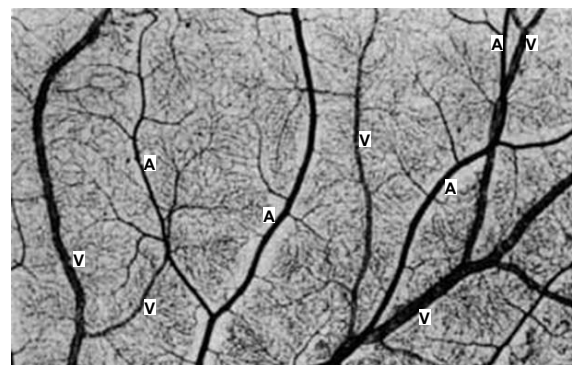


Fig. 8. Human retinal vasculature, including arteries (A), veins (V), arterioles, venules and capillaries. Note capillary free zone around arteries. Modified data by Henking cited from (Park 2007).

diffusion of oxygen through the walls of the large retinal vessels (Cioffi et al. 2003). Additionally, retinal arteries and veins remain isolated from the retinal neural tissue throughout their course by surrounding astrocyte and Müller cell processes (Ashton 1963), which are in direct contact with the adventitia. These processes surround all retinal vessels to form the “perivascular limiting membrane of Kruckmann”. This glial cuff around arteries has a high concentration of collagen and differs from that around other retinal vessels (Park 2007).

Retinal capillaries

Overall capillaries can be classified as continuous, fenestrated or discontinuous (Fig. 6). *Continuous* capillaries are the most impermeable type. They can be found, for example, in the brain. Adjacent endothelial cells are connected here by an almost continuous network of tight junctions (Fig. 6, top). The wall of *fenestrated* capillaries is thin with openings, covered by a thin porous membrane (Fig. 6, bottom). They are generally found in tissues with large fluid movements between the intravascular and extravascular compartments (for example, kidney). *Discontinuous* capillaries permit blood cells to pass easily through the microvessel walls (for example, in liver and bone marrow). *Retinal capillaries represent the continuous type*. Microvessels of the choriocapillaris are fenestrated, for example. No discontinuous capillaries are found in the eye.

Retinal capillaries are spread like a vast cobweb through the retina between the arterial and venous systems. There are only three areas of the retina that are devoid of capillaries: the above mentioned foveal avascular zone and the zone adjacent to major arteries and veins as well as the far peripheral retina (Park 2007). There are no direct shunts between the arterioles and venules in this or any other terminal area of the retinal circulation. The only normal connection between retinal inflow and outflow systems is through the capillaries.

Retinal capillaries range in diameter from 4 to 6 μm . The capillary wall consists of a continuous layer of flattened and longitudinally oriented endothelial cells and an incomplete layer of longitudinally oriented pericytes (Fig. 6, top), which are believed to have a contractile function and to regulate retinal blood flow at the microvascular level (Helbig et al. 1992). The pericytes of retinal capillaries possess multiple arm-like processes that turn around the surrounding endothelial cells (Fig. 6). These processes cover about 85% of the entire circumference of the capillary endothelial tube (Frank et al. 1990). The capillary basement membrane between pericytes and endothelial cells is much thinner than the basement membrane covering the two types of cells. This arrangement probably allows increased communications between the cells. The pericytes are closely spaced, resulting in an approximate ratio of pericytes to endothelial cells of 1:1, a relatively high ratio compared with elsewhere in the central nervous system. The retinal capillary basement membrane is thicker than in most other capillaries in the body. In certain diseases such as diabetes, this thickness increases (Roh et al. 2007).

1.2.5 Quantitative parameters of ocular circulation

In the following chapter the principal fluidmechanical parameters of ocular blood flow are described.

1.2.5.1 Blood flow velocity

Blood flow velocity values in different vascular beds of the eye in normal volunteers are shown in Table 1.

Blood velocities in large ocular vessels were measured using color Doppler imaging by A. Ustymowicz et al. (2005) in 140 healthy volunteers and by H. Kaiser et al. (1996) in 189 healthy volunteers.

Since the blood flow in most large ocular arteries is pulsatile, the arterial velocity is a periodic function, which changes non-uniformly from its minimum (EDV – end diastolic velocity) to its maximum (PSV- pulse systolic velocity). The venous velocity changes periodically in an almost sinusoidal form during the cardiac cycle from its minimum (minV) to its maximum (maxV). These characteristic waves assessed with color Doppler imaging in a short PCA and in a vortex vein are shown in Fig. 9.

Logean et al. (2003) showed with confocal scanning laser Doppler velocimetry, that velocity profiles in large branch retinal arteries and veins are almost parabolic. Retinal arterial velocity also changes during the cardiac cycle (Table 1 and Fig. 10).

Table 1 shows also the data by Grunwald et al. (1996), who measured blood flow in large retinal veins with laser Doppler velocimetry. Blood flow velocities in large retinal arteries were measured by Nagaoka et al. (2002) using Canon scanning laser Doppler flowmetry and by Ferguson et al. (2004) with Tracking Scanning Laser Ophthalmoscope. Martin et al. (2005) measured the leukocyte velocity in the premacular region using adaptive optics in a scanning laser ophthalmoscopy.

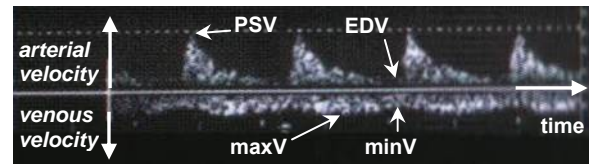


Fig. 9. Temporal changes of the blood flow velocity in a short posterior ciliary artery and in a vortex vein. Color Doppler imaging. Modified from (Kagemann et al. 1999).

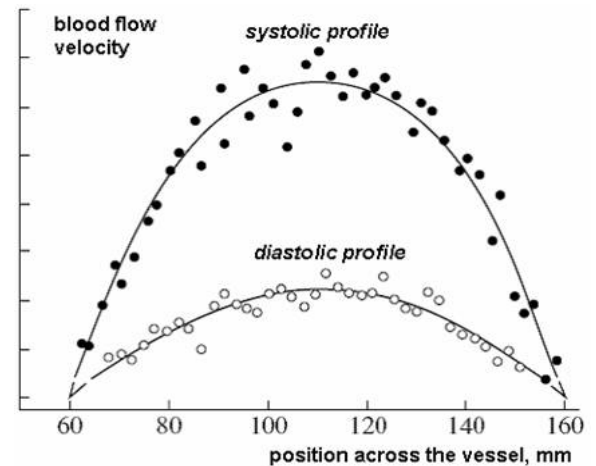


Fig. 10. Measured velocity values across a retinal arterial segment during systolic and diastolic phases of cardiac cycle and corresponding parabolic fits. Modified from (Logean et al. 2003).

Table 1. Physiological blood flow velocities in different vascular beds of the eye.

(PSV – pulse systolic velocity; EDV–end diastolic velocity; maxV/minV – maximal/minimal velocity)

Vessel	Age							
	Different ages (Kaiser et al. 1996)		< 40 years (Ustymowicz et al. 2005)		40-60 years (Ustymowicz et al. 2005)		> 60 years (Ustymowicz et al. 2005)	
	PSV, m/s	EDV, m/s	PSV, m/s	EDV, m/s	PSV, m/s	EDV, m/s	PSV, m/s	EDV, m/s
Ophthalmic artery	0,392±0,053	0,091±0,025	0,406±0,089	0,112±0,037	0,350±0,079	0,107±0,043	0,340±0,080	0,084±0,033
CRA	0,110±0,018	0,033±0,009	0,099±0,018	0,037±0,009	0,097±0,020	0,035±0,008	0,093±0,020	0,030±0,009
Short PCAs	0,110±0,017	0,037±0,010	0,138±0,026	0,057±0,015	0,135±0,029	0,053±0,015	0,128±0,024	0,043±0,012
	maxV, m/s	minV, m/s						
CRV	0,045±0,009	0,033±0,007						
Large retinal arteries, (see also 2.4.4.3)	0,020 0,0063 (Logean et al. 2003)							
	max. velocity, m/s							
	0,046±0,004 (Ferguson et al. 2004) 0,036±0,013 (Nagaoka et al. 2002)							
Large retinal veins	0,0179 ±0,0014 (Grunwald et al. 1996)							
Parafoveal capillaries	0,00137(0,00077÷0,00210) mean(range), 25-35 years old (Martin & Roorda 2005)							

Thus blood flow velocities vary in different vascular beds of the eye. Ocular blood velocities are age and gender dependent (Ustymowicz et al. 2005). They can be altered in different pathologies (Ahmetoglu et al. 2003)

and in response to physiological and drug stimuli (Harris et al. 1996). However the velocity in a vessel segment of a retinal artery can remain unchanged under physiologic conditions during several months (Riva et al. 1985). The velocity alone does not provide the information on the volumetric blood flow and hence on the blood supply of a tissue. The decrease of blood flow velocity does not imply a decrease of metabolism. Increased blood flow velocity in a vessel segment may be a sign of physiological local narrowing or partial vessel occlusion.

1.2.5.2 Vessel diameter

The vessel diameters are the essential adjusting elements of the ocular circulation at whole and in particular of autoregulation. They are influenced by age, pathologic and therapeutic changes. Diameter values of different ocular vessels in normal volunteers are shown in Table 2.

Table 2. Mean vessel diameters in healthy volunteers in different vascular beds of the eye. μm ($\text{m} \times 10^{-6}$)

Vessel	Mean diameter			
	whole vessel	prelaminar portion	laminar portion	retrolaminar portion
Ophthalmic artery	>1000,0 (Büchi 1996) 2020,0±460,0 33,0±7,0 y.o. (Orge et al. 2002) 1140,0±260,0 58,6±15,3 y.o. (Michelson & Schuierer 1991)			
Branches of the ophthalmic artery	100,0 ÷ 1000,0 (Büchi 1996)			
CRA	163,0±17,0 (Dorner et al. 2002)	144,9 (Yao et al. 2002) 230,0 (Bunin 1971)	137,9 (Yao et al. 2002)	139,1 (Yao et al. 2002) 280,0 (Bunin 1971)
CRV		176,9 (Yao et al. 2002)	130,1 (Yao et al. 2002)	99,8 (Yao et al. 2002)
Large retinal arteries	39,0÷134,0 (Riva et al. 1985) 115,8±5,0 (Harris et al. 2003)			
Large retinal veins	64,0÷177,0 (Riva et al. 1985) 166,0±12,0 (Grunwald et al. 1996)			
Radial iridal arteries	15,0÷50,0 (Roh et al. 2007)			
Radial iridal veins	30,0÷90,0 (Roh et al. 2007)			
Choriocapillaris	8,0÷20,0 (Bunin 1971)			
Capillaries of the ciliary processes	6,0÷30,0 (Bunin 1971)			
Retinal arterial capillaries	3,5÷6,0 (Bunin 1971)			
Retinal venous capillaries	14,8÷20,6 (Bunin 1971)			
Parafoveal capillaries	5,0÷15,0 (Ferguson et al. 2004)			

Large retinal vessels with diameters between 100 to 200 μm and less, influence retinal microcirculation and control blood flow, capillary pressure distributions and metabolism. The retinal vessel diameter changes constantly over time. Blood flow in a microcirculation system is modulated in its temporal domain due to active and passive oscillations of the vessel wall (Krupatkin 2003). Vasomotion processes

Table 3. Frequency ranges of temporal vessel wall modulation of peripheral non-ophthalmic vessels. (modified from Krupatkin (2003) and Sidorov (2001))

Band	Frequency interval		Peak frequency		Rhythm origin
	Hz	oscill./min	Hz	oscill./min	
I	0,0095÷0,02	0,57÷1,2	0,01	0,6	local, metabolic, endothelial (Kvermmo et al. 1999)
II	0,02÷0,06	1,2÷3,6	0,04	2,4	neurogenic (Kastrup et al. 1989; Sidorov et al. 2001)
III	0,06÷0,15	3,6÷9	0,1	6	myogenic (Sidorov et al. 2001)
IV	0,15÷0,4	9÷24	0,3	18	respiratory (Sidorov et al. 2001)
V	0,4÷1,6	24÷96	1	60	cardiac (Sidorov et al. 2001)

evoke fast and slow changes of the vessel diameter. They are superimposed with low and high frequency oscillations caused by the blood pressure, respiratory processes, IOP variations, aging, changes of illumination or

vasoactive medications. Active rhythms of the microcirculatory system are related to metabolic, endothelial, neurogenic and myogenic activity of control mechanisms (Table 3). Cardiac and respiratory rhythms represent passive influence factors for the microcirculation system (Krupatkin 2003). Oscillations of the vessel diameter reflect corresponding oscillations of the vessel wall. They can be characterised by their frequency and their magnitude. Table 3 contains 5 principal frequency intervals of vessel wall oscillations in microcirculatory systems introduced by Kvernmo et al. (1999) and interpreted by Krupatkin (2003).

Additionally the vessel diameter varies along the vessel forming wide and narrow segments. This latter feature will be thoroughly investigated in the present work. Most known methods for diameter measurement estimate only one diameter value off line at one local measuring point and at one time point (Hubbard et al. 1999). They cannot provide necessary information about functional temporal and local vessel behaviour. Dynamic analysis of retinal vessels with the Retinal Vessel Analyzer (RVA) introduced by Vilser et al. (1991; 2002) and applied in the present work is able to examine function and individual capacities of vessel segments along the vessels. It is based on on-line diameter measurements. Vessel analysis with RVA is able to recognize diameter changes in response to functional demands and changes due to compensation of disturbances in microcirculation. It may define vascular risk factors, early but still reversible pathologic changes and therapeutic effects (Vilser et al. 2002).

It is important to be aware to specify the measurement methods for diameter assessment. Most optical methods assessing retinal vessels, including the RVA, can measure only the diameter of the red blood cell column – the visible part of a retinal vessel (Vilser et al. 2002) (Fig. 11). However sometimes the whole vessel diameter is measured including vessel wall thickness and plasma layer (Michelson et al. 2001; Michelson et al. 2007). The latter varies in small vessels from 1 to 3 μm dependent on blood rheology, flow rate and absolute vessel diameter (Fung 1990). Michelson et al. (2007)

reported a clinically measured $14,0 \pm 5,3 \mu\text{m}$ thickness of a retinal arterial wall in arteries with external diameter of $110,4 \pm 16,8 \mu\text{m}$. This result is consistent with $18 \mu\text{m}$ thickness measured in-vitro in paraffin sections of human retinal arteries with a luminal diameter (red blood cell column + plasma layer) of $100 \mu\text{m}$ (Hogan et al. 1971). Additionally the thickness of a retinal venous wall amounted to $18,1 \pm 7,5 \mu\text{m}$ in arteries with external diameter of $134,1 \pm 0,1 \mu\text{m}$ in the study by G. Michelson et al. (2007).

1.2.5.3 Blood flow

Blood flow (volumetric flow rate, minute volume) represents the blood volume, streaming through a vessel or vascular bed per minute (per unit time in the general case). In experiments in monkeys the whole ocular blood flow amounted to $800 \mu\text{l}/\text{min}$ (Alm 1992). Choroidal flow contributes with $677 \mu\text{l}/\text{min}$ (85%); the iris - with $8 \mu\text{l}/\text{min}$ (1%); the ciliary body - with $81 \mu\text{l}/\text{min}$ (8%) and the retina – with $34 \mu\text{l}/\text{min}$ (4%).

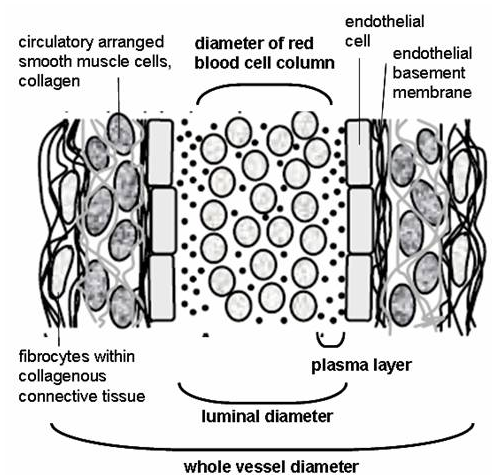


Fig. 11. Histologic scheme of a large retinal artery and definitions of different vessel diameters. Modified from (Michelson et al. 2007).

This proportion is true for the human eye as well. Thus the ocular blood flow is mainly choroidal and the retinal blood flow represents 5% or less of the total ocular blood flow (Alm 1992). Data on the blood flow in different vascular beds of the eye is represented in Table 4. Sometimes data measured with different techniques varies notably. About 1 ml of blood flows through the human eye per 1 minute: the flow rate of ophthalmic artery. 75% (724 μ l/min, (Silver et al. 1989)) of this quantity is due to pulsatile flow.

The flow in CRA and CRV has never been measured directly and was estimated as a summation flow of all retinal arteries or veins (Grunwald et al. 1996; Dorner et al. 2002). As follows from the law of conservation of mass, the whole blood flow in retinal arteries and veins or in CRA and CRV should be the same. Riva et al. confirmed this conclusion experimentally (Riva et al. 1985).

Blood flow in the retinal arterioles and venules is laminar. With vascular disease, turbulence of flow may ensue (Roh et al. 2007). Blood flow in retinal vessels has a small pulsatile component (Dollery 1968). Scanning laser Doppler flowmetry studies showed that the volume of blood flow in the nasal retina is significantly lower than that in the temporal retina as a result of smaller retinal vessels and slower blood flow velocity in the nasal retina (Rassam et al. 1996). This is consistent with the higher metabolic demand expected of the temporal retina from its larger size and the presence of the metabolically active foveal region.

Table 4. Mean blood flow in healthy volunteers in different vascular beds of the eye. [μ l/min ($\text{m}^3/\text{s} \times 1,67 \times 10^{-10}$)]. (CDI – color Doppler Imaging, DSA – digitised subtraction angiography; LDV – Laser Doppler velocimetry, CLDF – Canon laser Doppler flowmetry; HLDF - Heidelberg laser Doppler flowmetry).

Vessel or organ	Mean blood flow	Method of assessment
Ophthalmic artery	9740 \pm 3910 33,0 \pm 7,0 years old (Orge et al. 2002)	CDI
	6750 \pm 3490 58,6 \pm 15,3 years old (Michelson & Schuierer 1991)	DSA + CDI
CRA (all retinal arteries)	37,0 \pm 4,9 (Grunwald et al. 1996)	LDV
	38,1 \pm 9,1 (Dorner et al. 2002)	LDV
	33,0 \pm 9,6 (Riva et al. 1985)	LDV
	80,0 \pm 12,0 (Feke et al. 1989)	LDV
CRV (all retinal veins)	34,0 \pm 6,3 (Riva et al. 1985)	LDV
Large retinal arteries	9,6 (Nagaoka et al. 2002)	CLDF
	8,8 (Guan et al. 2003)	CLDF
Large retinal veins	14,7 \pm 2,6 (Grunwald et al. 1996)	LDV
Whole ocular blood flow	1000 (Volkov 2001)	HLDF
Minute cardiac volume	2900000 \div 4400000 (Bunin 1971)	

Experiments in monkeys showed the retinal and the choroidal blood flow to be 10 times higher than the cerebral one per 100 grams of corresponding tissue supplied (Alm 1992). Since there is no big differences in the metabolic activity of compared tissues, they suppose that from the large amount of blood flowing in the choroid only a small amount of nutrients is utilized by the retina (for example, only 5 – 8% of oxygen). The oxygen uptake from retinal vessels is higher and amounted to 38% (Shamshinova & Volkov 1998).

The blood flow in ocular vessels (**Q**) has been measured indirectly with methods of ophthalmodynamometry (ophthalmotonometry) or was calculated on the base of the average blood velocity (v_{av}) and vessel diameter measurements (**d**). If the velocity would be constant in all the points of its cross-section, then the volumetric flow could be calculated as product of this velocity and the cross-sectional area (Blevins 1984). If the velocity would be constant in all the points of its cross-section $v = v_{av}$, then the volumetric flow could be calculated as product of this average velocity and the cross-sectional area (Blevins 1984). For a round cross-section this will be calculated as:

$$Q = \frac{\pi \cdot d^2}{4} \cdot v_{av} \quad (1)$$

Since the velocity profile in blood vessels have another almost parabolic form (Logean et al. 2003), Fig. 10, Hagen-Poiseuille's Law has been commonly applied for the blood flow calculations. According to this Law the blood flow is proportional to the vessel diameter at a power of 4:

$$Q = \frac{\pi \cdot \Delta p}{128 l \eta} \cdot d^4 = \frac{\Delta p}{R} \quad (2)$$

Here η represents the apparent blood viscosity (see 1.3.2.1); l – the length of the chosen vessel segment, Δp – pressure loss along this vessel segment. R – coefficient of flow resistance (Fung 1990). However the Hagen-Poiseuille's Law has certain limitations: the flow should be laminar and stationary, the liquid is homogenous and isotropic, the vessel cross-section is constant and round (Blevins 1984; Loytsyanskiy 1987). Since the ocular blood flow is mainly pulsatile (Silver et al. 1989), the blood is not homogeneous and anisotropic (Fung 1990) and the cross-section might change along the vessel and over time (Kvernmo et al. 1999; Kotliar et al. 2007). Therefore Hagen-Poiseuille's Law can only provide an estimation of the true volumetric flow in ocular vessels.

Though the blood flow profiles in vessels are known to be blunted near the vessel axis (Fung 1990), for arteries and veins of the size found in the retina it is considered, that the deviations of flow from that predicted by the Hagen-Poiseuille's law should be small, provided that accurate estimates of local viscosity can be made (Charm & Kurland 1974; Roh et al. 2007). Feke et al. (1989) concluded on the base of their experiments that the blood flow in large retinal arteries and veins is proportional to the vessel diameter at a power of 4,1 and is therefore in accordance with Hagen-Poiseuille's Law. However the precision of these results seems to be doubtful. Indeed, in healthy volunteers the total diameter of all retinal veins exceeds the total diameter of retinal arteries (Hubbard et al. 1999). Since the total blood flow in retinal arteries and veins is equal, the power of vessel diameter for arteries and veins in relationships like (2) should be different. Alternatively the venous blood viscosity should considerably differ from the arterial one.

Riva et al. (1985) recalculated the flow rate from experimentally measured velocity and vessel diameter with formula (1) and concluded that retinal arterial flow is proportional to the vessel diameter by a power of $2,76 \pm 0,16$. The venous flow in the retina was proportional to the diameter by a power of $2,84 \pm 0,12$. Thus they contradict formula (2). The question of the relationship between the blood flow and the vessel diameter in the microcirculation system of the retina has been unanswered so far. According to contemporary data the normal physiological blood flow in small arteries of $50 \div 120 \mu\text{m}$ in diameter is proportional to the vessel diameter by a power of 3, the flow in similar veins is proportional to the diameter by a power of 1 (W. Vilser, personal communication).

1.2.5.4 Blood pressure, perfusion pressure and flow resistance

When the blood flows through the circulation system, a pressure loss arises because of the resistance to flow. In classical hydrodynamics and hemodynamics the pressure loss is considered as a measure of the flow resistance (Loytsyanskiy 1987; Fung 1990). The pressure loss can be characterised by the pressure gradient: the ratio of pressure difference between two points to the distance between those points (Bunin 1971). The blood

velocity is proportional to the pressure gradient. Consequently there exists a relationship between the main hemodynamic characteristics: blood pressure, flow velocity, flow resistance and vessel diameter (2).

The flow resistance of arterioles and capillaries amounts to 70 – 80% of the total resistance of the vascular bed. Arteries contribute with 20% and veins with 10% (Bunin 1971). The pressure distribution in the ocular vascular beds is analyzed in detail elsewhere on the base of numerous experimental and clinical studies (Bunin 1971; Alm 1992; Cioffi et al. 2003).

Quantitative data on the absolute pressure in different vascular beds of the eye are summarised in Table 5.

Table 5. Mean blood pressure in healthy volunteers in different vascular beds of the eye. [mmHg (Pa×133,32)]

Vessel or organ	Mean blood pressure		References
	sistolic	diastolic	
Ophthalmic artery	114,5	81,2	(DaSilva et al. 1979)
	73,5±10,0		(Astakhov & Dzhalishvili 1990)
CRA	75	40	(Ohashi et al. 1958)
	90	60	(Weigert et al. 2005)
CRV	30	20	(Ohashi et al. 1958)
		18÷30	(Bunin 1971)
Choroidal arteries		45÷60	(Bunin 1971)
Vortex veins	23÷35		(Ohashi et al. 1958)
Arteries of the iris	76	57	(Bunin 1971)
Anterior ciliary arteries	60	35	(Rethy 1963)
Retinal capillaries	50	30	(Ohashi et al. 1958)
Capillaries of the systemic circuit (for the comparison)	15÷25		(Bunin 1971)
Episcleral veins	6÷14		(Bunin 1971)
	9,7		(Goldmann 1962)

Since PCAs supplying the choroid and CRA are direct branches of the ophthalmic artery, the blood pressure in arteries nourishing the choroid and the retina should be of the same order. The normal circulation in choroidal vessels is maintained despite of a relatively small pressure difference between the arterial and the venous systems and considerable blood volume. This becomes possible due to the low resistance of choroidal vessels (the total vessel lumen of choroidal vessels is large) in comparison to the resistance of retinal vasculature.

The pressure in retinal capillaries is considerably higher than in other capillary beds of the macrocirculation circuit. The pressure difference between arterial and venous retinal capillaries is relatively high and amounts to 10 – 20 mmHg. This serves to maintain the intense blood supply and the high rate of metabolism in the retinal tissue.

The perfusion pressure mentioned in 1.2.3 characterises the level of metabolism between blood and ocular tissues. For an organ or a tissue the perfusion pressure is the difference between the arterial pressure in the supplying vessels and the local tissue pressure. This parameter varies intra- and interindividually but it needs to be at a certain level to provide the normal trophism of the tissue. Specifying the definition given earlier (1.2.3), ocular perfusion pressure is defined as difference between the mean arterial pressure in the ophthalmic artery and IOP (Volkov 2001). Several approaches are proposed to the calculation of the ocular perfusion pressure. Ideally the pressure in supplying arteries, which is different from the pressure in the ophthalmic artery, and the tissue pressure, which can also differ from IOP, need to be measured.

Commonly formula (11) is used for the calculation of the mean arterial pressure from systolic and diastolic values. The arterial pressure in the ophthalmic artery can be estimated from routine Riva-Rocci's measurements of systemic arterial pressure with the brachium cuff (RR). For example, if this pressure is equal to 125/80 mmHg (meanRR=95mmHg), the pressure in the ophthalmic artery amounts to 75 mmHg. Assuming the normal IOP of 15 mmHg one can derive the normal perfusion pressure of 60 mmHg (Volkov 2001). This approach is applicable in healthy volunteers with the difference between meanRR and the ophthalmic artery being interindividually similar. However in some systemic vascular diseases such an approach would provide a systematic error.

Since the systemic blood pressure and the IOP are components of the perfusion pressure, various systemic vascular diseases, like arterial hypertension and hypotension as well as pathological IOP increase might unfavourably influence the ocular circulation.

1.2.6 Normal vascular endothelial function

Since the inner wall structure of retinal vessels is investigated in the present work the innermost layer of the vessel wall, the vascular endothelium (Fig. 6, Fig. 7) needs to be taken into account. It is not only a static physical barrier that simply separates blood from tissue. See (Pearson 1991; Haefliger et al. 1994; Cines et al. 1998; Yildiz 2007) for detailed reviews on the vascular endothelium and its function.

The vascular endothelium represents the thin layer of cells that line the interior surface of blood vessels, forming an interface between circulating blood in the lumen and the rest of the vessel wall. It is considered, that this is “a critically strategic interface between blood and body” (Schafer 1997). Endothelial cells line the entire circulatory system, from the heart to the smallest capillary. These cells reduce friction of the blood flow allowing the fluid to propagate further. Moreover endothelium is a dynamic, disseminated organ that possesses vital secretory, synthetic, metabolic, and immunologic functions (Cines et al. 1998). In an average-sized 70 kg man the mass of this organ is equivalent to five hearts and the surface area potentially being covered with endothelium is equivalent to a half dozen tennis courts (Henderson 1991).

The endothelium is not a homogeneous organ (Cines et al. 1998). Endothelial cells from different vascular beds show highly differentiated functions as a consequence of genetic diversity and the impact of specialized surroundings. In some organs, there are highly differentiated endothelial cells to perform specialized 'filtering' functions. Examples of such endothelial structures include the renal glomerulus as well as mentioned above blood-brain and blood-retinal barriers. Both blood and lymphatic vessels and capillaries possess a single layer of endothelial cells. Endothelial tissue is a specialized type of epithelium tissue (one of the four types of biological tissue in animals).

Anatomical peculiarities of the vascular endothelium were described above; see chapters 1.2.2, 1.2.3 and Fig. 6, Fig. 7. The main activities of vascular endothelium and corresponding substances being secreted are summarized in Table 6. Endothelial cells are involved in many aspects of vascular biology, including:

- **regulation of vessel tone:** vasoconstriction and vasodilation, and hence the control of blood pressure. This activity is most instrumental for the present work and was therefore already mentioned briefly regarding retinal vessels. Endothelial cells are able to monitor changes in blood pressure, oxygen tension and blood flow by as yet unknown mechanisms. Information sensed on the luminal surface of the endothelium can be transmitted either by direct permeation or by active transport of secreting substances. Endothelial cells contribute to the regulation of blood pressure and blood flow by releasing vasodilators such as nitric oxide (NO) and prostacyclin (PGI₂), as well as vasoconstrictors, including endothelin (ET) and platelet activating factor (PAF) (Table 6). The major biologic effects of these chemically diverse compounds are regulated by localization of specific receptors on vascular cells. NO is constitutively secreted by endothelial cells, but its production is modulated by a number of exogenous chemical and physical stimuli. For example, the increase in NO secretion evoked by shear stress contributes to the phenomenon of flow-mediated vasodilatation, an important autoregulatory mechanism by which blood flow

increases in response to exercise. The other known vasoregulating mediators (PGI₂, ET, and PAF (Table 6)) are synthesized primarily in response to changes in the external environment.

- **blood coagulation/clotting (thrombosis and fibrinolysis).** Under normal circumstances the endothelial surface prevents blood clotting and allows smooth flowing of the blood.
- **atherosclerosis.** Endothelial dysfunction, or loss of normal endothelial function, is a manifestation of vascular pathology, which may lead to atherosclerosis (see 1.2.7.1 for details). This is very common in patients with diabetes mellitus, systemic hypertension or other systemic vascular diseases. One of the main mechanisms of endothelial dysfunction is the diminishing of nitric oxide.
- **formation of new blood vessels (vasculogenesis and angiogenesis).** Vasculogenesis, the primary organization of endothelial cells into tubal structures and then into vessels in the absence of preexisting vascular structures, and angiogenesis, the continued expansion of the vascular tree, take place through the expression of growth factors.
- **inflammation.** The endothelium can adapt rapidly to changes in its environment. Under certain circumstances, especially in response to adverse stimuli such as wounds, infections or irritation (e.g. insect sting), the endothelium may become activated and change its function. First of all the endothelium prevents physical disruption of the vessel wall by trauma, toxins, or other threats to the maintenance of intravascular volume and oxygen delivery. Endothelial cells control the passage of materials and the transit of platelets and leukocytes (white blood cells) into and out of the bloodstream (see 1.2.7.1 for details).

- **swelling (edema).** Endothelium is normally locally impermeable to substances in the blood. Under the effects of certain factors, for example histamine, endothelial cells lose attachment to each other and retract. This allows fluid and proteins to diffuse out into the local tissues causing tissue swelling termed edema. This reorganization of cell-cell junctions is rapid and reversible and takes place within few minutes. The endothelium may become activated and develop specialization for emigration of lymphoid cells. The endothelial cells become cuboidal in shape and express surface adhesion molecules which facilitate lymphocyte adhesion and migration.

Table 6. Activities of vascular endothelium and synthesized vasoactive substances. Modified from (Cines et al. 1998).

Activities	Factor secreted by the endothelium
vasodilation, inhibition of platelet aggregation and deposition	prostacyclin (PGI ₂)
vasodilation, inhibition of leukocyte adhesion, platelet adhesion, activation and aggregation, maintenance of the vessel basal tone, inhibition of muscle cell migration and proliferation	nitric oxide (NO)
vascular smooth muscle relaxation	endothelium derived hyperpolarizing factor (EDHF)
regulation of fibrinolysis	tissue plasminogen activator (tPA)
anticoagulant activity	thrombomodulin
promotion of blood coagulation	thromboplastin
vasoconstriction, mitogen for smooth muscle cells	endothelin-1 (ET-1)
vasoconstriction, activation of platelets and neutrophils, promotion of leukocyte adhesion at cell surface	platelet activating factor (PAF)
promotion of platelet adhesion and activation of blood coagulation	von Willebrand Factor

Vascular endothelium is exposed continuously to fluid shear stresses. Shear-induced changes in transduced biomechanical forces can cause not only cytoskeletal rearrangement and altered morphology but changes in endothelial gene expression (Malek & Izumo 1995). Most studies have examined primarily changes that occur within hours of initiating flow, but the adaptive response of endothelium to shear forces is less well characterized. An effect of shear on vascular biology is suggested, for example, by the observation of decreased vasodilator function at coronary branch points that have a predilection for atherosclerosis (McLenachan et al. 1990). Consistent

with this notion, a number of genes relevant to the development of atherosclerosis expressed by endothelium have shear stress response elements that coordinate their induction. Shear stress modulates endothelium secretion of factors regulating vasoconstriction and dilation, vessel growth, fibrinolysis and cell adhesion (Malek & Izumo 1995).

It is currently believed that endothelium must remain in a resting or unperturbed state to optimize expression of anticoagulant activities which prevent thrombus formation. An extensive experimental literature supports the notion that several common human vascular diseases are related to endothelial dysfunction. i.e., that prolonged or exaggerated endothelial activation leads to dysfunction that is an early, often preclinical component of vascular disease (Antonov et al. 1997).

To conclude, *vascular tone depends upon a balance between the endothelial vasodilators (e.g. nitric oxide) and vasoconstrictors (e.g., endothelin) with reduced formation of vasodilators resulting in vasoconstriction. Endothelial cells thus play an important role in modulating the microvascular tone and in autoregulation.*

1.2.7 **Pathological changes of vessel structure and vascular endothelial alterations in select systemic and ocular diseases**

1.2.7.1 Atherosclerosis

Atherosclerosis is a disease affecting arterial blood vessels. It is a chronic inflammatory response in the walls of arteries, in large part due to the formation of multiple plaques within the arteries. They are called atheromatous plaques, from Greek “athera”= porridge, which is the accumulation of a soft, flaky, yellowish material nearest the lumen of the artery. Atherosclerosis is commonly referred to as a "hardening" of the arteries.

Atherosclerosis is the most prevalent vascular disease in developed countries. This is a multifactorial disease with numerous predisposing factors, including smoking, diabetes, hyperlipidemia, aging, mechanical stress and inflammation, hypertension, obesity (Cines et al. 1998). Hence, the contemporary concepts on the pathogenesis (origin) and development of atherosclerosis need to be elucidated in order to understand possible mechanisms of vascular abnormalities in aging and in pathologies considered in the present work: glaucoma, arterial hypertension, metabolic syndrome.

The following terms are similar, yet distinct, in both spelling and meaning, and can be easily confused: **arteriosclerosis**, **arteriolosclerosis**, and **atherosclerosis**. Arteriosclerosis is a general term describing any loss of elasticity of arteries (Greek “arterio”=artery, “sclerosis” = hardening). Arteriolosclerosis is atherosclerosis mainly affecting small arteries (arterioles). Atherosclerosis is a hardening of an artery specifically due to an atheromatous plaque. Thus, atherosclerosis is a form of arteriosclerosis.

Microinflammation and atherosclerotic lesion formation.

Healthy endothelial cells contribute to the prevention of atherosclerosis in medium to large arteries by inhibiting platelet activation, limiting the entry of cells and lipids into the vessel wall, maintaining a non proliferative and biochemically quiescent intima, and secreting products that limit potentially injurious responses

(Cines et al. 1998). There is now extensive evidence that the morphologically abnormal endothelium is also dysfunctional and actually contributes to the development of atherosclerosis.

The most common recent theory of the atheromatous plaques formation is presented in Fig. 12 (Ross 1999). Leukocytes coordinate their activity by signaling each other with substances, called cytokines. The cytokines signal the leukocytes to attack invading microbes or to gather around a splinter to float it to the surface of the skin. There are low levels of these signals all over the body at all times. They are part of the background state of alertness of the immune system. This condition is called microinflammation or chronic systemic inflammation by different authors. During inflammation, leukocytes tether to and roll slowly on the endothelium surface. The cells then adhere in the site of inflammation, arrest, spread, and finally emigrate between endothelial cells to reach the underlying tissues (Fig. 12a). At sites of bleeding leukocytes tether to and roll on adherent platelets.

Like any other organ, the vascular endothelium ages and can be damaged. Microinflammation is a major player in causing this damage. The primary steps are the following (Stevens et al. 2005):

- Excess cholesterol in the bloodstream collects in the endothelium, forming small subendothelial deposits of lipid (so called “fatty streaks” (Cines et al. 1998)). The exact cause for this process is unknown, and fatty streaks may appear and disappear.
- Some of that cholesterol is oxidized, which adds to the usual background level of inflammatory signals. If this rises above a certain threshold, the endothelium becomes sticky, attracting leukocytes. The leukocytes need to pass between the endothelial cells to clean up the oxidized cholesterol. Being activated by inflammatory signals the leukocytes are beginning to enter the artery wall from the bloodstream, with platelets adhering to the area of insult, and to migrate through the endothelium (Fig. 12a).

The more damage that occurs, the more inflammatory signals are sent. With heightened microinflammation, this first response can become self-perpetuating. When this happens, the area between the endothelium and the elastic/muscular coat of the artery becomes swollen with leukocytes engulfed oxidized cholesterol. These leukocytes are called macrophages. After they consume oxidized cholesterol, they take on a foamy appearance and are called “foam cells” (Fig. 12b).

Smooth muscle cells respond to the inflammatory signals by migrating out into the plaque. While the artery is narrowed by about 25%, the vascular endothelium is, apparently, still intact so blood flows past in a normal fashion. At this point, there are still no symptoms. Depending on

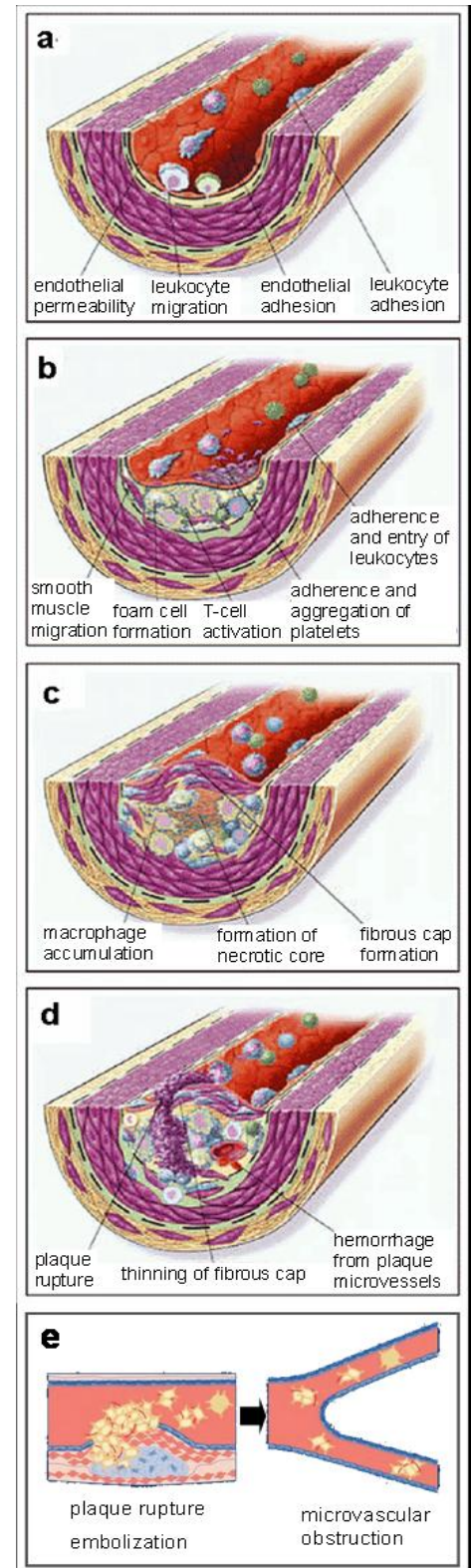


Fig. 12. Process of atherosclerotic lesion formation. See explanation in the text. Modified from (Falk et al. 1995; Ross 1999; Topol & Yadav 2000).

the general level of microinflammation, blood sugar levels, cholesterol levels, and other factors, this particular area of plaque may stop at this stage or continue to grow.

With sustained insult, the process continues, as shown in Fig. 12c, where the artery is already over 50% occluded. More white blood cells have been attracted. Eventually the foam cells die and contribute to dead or "necrotic" tissue within the arterial wall. The artery is under continual stress from the pulsing pressure of the blood, so smooth muscle cells will collect under the endothelium. They form a "fibrous cap", which separates the soft and weakened necrotic area.

These capped fatty deposits (now called atheromas) may produce enzymes that cause the artery to enlarge over time. As long as the artery enlarges sufficiently to compensate for the extra thickness of the atheroma, then no narrowing of the lumen occurs. The artery becomes expanded with an egg-shaped cross-section and still with a circular opening (fibro-fatty plaque). If the enlargement is beyond proportion to the atheroma thickness, then an aneurysm is created, a localized, blood-filled dilation of a blood vessel caused by weakening of the vessel wall, (Glagov et al. 1987). This might result in thickening and expansion of the wall and, sometimes, spotty localized narrowing of the lumen with some atrophy of the muscular layer (fibrous plaque) (Tuzcu et al. 2001).

In addition, the calcification deposits between the outer portion of the atheroma and the muscular wall, as they progress, lead to a loss of elasticity and stiffening of the artery as a whole.

The process goes on (Fig. 12d). The tiny blood vessels within the plaque break and bleed further enlarging the plaque. Microinflammatory signals lead to dissolution of part of the fibrous cap covering the diseased plaque. The endothelium ruptures. When the tissue from within the plaque hit the blood, a clot forms. Such clots will travel with the blood downstream (Fig. 12e) and may occlude smaller vessels somewhere within the body, inducing stroke, heart attack, arterial embolisms etc. Following another possible scenario, blood enters the ruptured plaque and sometimes results in a sudden expansion of the atheroma size. Tissue fragments, containing collagen and tissue factor activate the system of coagulation. The result is the formation of a blood clot overlying the atheroma, which obstructs blood flow acutely directly at the place of ruptured atheroma.

In atherosclerosis, the histological changes vary depending on the region of the retinal artery involved. Atherosclerosis, consisting of subendothelial plaque formation and enlargement of the intimal and endothelial layers, can occur along any portion of the retinal artery. Markedly the hyalinization (pathologic formation of the hyaline, the substance with a glassy, pink appearance) affects the intraocular portion of the artery and spares the intraneural portion. This is because hyalinization occurs only at those segments of the arterial tree where the internal elastic lamina contains collagenous fibrils embedded in a matrix of basement membrane (Park 2007).

To conclude, atherosclerosis causes two main problems. First, the plaques, though long compensated for by artery enlargement eventually lead to plaque ruptures and narrowing of the artery or small arteries downstream and, therefore, an insufficient blood supply to the organ they feeds. If the enlargement process in the compensating artery is excessive then an aneurysm results. These complications are chronic, slowly progressing and cumulative. The injurious processes that initiate atherosclerosis appear to persist throughout life in most individuals (Cines et al. 1998). Studies are now being conducted to determine the extent to which the biochemical and functional changes in the vessel wall can be reversed at different stages of the disease.

1.2.7.2 Aging

Aging is one of the main risk factors for the development of atherosclerosis and, therefore, for coronary artery disease. The term **risk factor** is widely used in the medicine. It is a variable associated with an increased risk of disease or infection (Dawber & Kannel 1961). Risk factors are correlational and not necessarily causal. Arteriosclerotic changes occur in blood vessels with age even in the absence of arteriosclerotic risk factors (Dohi et al. 1995; Stork et al. 2006). Age associated remodeling of the vascular wall includes luminal enlargement, thickening of intima and media (Fig. 7), and increased vascular stiffness. Aging large arteries are elongated and tortuous (Virmani et al. 1991). As aging occurs, smooth muscle cells progressively migrate from the tunica media and accumulate into the tunica intima. Aging is also associated with changes of proliferative and apoptotic smooth muscle behaviour and their response to growth factors (Yildiz 2007). Arteriosclerosis involves the whole vascular system in a somewhat patchy appearance (Stary et al. 1992). It is also known that small vessels are affected differently from major vessels like the carotid artery (Criqui et al. 1989).

Apart from age-associated remodeling of the vascular wall, endothelial function declines with age. This is most obvious from the attenuation of endothelium-dependent dilator responses (Davies & Hagen 1993). In fact, in the course of aging, there is an alteration in the equilibrium between relaxing and contracting factors released by the endothelium. Aging is also associated with a reduction in the regenerative capacity of the endothelium and endothelial aging, which is characterized by an increased rate of endothelial cell apoptosis. Aging induces several changes in the vascular endothelium gradually altering its nature from an anti- to a proatherosclerotic one. According to Yildiz (2007), arteries from healthy elderly subjects show no endothelial lesions or discontinuities; endothelial cells may, however, be irregular in shape and have increased height; there may be exaggerated deposition of collagen and elastin with abnormal abundance of leukocytes and macrophages.

The age-related functional alterations mentioned above have been observed in normotensive individuals without atherosclerosis. However most of them are also present in atherosclerotic vessels, which are also known to be stiffer than normal but in which, unlike in aging, focal lesions, vessel stenosis, and plaque rupture eventually develop. Hence, vessel aging may be viewed as representing the primary stage of atherosclerosis or, conversely, atherosclerosis may be viewed as a form of accelerated arterial aging, because aging and atherosclerosis run along very similar biochemical pathways and determine many similar vascular alterations (Ferrari et al. 2003).

Age-related studies of large retinal vessels show narrowing of the retinal arteries. This appears to be due to the fibrous replacement of contractile elements (Seitz 1964; Wise et al. 1971). These morphologic findings may account for the decrease in reactivity of retinal arteries and arterioles to blood pressure and oxygen tension changes with age. A similar decrease in myogenic tone of the PCAs with age has also been reported (Nyborg & Nielsen 1990). With aging there occurs a gradual loss of endothelial cells in retinal capillaries, followed by degeneration of pericytes, an increase in capillary diameter, and a thickening of the capillary basement membrane surrounding the external surface of the pericyte. The peripheral vessels begin to lose both their endothelial cells and their intramural pericytes by age 40. As long as one or the other cell type survives, the capillary channel remains patent. When both cells die, the capillary lumen collapses and becomes devoid of blood (Park 2007).

On the base of their studies Harris et al. (2001) concluded that aging and atherosclerosis reduce the ability of the eye to autoregulate blood flow when ocular perfusion pressure changes. Embleton et al. (2002) reported that

capillary blood flow in the retina, neuroretinal rim and lamina cribrosa decreases with advancing age. Additionally according to (Grunwald et al. 1998), foveolar choroidal blood flow decreases with age. The authors considered this change to relate to the decrease in density and diameter of the choriocapillaries that occurs with increasing age.

***In conclusion,** it becomes increasingly evident that the aging is associated with blood vessel structural and functional disturbances. Although typical atherosclerotic lesions are confined to large and medium arteries, vessels of microcirculation also are affected. The border between physiological aging and pathological arteriosclerosis is not well defined. Both undergo similar biochemical processes and result in similar changes in the vasculature (Ferrari et al. 2003; Yildiz 2007). See (Dohi et al. 1995; Yildiz 2007) for detailed reviews on age-related vascular changes. In order to assess changes in microvasculature due to age, healthy volunteers of different age groups were examined and the behaviour of their retinal vessels to flickering light. From the obtained data before, during and after stimulation a longitudinal vessel profile was determined and irregularities of the vessel wall were assessed.*

1.2.7.3 Primary open-angle glaucoma

Glaucoma is a group of diseases of the optic nerve involving loss of retinal ganglion cells (Fig. 1) in a characteristic pattern of optic neuropathy. Although raised intraocular pressure is a significant risk factor for developing glaucoma, there is no defined threshold for IOP that necessarily causes glaucoma. One person may develop nerve damage at a relatively low pressure (normal-tension glaucoma), while another person may have high eye pressure for years and yet never develop damage (ocular hypertension). Untreated glaucoma leads to permanent damage of the optic nerve and resultant visual field loss, which can progress to blindness. The worldwide incidence of glaucoma has been estimated by various authors as between 0,47% and 8% (Sassani 2007). It is the second leading cause of blindness. **Primary open-angle glaucoma** (POAG) is the most common form of adult glaucoma. POAG is characterized by open anterior chamber angle, chronic progressive loss of retinal ganglion cells and typical patterns of visual field loss in the advanced stages (Kwon & Caprioli 2007).

The pathogenesis of POAG is incompletely understood. Proponents of the vascular theory argue that microvascular changes in the optic nerve head are responsible for glaucomatous optic nerve damage (Hayreh et al. 1999). Blood flow and its regulation might be of paramount importance in the development of glaucomatous damage (Alm 1992; Buckley et al. 1997; Flammer et al. 1999; Hayreh 1999). It is well known that a nocturnal systemic hypotension (Graham & Drance 1999; Hayreh 1999; Jonas 2003) and vasospastic reactions (Drance et al. 1988; Gasser & Flammer 1991; Flammer et al. 1999) are linked with progression of glaucomatous damage.

In healthy eyes the local autoregulation of microcirculation within the retina and optic nerve head is able to counterbalance within certain limits an increase or decrease in perfusion pressure and therefore protects tissue from damage. C. Riva (1981) demonstrated retinal autoregulation in response to intraocular pressure increase, and F. Robinson (1986) showed retinal autoregulation in response to systemic blood pressure increase. Misbalanced local blood flow regulation appears to be an important pathogenic factor in POAG progression (Stodtmeister & Pillunat 1991; Anderson 1999). The vast majority of published studies on blood flow in glaucoma report a reduced ocular perfusion in glaucoma patients compared with normal subjects. This reduction of ocular blood flow often precedes the damage. The major cause of this reduction is not atherosclerosis, and not only a consequence of elevated IOP (and in turn decreased ocular perfusion pressure) or reduced number of retinal ganglion cells but, at least in part,

rather a vascular dysregulation (Garhofer et al. 2004), leading to insufficient autoregulation. This in turn may lead to unstable ocular perfusion and thereby to the tissue damage (Flammer et al. 2002). Moreover, vascular dysregulation appears to be an early manifestation in glaucoma (Flammer et al. 2002; Fuchsjaeger-Mayrl et al. 2004).

Vascular dysregulation could imply inadequate retinal constriction and dilation in response to changes in IOP or altered metabolic demand (Garhofer et al. 2004). Nagel et al. reported that a short-term rise in IOP leads to less retinal venous reaction in POAG patients than in healthy volunteers (Nagel et al. 2001). Garhofer et al. (2004) showed that flicker induced vasodilation of retinal veins is significantly diminished in patients with early stage POAG. Seidova et al. (2007) found, that functional retinal arterial and venous dilation in response to flicker stimulation does not differ between POAG patients and healthy subjects. However reactive arterial constriction following the stimulation appeared later and venous restoration occurred faster in POAG. Additionally this research group reported that low frequency non-stimulated oscillations of arterial diameter were well expressed in healthy seniors and almost absent in POAG patients, while high frequency venous pulsation was less intensive in POAG (Kotliar et al. 2007). In the mentioned clinical studies it was not possible to exclude that increased IOP alters autoregulatory capacity of retinal vessels, which in turn, could lead to reduced vessel responses. It is not yet clarified whether this impaired regulation of retinal branch vessels contributes to the progression of the disease.

The author has been found no studies on blood flow in retinal branch vessels in POAG or studies on the structure of retinal vessels in this disease in the literature. A former study by Grunwald et al. (1984), who showed with blue field entoptic technique the abnormal autoregulation of macular retinal blood flow in open-angle glaucoma, is an exception. A number of studies with color Doppler imaging showed abnormal hemodynamics of central retinal artery and vein in POAG, which was supposed to affect the blood supply to the optic disc and the retina (Liu et al. 1998; Zaluczowska-Marcela et al. 2000). Liu et al. (1999) and Plange et al. (2006) reported additionally, that alterations in hemodynamics of CRA and CRV are correlated with the optic nerve damage in POAG.

Medications used to treat POAG include many classes of drugs, all designed to lower IOP. Carbonic anhydrase inhibitors such as dorzolamide reduce production of aqueous humor. Recently it was shown, that dorzolamide additionally improves the autoregulation of retinal vessels after artificial changes in perfusion pressure in eyes suffering from POAG (Nagel et al. 2002; Nagel et al. 2005). It seems, that topically (eye drops) applied dorzolamide may reach the retina (Sugrue 1996) and inhibits carbonic anhydrase localised in retinal capillaries. This may lead to capillary dilatation. Improving the presumed capillary response to a disturbance in perfusion pressure leads to less tissue damage as well as to a shorter reaction time in the regulating diameter of arteries and veins (Nagel et al. 2005).

To conclude, local blood flow regulation is misbalanced in POAG. This appears to be an early manifestation of the disease. In detail, CRA, supplying the retina, and CRV, draining the retina, show abnormal hemodynamics in POAG. Temporal reaction of large retinal vessels is impaired in POAG. Application of dorzolamide may improve the autoregulation of retinal vessels. Whether retinal branch arteries of healthy subjects, untreated and treated POAG patients show irregular local patterns in the longitudinal vessel profile during their dynamic reaction to short-term and moderate IOP increase, was investigated in the glaucoma study.

1.2.7.4 Systemic hypertension

Systemic or arterial hypertension, commonly referred to as "high blood pressure", is a medical condition in which the blood pressure is chronically elevated. Persistent hypertension is one of the risk factors for strokes, heart attacks, heart failure and arterial aneurysm, and is a leading cause of chronic renal failure. The incidence of arterial hypertension in the adult USA population amounted to 31% (Burt et al. 1995). Hypertension is considered to be present when systolic blood pressure of a person is consistently 140 mmHg or greater, and/or their diastolic blood pressure is consistently 90 mmHg or greater (JNC 1993). In patients with diabetes mellitus or kidney disease studies have shown that blood pressure over 130/80 mmHg should be considered high and requires further treatment (Chobanian et al. 2003).

Currently, the retina remains the most accessible organ for the clinician to detect undiagnosed hypertension and to monitor blood pressure control (Walsh et al. 2007). The **hypertensive retinopathy** represents one of three distinct types of systemic hypertension visible in the eye (Fig. 5) (with two others being hypertensive choroidopathy, and hypertensive optic neuropathy). Clinical findings seen in the retinal vasculature in hypertensive retinopathy include the following (Walsh et al. 2007):

- **arterial narrowing** (focal and diffuse). This is one of the earliest and classic signs of hypertensive retinopathy. An increase in vascular wall tone in response to autoregulatory mechanisms causes a decrease in the arterial caliber (vasoconstrictive phase) (Tso & Jampol 1982). This vasoconstrictive state may be observed in a more focal or diffuse way, depending on the initial condition of retinal arteries. Following elevation of intraluminal arterial pressure vessels with areas of sclerosis lose their muscle tone and dilate, whereas nonsclerotic vessels remain narrow because of intact muscular walls and preserved autoregulatory response. Recently Hayreh (1996) found no narrowing of arterioles, when comparing normal fundus angiograms (eye-ground photos with dye solution in retinal vessels) to those with hypertensive retinopathy. He concluded that the apparent narrowing was caused by an artefact produced by retinal edema masking the arterial walls along with the contrast of dilated venules, which made the arteries appear narrower in turn.
- **arteriosclerotic changes** are observed within the vessel walls if constriction of the retinal vasculature persists. The wall of a retinal artery is transparent. As the wall thickens from continuous vasoconstriction, the light reflex becomes more diffuse and partially obscures the blood column, giving the artery a yellowish appearance. Progression of the thickening and sclerotic changes eventually obscures the blood column completely, producing a whitish appearance. Moreover, in humans systemic hypertension has been shown to be associated with a remodeling in peripheral resistance vessels (Schiffrin & Hayoz 1997). Progression of arteriosclerosis leads to endothelial damage and necrosis of the muscular component of the vessel walls. This may lead to a damage of the blood-retinal barrier, causing leakage into the retina. The consequent thrombosis within the vessel may cause closure of the vessel lumen, resulting in retinal tissue damage (Tso & Jampol 1982). Hence, artery and vein occlusion (closing) and microaneurysms are the most common results of persistent arteriosclerotic changes.
- Along with reflective changes, the thickening produces **arterio-venous crossing changes**. As the arterial wall thickens at their crossing points, the vein appears locally narrowed if posterior to the artery or elevated if above to the artery (Marcus Gunn's sign, first described in 1898).

- Other characteristic changes common to arteriosclerosis are **increased tortuosity** of retinal vessels and **increased arterial branching angles**, known as perpendicularization.

Consistent with the mentioned vascular manifestations of hypertensive retinopathy, clinical studies showed abnormalities of retinal microcirculation and retinal vessel reactivity in systemic hypertension. According to Wolf et al. (1994), the retinal microcirculation of hypertensive patients in the retinal capillary network near the fovea showed significant alterations. Both the capillary density and capillary flow velocities were significantly reduced compared with the control group in this study. Delles et al. (2004) reported the impairment of endothelial function of the retinal vasculature in early systemic hypertension. Nagel et al.(2004) showed, that arterial hypertension appears to be associated with a reduced response of retinal arteries to metabolic demand. Already in early hypertension Michelson et al. (2006) confirmed the impairment of the NOS-dependent vascular tone in retinal arteries and capillaries as well as the independence of retinal capillary flow regulation from systemic circulation.

***To conclude,** retinal blood flow and its regulation are impaired in systemic hypertension. Chronic systemic hypertension manifests in the retinal vasculature with irregular-appearing narrowed arteries and arteriosclerotic changes including arterio-venous crossing changes, increased vascular tortuosity as well as with increased arterial branching angles. In the present work possible structural changes in retinal arterial and venous vasculature in systemic hypertension were attempted to detect, which has been reported earlier elsewhere in other microcirculatory beds (Foster et al. 1968; Jacobsen et al. 2002). Whether longitudinal retinal arterial and venous profiles in moderate systemic hypertension are altered was investigated.*

1.2.7.5 Obesity

A healthy human body requires a minimum amount of fat for the proper functioning of its hormonal, reproductive, and immune systems. The accumulation of too much storage fat can impair movement and flexibility, and can alter the appearance of the body. **Obesity** represents a condition in which the natural energy reserve, stored in the fatty tissue, is increased to a point where it is associated with certain health conditions or increased mortality. The USA has the highest rates of obesity in the developed world: from 2003 to 2004 32,2% of adult population were obese (Ogden et al. 2006). Obesity is typically evaluated in absolute terms by measuring body mass index (BMI), but also in terms of its distribution through waist circumference (waist-hip circumference ratio measurements) (Janssen et al. 2004). Additionally, the presence of obesity is regarded in the context of other risk factors and comorbidities (other medical conditions that could influence risk of complications) (NIH 2000). BMI is calculated by dividing the subject's weight by the square of his/her height (Quetelet 1871):

$$BMI = weight[kg]/(body\ length\ [m])^2 \quad . \quad (3)$$

A BMI of 18,5 ÷ 24,9 is considered as normal weight. A BMI of 30,0 and more is obese. (WHO 2000). However many factors can affect the interpretation of BMI, for example, BMI overestimates body fat in persons who are very muscular.

Obesity is an individual clinical condition, not necessarily a disease. Though it is increasingly viewed as a serious and growing public health problem: excessive body weight has been shown to predispose to various life-

threatening diseases: coronary heart disease, type 2 diabetes, sleep apnea (NIH 2000). Obesity is the main risk factor for metabolic syndrome – the clustering of diseases, including type 2 diabetes, systemic hypertension and hyperlipidemia.

Although obesity is linked with large vessel atherosclerosis and diabetes, its association with microvascular changes is less clear. Only few data on retinal vessel abnormalities in obesity is published yet. Wang et al. (2006) concluded from the data of large epidemiologic study, that microvascular function is impaired in the course of weight gain. Wider retinal venular (but not arteriolar) diameter is associated with risk of obesity, independent of hypertension, diabetes, lipids, and cigarette smoking. Also in the study by Cheung et al. (2007) in healthy children greater BMI and weight were associated with larger retinal venous (but not arterial) caliber. Retinal arteriolar narrowing, venular dilation and isolated retinopathy signs have been shown by Nguyen & Wong (2006) to be associated with obesity and metabolic disorders.

In conclusion, obesity is related to a number of vascular diseases. Thus retinal vessel abnormalities might be expected in obesity like early vascular changes linked with atherosclerosis (1.2.7.1), diabetic (Kador 2007) and hypertensive (1.2.7.4) retinopathy. There are only few reports on retinal vessels structure and function in obese persons. Enlarged retinal venous diameter is the most common finding. Retinal arteries are less investigated. Whether longitudinal retinal arterial profiles in obese persons are altered was investigated in the present work.

1.2.8 Abnormalities of longitudinal vessel profiles in micro- and macrocirculation

Normal human vessels are not straight tubes. Both arteries and veins rather possess narrow and wide segments, which are relatively uniformly distributed along a vessel (Fig. 13, Fig. 14). Whether this vessel structure changes during vessel reaction and with increasing age has not yet been elucidated.

From clinical and experimental studies it is well-known that arteries in a pathologically changed micro- or macro circulation system might possess local microirregularities, which can influence blood flow (Alm 1992; Alstrøm et al. 1999; Jacobsen et al. 2002). A pattern of alternating constrictions and dilations along the vessel has been shown for microcirculation using in-vivo microscopy and in larger vessels during arteriography (Giese 1964). This structure of longitudinal vessel profiles was termed “stationary arterial waves” (Theander 1960; New 1966) or “corrugated arteries” (Foster et al. 1968) by different authors. Primarily the phenomenon was reported in femoral arteries (Theander 1960). Subsequently it has been observed in carotid, radial, splenic, superior mesenteric, and renal arteries (Foster et al. 1968). In large vessels the phenomenon has been detected proximal from obstructive vascular lesions and in patients with various vascular diseases, e.g., Buerger’s disease. (Jacobsen et al. 2002).

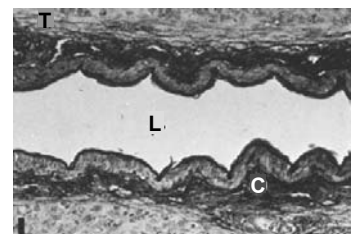


Fig. 13. Longitudinal section of arteriole in the contracted spleen of a cat. Vessel lumen (L); within pleated wall: internal elastic lamina, smooth muscle layer, darkly staining collagen (C), and trabecular smooth muscle (T). Short bar: 10 μ m. Amplification x 500. Modified from Schmidt et al. (1983).

As it was already mentioned, arterial narrowing in systemic hypertension sometimes has a focal appearance (1.2.7.4). Additionally, another peculiar structure of longitudinal arterial profiles, the so-called “sausage-string appearance”, occurs when severe experimental hypertension is provoked in

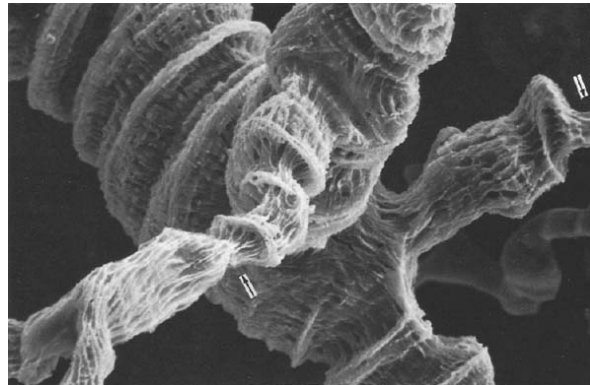


Fig. 14. Arteriolar cast from the contracted spleen of a cat. Note sharp ridges due to pleated vessel wall, and fine surface detail. Dramatic narrowing of luminal diameter (black arrows) is apparently caused by contraction of vascular smooth muscle. Short bars: 10 μm . Amplification $\times 360$. Modified from Schmidt et al. (1983).

a microcirculation system (Alstrøm et al. 1999; Jacobsen et al. 2002). This vascular pattern has been demonstrated in small blood vessels in various vascular beds, including mesentery, intestine, kidney, eye, ear, and brain. The phenomenon is of a functional nature, since it disappears on lowering of the arterial pressure and reappears if the pressure is increased once more. The sausage-string pattern in microcirculation is related to the development of vascular damage (Giese 1964). It was noted long ago (Goldblatt 1938), that arteriolar fibrinoid necrosis associated with severe hypertension is not distributed uniformly along the affected vessels. In fact, on microscopic examination of longitudinal sections of arterioles exposed to severe hypertension fibrinoid necrosis alternates with apparently normal vascular wall segments. It is likely that such a patchy distribution of arteriolar wall necrosis can also influence longitudinal vessel profiles.

To conclude, normal human vessels possess narrow and wide segments in their course. It seems, that small vessels, mostly arteries, in a pathologically changed micro- or macro circulation system might possess an abnormal longitudinal profile because of several reasons: instability of thin vessel walls, which become more rigid with age (Jacobsen et al. 2002); partial endothelial damage of retinal arteries (Haefliger et al. 1994); partial degradation of smooth musculature of retinal arterial walls (Jacobsen et al. 2002; Vilser et al. 2002). Whether such structural abnormalities can be found in large human retinal arteries and veins and whether these changes, if any, might influence hydraulic parameters of a vessel is investigated in the present work.

1.3 Blood Properties and Blood Rheology

1.3.1 Blood, its constituents and properties

Blood is the fluid, transporting oxygen, carbon dioxide, nutrients, salts, hormones, metabolites and many other components that make it possible to maintain life. It is also a crucial component of thermoregulation, as it absorbs and redistributes excess heat in the body. From a rheological point of view, blood is a heterogeneous suspension in an aqueous solution of electrolytes and nonelectrolytes. In the typical adult human, blood is composed of plasma, and heterogeneous mixture of cellular components. The percentage of total volume of these cellular components is called **hematocrit**. The average hematocrit is 40–52% for men, and 35–47% for women. In the normal cerebral microvasculature, the hematocrit drops to 85 % of the macrovascular hematocrit but in pathological tissue, such as in tumors, the microvascular hematocrit varies greatly.

The major constituents of this formed element group include: red blood cells (RBCs), or erythrocytes; white blood cells (WBCs), or leukocytes; and platelets, or thrombocytes. 1 mm³ of normal human blood consists of approximately 5.000.000 RBCs, 5.000 to 10.000 WBCs, and 200.000 to 300.000 platelets (Fung 1990). Thus, leukocytes, and platelets occupy less than one percent of the total blood volume. The average healthy adult maintains one-eleventh of their body weight as blood, representing a volume between 4,5 and 6 litres.

Plasma

The fluid in which the aforementioned cells are suspended is known as plasma. It is a yellowish fluid with a specific gravity in humans ranging between 1,056 to 1,066 (Fung 1990). Plasma is a viscous fluid that is 90% water and 10% solid matter, which consists of: clotting proteins (albumin, globulin and fibrinogen), immunoglobulins, carbohydrates, salts, vitamins, and other particles. In healthy subjects, research has shown plasma to act as a Newtonian viscous fluid (Merrill et al. 1965) with a coefficient of viscosity about 0,0012 Pa*s (Gregersen et al. 1967; Chien et al. 1971). However there are some pathological conditions, which could lead to dissolution of the blood cells and spillage of their contents into the plasma. Under these conditions plasma might become Non-Newtonian. Most plasmas show 2 – 3% decrease of viscosity with each 1°C increase in temperature over the range 15°C to 40°C. Normal plasma viscosities ranges 0,0017 to 0,0019 Pa*s at 20°C; 0,0015 to 0,00172 Pa*s at 25% and 0,00116 to 0,00135 Pa*s at 37°C (Harkness 1971). At temperature higher than 42°C irreversible changes might occur in some plasma constituents resulting in increased viscosities. When blood is left undisturbed, the cells start to coagulate. The process is called blood clotting, and is initiated by the plasma protein fibrinogen. A straw-colored fluid, called serum appears in the plasma, when the clot contracts. Serum is similar to plasma in composition but with fibrinogen removed, while forming the clot. Fibrinogen has been shown to have little or no effect on the Newtonian properties of blood. In the blood flow there is always a small plasma layer near the vessel wall which is about 10 µm thick in large vessels and decreases with decreasing vessel diameter (see also 1.2.5.2). In small vessels the plasma layer reduces the pressure gradient needed for a given flow rate (Cockelet 1986).

Erythrocytes

Red blood cells, erythrocytes, are specialized cells for delivering oxygen from the lungs to the rest of the body. Human RBCs of healthy subjects possess a fine flexible membrane that surrounds the haemoglobin. They are

biconcave disk shaped, with a diameter of 7,6 μm and thickness of 2,8 μm (the thickness at the disk center is less than 1 μm) (Fung 1990). The mean volume of a RBC is about 87 μm^3 (Cokelet 1986). The RBC shape maximizes the surface area for O_2 diffusion and minimizes the diffusion distance in the cell. It also permits extensive deformations, a characteristic needed in passage through small capillaries, as well as large changes in the cell volume. Specific gravity of RBCs amounts to 1,10 (Fung 1990). Under hypotonic conditions, an erythrocyte can almost double its volume, achieving a spherical form, but if excessive changes in surface area are required, the cell will rupture, resulting in hemolysis (Hoffman et al. 2000).

Leukocytes

The white blood cells are an integral part of the immune system, providing protection against microorganisms and other foreign matter. They have form of a wrinkle-surfaced sphere and have diameter of about 8 – 20 μm . A normal concentration of leukocytes is 4,5 to 11 million per litre. This level can increase during infection to 16 million per litre or higher. There are several different types of white blood cells. One primary technique to classify them is to look for the presence of granules, which allows the differentiation of cells into the categories granulocytes with mean diameter of 9,4 μm and mean volume of 440 μm^3 (neutrophils (65%), basophils (1%), and eosinophils (4%)) and agranulocytes (lymphocytes (25%, mean diameter 7,4 μm , mean volume 210 μm^3), monocytes (6%, mean diameter 9,5 μm , mean volume 460 μm^3), and macrophages (differentiated monocytes)) (Cokelet 1986; Alberts et al. 2002). While the white blood cells and platelets play very important roles in maintaining the immune system and maintaining hemostasis, respectively, their concentrations are so much below that of the RBCs that their contribution to the viscosity of blood is negligible when compared to the effects of the RBCs. At high flow rates WBCs are concentrated at the vessel axis, while at lower flow rates they move to regions next to the vessel wall (Cokelet 1986).

Platelets

Platelets, or thrombocytes, are the cells circulating in the blood that are involved in the cellular mechanisms of primary hemostasis leading to the formation of blood clots. Platelets are much smaller than RBC. They have form of an irregular disk and measure 1,5 ÷ 3,0 μm in diameter and 15 μm^3 in mean volume (Cokelet 1986; Fung 1990). In flowing blood the platelet concentration is highest near the vessel wall (Cokelet 1986).

1.3.2 Blood flow in macro- and microcirculation

1.3.2.1 Newtonian behaviour of blood. Blood viscosity and viscoelasticity.

At high shear rate $\dot{\gamma} : \dot{\gamma} > 1000 \text{ s}^{-1}$ whole blood behaves like a Newtonian fluid with a constant coefficient of viscosity η :

$$\tau = \eta \dot{\gamma} \quad \text{or} \quad \sqrt{\tau} = \sqrt{\eta \dot{\gamma}}, \quad \eta = \text{const} , \quad (4)$$

where τ represents the shear stress. Normally the blood flow can be considered as Newtonian in blood vessels larger than 500 μm in diameter (Cokelet 1986).

In a Newtonian sense viscosity η may be defined as the force required to move a unit area through a fluid to create a unit velocity gradient. For blood the viscosity depends mainly on the protein concentration of the plasma, the RBC deformability and their aggregation. Consequently blood viscosity varies with the shear rate of the flow. It increases with decreasing shear rate, increasing hematocrit, decreasing temperature, and with the tendency of RBC to aggregate. Viscosity is also patient dependent. Additional factors may affect the viscosity in microvessels (for example, Fahreaus effect (dependence of hematocrit on vessel diameter) and Fahreaus-Lindquist effect (dependence of viscosity on vessel diameter) (Cockelet 1986; Fung 1990)). In some fluids, called shear-thickening fluids, viscosity increases with shear rate; in others, known as shear-thinning fluids, viscosity decreases with increasing shear rate. Depending on its parameters blood may show both thickening and thinning behaviour (Artoli 2003).

For some unsteady flows such as blood flow in the human circulation, the liquid generally demonstrates both a viscous and an elastic effect. These effects determine the stress-strain relationship of liquid. Such liquids are called viscoelastic. Blood plasma shows viscosity, while whole blood is both viscous and elastic. The viscosity is related to the energy dissipated during the flow. The elasticity is related to the energy stored during the flow due to orientation and deformation of RBCs (Thurston 1972; Sharpa et al. 1996). The viscoelastic characteristics of blood change with the level of strain and strain history. Such fluids are called thixotropic. Although these complex blood properties are probably unimportant in normal circulatory physiology, they might be significant when blood rheology is used as a basis of clinical applications to diagnosis of diseases, pathologies and biochemical studies (Fung 1990).

Newtonian laminar flow through a cylindrical tube obeys the Hagen-Poiseuille formula (1). If the fluid is blood and tube (vessel) diameter is less than 500 μm (Cockelet 1986), the flow does not obey the Hagen-Poiseuille Law, but one can still measure the volumetric flow rate and the ratio $\Delta p/l$ to calculate the parameter η , which used to be viscosity in Hagen-Poiseuille formula:

$$\eta = \frac{\pi \cdot d^4}{128Q} \cdot \frac{\Delta p}{l} \quad (5)$$

So computed η is defined then as apparent blood viscosity. In large vessels with $d > 500 \mu\text{m}$ the equation (5) is obeyed, and η is constant for given blood at a fixed hematocrit. In small tubes η is less than the large tube value (Fahreaus-Lindquist effect). The concept of apparent blood viscosity can be extended to any flow regime including turbulence flow as long as one can compute it from a formula that is known to be obeyed for a homogeneous Newtonian fluid (Fung 1990).

1.3.2.2 Non-Newtonian behaviour of blood

As plasma is showing Newtonian characteristics, it is evident that the RBCs are responsible for the Non-Newtonian behaviour. Red blood cells are relatively big in the sense that their Brownian motion has little effect on the flow. RBCs are responsible for the mentioned shear thinning effect. The physical explanation for this phenomenon is the cells flexibility and tendency to align with the flow. The red blood cells align in such a way that the largest dimension is paralleled with the direction of the flow. The fraction of aligned RBCs is seen to increase

with the shear rate, which is in contrast with artificially hardened cells. RBCs of humans in plasma can form aggregates known as rouleaux. RBC aggregation results from the action of large plasma proteins. Rouleaux formation is primarily dependent on the shear rate and hematocrit in addition to fibrinogen concentration. As shear rate rises, the aggregates are torn apart until no aggregates remain when shear rate reaches about 100 s^{-1} . With increasing hematocrit, the rate and size of rouleaux will increase rapidly. The shear rate dependence of viscosity in whole blood increases very rapidly with hematocrit reaching a maximum at about 70%. High viscosity at low shear rate due to rouleaux formation produced by the fibrinogen leads to blunting of the flow profile and has a significant influence on flow rate. When the shear rate tends towards zero, it is speculated that the human blood becomes one big aggregate, which then behaves like a solid (Fung 1990). Red cell aggregation as well as red cell deformability also affects the shear dependence of blood viscosity as shown in Fig. 15.

Detailed study on RBC deformability was performed by Goldsmith (1972) by observing blood flow in small cylindrical glass tubes of $65 - 200 \mu\text{m}$ in diameter. The viscosity of blood at shear rate $> 100 \text{ s}^{-1}$ (aggregation is negligible) was compared with other suspensions and emulsions. The flow of oil droplets in water was, as for blood, maintained at very high volume fractions. It was therefore, concluded that droplets and RBCs have a similar elastic behaviour. High deformability of the RBCs makes blood a remarkable fluid. It was shown that, when the volume fraction exceeded 50%, most other fluids stopped to flow. Blood and droplets, however, were able to maintain the flow until hematocrits of 98%. Still, a suspension of oil droplets remained more viscous than a suspension of red cells (Goldsmith 1972). It is therefore believed that a RBC is even more deformable than a droplet.

Logean et al. (2003) reported the following wall shear rates in large retinal vessels: retinal arteries: $950 \pm 200 \text{ s}^{-1}$ during the systole and $250 \pm 100 \text{ s}^{-1}$ in diastolic phase; retinal veins: $520 \pm 70 \text{ s}^{-1}$.

Corresponding wall shear stresses in large retinal arteries and veins, calculated with a viscosity of $0,0035 \text{ Pa}\cdot\text{s}$ (Miyazoe et al. 1999; Andrews et al. 2000) were $3,33 \pm 0,70 \text{ Pa}$; $0,86 \pm 0,35 \text{ Pa}$ and $1,82 \pm 0,25 \text{ Pa}$ respectively (Logean et al. 2003).

To conclude, parts 1.3.2.1 and 1.3.2.2, apparent blood viscosity is decreasing rapidly at low shear rates with RBC aggregation and is decreasing slowly at high shear rates with RBC deformability. Experimentally, three main regions, which characterize the relationship between shear stress and blood viscoelasticity, have been observed (Fung 1990; Liepsch et al. 1991; Artoli 2003), Fig. 15:

- at low shear rate ($\dot{\gamma} < 10 \text{ s}^{-1}$) the cells are clustered in rouleaux with diminishing nature as the shear rate is increased. The viscosity and the elasticity are of the order of $10^2 \text{ Pa}\cdot\text{s}$. In this region blood is absolutely Non-Newtonian;

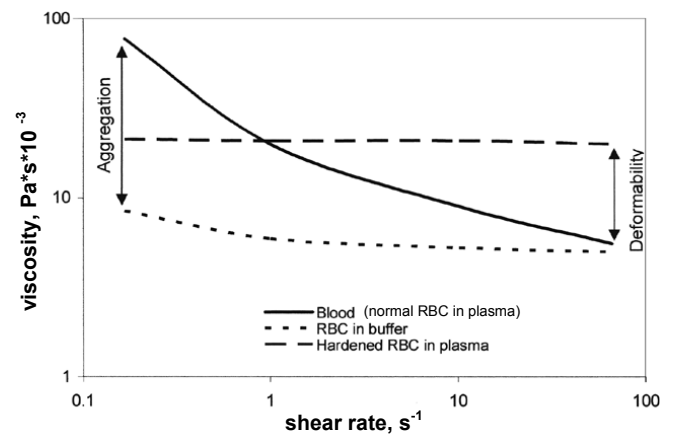


Fig. 15. Diagrammatic logarithmic representation of the effects of red cell aggregation and red cell deformation on the shear dependence of blood viscosity. Modified from (Chien et al. 1971).

- at medium shear rate ($10 < \dot{\gamma} < 100 \text{ s}^{-1}$), the rouleaux are disintegrated and forced to be oriented. The viscosity is of the order $10^{-3} \div 10^{-4} \text{ Pa}\cdot\text{s}$ decreasing with increasing shear rate. The elasticity is of the order of $10^2 \text{ Pa}\cdot\text{s}$ but slightly less than at low shear rate;
- with increasing shear rate ($\dot{\gamma} > 100 \text{ s}^{-1}$) the cells are deformed and they tend to form layers that slide on plasma. To a fair approximation, blood might be treated as Newtonian fluid in this region. When the shear rate is about 1000 s^{-1} , a typical value in large vessels, the Non-Newtonian behaviour becomes insignificant and the apparent viscosity reaches the values in the range of $0,003 \div 0,004 \text{ Pa}\cdot\text{s}$ (Caro et al. 1978). The elasticity remains in the order of $10^2 \text{ Pa}\cdot\text{s}$ but slightly less than at medium shear rate.

Hence the Newtonian model might be a reasonable approximation for the blood flow in large retinal vessels but Non-Newtonian effects can still be revealed. For the first approximation blood was considered to be Newtonian, isotropic, homogeneous and incompressible. In the extended model blood was considered as Non-Newtonian fluid in order to study possible additional effects of blood rheology.

1.3.3 Fluid-structure interaction

Vessel walls are distensible tubes with complex elastic behaviour. Vessel diameter varies with the pulsating pressure. Being elastic vessel walls also propagate pressure and flow waves generated by the heart at a velocity rate, which is mainly determined by the elastic properties of the wall and the pressure gradient. The distensibility of the vessel wall is essential for the wave propagation (Pontrelli & Rossoni 2003). The fluid-structure interaction is of primary interest in modeling blood flow, because of the arterial wall remodeling process and the subsequent altered flow pattern in pathologic states (Pontrelli 2001). The fluid blood and the vessel structure constitute an intrinsically coupled system. However, fluid-structure interaction is rather a challenge for hemodynamics due to the complex structure of the arterial wall (fibrous elastin and collagen supported in a fluid) and its elastomer behaviour (elastomers are easily extensible) (Artoli 2003). In medium vessels, such as large retinal arteries and veins, a maximal change of 5% in vessel diameter during vessel pulsation is expected. This results in the same order change of the Reynolds number. The effect is therefore quite minor for the investigated vessels. Therefore, for the first approximation, vessel walls were considered to be rigid in the present study.

1.3.4 Rheological models and constitutive equations of blood

Rheological models of blood describe the behaviour of blood constituents, mainly RBCs, including their aggregation and deformability. A constitutive (descriptive) equation describes a physical property of a material. Since it must be independent of any particular set of coordinates of reference, it must be a tensor equation (Fung 1990). From a modeling point of view, it is necessary to know that constitutive equation of blood can describe the deformations in the fluid. By the constitutive equation a relation between specific blood properties and the dynamical equations is established. Because of their importance, hematocrit and shear rate are the primary independent variables for describing apparent viscosity of blood or RBC suspensions. Other independent variables

such as temperature and concentration of substances causing RBC aggregation, are usually of less practical importance in a constitutive equation because they are constant in a given problem (Cockelet 1986). Because of the complexity of blood, especially due to its high particles' volume fraction, it has not been possible to develop constitutive equations without introduction of some empiricism or the use of approximations (Table 7).

Table 7. Various blood constitutive equations and their parameters. Review from (Fung 1990; Luo & Kuang 1992; Zhang & Kuang 2000; Bitsch 2002; Artoli 2003) and sources mentioned in the table.

No	Equation (source)	Type	Expression for shear rate $\dot{\gamma}$	Blood constitutive parameters
1	Newtonian (Fung 1990)	Linear	$\tau = \mu \dot{\gamma}$	μ – Newtonian viscosity
2	Casson (Casson 1959)	Casson	$\sqrt{\tau} = \sqrt{\tau_y} + \sqrt{\eta_y \dot{\gamma}}$	τ_y – yield stress; η_y
3	Quemada (Quemada 1981)	Casson	$\tau = k_\infty \left(\frac{1 + \vartheta}{\chi + \vartheta} \right)^2$ $\chi = \sqrt{k_\infty / k_0}$ $\vartheta = \sqrt{\theta \dot{\gamma}}$	k_0, k_∞, θ ; θ – critical time, which characterizes the evolution of the structure k_∞ – viscosity index (intrinsic viscosity) related to RBC deformability; k_0 – viscosity index (intrinsic viscosity) related to RBC aggregation
4	K-L (Luo & Kuang 1992)	Casson	$\tau = \tau_y + \eta_p \left(\alpha_1 \dot{\gamma} + \alpha_2 \sqrt{\dot{\gamma}} \right)$	η_{plasma} – plasma viscosity; τ_y – yield stress; α_1 – viscosity index related to RBC deformability; α_1 / α_2 related to RBC aggregative level
5	Bi-exponent (Zhang & Kuang 2000)		$\eta = \eta_e + \eta_D e^{-\sqrt{t_D \dot{\gamma}}} + \eta_A e^{-\sqrt{t_A \dot{\gamma}}}$	$\eta_e, \eta_D, t_D, \eta_A, t_A$ $\eta_D / \eta_e - 1$ – viscosity index related to RBC deformability; $\eta_A / \eta_e - 1$ – related to RBC aggregation; t_D, t_A represent sensitivity of RBC deformability and aggregation to shear rate
6	Cross (Cross 1965)	Casson	$\frac{\eta - \eta_\infty}{\eta_0 - \eta_\infty} = \frac{1}{(1 + (k_c \dot{\gamma}_c)^{m_c})}$	η_0, η_∞ – asymptotic apparent viscosities as $\dot{\gamma} \rightarrow \infty$ and $\dot{\gamma} \rightarrow 0$; k_c, m_c
7	Wang (Wang & Stoltz 1994)	Casson	$\tau = \eta_p \left(\beta_1 \dot{\gamma} + \beta_2 \sqrt{\dot{\gamma}} \right)$	η_{plasma} – plasma viscosity; β_1, β_2
8	Power Law (Hussain et al. 1994)	Power Law	$\tau = A_p \dot{\gamma}^{n_p}$	A_p, n_p
9	Weaver (Weaver et al. 1969)	Power Law	$\log \eta = \log \eta_p + (0,03 - 0,0076 \log \dot{\gamma}) H$	η_{plasma} – plasma viscosity; H – hematocrit
10	Walburn (Walburn & Schneck 1976)	Power Law	$\tau = C_1 \exp(C_2 H + C_4 TPMA / H^2) \dot{\gamma}^{1 - C_3 H}$	TPMA – plasma protein level; H – hematocrit
11	Generalized Newtonian (Bird et al. 1987; Baaijens et al. 1993; Artoli 2003)		$\tau = \eta(A) A$ $A = L + L^T$ $L = \nabla \bar{v}$ $\eta(A) = \eta_\infty + (\eta_0 - \eta_\infty) \left[\frac{1 + \log(1 + \Gamma \dot{\gamma})}{1 + \Gamma \dot{\gamma}} \right]$	$\dot{\gamma} = \sqrt{\frac{tr(A^2)}{2}}$ Γ – material const., repres. degree of shear thinning; η_0, η_∞ – asymptotic apparent viscosities as $\dot{\gamma} \rightarrow \infty$ and $\dot{\gamma} \rightarrow 0$
12	Oldroyd B (Oldroyd 1958)		$\tau + \lambda_1 (\dot{\tau} - L\tau - \tau L^T) = \eta(A + \lambda_2 (\dot{A} - LA - AL^T))$ $A = L + L^T$ $L = \nabla \bar{v}$	λ_1, λ_2 – relaxation and retardation constants; η – const.
13	Generalized Oldroyd B (Pontrelli 1997) (Yeleswarapu 1996)		$\tau + \lambda_1 (\dot{\tau} - L\tau - \tau L^T) = \eta(A) A + \eta_0 \lambda_2 (\dot{A} - LA - AL^T)$ $A = L + L^T$ $L = \nabla \bar{v}$ $\eta(A) = \eta_\infty + (\eta_0 - \eta_\infty) \left[\frac{1 + \log(1 + \Gamma \dot{\gamma})}{1 + \Gamma \dot{\gamma}} \right]$	$\dot{\gamma} = \sqrt{\frac{tr(A^2)}{2}}$ Γ – material const., repres. degree of shear thinning; η_0, η_∞ – asymptotic apparent viscosities as $\dot{\gamma} \rightarrow \infty$ and $\dot{\gamma} \rightarrow 0$ λ_1, λ_2 – relaxation and retardation constants;

Comments to Table 7: Not all available constitutive models are shown. The intention of the table was to provide an impression on constitutive equations. For more details on each model the corresponding sources given in the table should be considered.

A dot over a variable denotes the substantial derivative: $\frac{D}{Dt} = \frac{\partial}{\partial t} + \vec{v} \cdot \nabla$

The generalized Newtonian fluid model (Table 7:11) is a simple extension of the theory for Newtonian fluids, as the viscosity instead of being a constant, is a scalar function of the scalar invariants of the shear rate tensor. It applies to an incompressible shear flow (Bird et al. 1987).

Hematocrit plays an important role in hemorheology. At zero hematocrit (blood plasma) all the fluids behave in a Newtonian manner. At small shear rates cell aggregation has a large influence on the viscosity. The effect of cell aggregation is largest at moderate hematocrits (Bitsch 2002). The most constitutive parameters mentioned in Table 7 (e.g. $\alpha_1, \tau_y, \eta_0, \eta_\infty, \theta, \eta_e, \eta_D, t_D, \eta_A, t_A, \lambda_1, \lambda_2$) are dependent of hematocrit (Zhang & Kuang 2000).

τ_y is used in several models. It represents the so called **yield stress**: the stress of blood as $\dot{\gamma} \rightarrow 0$. The existence of the finite yield stress τ_y has been controversial (Walburn & Schneck 1976; Fung 1990). Experiments by Merrill et al. (1965) reveal that yield stress does not exist for hematocrit H less than the critical value H_c . However, when $H > H_c$, τ_y obeys:

$$\tau_y = 0,08(H - H_c)^3$$

where $H_c = 5 \div 8\%$ (Luo & Kuang 1992). τ_y is almost independent of the temperature in the range $10 \div 37^\circ\text{C}$. The unit of τ_y is Pa.

The common Casson equation (Table 7, 2) might be applicable at low shear rates, and hematocrit smaller than 39% (at 37°C). However, at shear rates above 5 s^{-1} it is starting to deviate, and another model is required until the Newtonian region at higher shear rates is reached. In the literature, different kinds of constitutive equations have been suggested (Table 7). Zhang and Kuang (2000) have performed an analysis study, where they fitted a large variety of constitutive equations to measurements obtained in a concentric cylinder (Table 7, 1-10). By means of a least squares fit they concluded that the **Quemada**, Bi-exponent and L-K equations were best applicable for human and canine blood. Equations 11-13 in Table 7 were not used in the study by Zhang and Kuang. The generalized Oldroyd B model (Table 7, 13) (Yeleswarapu 1996; Pontrelli 1997) was issued after this analysing study. It considers the *creep*, the normal stress relaxation effects with constant viscosity, and combines the generalized Newtonian model (Table 7, 11) with the Oldroyd B model (Table 7, 12). Since the Generalized Oldroyd B model captures most of the important characteristics of blood it is also well applicable for blood modeling (Artoli 2003).

Most of the equations gathered in Table 7 are established for clinical purposes, since a constitutive equation contains information of the rigidity of RBC. For example, the parameters in the Bi-exponent equation are directly related to aggregation and deformability, and can be used to make a patient diagnosis. Blood rheology in the macroscopic domain has been used extensively for that purpose, see for example Fung (1990).

1.3.5 Principles of rheological model by Quemada

In order to describe Non-Newtonian blood rheology in the present work Quemada's rheological model was used, since it was shown to be well applicable for human blood in independent analysing studies (Eastoppe & Brooks 1980; Zhang & Kuang 2000) and since it represents the rheological data for blood and RBC suspensions over a wide range of conditions (Cockelet 1986).

Quemada introduced the term effective intrinsic viscosity \mathbf{k} , which was involved in his viscosity equation proposed (Quemada 1978; Quemada 1981):

$$\eta_r = \eta / \eta_{plasma} = \sqrt{1 - \frac{1}{2}kH} \quad , \quad (6)$$

where η_r represents relative blood viscosity, η_{plasma} is blood plasma viscosity, \mathbf{H} – hematocrit. In very dilute systems with $\mathbf{H} \rightarrow 0$ the equation (6) tends to the Einstein equation: $\eta_r = 1 + k\mathbf{H}$ and \mathbf{k} appears as true intrinsic viscosity. As \mathbf{H} is raised, it becomes the volume fraction of RBC and \mathbf{k} becomes effective intrinsic viscosity, which involves all changes in the effective volume of RBCs. \mathbf{k} is then \mathbf{H} and $\dot{\gamma}$ dependent. Quemada proposed to consider \mathbf{k} from viscosimetric measurements at given \mathbf{H} and $\dot{\gamma}$ as characterizing the structure of the suspension. Under steady shear rate and constant hematocrit \mathbf{k} reaches the equilibrium value:

$$k = k(\dot{\gamma}) = k_\infty + \frac{k_0 - k_\infty}{1 + \sqrt{\theta \dot{\gamma}}} \quad , \quad (7)$$

where \mathbf{k}_0 represents low share rate intrinsic viscosity, \mathbf{k}_∞ is high share rate intrinsic viscosity and θ – critical time, which characterizes the evolution of the structure, as for example the time for particle aggregation. Cockslet characterized this parameter as “relaxation time for the dominant structural unit causing the suspension to be Non-Newtonian” (Cockslet 1986). Alternatively $\dot{\gamma}_c = \theta^{-1}$ (critical shear rate) was introduced, which is related to the critical shear stress under which the structure is broken (Quemada 1981). \mathbf{k}_0 , \mathbf{k}_∞ and $\dot{\gamma}_c$ form a set of structural parameters for rheological characterization of blood, which are experimentally measured. All three parameters depend on the hematocrit value (Quemada 1981; Cockslet 1986). These dependences on hematocrit are depicted in Fig. 16 (see 2.4.4.5 and legend to the figure for additional explanation on methods they were obtained).

The properties of the equations (6)(7) which are pertinent to blood rheology are the following (Cockslet 1986):

- $\mathbf{k}_0 > 0$ and $\mathbf{k}_\infty > 0$. For shear-thinning suspensions including human blood $\mathbf{k}_0 > \mathbf{k}_\infty$;
- if the suspension is Newtonian the equations reduce to:

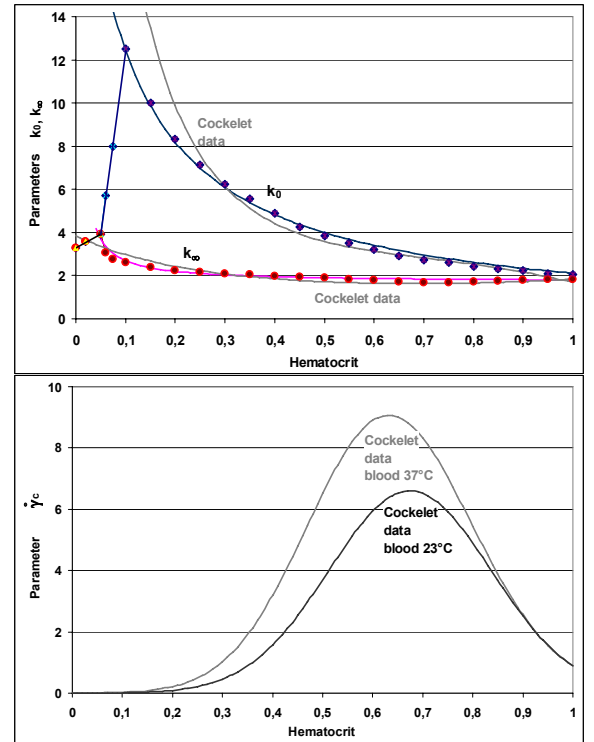


Fig. 16. Parameters of the Non-Newtonian Quemada model derived from (Dufax et al. 1980; Quemada 1981; Cockslet 1986)): **Top:** the low and the high shear rate intrinsic viscosities \mathbf{k}_0 (blue line) and \mathbf{k}_∞ (red line) depicted recalculated and fitted from experimental data by Quemada (1981). Grey lines represent the data on Quemada model for blood at 37°C from (Dufax et al. 1980) reported by Cockslet (1986). **Bottom:** critical shear rate $\dot{\gamma}_c$ for blood at 23°C and 37°C. Distributions were modified from the data by Cockslet (1986).

$\eta_r = \frac{1}{\sqrt{1-1/2(kH)}}$, where $\mathbf{k} = \mathbf{k}_0$, if $\dot{\gamma} \ll \dot{\gamma}_c$; $\mathbf{k} = \mathbf{k}_\infty$, if $\dot{\gamma} \gg \dot{\gamma}_c$ or $\mathbf{k} = \mathbf{k}_0 = \mathbf{k}_\infty$, if $\dot{\gamma}_c$ is within the range of

$\dot{\gamma}$ for which the RBC suspension is Newtonian;

- the Casson equation (Table 1 2) can be recovered from the Quemada equation at high θ ($\dot{\gamma} \gg \dot{\gamma}_c$). At such large shear rates RBC aggregation would not be expected and this limiting case is built on the model of particle aggregation;
- when relative viscosity reaches infinity at the high \mathbf{H} , the equations (6)(7) reduce to: $\mathbf{k}_0 = 2/\mathbf{H}_m$, where \mathbf{H}_m is the maximum volume fraction (or hematocrit for blood) physically permissible in the suspension if particles are in the form prevalent at $\dot{\gamma} \ll \dot{\gamma}_c$.

2 Methods

2.1 Functional in-vivo measurements with the Retinal Vessel Analyzer (RVA)

2.1.1 Principles of RVA measurements

The vessel diameter was measured on-line with the Retinal Vessel Analyzer (RVA, IMEDOS GmbH, Jena, Germany, Fig. 17). The device allows non-invasive on-line assessment of the vessel diameter depending on time and location along the vessel. Before, during and after

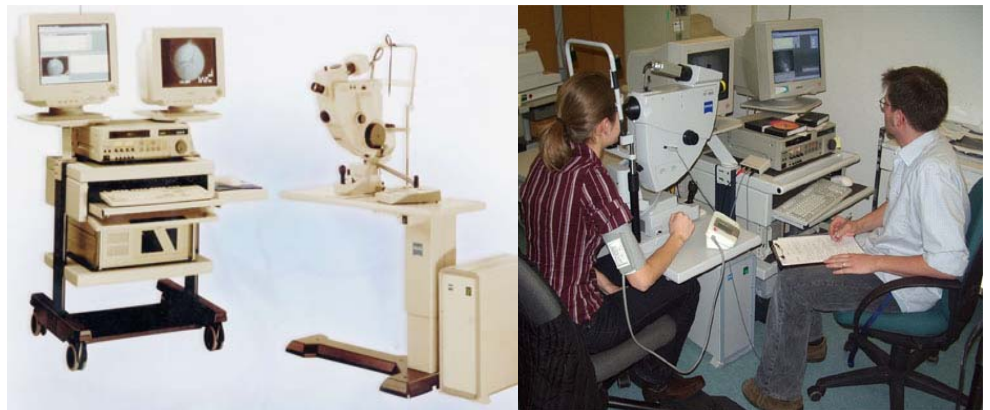


Fig. 17. Retinal Vessel Analyzer

provocations arterial and venous diameters can be assessed. For that purpose the RVA consists of a retinal camera (Zeiss 450 FF), a CCD-camera for electronic on-line imaging and a PC for system control, analysing and recording of the obtained data (Fig. 17). More detailed description of this device and its process of vessel diameter measurement can be found for example in (Polak et al. 2000; Vilser et al. 2002).

An arterial segment of approximately 1 mm in length was evaluated in each eye (Fig. 18). Selection criteria for the segment were: location within a circular area of two disc diameters, no crossing or bifurcation in the measuring segment, curvature of not more than 30° , distance to neighboring vessels of at least one vessel diameter and sufficient contrast to the surrounding fundus. The selected vessel segment was placed in the middle part of the fundus image by eye movement, by using the inner fixation of the camera before the vessel measurement began (Fig. 18). The vessel segment was scanned randomly 25 times a second in the measurement window under optimal conditions. The position of the vessel edges, the vessel course, the vessel diameter, and correction for ocular movements were calculated automatically on-line. Since the image scale of each eye was unknown the measured values were expressed in relative units (RU). These units correspond to micrometers if the examination eye has the dimensions of the normal Gullstrand eye. 30 seconds before every flicker provocation was taken as the baseline, to which the subsequent diameter response was normalized.

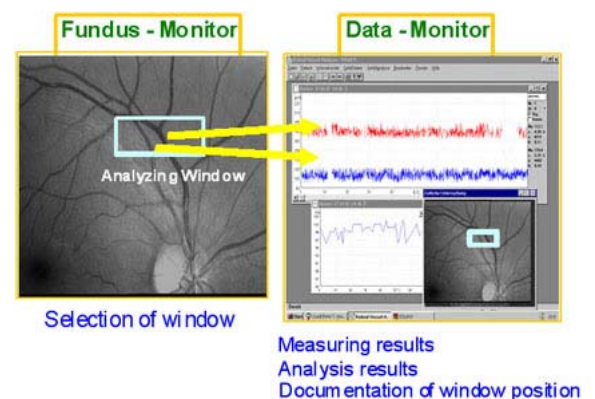


Fig. 18. Principles of the Retinal Vessel Analyzer measurements

2.1.2 **Functional stimulation of retinal vessels (Flickering light, OODG by Ulrich, etc.)**

Retinal autoregulation is difficult to measure since it is by definition a functional response (1.2.3). Clearly, autoregulation, its disturbances and possible influences on it by pharmaceutical agents are not detectable in a full-scale when assessing only the static state (Hubbard et al. 1999). This complicated entity can only be evaluated correctly when regarding the process in its dynamic regulation (Vilser et al. 1991; Vilser et al. 2002; Nagel & Vilser 2004). In order to achieve this goal ocular perfusion ought to be altered by a standardized stimulus that is provoking the autoregulation process which then can be measured. A dedicated analysis of the measurement results gives an insight into different autoregulative mechanisms, which compensate for disturbances of or demands on microcirculation (Seifert & Vilser 2002). Changes in autoregulative reserve could be used for early recognition. Since the retinal autoregulation is quite sensitive to changes in perfusion pressure, tissue levels of oxygen and carbon dioxide, to local factors and to some vasoactive agents and medicaments possible methods of functional provocation of retinal vessels are follows:

- provocation using Bayliss effect (Bayliss 1902; Blum et al. 1999): evokes vessel constriction with ensuing regulating phase of reactive vessel dilation;
- oxygen breathing (Lanzl et al. 2000): evokes strong vessel constriction with ensuing regulating phase of reactive vessel dilation;
- pharmacological provocations of any kind, for example phenylephrine 10% eye drops (Kotliar et al. 2000): different vascular reactions;
- reverse breathing and increase of CO₂ in blood (Seifert & Vilser 2002): evokes vessel dilation with ensuing regulating phase of vessel constriction;
- artificial IOP increase (Nagel et al. 2000; Nagel et al. 2001; Nagel & Vilser 2004): complex vessel reaction different for arteries and veins;
- photo stimulation with flickering light (Michelson et al. 2002; Polak et al. 2002; Kotliar et al. 2004; Nagel et al. 2004): prompt vessel dilation with ensuing arterial constriction and venous relaxation

In the present work provocations of retinal vessels with two latter methods were used. These will be presented in detail below.

Artificial IOP increase with oculo-oscillo-dynamography by Ulrich (OODG)

In 1985 Ulrich and Ulrich proposed a new method to measure the pressure in the central retinal artery and in the ciliary arteries (Ulrich & Ulrich 1985) (Fig. 19) - oculo-oscillo-dynamography by Ulrich (OODG). The method provides continuous bilateral registration of ocular volume pulsations and includes ophthalmodynamometry, ophthalmodynamography and ocular pneumoplethysmography. Using the suction cup attached to the sclera IOP is increased, and the ocular pulsations can be assessed (Fig. 19, left). The ocular pulse depends on IOP changes and on the blood volume in the eye. The latter depends on the cardiac cycle (ocular pulse). All the arterial vessels in the eye influence the pulse wave.

OODG device consists of a scleral vacuum suction cup (with diameter of 11, 12 or 13 mm), a suction pump and an infrasound pressure converter. The latter converts changing IOP into the electric signal, which is transferred

to the microcomputer and is recorded in form of an oscillating pulse wave. During the provocation the suction cup is attached to the sclera laterally from the cornea and a rarefaction is performed with the suction pump (Fig. 19, right). IOP increases through this manipulation to a certain level and the ocular pulse curve flattens. The pulse wave disappears in the vessels at an instant that the systolic pressure becomes less than IOP. Then the rarefaction can be decreased and the pulse wave comes back in the vessel. At first the pulsation appears in the central retinal artery. Later it can be seen in choroidal and ciliary vessels. Finally IOP becomes less than the diastolic pressure in ocular vessels and the ocular pulse increment ceases. When combining fluorescent angiography with OODG the pulse wave source can be detected and the information on the ocular pulse can be correlated with corresponding vessels (Ulrich & Ulrich 1985).

The authors of OODG proposed this method for the assessment of several hemodynamic characteristics such as perfusion pressure, systolic pressure in retinal and choroidal vessels, diastolic pressure in these and other ocular vessels), pulse blood volume, temporal pulse characteristics, anacrotic and catacrotic angles (Ulrich & Ulrich 1985).

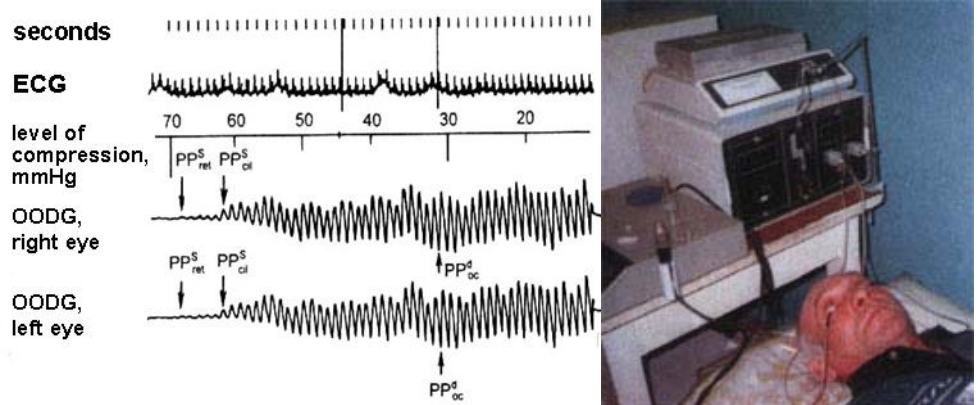


Fig. 19. Left: Oculooscillograms of paired eyes of a healthy volunteer 32 years old. PP_{ret}^s – systolic perfusion pressure in the retina; PP_{cil}^s – systolic perfusion pressure in the ciliary body; PP_{oc}^d – diastolic perfusion pressure. **Right:** OODG-provocation and measurements. Modified from (Volkov 2001).

OODG is used in combination with other methods to assess the ocular hemodynamics. In a number of studies OODG was used as a dosed provocation of intraocular microcirculation by artificial acute IOP increase (Riva et al. 1986; Zetlan et al. 1992; Michelson et al. 1996; Pillunat et al. 1997). This provocation seems to mimic events of naturally occurring IOP peaks in glaucoma or short-term decrease of systemic blood pressure.

The method is formally reconed as non-invasive. However it is tedious in implementation and burden to an examined person is high enough during the provocation. Therefore OODG is nowadays gradually being replaced by contemporary ophthalmodynamometry methods like ophthalmodynamometry with a contact lens by Löw (Jonas 2003) or dynamic contour tonometry by Kanngiesser (2005).

Flickering light

Dilation of retinal vessels can be achieved by changing the illumination level of the retina (Polak et al. 2002; Kotliar et al. 2004). This effect is called neurovascular coupling and has been studied extensively in the ophthalmic community (Logean et al. 2001; Riva et al. 2001; Schmetterer et al. 2001).

The hypothesis of neuro-vascular coupling described by Roy and Sherington in 1890 (Roy & Sherington 1890) has been verified since using different techniques to measure regional cerebral blood flow. Neurovascular coupling is defined by neuronal activity evoking local change in blood flow. In the central nervous system neurovascular coupling has been shown to be unaffected during normal aging (Rosengarten et al. 2003). The effect is highly dependent on glial cell activity as has been shown in isolated mammalian retina (Metea & Newman 2006).

Within the visual system stimuli are processed and reinforced to create the visual image. Difference in brightness represents such a stimulus, colors – another one. The primate visual pathway is characterized by two main cellular systems. Prompt changes in the luminance level on the retina represent a strong stimulus for the magnocellular system. On the other hand, low temporal frequency, counter-phase modulation of red and green fields are known to be optimal stimuli for the parvocellular system (Riva et al. 2001). These neurophysiological considerations served as a basis to construct a possible stimulus to investigate the interaction of neural and metabolic processes in the retina. Retinal blood flow in reaction to flickering light was examined in 1990 by A. Bill and G. Sperber (1990). They found an increase in retinal blood flow in monkeys after stimulation with flickering light. C. Riva, B. Falsini and E. Logean (2001) were able to observe this effect in healthy human volunteers. In their experiment the retinal blood flow in the optic nerve head was measured using laser Doppler flowmetry with the finding of an increase of retinal blood flow after application of stroboscopic light with a frequency of 15 Hz. Later on, K. Polak, L. Schmetterer and C. Riva (2002) examined the flicker evoked increase in retinal arterial and venous diameter for luminance flicker with frequencies of $2 \div 64$ Hz and stimulus duration of 1 min. The most effective stimulus for the human retina consists in the application of a rectangular flicker light with a frequency of $8 \div 20$ Hz (Polak et al. 2002; Nagel et al. 2004; Kotliar et al. 2006).

In RVA and DVA an optoelectronic shutter is inserted in the retinal camera in place of an additional optical filter. The shutter interrupts the observation light (530–600 nm, irradiance at the fundus approximately $1,96 \times 10^{-4}$ W/cm² over 30° visual field of the retinal camera and works with a bright-to-dark ratio of 25:1 (Vilser et al. 2002; Nagel et al. 2004). The chosen frequency of 12,5 Hz of rectangular light interruption provided a sequence of one normal illuminated and one dark single frame at a video frequency of 25 Hz. This frequency lies in the mentioned range of the maximally exciting flicker frequency (Polak et al. 2000; Riva et al. 2001). The optoelectronic shutter is controlled by a special program running on the RVA computer. For that purpose the RVA consists of a retinal camera (Zeiss 450 FF), a CCD-camera for electronic on-line imaging and a PC for system control, analysing and recording of the obtained data (Fig. 17).

In RVA the duration of flicker stimulation as well as the observation pauses between stimulation can be adjusted manually and depended on experimental design. Generally the pauses need to be long enough to allow the vessel diameter to return back to the baseline after provocation (Kotliar et al. 2004). In modern DVA-system measurement of the baseline vessel diameter for 50 seconds in continuous light was followed by three cycles of 20-second flicker provocation and 80 s observation. This standard protocol, introduced by the manufacturer, runs automatically and could be changed in the scientific version of the device. In order to reduce inaccuracies and noise in data evaluation an averaging procedure is applied. The same averaging procedures are used for visual evoked potential examinations. In DVA, for example, 3 single measurements for each volunteer are summed up: consisting of 30 s of baseline before the flicker application, 20 s of flicker application and 80 s thereafter. Because of the wide variation of vessels diameters between individuals, the mean diameter resulting from baseline measurements before application of the stimulus is normally

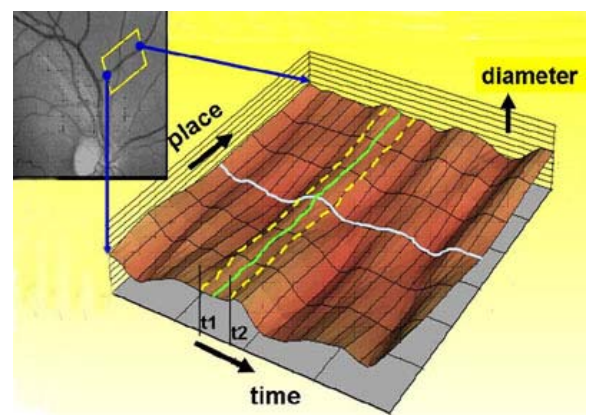


Fig. 20. Data representation in the RVA. 3D –time-space matrix

defined as 100% and the ensuing vessel diameter changes correlated to the baseline value.

2.1.3 Assessment of temporal vessel reaction

The result of RVA-scanning procedure is a matrix of data, which is demonstrated as 3D display in Fig. 20. Temporal assessment of retinal arterial behaviour in response to stimuli is the most common feature of the device already published in a number of studies (Polak et al. 2003; Nagel & Vilser 2004; Nagel et al. 2004). For this feature changes in vessel segment diameter mean over time are traced (white solid line in Fig. 20).

2.1.4 Assessment of longitudinal vessel profiles

The obtained data additionally allows to detect spatial changes in vessel diameter along a chosen segment during a defined time period can be assessed. (e.g. time interval between the two dashed yellow lines in Fig. 20).

For each pixel (point of the segment) the mean of all measurements in this location during the chosen time interval is calculated. The result is termed “longitudinal vessel profile” (green solid line in Fig. 20). This corresponds to the configuration of the vessel wall in its longitudinal section, when assuming the vessel to be axially symmetrical (Fig. 21). Profiles obtained at different time intervals can be compared. Through this local vessel analysis is possible to assess in vivo non-invasively dynamic variations in longitudinal vessel configuration in humans during different states of stimulation (Fig. 22). The method of data acquisition for local vessel analysis with RVA was explained in detail before (Kotliar et al. 2006).

The lengths of vessel segments were measured in the same units (RU, MU) used for evaluation of vessel diameters (Vilser et al. 2002). External data transfer of spatial curves in RVA is performed in measurement units (MU). 1 MU equals to 12,5 µm in a normal Gullstrand eye.

In order to describe the longitudinal profile of a vessel and its caliber changes the frequency of these

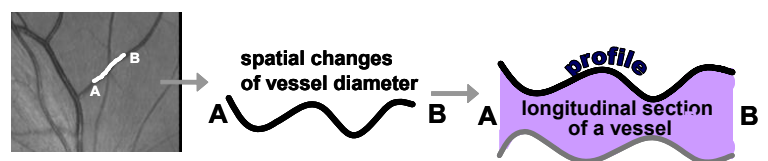


Fig. 21. Definition of longitudinal vessel profile

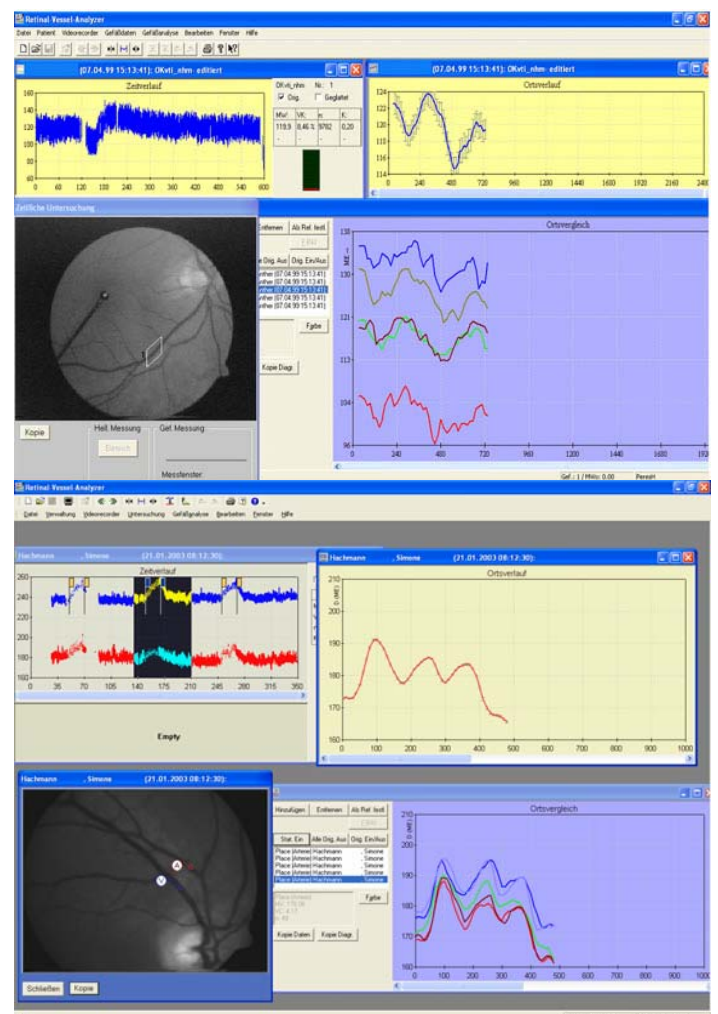


Fig. 22. Assessment of longitudinal vessel profiles. Longitudinal vessel profiles during baseline (green), constriction (red), dilation (blue) and relaxation (grey and brown) as displayed. **Top**: in RVA-system in glaucoma study. **Bottom**: in DVA-system in systemic hypertension study. Assessed temporal cycle is marked within the whole temporal vessel diameter course.

changes needs to be characterized. Waves along a curve (temporal or a spatial) can be defined by their frequency and amplitude. Applying these principles to the longitudinal retinal vessel profile waves of different frequency can be determined, namely high frequency waves (HFW) including waves in the longitudinal vessel profiles with 10 to 20 oscillations per 1 mm of the vessel segment and a magnitude between 1,5 and 15 μm and low frequency waves (LFW) defined as 0,2 to 5 oscillations per 1 mm of vessel segment and a magnitude of 15 to 40 μm .

2.1.5 Spectral analysis of longitudinal vessel profiles

To characterize the longitudinal vessel profile the power spectrum for the local vessel diameter curve of each subject was obtained by Fast Fourier Transform (Fig. 23). Each power spectrum was reduced by dividing each value in the frequency distribution by the whole area of the power spectrum as described in detail elsewhere (Bronzino et al. 1987).

*Obviously original power spectra of a group cannot be simply averaged to a mean power spectrum: for instance, a high magnitude peak of an individual at a certain frequency would obscure all other peaks at other frequencies. A **reduced power spectrum** looks like the power-spectrum in Fig. 23, right panel. There remains frequency in **Hertz (Hz)** along the abscissa-axis and by definition, the power in $\text{MU}^2/(\text{MU}^2*\text{Hz}) = \text{Hz}^{-1}$ along the ordinate-axis. The reduced power spectrum conserves all the key frequencies and corresponding peaks as well as proportions of peak heights of the initial original power spectrum. An individual reduced power spectrum becomes simply a probability distribution of frequencies in the corresponding analyzed curve. The whole area under the reduced power spectrum equals to 1. Individual reduced power spectra are averageable using this method.*

For each type of spatial curves and for each age group the **average reduced power spectra** (ARPS) were derived from these individual reduced power spectra by calculation of the median value in the group for each point of frequency distribution as suggested by other authors for brain vessels (Bronzino et al. 1987). Following parameters of ARPS were evaluated: Spectral Edge Frequency, average frequencies of peaks and average area under the spectrum within chosen frequency bands.

The frequencies in all power-spectrum charts were calculated in reciprocal local measurement units: MU^{-1} . The term “frequency” measured in Hz is commonly related to the temporal changes. For the purposes of the present work the term “spatial frequency” was introduced, which shows that it is dealing with spatial, not with temporal curves. The measure of “spatial frequency” is calculated in Hz. Like the temporal meaning of Hz (one oscillation per second) the latter means one oscillation per local measurement unit 1 MU (Vilser et al. 2002). Consequently, for example the spatial frequency of 0,1 Hz corresponds to one whole oscillation of a longitudinal vessel profile in 10 MU or in 125 μm in a Gullstrand eye. Thus in the present work the following remains valid:

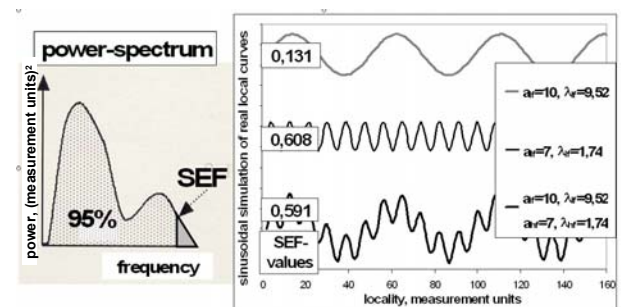


Fig. 23. Characteristic parameter of the high frequency waviness of arterial segments: spectral edge frequency (SEF). Examples of harmonic functions on the right show the range of calculated SEF-values. a, λ – corresponding parameters of the formula (10).

$$[\text{spatial frequency}] = MU^{-1} = \text{Hz} . \quad (8)$$

Note that consequently both the area under a reduced power spectrum as well as the area under ARPS are dimensionless values:

$$[\text{ARPS area}] = \text{Hz} * \text{Hz}^{-1} = 1. \quad (9)$$

Spectral Edge Frequency (SEF)

The parameter SEF was introduced and calculated for each subject for each considered time interval. SEF is a quantitative parameter to describe the presence of high frequencies and to characterize high frequencies. It is derived from the power spectrum of the vessel profile, created with Fast Fourier Transform (Bronzino et al. 1987). SEF divides the whole area under the power spectrum in two non equal parts: 95% and 5% (Schwender et al. 1996; Nieuwenhuijs et al. 2002) (Fig. 23). In general high SEF-values describe a more wavy curve (higher sinus frequency), and accordingly small SEF-values describe a less wavy curve.

In order to explain the concept of SEF a harmonic function consisting of a combination of sinus curves with a variable x is considered: a low frequency one with a magnitude \mathbf{a}_{lf} and a period λ_{lf} and a high frequency one with $\mathbf{a}_{hf}, \lambda_{hf}$:

$$\mathbf{g} = \mathbf{a}_{lf} \sin((2\pi/\lambda_{lf})x) + \mathbf{a}_{hf} \sin((2\pi/\lambda_{hf})x) . \quad (10)$$

Calculated SEF values for different values of parameters are represented in the left panel of Fig. 23, showing how this parameter can be applied to standard mathematical functions. One can see that the more wavy the curve is (the more high frequencies and the less low frequencies it has), the higher is the corresponding SEF-value.

When calculating SEF of a one parametric sinus (2 upper curves in the right panel of Fig. 23) one obtains approximately the eigenfrequency of the function since it is represented with one single peak in the power spectrum. A two-parametric sinus-curve (a lower curve in the right panel of Fig. 23) is already represented with two separate peaks in the power spectrum. This situation is closer to the real one: SEF will be closer to the higher peak dependent on the relationship between the corresponding magnitudes and eigenfrequencies.

With certain limitations the parameter SEF can be applied to the analysis of retinal vessel microirregularities. SEF may reflect variations of HFW for a subject at different time intervals and variability of HFW between subjects. This parameter shows whether relatively high frequency waves are represented on the curve: the more high frequencies the real curve has, the higher is the corresponding SEF value. However by definition SEF is dependent from the area of the power spectrum: that is even if high frequency waves are well represented they could show relatively small SEF, if low frequency and middle frequency waves have large amplitudes. On the other hand if moderate and low frequencies on the curve possess relatively small amplitudes, SEF can overestimate. A high SEF value implies that higher frequencies representing higher rates of change in lumen are present, though a small SEF value does not necessarily exclude higher frequencies.

2.2 Study designs

2.2.1 Age-related study

Measurements

20 min after pupil dilation with one drop of Mydriaticum Stulln® (Pharma Stulln Ltd, Germany) continuous measurement of retinal venous diameters was performed using RVA. Measurement of the baseline vessel diameter for 100 s in continuous light was followed by two cycles of 60 s flicker provocation and 150 s observation. Total duration of the measurements was 9 min. One cycle with enough measurement points was chosen for local vessel assessment as it is shown in Fig. 22, bottom. Measurements of the arterial reactions were taken later off-line from video tape.

Pulse and blood pressure

During the examination time blood pressure measurements by Riva-Rocci (RR) were taken once a minute. From those data the mean systemic arterial blood pressure (MAP, meanRR) was calculated as:

$$\text{meanRR} = \text{RR diastole} + 1/3 * (\text{RR systole} - \text{RR diastole}) \text{ mmHg.} \quad (11)$$

Data evaluation and statistical methods

Definition of observation time intervals

The time course of vessel diameter change in all subgroups was plotted (Fig. 24). The ensuing slope of the temporal response was consistent in all subjects and corresponded to results in healthy subjects reported by other authors (Polak et al. 2002; Nagel et al. 2004). This time response was not the subject of the present study. However since it represents the basis for the definition of time segments in the study design it is briefly described.

Arteries. Average vessel diameter over time demonstrated a diameter increase during provocation; a reactive vessel constriction was observed after releasing the stimulus with an ensuing return to initial baseline values (Fig. 24, upper panel). These temporal phases were observed in all groups. Four time intervals for examination were defined as shown in Fig. 24.

Veins. Flicker stimulation increased the venous diameter over time. After cessation of flicker the venous diameter decreased slowly back to initial baseline values (Fig.

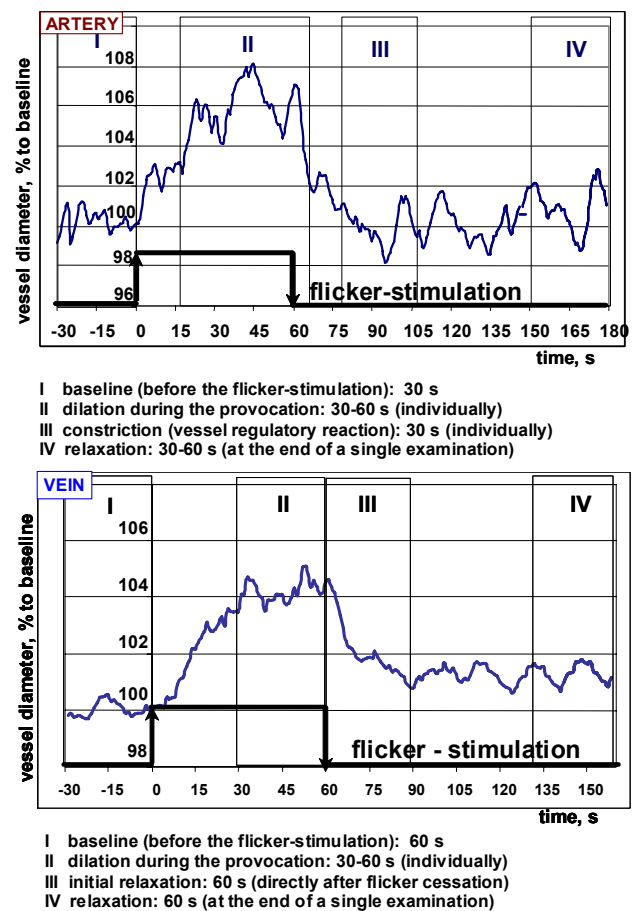


Fig. 24. Temporal arterial (top) and venous (bottom) vessel reaction to flicker provocation and explanation of time intervals of local vessel reaction assessment.

24, bottom panel). These temporal phases were observed in all groups. Four time intervals for examination were defined as shown in the bottom of Fig. 24.

Start of time segments II and III in arteries and of segment II in veins (Fig. 24) were assigned individually. For each subject an individual time interval included the point of maximal dilation or constriction and was chosen so that changes in vessel diameter during the interval were minimal.

Longitudinal vessel profiles during selected time segments were assessed at defined time intervals (Fig. 24) for each subject and compared intra- (Fig. 22, bottom panel) and interindividually.

A program was created in MATLAB 6.1 in order to plot power spectra with Fast Fourier Transform and evaluate the chosen parameter. Since Fast Fourier Transform needs the data vectors of the length, which is a power of 2, longitudinal vessel profile segments of $\sim 400\mu\text{m}$ in length (which corresponds to $2^5 = 32$ MU) were taken for each subject. A template with corresponding macros in MS Excel was created for each subject in order to filter, process and analyse the numerical data from the RVA. Since it was impossible to prove the normal distribution of measurement data, non-parametric Kruskal-Wallis Test and Mann-Whitney Test for independent samples were used in order to assess statistical differences of the evaluated characteristics. Since comparing three groups of volunteers regarding 1 parameter, necessary adjustment for multiple comparisons was considered by the Dunnett method (Glantz 1999) with a coefficient of 3. Because of the small number of subjects the statistical tests were applied on the level of significance of $p = 0,05$ for each evaluated parameter. Non parametric statistics were calculated in SPSS 11.0 for Windows.

2.2.2 Glaucoma study

20 min after pupil dilation with one drop of tropicamide Mydriaticum Stulln® (Pharma Stulln Ltd, Germany) continuous measurement of retinal venous diameter was performed with RVA. Measurements of the arterial reactions were taken later off-line from video tape. Total duration of the measurements was 10 min. Vessel diameter was assessed for two minutes in order to obtain baseline values. IOP increase was induced applying the principle of oculo-oscillo-dynamography by Ulrich (Taberna pro medicum, Lüneburg, Germany) (Ulrich & Ulrich 1985). Topical anesthesia was achieved by oxybuprocain eye drops before fitting the suction-cup (diameter 11 mm) of the OODG to the lateral portion of the globe.

2.2.2.1 Study 1 with acute suprasystolic IOP-increase

The standardized examination program increased IOP for three seconds to suprasystolic values. Systolic retinal and ciliary blood pressure was measured with OODG device during 40 s linear release of the increased IOP (Fig. 25, top).

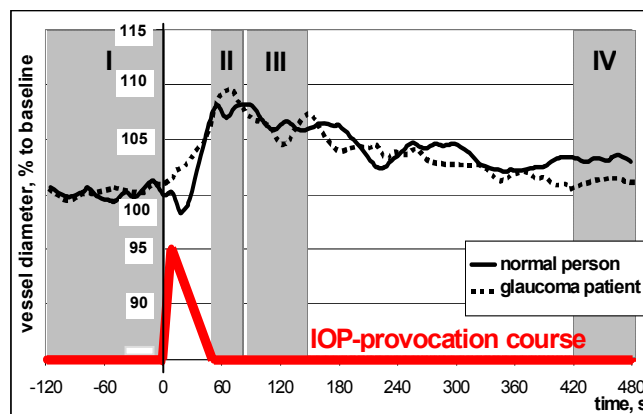
2.2.2.2 Study 2 with moderate 100 s IOP-increase

After 100 s of applying the suction cup to a pressure of 35 mmHg on the device, the suction cup was released.

Immediately after the RVA measurement, the contact lens was removed, IOP was assessed by applanation tonometry and then again briefly elevated, using the same suction cup parameters and the IOP actually achieved was measured by applanation tonometry. This second measurement was used to determine the individual IOP produced during the provocation with the limit of ignoring the oculopressure effect obtained by the first suction cup procedure.

Pulse and blood pressure

During the examination time blood pressure measurements by Riva-Rocci (RR) were taken once a minute. From those data MAP was calculated with formula (11).



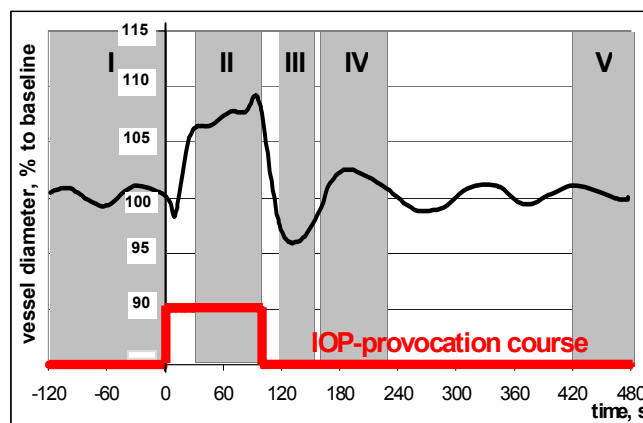
- I baseline: 120 s
- II dilation after IOP-provocation: 30 s individually
- III initial restoration: 60 s immediately after phase II
- IV restoration: 60 s at the end of the examination

Data evaluation and statistical methods

Definition of observation time intervals

Studies 1 and 2

The time courses of arterial diameter change in all subgroups were plotted. The ensuing slope of the temporal response showed dilation of the arterial vessel during provocation in all subjects (Fig. 25), which was reported previously (Nagel et al. 2001; Nagel & Vilser 2004). This time response was not the subject of the present study. Since it represents the basis for the definition of time segments in the study design it is briefly described.



- I baseline: 120 s
- II dilation during IOP-provocation: 30-60 s individually
- III constriction (vessel regulation reaction): 30 s individually
- IV initial restoration: 60 s immediately after phase III
- V restoration: 60 s at the end of the examination

Fig. 25. Temporal arterial reaction to pressure provocation (graphs are modified from (Nagel et al. 2001; Nagel et al. 2002)) and definition of time intervals for local vessel reaction assessment. **Top:** study 1 (suprasystolic IOP provocation): summary of temporal reaction of all normal persons and glaucoma patients; **Bottom:** study 2 (moderate 100 s IOP provocation): individual temporal vessel reaction of a healthy subject.

Study 1. Suprasystolic IOP provocation (Fig. 25, top)

The time course of the average vessel diameter demonstrated a slight diameter decrease during provocation; dilation was observed after releasing the stimulus with an ensuing return to initial baseline values (Fig. 25, top). During application of the suction cup and acute IOP-increase RVA measurements data could not be gathered for every time point in all subjects. Therefore the IOP increase time was disregarded and four time intervals for examination were defined as shown in Fig. 25, top panel.

Study 2. 100 s moderate IOP-increase (Fig. 25, bottom)

The artificially elevated IOP increased the arterial diameter over time. After normalization of the IOP the arterial diameter decreased below baseline values (constriction) with a subsequent return to initial baseline values

(Fig. 25, bottom). These temporal phases were observed in all groups. The five time intervals studied are shown in fig. 2A. The constriction phase was not observed in study 1. Therefore the number of observed time intervals is not equal in both studies.

Studies 1 and 2

Start of time segment II in study 1 (Fig. 25, top) and segments II and III in study 2 (Fig. 25, bottom) were assigned individually. For each subject the individual time interval contained the point of maximal dilation or constriction. This point was located within the interval so that the interval includes the maximal absolute sum of dilation (constriction) values. Longitudinal vessel profiles during selected time segments were assessed at defined time intervals for each subject and compared intra- and interindividually.

A program was created in MATLAB 6.1 in order to plot power spectra with Fast Fourier Transform and evaluate the chosen parameter. Longitudinal vessel profile segments of $\sim 400\mu\text{m}$ in length (which corresponds to $2^5 = 32$ MU) were taken for each subject similar to the study 2.2.1. Data transfer to MS Excel for evaluation was performed in MU.

A template with corresponding macros in MS Excel 2000 was created for both studies for each subject in order to filter, process and analyse the numerical data obtained from RVA. Since it was impossible to prove the normal distribution of measurement data, the non parametric Wilcoxon-Test for dependent samples (glaucoma patients before and after treatment) and the Mann-Whitney Test for independent samples (normal subjects and POAG patients) were used in order to assess statistical differences of the evaluated characteristics. Since comparing three groups of patients (normal subjects, glaucoma patients before and after the treatment) regarding 1 parameter, necessary adjustment for multiple comparisons were considered by means of Newman-Keuls method and Dunnet method (Glantz 1999) with a coefficient of three. Because of the small number of subjects the non parametric tests were applied on the level of significance of $p = 0,05$ for each evaluated parameter. Non parametric statistic was calculated in SPSS 11.0 for Windows (Bühl & Zöfel 2002). Linear slopes were calculated applying the least square method.

2.2.3 Systemic hypertension study

Measurements

30 min after pupil dilation with one drop of tropicamide continuous measurement of retinal vessel diameter was performed using RVA (Nagel et al. 2004). Measurement of the baseline vessel diameter for 100 seconds in continuous light was followed by five cycles of 20-second flicker provocation and 80-second observation. One cycle

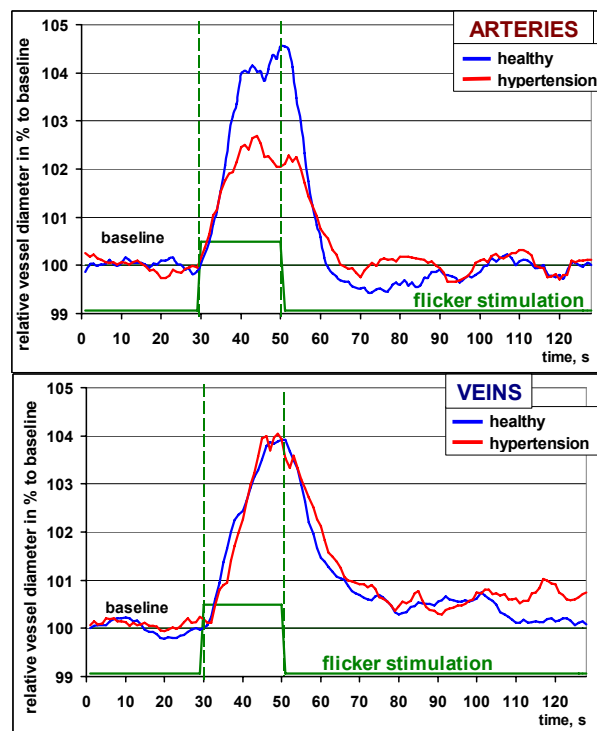


Fig. 26. Systemic hypertension study. Summary temporal arterial (top) and venous (bottom) reaction to flicker in the examined groups (N=15).

with enough measurement points was chosen for local vessel assessment as it is shown in Fig. 22, bottom.

Off-line re-measurement of data.

In order to provide higher precision and accuracy the measurements of both arterial and venous reactions in this study were taken later off-line from video tape recordings with the novel version of RVA, Dynamic Vessel Analyzer. The peculiarities of DVA and its advantages on RVA were described before (Gugleta et al. 2006). I mention only that in DVA each pixel of the measured vessel segment is scanned 25 times a second under optimal conditions. Two vessel segments simultaneously, e.g. an arterial and a venous one, can be assessed in DVA.

Pulse and blood pressure

Automatic blood pressure measurement was obtained with the intensive care monitor (Cardiocup II; Datex Ohmeda, Louisville, CO). The measurement took approximately 33 s and was repeated at 1-minute intervals. From those data the mean systemic arterial blood pressure was calculated with formula (11).

Data evaluation and statistical methods

Definition of observation time intervals

The time course of vessel diameter change in both groups was plotted. This time response was partially reported previously (Nagel et al. 2004) and it is not the subject of the present study. However since it represents the basis for the definition of time segments in the study design it is briefly described.

Arteries

Average vessel diameter over time demonstrated a diameter increase during provocation; a reactive vessel constriction was observed after releasing the stimulus mainly in the control group with an ensuing return to initial baseline values (Fig. 26, top panel).

Veins

Flicker stimulation increased the venous diameter over time. After cessation of the flicker the venous diameter decreased slowly back to initial baseline values (Fig. 26, bottom panel).

As the basis for spatial analysis from the whole vessel examination described above one temporal cycle (from 5 assessed cycles) was chosen for each subject. It consisted of 30 s of baseline, 20 s of flicker stimulation and

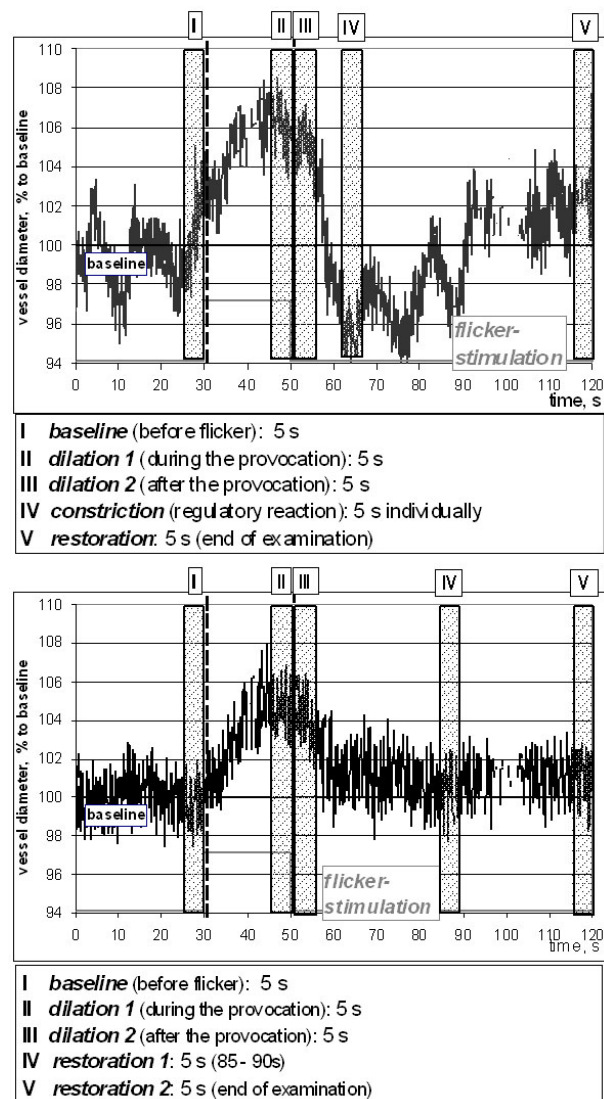


Fig. 27. Examples of temporal arterial (top) and venous (bottom) vessel reaction to flicker provocation and explanation of time intervals of local vessel reaction assessment.

80 s observation period (Fig. 26). Five time intervals for examination were defined for arteries and for veins as shown in Fig. 27.

Start of the time segment IV (Fig. 27) in arteries was assigned individually. For each subject an individual time interval included the point of maximal constriction and was chosen so, that changes in vessel diameter during the interval were minimal. Longitudinal vessel profiles during selected time segments were assessed at defined time intervals for each subject and compared intra- and interindividually.

Mathematical and statistical analysis

To characterize the longitudinal vessel profile the power spectrum for the local vessel diameter curve of each subject was obtained and ARPS was calculated. Following parameters of ARPS were evaluated: average frequencies of peaks and average area under the spectrum within chosen frequency bands.

A program was created in MATLAB 6.1 in order to plot power spectra with Fast Fourier Transform and evaluate the chosen parameter. Longitudinal vessel profile segments of $\sim 800\mu\text{m}$ in length (which corresponds to $2^6 = 64$ MU) were taken for each subject unlike the previous studies 2.2.1, 2.2.2.

A template with corresponding macros in MS Excel for Windows was created for each subject in order to filter, process and analyse the numerical data from DVA. Since it was impossible to prove the normal distribution of the most measurement data (the Kolmogorov-Smirnoff-test), the Mann-Whitney test and the Wilcoxon test were used in order to assess statistical differences of the evaluated characteristics. Non-parametric data were represented in the form: median(1 quartile; 3 quartile), parametric data were represented in form: mean \pm standard deviation. When comparing five different phases of vessel reaction regarding 1 parameter, necessary adjustment for multiple comparisons was considered by the Dunnett method (Glantz 1999) with a coefficient of 5. Because of the small number of subjects the non-parametric tests were applied on the level of significance of $p = 0,05$ for each evaluated parameter. Non-parametric statistics were calculated in SPSS 11.0 for Windows and Primer of Biostatistics, version 4.03 by S. Glantz (1999).

2.2.4 Obesity study

Measurements

20 min after pupil dilation with one drop of tropicamide continuous measurement of retinal venous diameter was performed using DVA. Measurement of the baseline vessel diameter for 50 seconds in continuous light was followed by three cycles of 20-second flicker provocation and 80-second observation. One cycle with enough measurement points was chosen for local vessel assessment as it was the case in the age-dependence and in the systemic hypertension studies (Fig. 22, bottom).

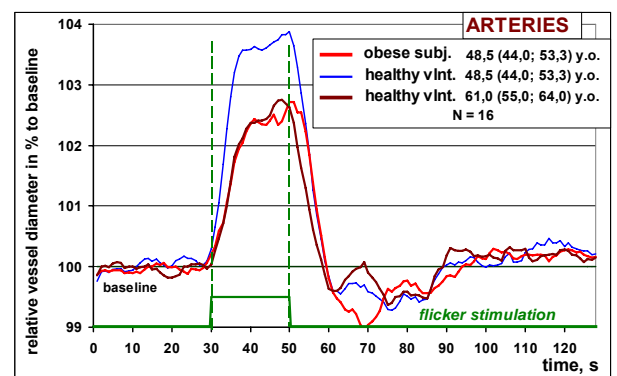


Fig. 28. Obesity study. Summary of temporal arterial reaction to flicker in examined groups (N=16).

Pulse and blood pressure

During the examination time blood pressure measurements by Riva-Rocci (RR) were taken once a minute. From those data the mean systemic arterial blood pressure was calculated with formula (11).

Data evaluation and statistical methods

Definition of observation time intervals

The time course of vessel diameter change in both groups was plotted in Fig. 28.

Arteries

Average vessel diameter over time demonstrated a diameter increase during provocation; a reactive vessel constriction was observed after releasing the stimulus mainly in the both groups with an ensuing return to initial baseline values (Fig. 28, top panel).

Veins

Flicker stimulation increased the venous diameter over time. After cessation of flicker the venous diameter decreased slowly back to initial baseline values (Fig. 28, bottom panel).

As the basis for spatial analysis from the whole vessel examination described above one temporal cycle (from 3 assessed) was chosen for each subject. As in the systemic hypertension study (2.2.3) it consisted of 30 s of baseline, 20 s of flicker stimulation and 80 s of observation period (Fig. 28). Five time intervals for examination were defined for arteries and for veins, similar to the systemic hypertension study (2.2.3) (Fig. 27). Start of the time segment IV (Fig. 27) in arteries was assigned individually. For each subject an individual time interval included the point of maximal constriction and was chosen so that changes in vessel diameter during the interval were minimal. Longitudinal vessel profiles during selected time segments were assessed at defined time intervals for each subject and compared intra- and interindividually.

Mathematical and statistical analysis

A program was created in MATLAB 6.1 in order to plot power spectra with Fast Fourier Transform and evaluate the chosen parameter. Longitudinal vessel profile segments of $\sim 400 \mu\text{m}$ in length (which corresponds to $2^5 = 32$ MU) were taken for each subject similar to the studies 2.2.1, 2.2.2. The mathematical and statistical analysis were performed according to the principles described above for the systemic hypertension study (2.2.3).

2.2.5 Repeatability and reproducibility of longitudinal vessel profile assessment and analysis

The method of longitudinal vessel profile assessment and analysis developed in the present work needs to be validated, that is its accuracy and precision should be tested.

Under the auspices of the present work the **accuracy** of the method, the degree of conformity of a measured or calculated quantity to its true value, was not checked. For such a validation histological studies described further in detail (5.2.2) need to be performed. The accuracy of some analytic elements of the method (4.1.5.1) was checked and discussed in the present work. Additionally the **precision** of the method, the degree to which further

measurements or calculations show the same or similar results was tested in the present work comprehensively. Precision is stratified into:

- **repeatability** - the variation arising when all efforts are made to keep conditions constant by using the same instrument and operator, and repeating during a short time period, and
- **reproducibility** - the variation arising using the same measurement process among different instruments and operators, and over longer time periods.

Whether the method of longitudinal vessel profile assessment with RVA is repeatable and reproducible was investigated. The detailed study on reproducibility and repeatability is the matter of a separate scientific paper. In the present work pilot studies in small groups were performed. The short-term repeatability, the long-term and the spatial reproducibility of the method were analyzed.

2.2.5.1 Short-term repeatability

In this pilot study 5 medically healthy volunteers from all age groups 21, 32, 39, 52 and 69 years old were involved. DVA measurements according to the standard protocol described in 2.2.4 were performed. Analysed time intervals for the repeatability examination were defined for arteries and for veins as follows. From the first 50 s of the baseline assessment a 5 s interval in the beginning (*baseline 1*) was chosen: from 5 to 10 s of the examination; and a 5 s interval at the end of the baseline assessment (*baseline 2*): regularly from 40 to 45 s of the examination but individually corrected for vasomotions. In case of expressed vasomotions the interval *baseline 2* was taken at approximately 45 s shifted backwards to be in the same vasomotion phase as the interval *baseline 1*. The 5 s interval *dilation 1* was taken immediately at the cessation of the first flicker stimulation from 70 to 75 s of the DVA assessment. The 5 s interval *dilation 2* was taken immediately at the cessation of the second flicker stimulation from 170 to 175 s of DVA assessment. Longitudinal vessel profiles during selected time segments were assessed at defined time intervals for each subject and compared intra- and interindividually. A program was created in MATLAB 6.1 in order to plot power spectra with Fast Fourier Transform and evaluate the chosen parameter. Longitudinal vessel profile segments of $\sim 800\mu\text{m}$ in length (which corresponds to $2^6 = 64$ MU) were taken for each subject similar to the systemic hypertension study (2.2.3). Mathematical and statistical analyses were performed according to the principles described above (2.2.3, 2.2.4). The samples were compared with non-parametric Wilcoxon-test. Additionally the coefficient of variation (**VC**) for basic parameters of the power spectrum analysis used in the present work: absolute vessel diameter, SEF, area within the frequency band $0,03 \div 0,06$ Hz, as well as the frequency of the primary peak, was calculated for each subject as follows (Köhler et al. 1995):

$$VC = \frac{s}{\bar{x}} \cdot 100\% , \quad (12)$$

where s represents the standard deviation and \bar{x} the mean of the first and the second measurement. Then the average value of VC (median) was calculated for each parameter for the group of volunteers.

2.2.5.2 Long-term reproducibility

In this pilot study 5 obese persons of moderate age of 44, 44, 50, 54 and 54 years old were involved. DVA measurements according to the standard protocol described in 2.2.4 were performed. Retinal vessels of patients were assessed at the same place in the retina with the time interval of 6 months. During this time the health-improving M.O.B.I.L.I.S. program was offered to the patients, which included psychological support, regular sport exercises and nutritional care. This was not the reason to exclude the subjects from the pilot long-term reproducibility study.

Two analyzed time intervals for the reproducibility examination were defined for arteries and for veins for the first and for the second (in 6 months) examination as follows. From the first 50 s of the baseline assessment a 5 s interval at the end of the baseline assessment (*baseline*) was chosen: regularly from 40 to 45 s of the examination. The 5 s interval *dilation* was taken immediately at the cessation of the first flicker stimulation from 70 to 75 s of DVA assessment. Longitudinal vessel profiles during selected time segments were assessed at defined time intervals for each subject and compared intra- and interindividually. A program was created in MATLAB 6.1 in order to plot power spectra with Fast Fourier Transform and evaluate the chosen parameter. Longitudinal vessel profile segments of $\sim 800\mu\text{m}$ in length (corresponding to $2^6 = 64$ MU) were taken for each subject similar to the systemic hypertension study (2.2.3). Mathematical and statistical analyses were performed according to the principles described above (2.2.3, 2.2.4). The samples were compared with Wilcoxon-test. Additionally the variation coefficient (VC) for basic parameters of the power spectrum analysis used in the present work: absolute vessel diameter, SEF, area within the frequency band $0,03 \div 0,06$ Hz, as well as the frequency of the primary peak, were calculated for each subject using the formula (12). The average value of VC (median) was calculated for each parameter for the group of volunteers.

2.2.5.3 Dimensional and spatial reproducibility

The question whether the longitudinal vessel profile of a randomly chosen retinal vessel is representative for a subject and does not differ in its microstructure from other measurable retinal vessel segments in the same and in the other eye was examined in the study.

One medically healthy young volunteer of 23 years old was included in this pilot study. 30 min after pupil dilation with one drop of tropicamide continuous measurement of his arterial diameters was performed using RVA. Measurement of the baseline vessel diameter for 50 s in continuous light was followed by three cycles of 20 s flicker provocation and 80 s observation.

31 retinal arterial and 31 retinal venous segments from the whole with RVA assessable fundus in the right and in the left eye of the volunteer were taken later off-line from video tape recordings and included in the study. Average vessel diameters of measured segments ranged from 72RU to 153RU for arteries and from 70RU to 164 RU for veins. In order to provide higher precision and accuracy the longitudinal vessel profiles in this study were analyzed later off-line using the technique described in 2.1.4 with DVA, the novel version of RVA.

One temporal cycle from 3 measured with enough measurement points, as a rule the first one, was chosen for local vessel assessment. As in the systemic hypertension study (2.2.3) it consisted of 30 s of baseline, 20 s of flicker stimulation and 80 s of observation period (Fig. 28). Five time intervals for examination were defined for

arteries and for veins as in the systemic hypertension study (2.2.3) (Fig. 27). Start of the time segment IV (Fig. 27) in arteries was assigned individually. For each measured vessel an individual time interval included the point of maximal constriction and was chosen so that changes in vessel diameter during the interval were minimal. Longitudinal vessel profiles during selected time segments were assessed at defined time intervals for each vessel and compared intraindividually.

A program was created in MATLAB 6.1 in order to plot power spectra with Fast Fourier Transform and evaluate the chosen parameter. Longitudinal vessel profile segments of $\sim 800\mu\text{m}$ in length (corresponding to $2^6 = 64$ RU) were taken for each vessel similar to the systemic hypertension study (2.2.3). Mathematical and statistical analyses were performed according to the principles described above (2.2.3, 2.2.4). VC for basic parameters of the power spectrum analysis used in 2.2.5.1 and 2.2.5.2, was calculated for each vessel with the formula (12). The average value of VC (median) was calculated for each parameter for the group of vessels. Following aspects were considered:

Dimensional reproducibility

The inner microstructure of retinal vessels might be different in vessels with different diameter. Whether wave structure of longitudinal vessel profiles is different in small and in large retinal vessels was investigated. All arterial and venous longitudinal profiles were ranged from the minimal to the maximal one. Two groups of 15 subjects each with smallest and largest vessel diameters correspondingly were formed. In each group vessel segments were ranged according to their diameter in increasing order of magnitude. Basic parameters of the power spectrum analysis for retinal vessels were calculated and compared between groups with non-parametric Wilcoxon-test for each parameter during constriction, baseline and dilation1 for arteries and relaxation1, baseline and dilation1 for veins.

The author is aware that a correction for multiple comparisons needs to be performed. Although in this pilot study tendencies in the differences between groups are aimed to be shown for future detailed reproducibility studies. This statistical correctness was therefore abandoned for the benefit of the sensitivity of the study. However different characteristic parameters of power spectrum were tested, which might show significant differences between the examined groups (explorative approach). Additionally VCs were calculated for the pairwise comparison of the segments: the smallest in the first group was compared with the smallest in the second group and so on.

Spatial reproducibility

The inner microstructure of retinal vessels might be different in the vessels located in different parts of the retina or in different eyes. Whether wave structure of longitudinal vessel profiles is different in the mentioned locations was investigated.

First all arterial and venous longitudinal profiles were divided in two groups according to their location in the right and in the left eye. 10 arterial segments and 11 venous segments were measured in the right eye. These were compared with 20 arterial segments and 19 venous segments in the left eye. Non-parametric statistics with Dunn-Test for two samples of different size (Glantz 1999) was applied for the analysis.

Subsequently all arterial and venous longitudinal profiles in the left eye were divided in four groups according to their location within the retina: nasal inferior (4 arteries, 4 veins), temporal inferior (4 arteries, 4

veins), nasal superior (5 arteries, 5 veins), temporal superior (7 arteries, 6 veins). The mentioned basic parameters of the power spectrum analysis for retinal vessels in different parts of the retina were assessed and compared with each other using Dunn-Test for four samples of different size (Glantz 1999).

2.3 Healthy volunteers and patients

2.3.1 Anamnestically healthy volunteers of different age (age-dependence study)

11 healthy volunteers according to their general practitioner in each age group of 21 – 27 years (5 males, 6 females, age $24,9 \pm 1,9$ years); 40 – 60 years (3 males, 8 females, age $50,2 \pm 5,3$ years) and 60 – 85 years (4 males, 7 females, age $68,6 \pm 7,6$ years) were entered into the prospective clinical study. They had not used regular medication for 3 months prior to examination.

Patients with any eye disease or the following systemic affections were excluded:

- acute myocardial infarction;
- diabetes mellitus;
- blood pressure higher than 150/ 95 mmHg;
- heart disease state III and IV (NYHA).

At the beginning of every test a clinical ophthalmic examination consisting of measurement of visual acuity, objective refraction, keratometry, applanation tonometry and funduscopy was carried out.

2.3.2 Glaucoma patients and age-matched healthy volunteers (glaucoma study)

Two independent studies assessing retinal arterial diameters to artificial IOP-pressure increase by RVA in healthy volunteers and glaucoma patients were performed and analyzed. These both studies were performed in collaboration with Edgar Nagel, MD (Private Eye Consultant Rudolstadt) and Walthard Vilser, PhD (Department of Biomedical Engineering, Ilmenau University of Technology).

2.3.2.1 Study 1 with acute suprasystolic IOP-increase

9 healthy persons (7 males, 2 females, age $55,6 \pm 8,4$ years with a range of 42 to 70 years) and 9 age matched patients with POAG (5 male, 4 female, age $58,8 \pm 10,3$ years with a range of 44 to 78 years) were entered into the prospective clinical study. Mean IOP measured in normals was $13,7 \pm 1,6$ mmHg. In glaucoma patients this parameter amounted to $23,3 \pm 1,9$ mmHg before treatment and $17,6 \pm 2,2$ mmHg after three times per day (tid) treatment with dorzolamide for at least two weeks.

2.3.2.2 Study 2 with moderate 100 s IOP-increase

13 normal volunteers (4 males, 9 females, $62,6 \pm 6,7$ years old with a range of 50 to 73 years) and 14 age matched untreated POAG patients (7 males, 7 females, $61,2 \pm 7,6$ years old with a range of 45 to 72 years).

Mean IOP measured in normals was $13,8 \pm 2,9$ mmHg. In glaucoma patients this parameter amounted to $22,4 \pm 6,0$ mmHg before treatment and $16,8 \pm 3,0$ mmHg after tid treatment with dorzolamide.

In both studies POAG was defined according to the guidelines of the European Glaucoma Society by: IOP >21 mm Hg, visual field defects related to glaucoma on automated static perimetry Octopus 101 program G2 and / or a glaucomatous disc change.

The POAG patients were not yet treated for glaucoma or the treatment was discontinued for four weeks before the test (wash-out phase). Data was obtained twice: first without glaucoma medication (untreated POAG group) and second four weeks after continuously using dorzolamide eye drops three times daily (treated POAG group). One eye of each patient was included in the study. The eye with more advanced glaucomatous damage or higher IOP was chosen. If both eyes demonstrated equal IOP values the eye to be included was randomized. Ocular factors for exclusion of patients were:

- opacities of the optical media, visual acuity (VA) < 0.5 (= 20/40);
- astigmatism > 1.0 D, myopia > 7.0 D;
- previous surgery on the study eye or injuries of the study eye;
- contact lens wear within 24 hours of the examination.
- patients with the following systemic problems were excluded:
 - acute myocardial infarction;
 - diabetes mellitus ;
 - treated hypertension or blood pressure higher than 150/ 95;
 - heart disease state III and IV (NYHA);
 - anticoagulation therapy with cumarins, heparin or heparin analogues.

At the beginning of every test a clinical ophthalmic examination consisting of measurement of VA, objective refraction, keratometry, computerised perimetry by Octopus 101 program G2, slit lamp examination, applanation tonometry and funduscopy was carried out. After administration of tropicamide to induce mydriasis, a plano rigid contact lens was fitted to obtain a constant optic quality during the whole examination because the suction cup in itself induces astigmatism, which causes a distortion of the fundus image.

2.3.3 Patients with systemic hypertension and age-matched healthy volunteers (systemic hypertension study)

This study was performed in collaboration with Edgar Nagel, MD (Private Eye Consultant Rudolstadt) and Walthard Vilser, PhD (Department of Biomedical Engineering, Ilmenau University of Technology).

15 untreated patients with systemic hypertension (8 males, 7 females, age 50,5±12,2 years) and 15 age- and gender matched anamnesticly healthy volunteers (8 males, 7 females, age 50,9±11,9 years) were entered into the prospective clinical study.

Patients with any ocular disease or the following affections were excluded (Nagel et al. 2004):

- clouding of the refractory media;
- visual acuity less than 0.5;
- astigmatism more than 2.0D;
- myopia more than 7.0D;
- history of an ocular operation or injury in the examination eye;
- wearing of contact lenses within the previous 24 hours;
- acute infection;
- known diabetes mellitus;
- pregnancy and nursing.

At the start of the study a clinical ophthalmic examination was performed (measurement of visual acuity, objective refraction, slit lamp microscopy, applanation tonometry and funduscopy), after which the pupil was dilated with tropicamide eye drops. The preparation for the examination took at least 30 minutes, allowing enough time for the volunteer to acclimatize and for the blood pressure to normalize.

2.3.4 Patients with obesity and age-matched healthy volunteers (obesity study)

This study has been performed in collaboration with Department of Preventive and Rehabilitative Sport Medicine, Munich University of Technology (chair Prof. Martin Halle, PhD, MD). All the examined obese subjects participated in M.O.B.I.L.I.S. - programm (**m**ultizentrisch **o**rganisierte **b**ewegungsorientierte **I**nitiative zur **L**ebensstiländerung in **S**elbstverantwortung (<http://www.mobilis-programm.de/>): *multicenter organised motion oriented initiative for the lifestyle changing in self responsibility*) which has been initiated by the physicians and sport scientists from the University Freiburg and has been implemented in several clinics for rehabilitative medicine in Germany nowadays. For the present study retinal arterial reactions of the patients were examined before the beginning of the M.O.B.I.L.I.S. program, analyzed and compared with retinal arterial reaction of age matched healthy subjects

16 obese persons (4 males, 12 females, age [median(1.quartile; 3.quartile)]: 48,5 (44,0; 53,3) years and 16 age- and gender matched anamnesticly healthy volunteers were entered into the prospective clinical study.

Inclusion criteria were:

- persons, who had attained the age of 18;
- body mass index (formula (3): $30 - 40 \text{ kg/m}^2$ (ranged: $29,4 \text{ kg/m}^2$ to $40,8 \text{ kg/m}^2$);
- participation in the sport program is possible.

Subjects with any disease or the following affections were excluded:

- exercise performance $<75 \text{ W}$ during 2 minutes (according to ergometry);
- absolute or relative contraindication against physical activity:

absolute:

- acute cardiac infarction;
- instable angina pectoris;
- arrhythmia with symptomatic and/or limited hemodynamics;
- symptomatic hard arteriosclerosis;
- non compensated heart failure;
- acute lungs embolism;
- acute myocarditis;
- acute pericarditis;
- acute aortal dissection;

relative:

- main trunk stenosis;
- valve disorders of moderate degree;
- known electrolyte disorders;
- severe arterial hypertension ($RR_{\text{sys}} > 165 \text{ mmHg}$; $RR_{\text{diast}} > 115 \text{ mmHg}$);
- tachyarrhythmia or bradyarrhythmia;
- hypertrophic cardiomyopathy and other forms of outflow pathway obstruction;
- AV-stenosis of a high degree;
- psychological or physical fatigues.
- diabetes mellitus type I;
- kidney disorders: creatinine $> 1,2 \text{ mg/dl}$;
- intake of anorectics or weight loss medications;
- appetite loss;
- status after cancer (disease period < 5 years);

- *diabetic foot syndrome from the stage 1 (surface defects);*
- *polyneuropathies;*
- *severe diabetic retinopathy (visual acuity < 10% or bleeding in the eyeground).*

At the beginning of the study thorough clinical examination was performed consisting of funduscopy, measurements of electrocardiogram, blood analysis, spiro-ergometry, pulse wave velocity in large vessels etc, after which the pupil was dilated with tropicamide eye drops.

In all presented studies mentioned in 2.3 informed consents were obtained from the subjects after explanation of the nature and possible consequences of the study. The study designs have been reviewed and approved by the Ethics Committee of the Medical Clinic (Klinikum rechts der Isar) of the Munich University of Technology (age-dependence study, obesity study) and by the Ethics Committee of the Medical Association of Thuringia (glaucoma study, systemic hypertension study) and have been performed in accordance with the ethical standards laid down in the 1964 Declaration of Helsinki.

2.4 Methods of Computational Fluid Dynamics (CFD) for simulation of blood flow in retinal vessels

2.4.1 CFD code NS3DV43C (Institute of Fluid Mechanics, MUT) for solving of the Newtonian problem

For all simulations in Newtonian case, the three-dimensional, parallel solver NS3DV43C developed in the Institute for Fluid Mechanics, Munich University of Technology is used (Skoda 2003), which has been extensively validated (Schilling 2003; Böhm 2004). The detailed description of the solver can be found elsewhere (Skoda 2003; Skoda et al. 2007). Briefly, NS3DV43C is allocated, cell-centred, and block-structured finite volume method using the SIMPLE scheme for pressure-velocity coupling.

For the interpolation of the mass fluxes at the cell faces, Rhie and Chow's method was used (Rhie & Chow 1983). At the block interfaces, the grid lines do not need to match, while the accuracy of the discretization scheme is maintained by a locally unstructured treatment of the fluxes. This means that a cell adjacent to an interface may have an arbitrary number of faces. This approach is also utilized for sliding interfaces. The convective terms of all equations can be approximated by various schemes, such as CDS, MINMOD or SMART which are of second- and third-order accuracy. Stable convergence behaviour is reached through combination with a deferred correction approach.

The implicit three-level time discretization is of second-order accuracy. The parallelization of the code is based on MPI-libraries (message passing interface).

For turbulence modeling, two classes of eddy viscosity models are used, namely, the cubic low Reynolds number k - ε model by Lien et al. (1996) (LCL) and the v^2 - f model by Durbin (1995). The LCL model is able to take into account Reynolds-stress anisotropy effects by a cubic constitutive relation between the Reynolds stress tensor and the mean flow quantities. The LCL model proposes a realizability constraint, where C_μ in the eddy viscosity relation is expressed as a function of strain and rotation invariants \mathbf{S} and $\mathbf{\Omega}$. The time and length scales T_s and L_s are calculated with the realizability condition by Durbin (Durbin 1996; Skoda et al. 2007):

$$T_s = \min \left[\frac{k_t}{\sqrt{6C_\mu u_t^2 \sqrt{S_{ji} S_{ji}}}} \right] ; \quad (13)$$

$$L_s = C_L \min \left[\frac{k_t^{1,5}}{\varepsilon}, \frac{k_t^{1,5}}{\sqrt{6C_\mu u_t^2 \sqrt{S_{ji} S_{ji}}}} \right] . \quad (14)$$

No additional modification of the production term to suppress the stagnation point anomaly is applied. The Reynolds-stress tensor is calculated using Boussinesq approach. The constants specific to the v^2 - f model are $\mathbf{D}_1=1,4$; $\mathbf{D}_2=0,3$; $C_L=0,17$. In the ε -equation, the constants are $C_{\varepsilon 2}=1,92$ and the constant $C_{\varepsilon 1}=1,55+\exp(-0.00285 \cdot \mathbf{Re}_y^2)$ is a function of the turbulent Reynolds number $\mathbf{Re}_y = \sqrt{k_t} y/v_t$, where y is the wall distance, k_t represents the turbulence value. The eddy viscosity ν_t is calculated by $\nu_t = C_\mu v^2 T_s$ with $C_\mu = 0,19$; v^2 - the velocity scale. The turbulent velocity scale in (13) and (14) is $u_t^2=v^2$. The time and length scales are bounded from below by the corresponding Kolmogorov scales (Durbin 1995). In order to incorporate a more effective realizability condition in the LCL model, a bound of the time scale is incorporated according to (13), where u_t^2

$=f_{\mu} \cdot k_t$. This variant of the model is referred to as LCL-RD, and the eddy viscosity relation in the LCL-RD model was written as (Skoda et al. 2007):

$$v_t = \frac{2/3}{4 + S + 0,9 \cdot \Omega} f_{\mu} k_t T \quad . \quad (15)$$

The ε - equation is implemented in explicit dependence on the turbulent time scale T_s , in order to adopt realizability. The convergence criterion for each equation in any model is a decrease of the sum norm of the residuum of at least 6 orders of magnitude. For any test case considered, at the inlet, the velocity field and the turbulence values k_t and ε are prescribed, v^2 equals to $2/3k_t$, and the elliptic operator f is extrapolated. At the outlet, a constant value of the static pressure is specified.

Following input data files for the solver NS3DV43C were introduced in the present study: *3dpar.01* with parameters of CFD simulation; *3dgrid.01 - .04* with the geometry and grids for all 4 blocks of the model; *3dbcd.01 - .04* with boundary conditions for all external sides and matching conditions for all internal sides of 4 blocks. Two latter groups of data-files were created automatically using 3D-geometry program mentioned below (2.4.4.2).

2.4.2 CFD Code N3DV6C and its extension for simulation of Non-Newtonian blood flow behaviour

For all simulations in Non-Newtonian case, the three-dimensional, parallel solver N3DV6C, developed in the Institute for Fluid Mechanics, Munich University of Technology, is applied (Skoda 2003). This solver used to be an extension of NS3DV43C solver for problems with cavitations. Currently N3DV6C becomes the last working version of the institute's solver, which has been regularly updated. For the present work the N3DV6C solver was adapted by B. Flurl and M. Bogner (Institute of Fluid Mechanics, Munich University of Technology) for the Non-Newtonian blood Quemada model.

Following input data files for the solver N3DV6C were introduced in the present study: *3dplasma* with blood rheological data; *3dpar.01* with parameters of CFD simulation, that differed from the homonym file for NS3DV43C. *3dgrid.01 - .04* and *3dbcd.01 - .04* were the same as in the Newtonian case. They also were created automatically using 3D-geometry program mentioned below (2.4.4.2).

2.4.3 Post-processor N3D_POST

In order to transfer the summary data and calculated average values from CFD simulation output data set the post-processor program N3D_POST was developed by my predecessors in the Institute for Fluid Mechanics. The post-processor was adjusted for both solvers NS3DV43C and N3DV6C. N3D_POST created an output file *balance00000_C.dat* with summary output parameters both at the inflow and at the outflow, inter alia: the area of the vessel cross-section A_s , the volumetric flow rate Q , the pressure p_{total} and the static part of the pressure p_{stat} . This data of the output file was then processed and analyzed in MS Excel.

2.4.4 CFD model of a retinal vessel

2.4.4.1 General assumptions

Applying computational fluid dynamics the pressure drop Δp and the coefficient of hydraulic resistance ζ , along various vessel segments of the same length l and different waviness were calculated with the assumption, that the volumetric flow Q through its cross-section remains constant (Fig. 29a). Pressure drop along a tube segment represents a reciprocal measure of its hydraulic conductivity C defined from the relationship:

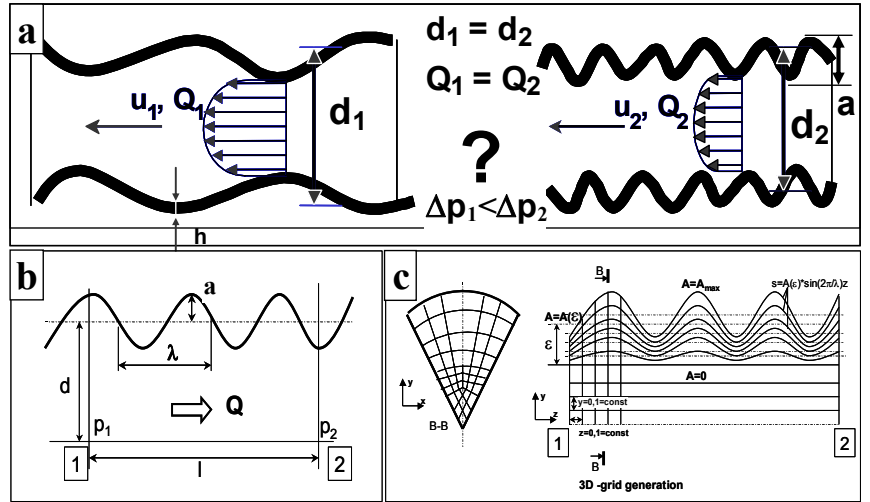


Fig. 29. Problem statement and parameters for the CFD-model. a: general problem statement. b: geometrical parameters of a wavy vessel segment. c: 3-dimensional grid generation for CFD simulation.

$$C = \frac{Q}{\Delta p} \quad , \quad (16)$$

that is, how does the tube resist to the fluid flow (Nesterov 1967). It depends on geometrical parameters of the vessel segment: the mean vessel diameter \bar{d} , the magnitude of waviness a and the period of waviness λ (Fig. 29b). Parameters l/\bar{d} , λ/\bar{d} and a/\bar{d} are dimensionless parameters of the model:

$$\Delta p = F \left\{ \frac{\lambda}{\bar{d}}; \frac{l}{\bar{d}}; \frac{a}{\bar{d}} \right\} \quad . \quad (17)$$

From the pressure drop the dimensionless coefficient of hydraulic resistance ζ_v (Loytsyanskiy 1987; Fung 1990) can be calculated:

$$\Delta p = \zeta_v \frac{\rho}{2} c^2 \quad ; \quad \bar{c} = \frac{Q}{\frac{\pi}{4} \bar{d}^2} \quad ; \quad (18)$$

where ρ represents the blood density.

Supposing: $Q = const$ one can obtain with:

$$L = \frac{l}{\bar{d}}; \quad \Lambda = \frac{\lambda}{\bar{d}}; \quad A = \frac{a}{\bar{d}}; \quad (19)$$

$$\zeta_v = f \{ L; \Lambda; A \} \quad .$$

Thus, it has been trying to find out, whether and how the resistance to blood flow is influenced by geometrical parameters of the vessel segment and particularly by parameters of vessel wall waviness.

2.4.4.2 3D-geometry generic model of a retinal vessel with a possibility to vary parameters of vessel wall configuration.

3D geometry of a retinal arterial segment and the corresponding computational grid were created manually with C++ program (Fig. 29c, Fig. 31). Thus, the geometric parameters of the model could be easily varied and prepared for each CFD simulation run.

In order to modify the waviness of the red block (Fig. 31, bottom) its outer wall was modeled with a combination of sinus curves in form of the function g (10). The variable x represents a coordinate along the segment. To vary the waviness the parameters of the sinus were changed. For most simulations represented here only the first term of the function g : e.g. $a = a_{lf}$, $\lambda = \lambda_{lf}$ has been applied

For the more common problem statement, accepted in the fluid mechanics the equation (10) may be converted into the dimensionless form:

$$G = \frac{g}{d} = A_{lf} \sin \left\{ \frac{2\pi}{\Lambda_{lf}} X^* \right\} + A_{hf} \sin \left\{ \frac{2\pi}{\Lambda_{hf}} X^* \right\} . \quad (20)$$

Here $X^* = x/\bar{d}$ is the dimensionless coordinate along the vessel segment and $X = X^*/\Lambda = x/\lambda$ is the reduced coordinate. Further, using this approach the conception of SEF can be rethought to the new fluidmechanical conception. The dimensionless Strouhal-number Sr (Strouhal 1878) is introduced as:

$$Sr = \frac{SEF \cdot \bar{d}}{c} . \quad (21)$$

In Fig. 30 examples of the dimensionless profiles and corresponding Sr -values for $\bar{c}_{in} = 5$ mm/s are represented by analogy with denominate profiles in Fig. 23 right panel.

A CFD model for Finite Volume Method represents the fluid inside the vessel divided into small hexagonal fluid elements. In order to reduce the calculation time, which depends partially on the amount of fluid elements, axial symmetry of the model was used. Calculations for 15° “piece of pie” sectors, that is for 1/24 of the whole model, were performed. After numerical calculation, such a “piece” was supplemented

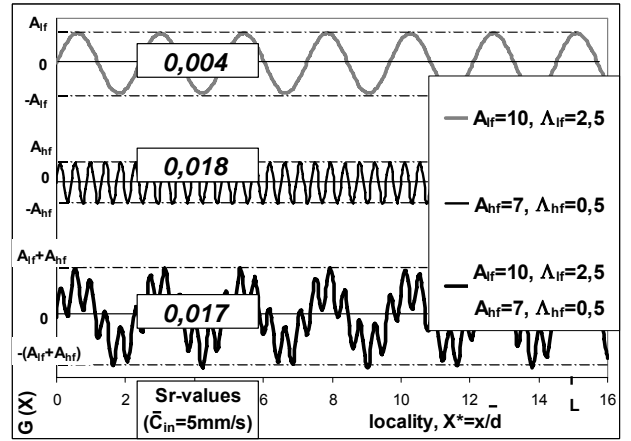


Fig. 30. Examples of the dimensionless profiles and corresponding Sr -values by analogy with denominate profiles in Fig. 23 right panel. L , A , Λ , – parameters of the formula (20).

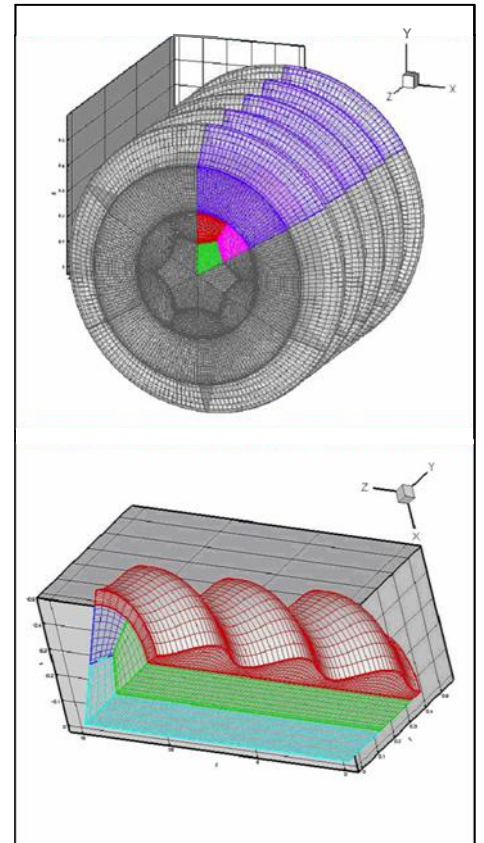


Fig. 31. 3-D geometry of Finite Volume Model of a wavy vessel segment. (compare with real vessels in Fig. 14). A 60° “piece of pie” sector of the whole model.

to a whole or to a half modeled vessel segment in the visualization program Tecplot 10.0. Since tetrahedron and wedge fluid elements were not allowed in the CFD model, an individual sector was divided into 4 blocks (Fig. 31): a part of solid revolution body with waviness (Fig. 31, bottom, red) and 3 hexahedrons (Fig. 31, bottom, light-blue, green and blue). The blocks were matched to each other at their interfaces. The geometry of each block was developed independently.

For the model sinusoidal simulations of the real vessel profiles the description with wavelength seems to be more appropriate and better understandable since the term “frequency” is commonly related to the temporal changes. The preliminary parameter analysis for the modeled profiles curves was performed with this wavelength description. However, the real vessel profiles are irregular and non-periodic (Fig. 72). Therefore, when dealing with a real experimentally obtained curve it was more appropriate to use frequency parameters than wavelength ones for the description of its waviness. For this purpose the *spatial frequency*, described above, was introduced.

Input data file *settings.dat* contained parameters of vessel waviness and grid generation was used for varying geometry parameters of vessel configuration (Table 8). Output data files: *3dgrid.01 - .04* with the geometry and grids for all 4 blocks of the model (Fig. 31) and *3dbcd.01 - .04* with boundary conditions for all external sides and matching conditions for all internal sides of 4 blocks were created as a result of 3D-geometry program run.

Table 8. Input parameters for 3D-geometry program. The content of the file *settings.dat*

Description of the parameters in Fig. 31, bottom	Parameters introduced	Parameter values for Fig. 31, bottom
number of elements along the Z axis +1	i_max	150
number of elements along the Y axis in the red block+1	j_max	15
number of elements in the third dimension of the red block+1	k_max_muss_ungerade_sein	11
number of elements along the Y axis in the light-blue block+1	j1_max	6
sectoral angle of the model, °	RotationsAngle	60
low frequency period of the vessel waviness, *10 ⁻⁴ m	PeriodLambda	5,00
high frequency period of the vessel waviness, *10 ⁻⁴ m	HochfrequentePeriodeLambda	0,00
low frequency magnitude of the vessel waviness, *10 ⁻⁴ m	Amplitude	0,05
high frequency magnitude of the vessel waviness, *10 ⁻⁴ m	HochfrequenteAmplitude	0,00
the length of the vessel segment, *10 ⁻⁴ m	Laenge_des_Gefaessessegmentes	15,00
mean vessel diameter, *10 ⁻⁴ m	Durchschnittl_Gefaessdurchm.	1,50
possibility of the concave form of vessel inlet and outlet for better numerical convergence yes/no	Kurviges_Inlet_ja1_nein0	0
whether the generic or real longitudinal vessel profile is simulated	Gefaessprofile_experimentell_ja1_nein0	0
order of B-Spline interpolation in case of real longitudinal vessel profile	B-SplineOrder	4

2.4.4.3 Parameters of CFD model.

The following range of model parameters were chosen (Table 9, Fig. 29b,c):

Table 9. Parameters of the Newtonian model

Parameter	Notation	Parameter range (÷) or value
length of the arterial segment	l	1,5÷3 mm
averaged internal diameter of each segment	\bar{d}	130 μ ÷170 μ
waviness of arterial wall:		
low frequency wavy walls		(0,2÷3 oscill./1 mm of vessel segment)
high frequency wavy walls		(3÷20 oscill./1 mm of vessel segment)
period of the waviness	λ : λ_{lf} , λ_{hf}	0÷1,5 mm
amplitude of the waviness	a	
low frequency waves,	a_{lf}	0÷40 μ ;
high frequency waves	a_{hf}	0÷20 μ ;
averaged inflow velocity	\bar{c}_{in}	1 ÷ 50 mm/s (Forrester et al. 2002) (Riva et al. 1985) (Ferguson et al. 2004) (Nagaoka et al. 2002) (Gilmore et al. 2005)
apparent cinematic blood viscosity:	$\nu=\eta/\rho$	3,317*10 ⁻⁶ m ² /s (Miyazoe et al. 1999; Andrews et al. 2000)
apparent dynamic blood viscosity	η	0,0035Pa*s (Miyazoe et al. 1999; Andrews et al. 2000)
blood density	ρ	1055kg/m ³ (Miyazoe et al. 1999; Andrews et al. 2000)

- *an estimation for the velocity rate c in a large retinal artery is 25 mm/s, given in the handbook (Forrester et al. 2002). In-depth literature search gave us the latest data on maximal blood velocities in large retinal arteries: measured by Riva et al (1985) with laser Doppler velocimetry it ranged from 15 to 40 mm/s in arteries of 100÷140 μ in diameter. It amounted to 46,0±4,0 mm/s measured by R. Ferguson et al. (2004) with Tracking Scanning Laser Ophthalmoscopy; to 36,0±13,0 mm/s measured by T. Nagaoka et al. (2002) and to 32,2±6,4 mm/s measured by E. Gilmore et al. (Gilmore et al. 2005) (2005) with Canon Laser Doppler Flowmetry (a laser Doppler velocimetry system that enables simultaneous measurements of blood velocity and vessel diameter in a retinal artery). Absolute velocities in retinal arteries decreased not significantly with increasing age (Ustymowicz et al. 2005). All these estimations give the centerline blood velocity measured at some arbitrary time point during the cardiac cycle (Ferguson et al. 2004) or averaged in time over the cardiac cycle (Riva et al. 1985; Nagaoka et al. 2002; Gilmore et al. 2005). The real flow in big retinal arteries is pulsatile and in average the centerline systolic velocity is about 3 times higher than the centerline diastolic velocity (Logean et al. 2003; Ustymowicz et al. 2005). In modeling the experiments the initial inflow velocity profile \bar{c}_{in} has been taken to be constant with a range of 1 ÷ 50 mm/s.*

2.4.4.4 CFD simulation of the blood flow in the generic model of a retinal vessel segment - Newtonian model.

Blood flow is modeled by the incompressible Navier-Stokes equations for a Newtonian fluid (Loytsyanskiy 1987; Skoda 2003):

$$\nabla \cdot c = 0$$

$$\rho \left(\frac{\partial c}{\partial t} + c \cdot \nabla c \right) = -\nabla p + \eta \nabla^2 c \quad . \quad (22)$$

Here \mathbf{c} is the velocity, p the pressure and η the dynamic blood viscosity. The linear differential operator in rectangular system of coordinates $(\mathbf{x}, \mathbf{y}, \mathbf{z})$: $\nabla = \frac{\partial}{\partial x} \vec{i} + \frac{\partial}{\partial y} \vec{j} + \frac{\partial}{\partial z} \vec{k}$, where $\vec{i}, \vec{j}, \vec{k}$ - are corresponding unit vectors of coordinate axes.

The governing equations were solved numerically in rectangular coordinate system using an implicit finite volume formulation. An in-house CFD code NS3DV43C has been used for numerical simulation. For each tested geometric parameter L , Λ or A a new geometric model (vessel segment configuration) was recalculated (Fig. 58 *a, b*) and the numerical simulation was performed, which took 1 – 3 hours and consisted of 15000 – 20000 cycles till the iteration process converged. At the end of such a run, the velocity and the pressure distribution along the vessel segment (Fig. 58*a* and *b* correspondingly) as well as main streamline directions and velocity vectors (Fig. 58*c* and *d* correspondingly) were analyzed by means of commercial software Tecplot 10.0. Finally, the numerical results of the simulation were post-processed (2.4.3).

For simplicity vessel wall displacements were also neglected. Fluid-structure interaction calculations taking into account the wall strains would require data on the material properties of the vessel wall, such as elasticity and wall thickness, which is difficult to obtain in vivo (1.3.3). The pulsatile character of the blood flow in arteries is usually regarded as second order in small arteries and arterioles (Fung 1990) and was also neglected in the presented approach. In order to check possible turbulence effects in the model a laminar and a turbulent flow model was used and both simulation results were compared to each other.

Generally, hydraulic resistances and other flow parameters of several vessel segments of the same length were compared prescribing the same initial constant (non-parabolic) velocity or volumetric flow rate at the inflow and zero pressure at the outflow, varying their geometric parameters including parameters of waviness. Non slip boundary conditions were prescribed at the vessel walls.

2.4.4.5 CFD simulation of the blood flow in the generic model of a retinal vessel segment. Non-Newtonian model.

Non-Newtonian blood rheology was described with Quemada model (Quemada 1981) using hematocrit distribution function by Lerche and Oelke (Lerche & Oelke 1990).

The blood viscosity is no more uniform in the vessel cross-section as it is in Newtonian models (Kotliar et al. 2005). It depends on local shear stresses, concentration of RBC and position within the cross-section. Derived from Quemada rheologic equations (6) and (7), the blood viscosity is described by the following function:

$$\eta(r) = \eta_{plasma} \left(1 - 0,5H(r, n) \frac{k_0 + k_\infty \sqrt{\frac{\dot{\gamma}}{\dot{\gamma}_c}}}{1 + \sqrt{\frac{\dot{\gamma}}{\dot{\gamma}_c}}} \right)^{-2} \quad (23)$$

Here \mathbf{r} represents reduced radius of a point within the cross-section $0 < \mathbf{r} < 1$, which is proportional to its distance from the vessel axis. For the represented model of a vessel with wavy walls the absolute radius \mathbf{r}_{abs} of the vessel

varied from 0 to r_{\max} , which also varies in its turn along the vessel axis (Fig. 29b): $r = r_{\text{abs}}/r_{\max}$. $\eta_{\text{plasma}} = 0,013 \text{ Pa}\cdot\text{s}$ is blood plasma viscosity (Fung 1990). $\mathbf{H}(\mathbf{r}, \mathbf{n})$ is the hematocrit inside the vessel. It is not constant in each point of the vessel cross-section and is depending on the position relative to the vessel axis. Having considered the axial migration of RBCs in small vessels (Fahreaus effect), Lerche and Oelke (1990) proposed to describe radial hematocrit distribution by a one-parameter equation as a function of a natural number \mathbf{n} : $5 < \mathbf{n} < 1000$:

$$H(r) = H_0 \left[-\frac{n(n+1)(n-1)}{2} \left(\frac{r^n}{n} - \frac{2r^{n-1}}{n-1} + \frac{r^{n-2}}{n-2} - \frac{2}{n(n-1)(n-2)} \right) \right]. \quad (24)$$

Its' possible distribution is represented in Fig. 32a. \mathbf{H}_0 represents average blood hematocrit, which is an individual characteristic of a person. $\mathbf{H}_0 = 0,45$ has been prescribed (Fung 1990).

\mathbf{k}_0 (low share rate intrinsic viscosity), \mathbf{k}_∞ (high share rate intrinsic viscosity) and $\dot{\gamma}_c$ (critical shear rate) are experimentally found dependences (Dufax et al. 1980; Quemada 1981; Cockett 1986). The intrinsic

viscosities \mathbf{k}_0 and \mathbf{k}_∞ have been approximated with best fits in form of piecewise continuous functions using MS Excel from corresponding data on actual packing concentration, obtained by Quemada (1978; 1981), see Fig. 16. $R^2 > 0,995$ served as criterion for the best fit. $\dot{\gamma}_c$ was approximated according to Cockett (1986):

$$k_0 = \begin{cases} 12,76H + 3,29 \rightarrow 0 < H < 0,05 \\ 170,40H - 4,61 \rightarrow 0,05 < H < 0,1 \\ -0,12 + \frac{2,45}{H + 0,095} \rightarrow 0,1 < H < 1 \end{cases} ; \quad k_\infty = \begin{cases} 12,76H + 3,29 \rightarrow 0 < H < 0,05 \\ 1,7 + \frac{0,1}{H} \rightarrow 0,05 < H < 1 \end{cases} ; \quad (25)$$

$$\dot{\gamma}_c = e^{(3,697H^3 - 25,60H^2 + 27,923H - 6,151)}$$

The radial distribution of these rheological parameters in a vessel depending on hematocrit \mathbf{H} was recalculated with formula (24), see Fig. 32b,c,d, in which $\dot{\gamma}$ represents the shear rate. Its invariant version for 3-D problem was derived using von Mises approach (Fung 1990):

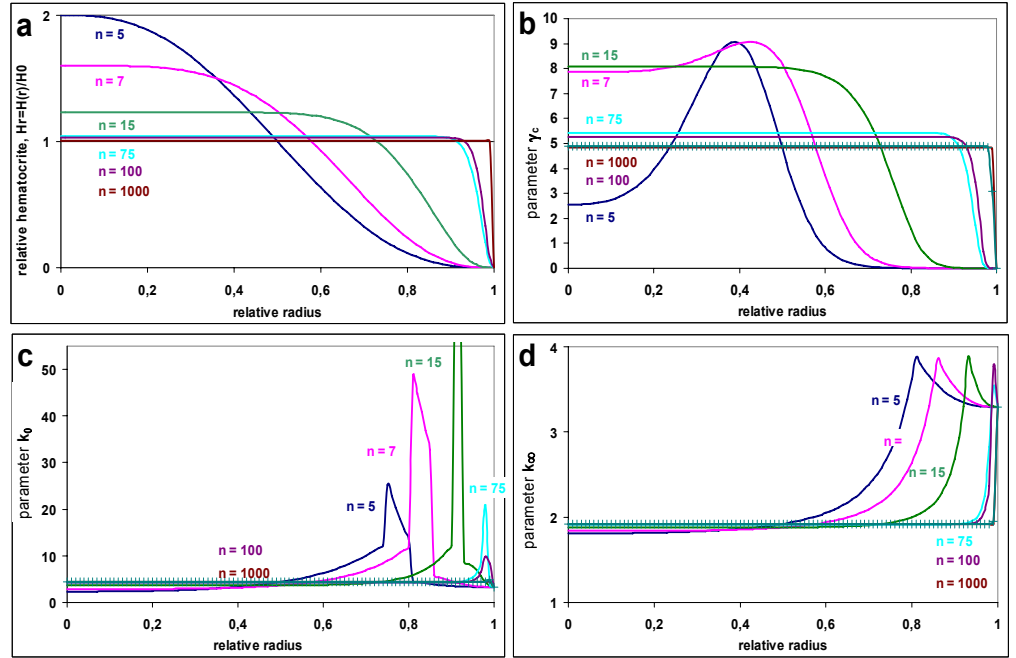


Fig. 32. Parameters of Non-Newtonian Quemada model (derived from (Quemada 1981; Lerche & Oelke 1990)): **a:** radial hematocrit profiles, normalized by mean capillary hematocrit; **b:** radial $\dot{\gamma}_c$ profiles; **c:** radial \mathbf{k}_0 profiles; **d:** radial \mathbf{k}_∞ profiles.

$$\dot{\gamma} = \sqrt{\text{trace}(S_{xyz}^2)}, \text{ where } S_{xyz} = \dot{\gamma}_{xyz} = \begin{bmatrix} \frac{\partial u}{\partial x} & \frac{1}{2}\left(\frac{\partial u}{\partial y} + \frac{\partial v}{\partial x}\right) & \frac{1}{2}\left(\frac{\partial u}{\partial z} + \frac{\partial w}{\partial x}\right) \\ \frac{1}{2}\left(\frac{\partial u}{\partial y} + \frac{\partial v}{\partial x}\right) & \frac{\partial v}{\partial y} & \frac{1}{2}\left(\frac{\partial v}{\partial z} + \frac{\partial w}{\partial y}\right) \\ \frac{1}{2}\left(\frac{\partial u}{\partial z} + \frac{\partial w}{\partial x}\right) & \frac{1}{2}\left(\frac{\partial v}{\partial z} + \frac{\partial w}{\partial y}\right) & \frac{\partial w}{\partial z} \end{bmatrix}, \quad (26)$$

where x, y, z are coordinates and $u(x, y, z), v(x, y, z), w(x, y, z)$ the velocity components; S_{xyz} represents the strain rate tensor.

I am aware that in some engineering and fluid dynamics books slightly another definition of the strain rate tensor is used (Artoli 2003): $S_{xyz}' = 2S_{xyz}$. Y. Fung (1990) called this another definition: "old definition".

Additionally, the blood density ρ_{blood} is also not more a constant in Non-Newtonian model. It depends on hematocrit:

$$\rho_{\text{blood}}(r, n) = \rho_{\text{plasma}}(1 - H(r, n)) + \rho_{\text{RBC}}H(r, n), \quad (27)$$

in which $\rho_{\text{plasma}} = 1025 \text{ kg/m}^3$ and $\rho_{\text{RBC}} = 1125 \text{ kg/m}^3$ (Benson 1999) are experimentally determined data.

In the presented model formulation the strain of the vessel wall was neglected for simplicity. Non slip boundary conditions were prescribed at the vessel walls. The pulsatile character of the blood flow in arteries is usually regarded as second order in small arteries and arterioles (Fung 1990) and was also neglected in the presented approach. A laminar flow model is used, since experimentally measured velocities in retinal arteries are relatively slow (Table 9), yielding small Reynolds-numbers:

$$0,03 \leq \text{Re} = \frac{\bar{c}_m \bar{d}}{\nu} \leq 3,0. \quad (28)$$

For the Non-Newtonian CFD simulation the same geometric model as for the Newtonian model was used (Fig. 29b,c) with corresponding quantitative parameters (Table 9). In order to reduce the calculation time and to present the flow near the vessel wall, where the most important flow patterns were expected, in more details, the uniformly distributed mesh of the red block (Fig. 31, bottom) is changed. Near the vessel wall the mesh becomes more comprehensive in the plane zOy (Fig. 33). The following formula was used for the decreased height of i^{th} from m fluid elements in the y direction inside the block:

$$(\text{height of the block}) * \left(1 - \frac{i^2 - (i-1)^2}{m^2}\right). \quad (29)$$

In order to avoid inconvenient narrow elements for the CFD simulations the current element was set equal to a half of rest distance to the block border if it became smaller than $0,05 * (\text{height of the block})$.

The governing equations were solved numerically using an implicit finite volume formulation. An in-house developed CFD code N3DV6C has been used for numerical simulation. Following calculation scheme was implemented:

$$\left. \begin{array}{l} n, r_{\max}, r \rightarrow H(r) \rightarrow \rho, k_0, k_\infty, \dot{\gamma}_c \\ \Delta p, \bar{u} \rightarrow \dot{\gamma} \end{array} \right\} \rightarrow \eta(r) \quad (30)$$

For each tested geometric parameter \mathbf{d} , \mathbf{a} or λ a new geometric model (vessel segment configuration) was calculated (Fig. 68) and a numerical simulation was performed, which took 8 – 40 hours and consisted of 45000-350000 cycles till the iteration process converged. At the end of such a run, the velocity, the pressure, the hematocrit and the viscosity distribution along the vessel segment (Fig. 68) as well as the main streamline directions and the velocity vectors were mapped by means of Tecplot 10.0. The numerical results were post-processed (2.4.3).

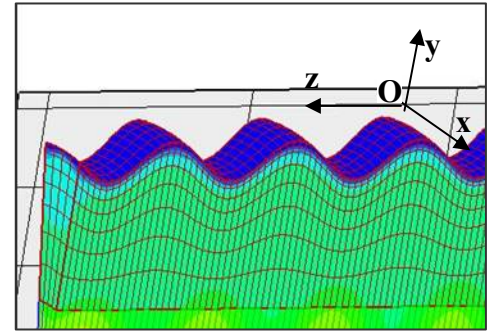


Fig. 33. Adaptive remeshing of a fluid element near the vessel wall.

2.4.4.6 Modeling of real human retinal vessels.

In order to perform CFD –simulation in real human retinal vessels the 3D geometry of real vessel segments was generated using DVA-data. Real vessel lumen configuration was recalculated from longitudinal vessel profiles with an assumption of axial symmetry. These data were saved in a .txt file, which was read by means of a geometry program. The interpolation was performed using B-splines. Formerly sinusoidal external border of the vessel lumen in the red block (Fig. 31, bottom) was changed to the real configuration. Three other blocks of the model remained unchanged. For the numerical simulations the solvers NS3DV43C (Newtonian case) and N3DV6C (Non-Newtonian case) were used. Different real vessel segments with equal length and inflow velocities or volumetric flow rates were tested. The main hemodynamic parameters of the model were post-processed.

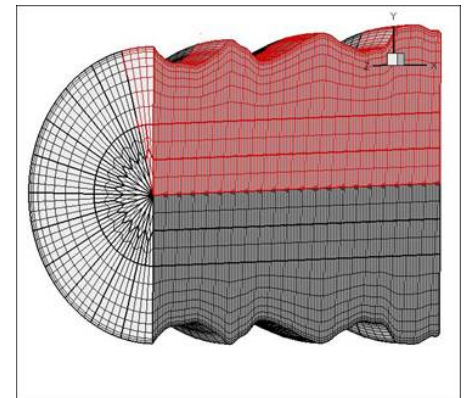


Fig. 34. 3-D geometry of Finite Volume Model of a real vessel segment (compare with Fig. 31). A 180° sector of the whole model. An example.

3 Results

3.1 Clinical studies on longitudinal retinal vessel profiles. Healthy aging, select systemic and ocular diseases

3.1.1 Age-dependence study

Circulation parameters

The mean systemic blood pressure did not vary significantly between groups at the beginning of the examination and did not change significantly within any group during the whole examination period.

Measured retinal vessel reactions

Typical longitudinal vessel profiles in the study can be seen in Fig. 35. Calculated ARPS of longitudinal arterial profiles for the three age groups for 4 phases of arterial reaction are represented in Fig. 36. The sequence of phases was chosen according to increase in diameter of the vessel from left to right.

In Fig. 37 HFW expressed by SEF is demonstrated according to the phase of arterial and venous reaction. In arteries SEF was significantly different between the young and senior age groups in each phase ($p < 0,05$, Dunnett test). SEF was also significantly different between the young and middle age group in dilation, constriction and relaxation ($p < 0,05$). No significant difference could be found between the young and middle age group for baseline tonus.

In veins no significant difference could be found between groups except for baseline tonus for the young and senior age groups ($p < 0,05$).

A statistically significant increase of HFW with age in arteries is demonstrated for each phase of the vessel reaction in Fig. 38, upper panel. The situation in veins is shown in Fig. 38, bottom panel. A significant age-related increase of HFW could only be demonstrated at baseline.

Conclusions for age-dependence study: High-frequency waviness of retinal vessel walls along longitudinal vessel sections increases significantly in anamnestic healthy volunteers with increasing age in all phases of arterial reaction and at the baseline in veins. In the elderly arteries assume a less regular profile, which might be an expression of endothelial damage.

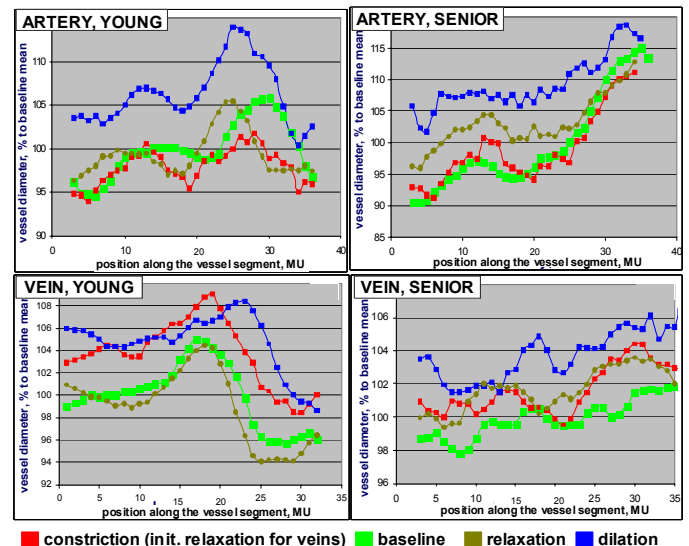


Fig. 35. Typical longitudinal vessel profiles in the age dependence study. Upper row shows longitudinal arterial profiles, the lower one – longitudinal venous profiles. On the left: vessel profiles of a young subject, on the right: vessel profiles of a senior volunteer.

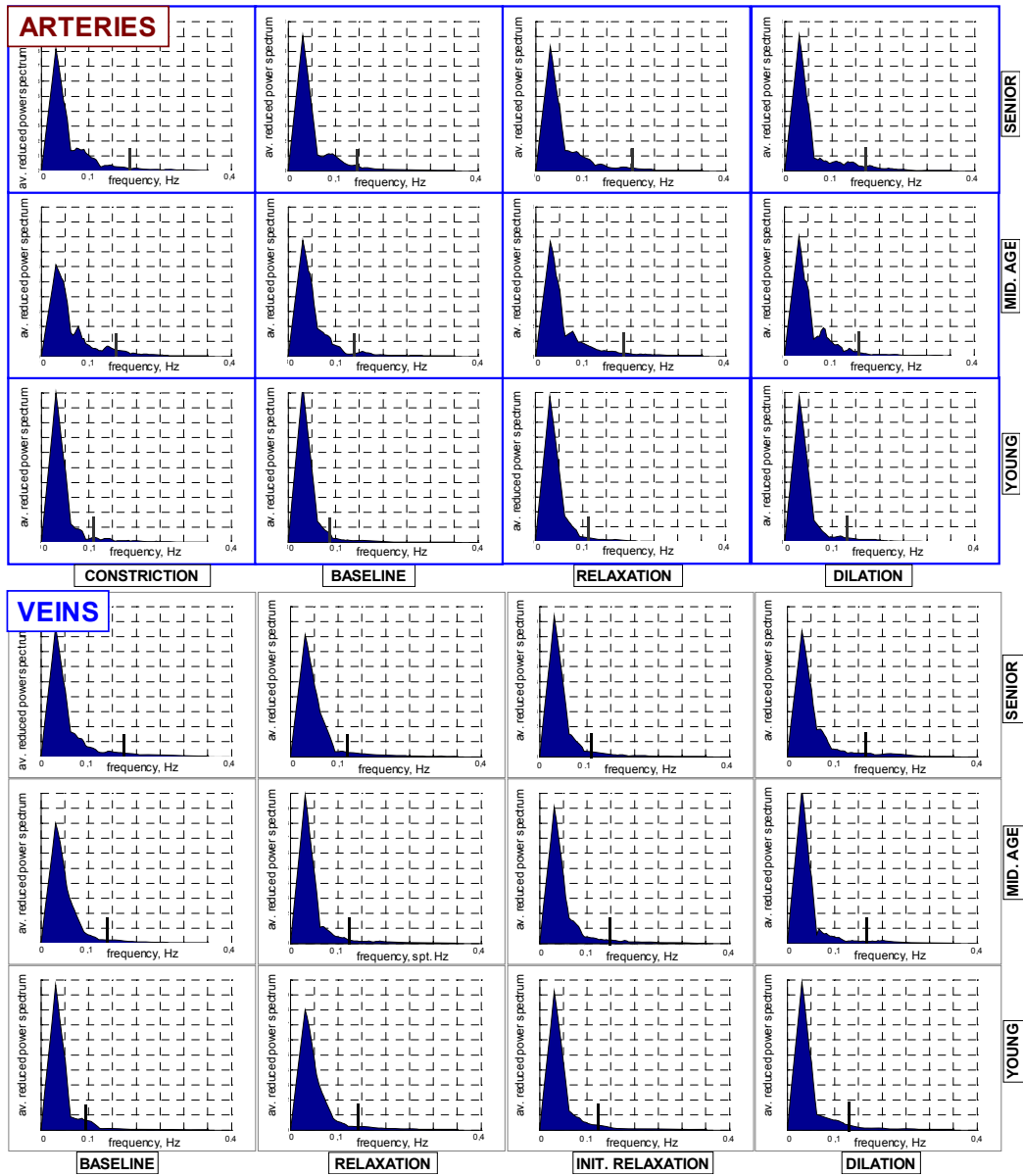


Fig. 36. Average reduced power spectra of spatial longitudinal vessel profiles for the three age groups at the 4 phases of vessel reaction during flicker stimulation assessment. Upper group: arteries; lower group: veins. The sequence of phases was chosen according to increase in diameter of the vessel from left to right. Small vertical black lines show median SEF-values for corresponding summarised longitudinal vessel profiles.

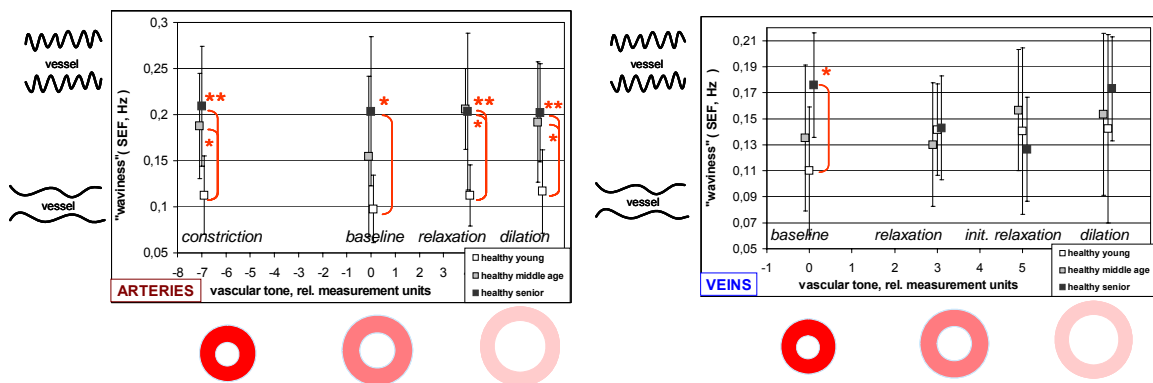


Fig. 37. High frequency waviness of longitudinal vessel profiles, expressed by SEF dependent on vascular tone. **Left:** arteries; **Right:** veins. Cartoons along the axes illustrate "waviness" and "tone". Vascular tone is represented in arbitrary units, which are ranged from -10 to 10, where -10 corresponds to the complete constriction, 0 – the baseline tonus, 10 – full vessel dilation.

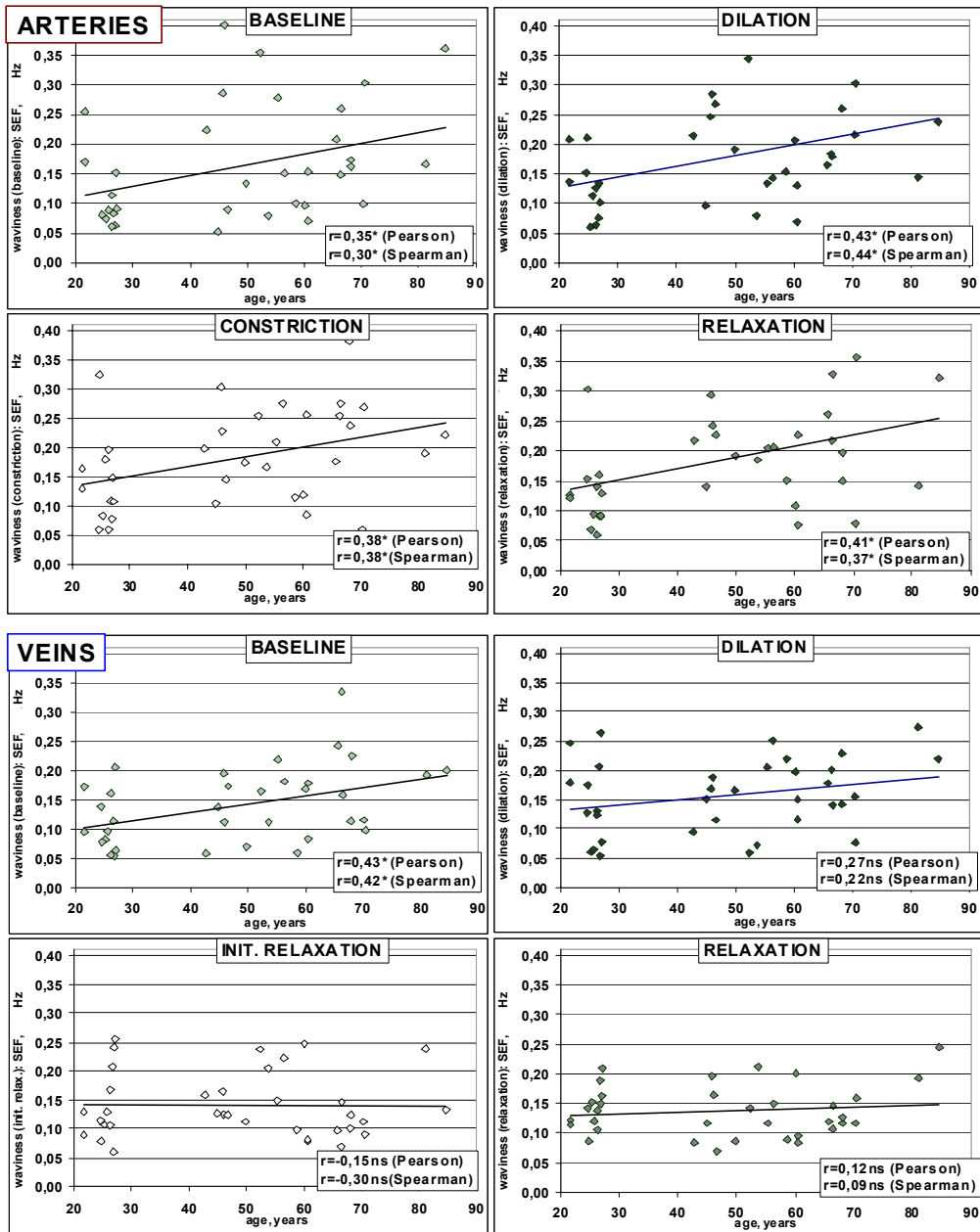


Fig. 38. High frequency waviness of longitudinal vessel profiles expressed by SEF dependent on age at the 4 phases of vessel reaction during flicker stimulation assessment. Each subject is represented by a diamond (♦). Top: arteries; Bottom: veins. Corresponding correlation coefficients and their significance (*) are represented.

3.1.2 Glaucoma study

IOP changes

In study 2 OODG raised the IOP of the healthy subjects from $13,7 \pm 2,9$ mmHg to $34,9 \pm 4,0$ mmHg ($p=0,003$). IOP increased from $22,4 \pm 6,0$ mmHg to $38,9 \pm 5,5$ mmHg ($p=0,007$) in the untreated POAG group and from $16,8 \pm 3,0$ mmHg to $37,3 \pm 4,0$ mmHg ($p=0,005$) in the treated POAG group (Nagel & Vilser 2004).

After the end of the measurement, i.e. approximately 8 minutes after suction cup release, the IOP was $-1,8 \pm 1,3$ mmHg (healthy subjects) $-3,6 \pm 3,3$ mmHg (untreated POAG patients) and $-2,3 \pm 3,3$ mmHg (treated POAG patients) below the respective baseline value.

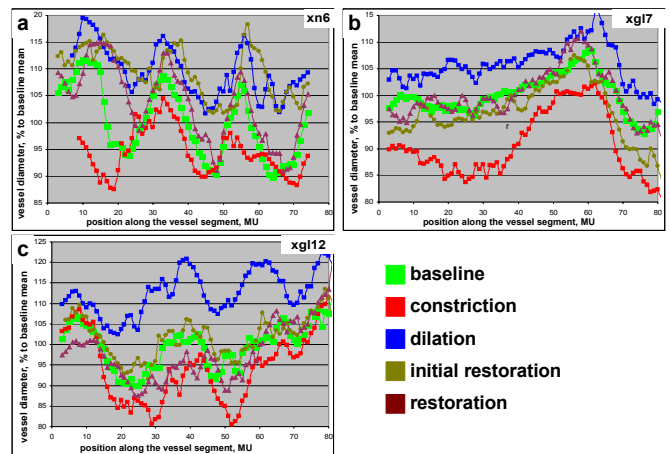


Fig. 39. Individual longitudinal vessel profiles in the glaucoma study 2. The profiles are derived from RVA data at one time point as described in Fig. 22 top, lower right insert. **a:** healthy age matched person; **b:** glaucoma patient; **c:** glaucoma patient after 4 week treatment with three times daily dorzolamide.

Circulation parameters

In both studies the mean systemic blood pressure did not vary significantly between groups at the beginning of the examination: study 1: 105,0 (95,0;118,0) mmHg; Study 2: 109,0 (93,0;120,0) mmHg (median (1.Quartile; 3.Quartile)); and did not change significantly within any group during the whole examination period, being in the end of the examination: 101,0 (91,0;115,0) mmHg (study 1); 102,0 (93,0;111,0) mmHg (study 2).

Measured retinal arterial reactions.

3.1.2.1 Study 1 with acute suprasystolic IOP-increase

In Fig. 40, Fig. 41 HFW of arterial segments, expressed by SEF is depicted dependent on vascular tone. Note, that according to formula (8): $MU^{-1} = Hz$, thus both Fig. 40 and Fig. 41 are presentations similar to Fig. 37.

No statistically significant changes in HFW were found in healthy subjects in different phases of the arterial reaction. A significant increase of HFW by changing vascular tone from baseline to dilation

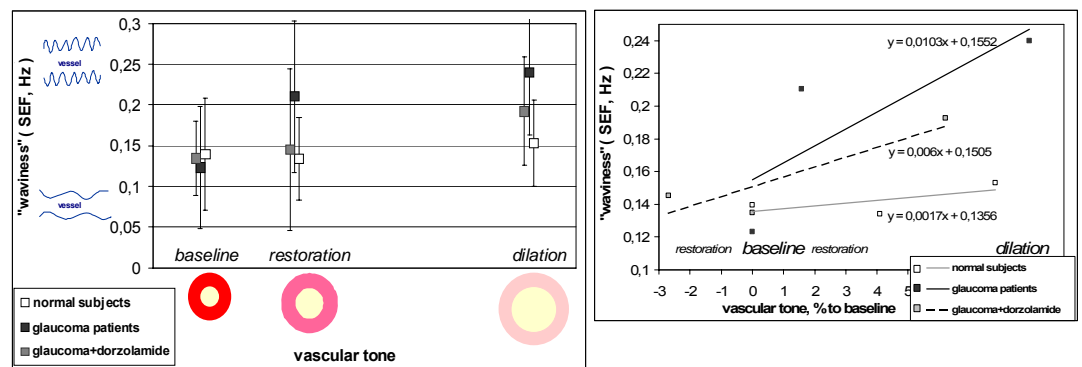


Fig. 40. High frequency waviness of arterial segments, expressed by SEF dependent on vascular tone. **Left:** results of study 1. **Right:** regression analysis of study 1. The chart on the right demonstrate lesser change in HFW after IOP provocation in healthy age matched normals shown by flatter incline of the grey linear regression slope.

($p < 0,03$) was found in POAG patients without treatment. See Fig. 39b and fig. 6, right panel for example, how does

HFW increase in the longitudinal vessel profile; see Fig. 40 for the statistical description. HFW was higher in untreated POAG patients than in normal persons during dilation ($p < 0,05$). HFW of POAG patients with treatment during dilation tends to be less than in the untreated POAG patients and more than in normals however the difference was not statistically significant ($p > 0,1$) (Fig. 40).

3.1.2.2 Study 2 with moderate 100 s IOP-increase

In Fig. 39 examples of typical local arterial reaction to the IOP provocation in study 2 are presented for the three examined groups.

No statistically significant changes in HFW described by SEF were found in healthy subjects in different phases of the arterial reaction (Fig. 39a, Fig. 41 left). A significant increase of HFW by changing vascular tone

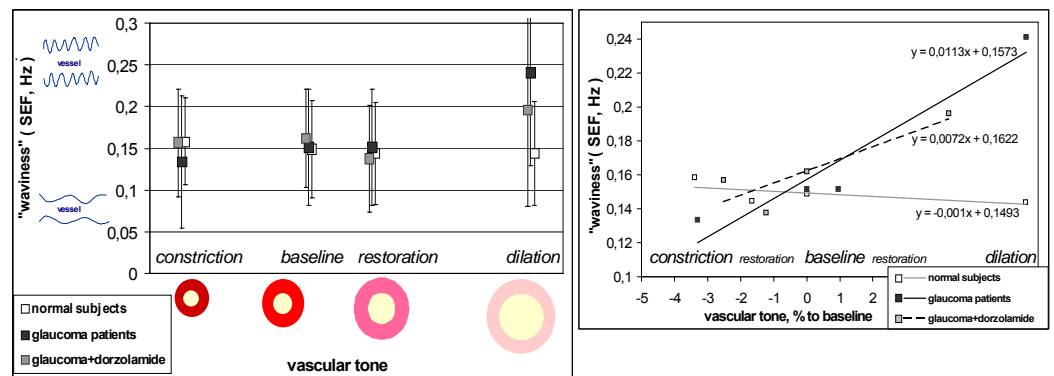


Fig. 41. High frequency waviness of arterial segments, expressed by SEF dependent on vascular tone. **Left:** results of study 2. **Right:** regression analysis of study 2. The chart on the right demonstrate lesser change in HFW after IOP provocation in healthy age matched normals shown by flatter incline of the grey linear regression slope.

from dilation to constriction ($p < 0,05$) was found in untreated POAG patients (Fig. 39b, Fig. 41 left). HFW was higher in POAG patients than in normal persons during dilation ($p < 0,05$, Fig. 41). However during constriction this parameter tends to be less in untreated glaucoma patients than in normals ($p > 0,08$). HFW of the treated POAG patients during dilation tends to be less than in the untreated POAG patients and more than in normals in both studies ($p > 0,1$).

Conclusion for glaucoma studies 1+2: The results of these studies indicate a local vessel wall difference in glaucoma patients compared to age matched controls. Significant increase of arterial microirregularities in the POAG retina during vascular dilation might be an indication for vascular endothelial alterations in glaucoma, leading to impaired perfusion in response to IOP increase.

3.1.3 Systemic hypertension study

The mean systemic arterial blood pressure amounted to $110,3 \pm 9,7$ mmHg in the hypertensive group and to $95,6 \pm 8,3$ mmHg in the control group (Nagel et al. 2004). No significant changes of the blood pressure occurred during the examination.

Arteries

There were no statistical significant difference between initial (baseline) average diameters of measured arterial segments in both groups ($p = 0,52$). This parameter amounted to: 119,6(109,2; 137,1) RU in the hypertensive

group and to 112,6(109,3; 127,0) RU in the control group. Typical longitudinal arterial profiles one can see in Fig. 42.

Calculated ARPS of longitudinal arterial profiles for 5 phases of arterial reaction are represented in Fig. 43 (upper panel) for both groups. The sequence of phases was chosen according to the increase in vessel diameter from the left to the right.

One can see, that in the control group ARPS do not differ when arteries change from the constriction to the dilation. This affirmation was proven statistically: No statistically significant differences in primary or secondary peak frequencies, peak values as well as in average areas under ARPS within any frequency band were found between different phases of arterial reaction in the control group ($p > 0,2$). This confirms the previous results for healthy subjects

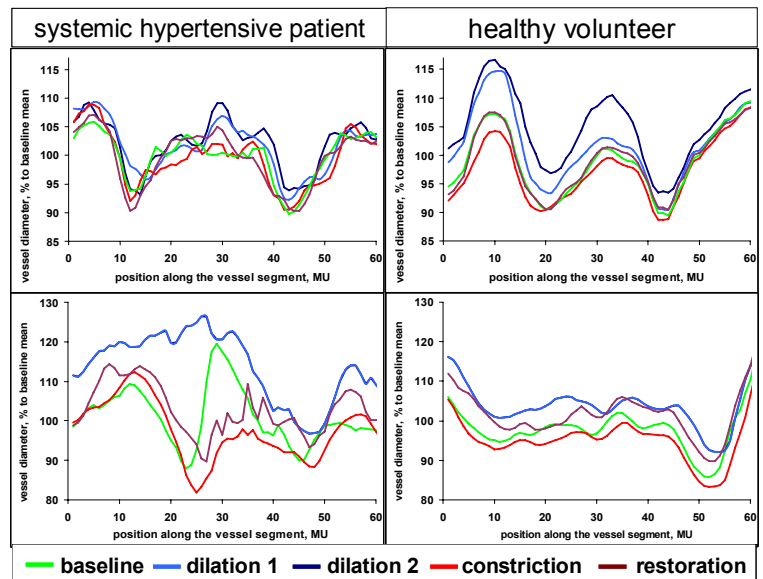


Fig. 42. Typical longitudinal arterial profiles in the examined groups. Systemic hypertension study. Arteries.

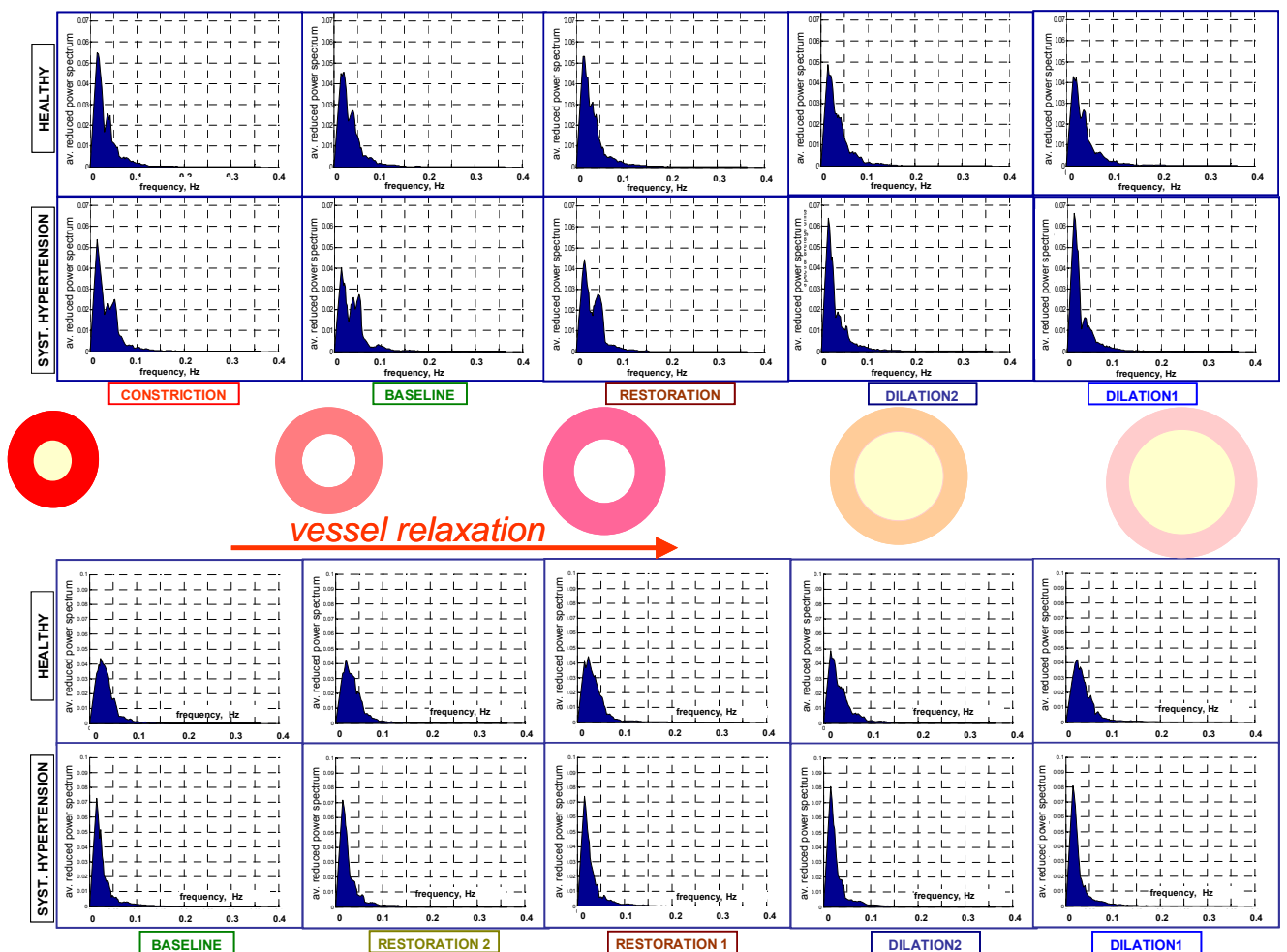


Fig. 43. Average reduced power spectra of spatial longitudinal vessel profiles for systemic hypertension study at the 5 phases of vessel reaction during flicker stimulation assessment. The sequence of phases was chosen according to the increase in vessel diameter from the left to the right. Upper group: arteries; lower group: veins.

(Kotliar et al. 2006; Kotliar et al. 2006) and (3.1.1). Examples in Fig. 42 (right panel) clear this finding: arterial profile shifts almost parallel during vessel reaction without changing the configuration of the longitudinal vessel profile. ARPS at all phases possess three peaks (Fig. 43, upper panel). The primary peak varies from 0,016 to 0,022 Hz at different phases (derived from ARPS), which corresponds to one oscillation in 45,5÷62,5 MU or in 568÷781 μm – a low frequency oscillation of a high magnitude. This characteristic frequency is superimposed with other oscillations in Fig. 42, top right panel and is conspicuous in the bottom right panel. The secondary peak of the power spectrum: 0,035÷0,042 Hz at different phases corresponds to one oscillation in 23,8÷28,6 MU or in 298÷357 μm – a mid frequency oscillation. This is clearly seen in Fig. 42, right panel top and bottom. There exists also a third small peak at 0,07 ÷ 0,08 Hz at all phases, which corresponds to one oscillation in 12,5÷14,2 MU or in 156÷179 μm – a high frequency oscillation of a low magnitude which is superimposed with other oscillations in Fig. 42, right panel top and is conspicuous in the bottom right panel.

In systemic hypertension group ARPS of constriction, baseline and restoration are analogous with each other and differs from both ARPS of dilation (Fig. 43, upper panel). This difference between dilation and other phases of vessel reaction is conspicuous in Fig. 42, left, bottom. Average area under reduced power spectra (dimensionless according to formula (9)) within the frequency band of 0,03÷0,06 Hz differs significantly in dilation1 (0,226(0,150; 0,292)) from constriction (0,317(0,221; 0,396)), baseline (0,371(0,241; 0,425)) and restoration (0,352(0,243; 0,412)) ($p<0,05$) (Fig. 44). This parameter differs significantly in dilation 2 (0,226(0,150; 0,364)) from the baseline ($p<0,05$).

Note, that because of the definition of ARPS, the statistical parameters (median, quartiles) of peak or band frequencies calculated from individual power spectra does not always coincide with peak frequencies seen in ARPS (e.g. Fig. 44): during averaging of power spectra individual primary peaks compensate each other building a peak somewhere not necessarily at the site of median peak frequency.

ARPS at constriction and baseline possess three main peaks: one primary and two secondary of almost the same height. At restoration two secondary peaks merge to one (Fig. 43, upper panel). The primary peak varies from 0,015 to 0,018 Hz at different phases, which corresponds to one oscillation in 55,5÷66,7 MU or in 694÷833 μm – a low frequency oscillation of a high magnitude. This characteristic frequency is superimposed with other oscillations in Fig. 42, left panel top and bottom. The primary peak frequency at baseline longitudinal arterial profile differs significantly in healthy group from systemic hypertension group ($p<0,05$). The secondary peak of the power spectrum: 0,038÷0,042 Hz at different phases corresponds to one oscillation in 23,8÷26,3 MU or in 298÷328 μm – a mid frequency oscillation. This is clearly seen in Fig. 42, left panel top and bottom. A third peak at 0,052÷0,055 Hz at baseline and constriction corresponds to one oscillation in 18,1÷19,2 MU or in 227÷240 μm – a mid frequency oscillation of a low magnitude which is also clearly seen in Fig. 42, left panel top

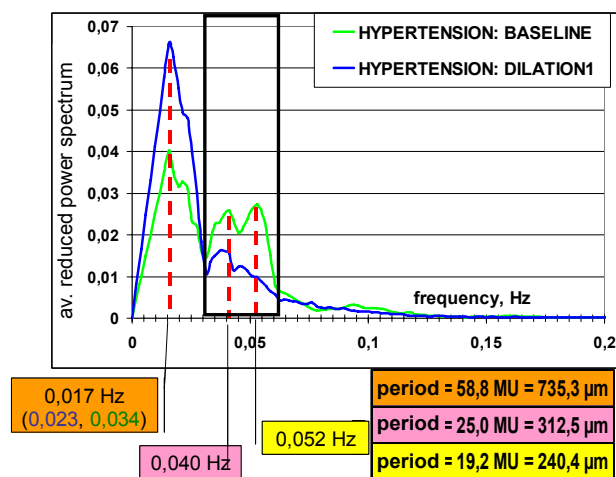


Fig. 44. Mathematical analysis on ARPS of arterial profiles. Different peaks correspond to dominating frequencies in spatial longitudinal arterial profiles. In syst. hypertension group the area under the power spectrum within the black frame differs significantly at baseline and dilation.

and bottom. The merged peak of 0,05 Hz at restoration (20 MU or 250 μm) is conspicuous in the left panel of Fig. 42 as well.

The average area under ARPS within the frequency band of 0,045÷0,060 Hz differs significantly in restoration between hypertension (0,172(0,053; 0,195)) and control group (0,050(0,038; 0,069)) ($p < 0,05$), showing significant dissimilitude between the groups in longitudinal vessel profiles in middle frequency range at restoration. There exists additionally a small high frequency peak at 0,092 Hz at the baseline (10,9 MU or 136 μm), which is conspicuous in the left panel of Fig. 42.

ARPS at dilation possess two main peaks. The primary peak has the same frequency range as it has at other phases of vessel reaction (see above) but it is significantly higher ($p < 0,05$). The secondary peak of ARPS: 0,035÷0,042 Hz (23,8÷28,6 MU or 298÷357 μm) – a mid frequency oscillation similar to the control group. This is clearly seen in Fig. 42, left panel top and bottom. There exists also a small high frequency peak at the dilation².

Although for each curve one can build a reduced power spectrum, there exists an infinite set of curves corresponding to the certain power spectrum chart: they all possess the frequency spectrum with different phases shifted to each other. The information of the phases shift is contained in the complex part of the Fast Fourier Transform. Thus the attempt to build an average *representative* profile of the group from ARPS seems to be nontrivial. A simple mean (median) of all profiles in the group would contain the confusing superposition of all oscillations in the different positions along individual profiles. The attempt to perform Fast Fourier Transform for all individual profiles, to reduce them, to build the average reduced Fourier Transform and to perform finally the inverse Fourier Transform would obviously lead to the same confusing superposition.

In order to explain the findings in the frequency domain I attempted to plot average representative longitudinal profiles for groups, which would correspond to ARPS in Fig. 43. A mathematical reconstruction was performed. A set of characteristic oscillations, showed by an average power spectrum was taken. These curves were shifted somehow to each other so that all the characteristic oscillations are present within the resultant curve. The sum of this shifted oscillation forms the resultant longitudinal vessel profile, which conforms to the corresponding average power spectrum and possesses characteristic peculiarities of longitudinal vessel profiles in the group. In Fig. 45 one can see an example of such a reconstruction for the baseline and the dilation in systemic hypertension group.

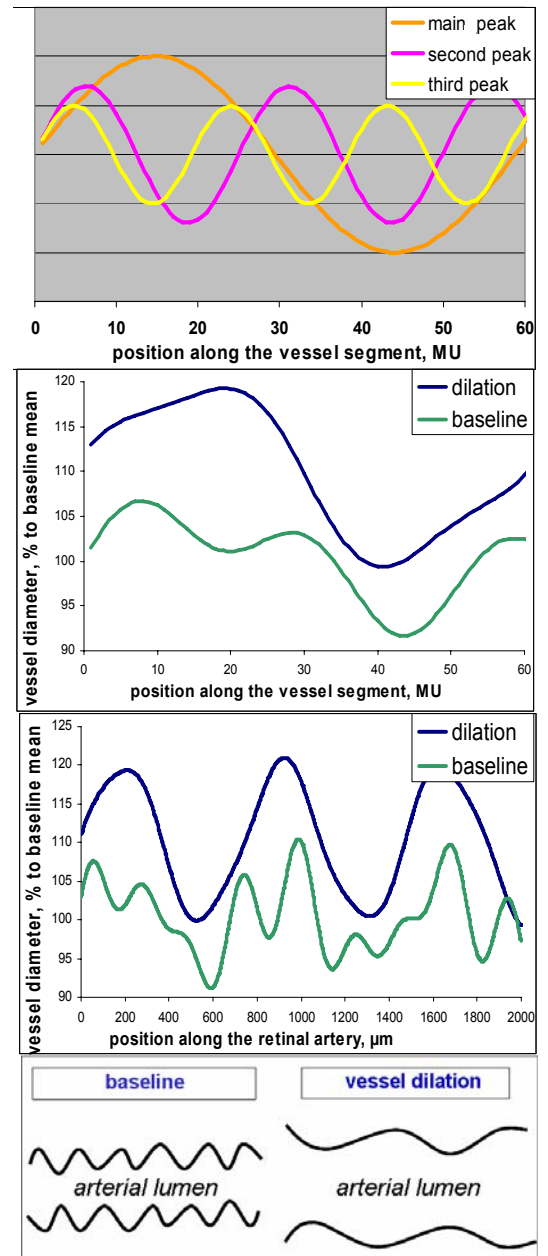


Fig. 45. Mathematical reconstruction of a characteristic spatial longitudinal arterial profile from power spectra in Fig. 43. **Top:** set of harmonic functions. Examples of representative longitudinal arterial profiles. **Middle:** vessel segment analyzed with RVA **Bottom:** retinal arterial segment of 2 mm length and graphic interpretation of obtained results.

Veins.

Although in both examined groups paired board by board running arteries and veins were assessed for each subject (Fig. 22, bottom panel) there was statistical significant difference between initial (baseline) average diameters of measured venous segments in both groups ($p < 0,03$). This parameter amounted to: 164,4(151,8; 168,4) RU in the hypertensive group and to 146,4(132,3; 152,1) RU in the control group. Besides there was statistical significant difference in the magnitude of the baseline (Fig. 46) in veins in both groups ($p < 0,02$). This amounted to 33,5(21,6; 35,8) RU in the hypertensive group and to 19,9(16,0; 23,6) RU in the control group. Calculated ARPS for 5 phases of arterial reaction are represented in Fig. 43 (bottom) for both groups. The sequence of phases was chosen according to the increase in vessel diameter from the left to the right.

One can see that in both groups ARPS do not differ when veins change from the baseline to the dilation. No statistically significant differences in primary or secondary peak frequencies, peak values as well as in average areas under ARPS within any frequency band were found between different phases of venous reaction in both groups ($p > 0,3$). The results for the control group confirm the previous own results for healthy subjects (Kotliar et al. 2006; Kotliar et al. 2006) and (3.1.1). Examples in Fig. 46 clear this finding: in both groups venous profile shifts almost parallel during vessel reaction without changing the configuration of the longitudinal vessel profile.

Venous ARPS of systemic hypertension group differs from ARPS of the control group. This difference is conspicuous in Fig. 46. Besides, the average area under ARPS within the frequency band of $0,03 \div 0,065$ Hz differs significantly between groups at dilation1 (hypertension: 0,171(0,113; 0,351); control: 0,366(0,328; 0,490)); restoration1 (hypertension: 0,213(0,134; 0,359); control: 0,382(0,303; 0,514)) and restoration2 (hypertension: 0,252(0,128; 0,374); control: 0,425(0,311; 0,496)), $p < 0,03$, Fig. 47. The average area under ARPS within the frequency band of $0 \div 0,025$ Hz differs significantly between groups at baseline (hypertension: 0,528(0,304; 0,709); control: 0,310(0,205; 0,422)); dilation1 (hypertension: 0,629(0,453; 0,696); control: 0,350(0,296; 0,505)) and restoration2 (hypertension: 0,564(0,349; 0,710); control: 0,296(0,187; 0,453)), $p < 0,05$, Fig. 47. The Median Frequency (MF) (dividing the whole area under power spectrum into two equal parts) differs significantly between groups at

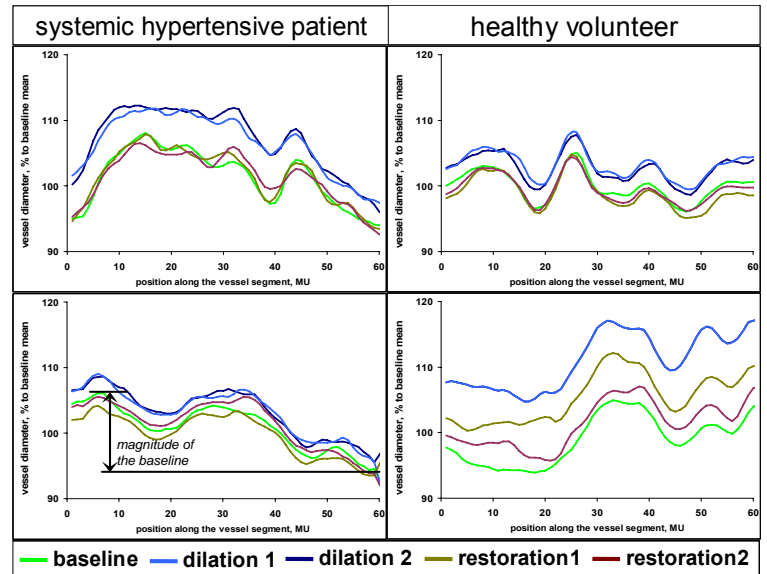


Fig. 46. Typical longitudinal venous profiles in the examined groups. Systemic hypertension study. Veins.

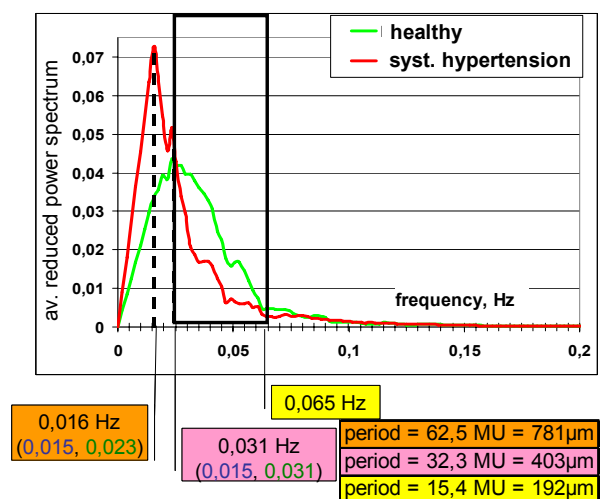


Fig. 47. Mathematical analysis on ARPS of venous profiles. Baseline. Peaks correspond to dominating frequencies in spatial longitudinal venous profiles. The area under the power spectrum within the black frame differs significantly at baseline, restoration 1,2 and dilation 1 between the examined groups.

dilation1 (hypertension: 0,020(0,018; 0,026) Hz; control: 0,031(0,025; 0,038)Hz) and restoration2 (hypertension: 0,021(0,018; 0,030) Hz; control: 0,031(0,026; 0,036)Hz) ($p < 0,05$)

ARPS in the control group possess one primary peak (Fig. 43, bottom panel) at all phases. Its frequency amounted to 0,031(0,016;0,031) Hz at baseline, dilation1, restoration1,2 and to 0,016(0,016;0,031) Hz at dilation2 (calculated from individual power spectra). These correspond to one oscillation in 32,2(32,2; 62,5) MU or in 403(403; 781) μm – a mid frequency oscillation and to one oscillation in 62,5(32,2; 62,5) MU or in 781(403; 781) μm – a low frequency oscillation. In the control group ARPS possess a number of small secondary peaks up to 0,1 Hz at different phases of vessel reaction, reflecting the presence of other oscillations of higher frequency at individual profiles.

ARPS in the systemic hypertension group possess one primary peak (Fig. 43, bottom panel) at all phases. Its frequency amounts to 0,016(0,016;0,023) Hz at all phases (calculated from individual power spectra). These correspond to one oscillation in 62,5(43,5; 62,5) MU or in 781(543; 781) μm – a low frequency oscillation of higher magnitude. ARPS in this group also possess a number of small secondary peaks up to 0,1 Hz at different phases of vessel reaction, reflecting the presence of other oscillations of higher frequency at individual profiles.

In order to summaries all the principal findings in longitudinal venous profiles in systemic hypertension study an example of mathematical reconstruction of a representative longitudinal baseline venous profile of a healthy volunteer and a patient with systemic hypertension (see Fig. 45 for the explanation) is represented in Fig. 48.

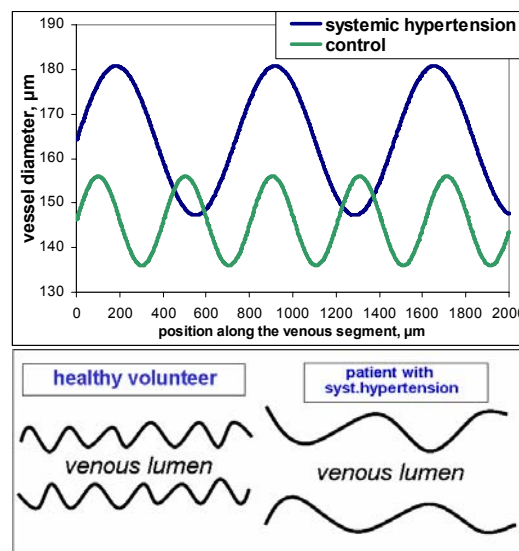


Fig. 48. Mathematical reconstruction of a characteristic spatial longitudinal venous profile from power spectra in Fig. 43. **Top:** retinal venous segment of 2 mm length. **Bottom:** graphic interpretation of the obtained results

Conclusions for systemic hypertension study: *While the microstructure of longitudinal arterial profiles in healthy volunteers does not change for different phases of the vessel reaction, the longitudinal arterial profiles in systemic hypertension become less irregular during vessel dilation. The microstructure of longitudinal venous profiles both in healthy volunteers and in patients with systemic hypertension does not change for different phases of the vessel reaction. The veins in systemic hypertension are pre-dilated and even pre-stretched. In longitudinal venous profiles in systemic hypertension low frequencies are more expressed and mid frequencies are more impaired than in the control group.*

3.1.4 Obesity study

There were no statistical significant difference between initial (baseline) average diameters of measured arterial segments in both groups ($p=0,28$). This parameter amounted to: 116,4 (105,7; 128,6) RU in the obesity group and to 109,7(103,2; 117,5) RU in the control group. Typical longitudinal arterial profiles one can see in Fig. 49.

Calculated ARPS of longitudinal arterial profiles for 5 phases of arterial reaction are represented in Fig. 50 for both groups. The sequence of phases was chosen according to the increase in vessel diameter from the left to the right. Interestingly the power spectra shape in all phases of vessel reaction in both examined groups are similar to the venous power spectra shapes in the systemic hypertension study (Fig. 43, bottom panel).

One can see, that in both groups ARPS do not differ when arteries change from the constriction to the dilation. No statistically significant differences in primary or secondary peak frequencies, peak values as well as in average areas under ARPS within any frequency band were found between different phases of arterial reaction in both groups ($p > 0,3$). The results for the control group confirm the previous own results for healthy subjects (Kotliar et al. 2006; Kotliar et al. 2006) and (3.1.1, 3.1.2, 3.1.3). Examples in Fig. 49 clear this finding: in both groups arterial profile shifts near parallel during vessel reaction almost without changing the configuration of the longitudinal vessel profile.

Nevertheless ARPS in the obesity group differ from ARPS of the control group. This difference is conspicuous in Fig. 49, Fig. 50. Besides, average area under ARPS within the frequency band of $0,055 \div 0,095$ Hz is smaller in obesity group for all phases of vessel reaction. It differs significantly between groups at dilation1 (obesity: $0,156(0,081; 0,196)$; control: $0,271(0,177; 0,408)$); dilation2 (obesity: $0,115(0,068; 0,215)$; control: $0,257(0,140; 0,247)$) and restoration (obesity: $0,137(0,066; 0,240)$; control: $0,314(0,136; 0,388)$), $p < 0,05$, Fig. 50 and Fig. 51.

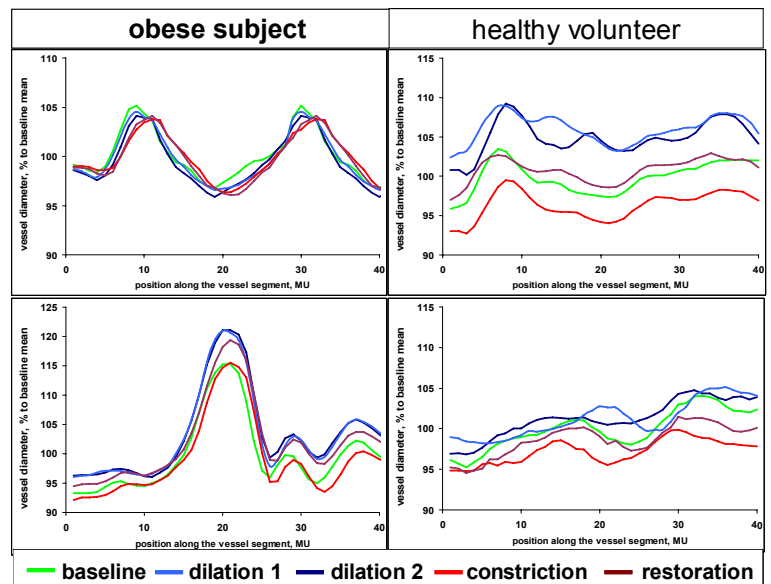


Fig. 49. Typical longitudinal arterial profiles in the examined groups. Obesity study. Arteries.

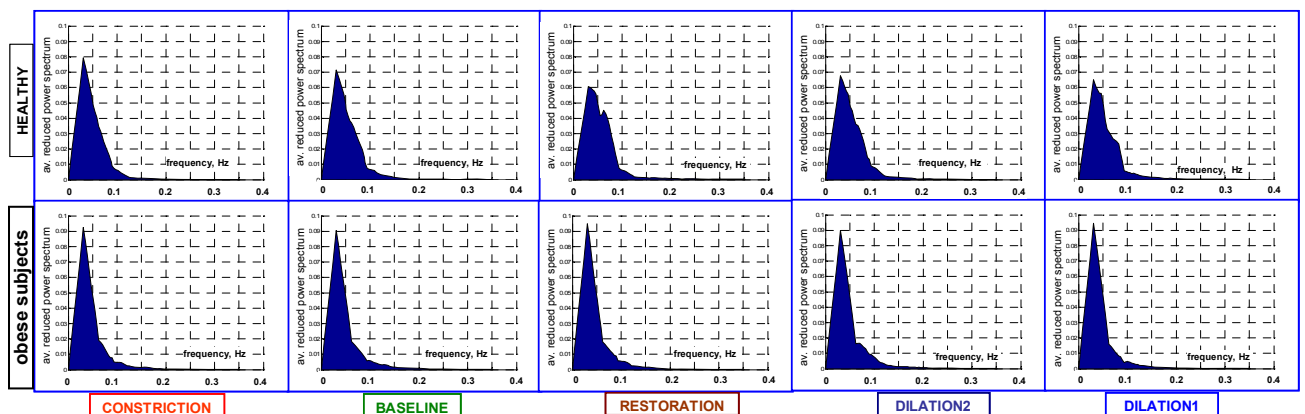


Fig. 50. Average reduced power spectra of spatial longitudinal arterial profiles for obesity study at the 5 phases of arterial reaction during flicker stimulation assessment. The sequence of phases was chosen according to the increase in vessel diameter from the left to the right, similar to Fig. 43.

Average area under ARPS within the frequency band of $0 \div 0,032$ Hz is larger in obesity group for all phases of vessel reaction. It differs significantly between groups at dilation1 (obesity: $0,404(0,345; 0,470)$; control: $0,305(0,133; 0,403)$) and restoration (obesity: $0,427(0,309; 0,465)$; control: $0,273(0,140; 0,438)$), $p < 0,05$, Fig. 50 and Fig. 51.

ARPS in the control group possess one primary peak (Fig. 50) at all phases. Its frequency amounted to 0,031(0,031;0,063) Hz at baseline, dilation1,2, restoration and to 0,031(0,031;0,039) Hz at constriction (calculated from indiv. power spectra). These correspond to one oscillation in 31,9(15,6/25,6; 31,9) MU or in 392(196/321; 392) μm – a mid frequency oscillation.

ARPS in the obesity group possess one sharp single peak (Fig. 50) at all phases. Its frequency amounted to 0,031(0,031;0,031) Hz at all phases (calculated from indiv. power spectra). These correspond to one oscillation in 62,5(62,5; 62,5) MU or in 781 (781; 781) μm – a mid frequency oscillation of a high magnitude.

SEF-values do not differ between groups at any phase of arterial reaction ($p>0,5$) being for the instance at baseline: obesity: 0,118(0,098; 0,135) Hz; control: 0,110(0,090; 0,166)Hz.

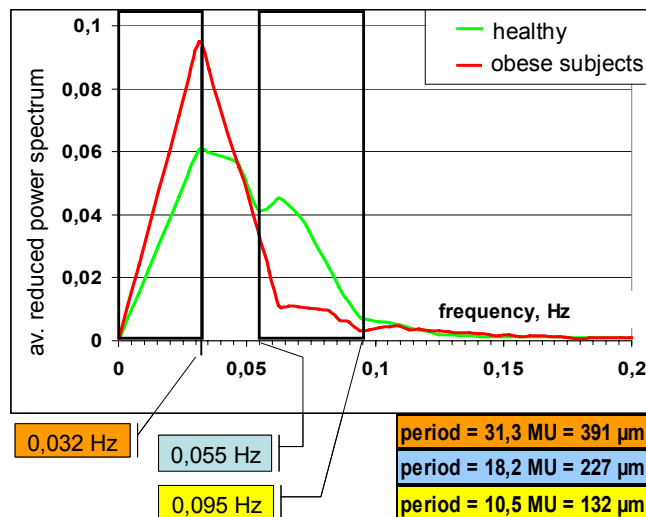


Fig. 51. Mathematical analysis on ARPS of arterial profiles. Restoration. Peaks correspond to dominating frequencies in spatial longitudinal arterial profiles. The areas under the power spectrum within black frames differ significantly at dilation 1, dilation 2 (for 0,055-0,095Hz only) and restoration between examined groups.

Conclusions for obesity study: Significant microstructural changes in longitudinal profiles of retinal arteries in patients with metabolic syndrome might be an indication for alterations in the vascular endothelium and smooth muscle cells in this disease, leading to impaired perfusion and regulation.

3.1.5 Repeatability and reproducibility of longitudinal vessel profile assessment and analysis

3.1.5.1 Short-term repeatability

Typical longitudinal vessel profiles are shown in Fig. 52. There were no statistical significant difference between initial and repeated parameters of measured longitudinal vessel profiles ($p > 0,5$). Calculated ARPS of longitudinal vessel profiles are represented in Fig. 53. Basic parameters of the study: absolute vessel diameter, SEF, area within the frequency band $0,03 \div 0,06$ Hz (*band sq.*), as well as the frequency of the primary peak (*pr. peak fr.*), and their VC are represented in tabular form (Table 10):

Table 10. Results of short-term repeatability pilot-study (median (1. quartile; 3. quartile))

		ARTERIES	VEINS
abs. diameter	baseline1, RU	113,3(102,2; 114,7)	146,5(126,7; 155,6)
	baseline2, RU	112,0(102,5; 114,0)	147,9(124,8; 156,1)
	VC, %	0,2(0,2; 0,4)	0,6(0,4; 1,0)
	dilation1, RU	113,3(102,2; 114,3)	149,0(127,3; 157,8)
	dilation2, RU	114,3(102,5; 114,9)	150,6(128,7; 160,2)
	VC, %	0,1(0,0; 0,2)	0,8(0,7; 1,1)
SEF	baseline1, Hz	0,053(0,053; 0,086)	0,095(0,094; 0,110)
	baseline2, Hz	0,070(0,064; 0,089)	0,093(0,086; 0,114)
	VC, %	9,5(4,9; 13,5)	7,4(4,0; 13,7)
	dilation1, Hz	0,084(0,045; 0,085)	0,100(0,098; 0,111)
	dilation2, Hz	0,080(0,067; 0,083)	0,106(0,063; 0,119)
	VC, %	2,1(1,6; 3,8)	16,2(5,9; 22,7)
band sq.	baseline1	0,356(0,349; 0,424)	0,277(0,219; 0,347)
	baseline2	0,419(0,362; 0,421)	0,285(0,260; 0,338)
	VC, %	1,1(1,1; 13,1)	7,8(2,2; 12,0)
	dilation1	0,401(0,384; 0,416)	0,295(0,254; 0,366)
	dilation2	0,402(0,348; 0,406)	0,368(0,268; 0,438)
	VC, %	6,0(3,6; 7,1)	13,8(12,9; 23,3)
pr. peak fr.	baseline1, Hz	0,016(0,016; 0,047)	0,016(0,016; 0,047)
	baseline2, Hz	0,016(0,016; 0,047)	0,016(0,016; 0,047)
	VC, %	0,0(0,0; 0,0)	0,0(0,0; 0,0)
	dilation1, Hz	0,016(0,016; 0,047)	0,016(0,016; 0,047)
	dilation2, Hz	0,016(0,016; 0,047)	0,016(0,016; 0,047)
	VC, %	0,0(0,0; 0,0)	0,0(0,0; 0,0)

3.1.5.2 Long-term reproducibility

Typical longitudinal vessel profiles are shown in Fig. 54. There were no statistical significant difference between initial and repeated parameters of measured longitudinal vessel profiles ($p > 0,5$). Calculated ARPS of longitudinal vessel profiles are represented in Fig. 55. Basic parameters of the study: absolute vessel diameter, SEF,

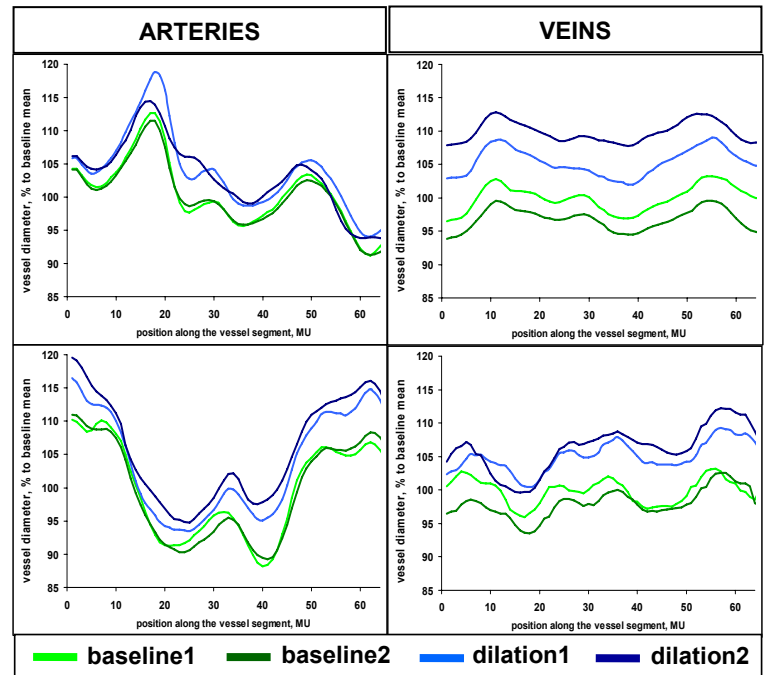


Fig. 52. Typical longitudinal arterial profiles of the examined volunteers. Short-term repeatability pilot-study. Medically healthy volunteers.

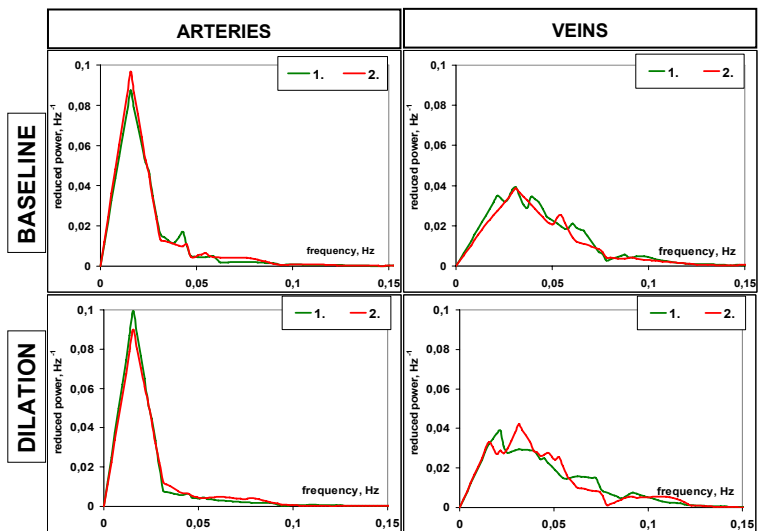


Fig. 53. Average reduced power spectra of spatial longitudinal arterial profiles for short-term repeatability pilot study at 2 phases of vessel reaction.

area within the frequency band $0,03 \div 0,06$ Hz (*band sq.*), as well as the frequency of the primary peak (*pr. peak fr.*), and their VC are represented in tabular form (Table 11):

Table 11. Results of long-term reproducibility pilot-study (median (1. quartile; 3. quartile))

		ARTERIES	VEINS
abs. diameter	baseline1, RU	125,4(105,5; 126,5)	144,2(136,7; 146,2)
	baseline2, RU	126,6(102,9; 126,7)	145,6(135,0; 146,2)
	VC, %	0,7(0,2; 2,5)	0,6(0,3; 0,8)
	dilation1, RU	127,1(105,3; 127,9)	145,9(138,3; 148,1)
	dilation2, RU	125,7(103,8; 129,3)	146,2(137,7; 149,9)
	VC, %	0,7(0,3; 0,7)	0,5(0,2; 0,8)
SEF	baseline1, Hz	0,127(0,088; 0,199)	0,126(0,093; 0,203)
	baseline2, Hz	0,125(0,109; 0,133)	0,162(0,128; 0,204)
	VC, %	29,2(21,9; 44,0)	17,5(8,1; 22,7)
	dilation1, Hz	0,134(0,089; 0,207)	0,124(0,068; 0,185)
	dilation2, Hz	0,118(0,117; 0,132)	0,106(0,063; 0,119)
	VC, %	31,3(23,1; 32,5)	46,3(39,2; 60,6)
band sq.	baseline1	0,343(0,318; 0,354)	0,358(0,255; 0,424)
	baseline2	0,269(0,260; 0,296)	0,320(0,226; 0,372)
	VC, %	34,8(5,1; 61,8)	8,5(6,0; 10,5)
	dilation1	0,321(0,238; 0,349)	0,325(0,235; 0,435)
	dilation2	0,314(0,191; 0,330)	0,368(0,268; 0,438)
	VC, %	29,8(23,2; 35,8)	21,0(14,5; 31,0)
pr. peak fr.	baseline1, Hz	0,031(0,031; 0,031)	0,031(0,031; 0,031)
	baseline2, Hz	0,031(0,031; 0,063)	0,031(0,031; 0,031)
	VC, %	0,0(0,0; 0,0)	0,0(0,0; 0,0)
	dilation1, Hz	0,031(0,031; 0,031)	0,031(0,031; 0,031)
	dilation2, Hz	0,031(0,031; 0,094)	0,016(0,016; 0,047)
	VC, %	47,1(0,0; 70,7)	47,1(47,1; 47,1)

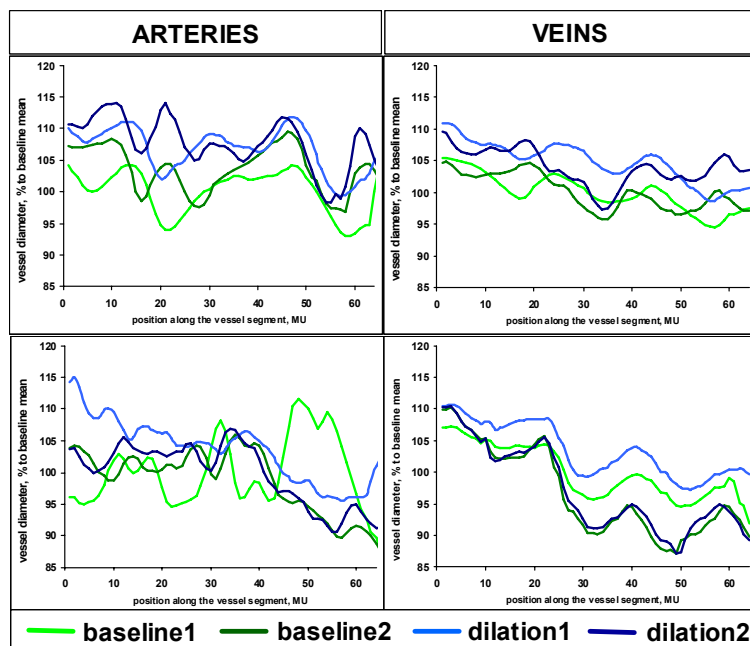


Fig. 54. Typical longitudinal arterial profiles of the examined patients. Long-term reproducibility pilot study. Patients with metabolic syndrome

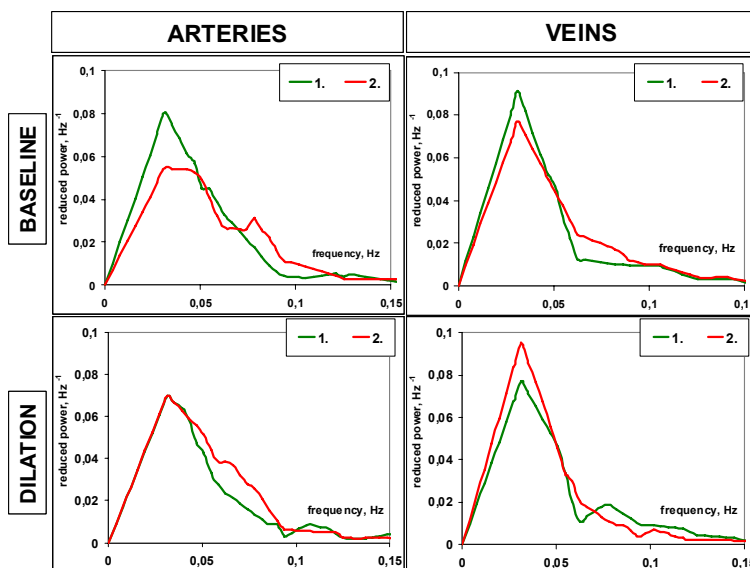


Fig. 55. Average reduced power spectra of spatial longitudinal arterial profiles for long-term reproducibility pilot study at 2 phases of vessel reaction.

3.1.5.3 Dimensional and spatial reproducibility

Dimensional reproducibility

One can see typical longitudinal vessel profiles of small and large vessels in Fig. 56. Basic parameters of the study: absolute vessel diameter, SEF, area within the frequency band $0 \div 0,026$ Hz (*band sq.*), frequency of the primary peak (*pr. peak fr.*), the VC of both investigated groups and their p-values (Wilcoxon-test) are represented in tabular form (Table 12).

Vessel diameters both for arteries and for veins were statistically different in both groups for all phases of vessel reaction ($p < 0,001$, Table 12). SEF values did not differ between groups, showing however a relatively high variation both for arteries and for veins.

Differences in arterial ARPS between groups is obvious in Fig. 57. In arteries there were differences in arterial ARPS, which is shown with quantitative parameter *band sq.* (Table 12).

The latter was significantly different between the groups ($p < 0,05$) for all examined phases of vessel reaction (Table 12). Parameter *pr. peak fr.* differs in arteries during constriction ($p < 0,02$). It was higher in the group of small vessels. There were no statistical significant differences between parameters of longitudinal venous profiles in small and large vessels ($p > 0,4$) (Table 12).

Venous ARPS seem to be quite similar in both groups (Fig. 57 bottom). Although non-parametric Wilcoxon test shows a difference for *pr. peak fr.* at baseline in veins ($p = 0,021$). This reflects greater primary peak frequency spread in small vessels not the differences in the median values.

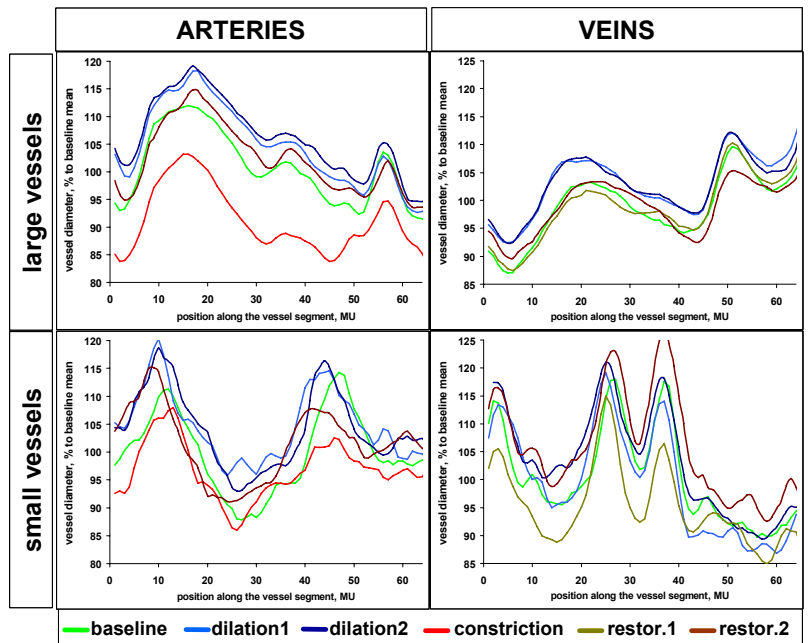


Fig. 56. Typical longitudinal arterial profiles of the examined vessels. Dimensional reproducibility pilot study. Young healthy volunteers.

Table 12. Results of dimensional reproducibility pilot-study (median (1. quartile; 3. quartile). BAS-baseline, DIL1-dilation1, CON-constriction; RES1-restoration1

		ARTERIES		VEINS				ARTERIES		VEINS			
abs. diameter	small diam., RU	87,8(83,6; 98,9)	110,4(93,3; 119,5)	0,274(0,184; 0,473)	0,380(0,162; 0,538)	band sq.	small diam.	0,274(0,184; 0,473)	0,380(0,162; 0,538)	pr. peak fr.	small diam., Hz	0,031(0,016; 0,031)	0,016(0,016; 0,047)
	large diam., RU	112,8(107,4; 131,4)	146,4(136,9; 160,1)	0,526(0,446; 0,775)	0,481(0,369; 0,577)		large diam.	0,526(0,446; 0,775)	0,481(0,369; 0,577)		large diam., Hz	0,016(0,016; 0,016)	0,016(0,016; 0,023)
	VC, %	18,9(16,5; 23,8)	21,8(19,6; 28,1)	66,1(26,6; 79,1)	36,4(14,0; 89,5)		VC, %	66,1(26,6; 79,1)	36,4(14,0; 89,5)		VC, %	47,1(23,5; 47,1)	23,5(0,0; 64,8)
	p-value	0,000	0,000	0,004	0,414		p-value	0,004	0,414		p-value	0,012	0,203
	small diam., RU	86,8(82,4; 96,5)	105,5(91,6; 114,0)	0,320(0,164; 0,500)	0,383(0,264; 0,547)		small diam.	0,320(0,164; 0,500)	0,383(0,264; 0,547)		small diam., Hz	0,031(0,016; 0,031)	0,016(0,016; 0,039)
	large diam., RU	110,8(105,6; 130,2)	143,9(132,0; 157,1)	0,563(0,381; 0,738)	0,442(0,372; 0,588)		large diam.	0,563(0,381; 0,738)	0,442(0,372; 0,588)		large diam., Hz	0,016(0,016; 0,016)	0,016(0,016; 0,016)
VC, %	18,5(16,5; 24,4)	22,8(20,2; 27,7)	45,6(11,4; 76,4)	28,8(17,8; 77,7)	VC, %	45,6(11,4; 76,4)	28,8(17,8; 77,7)	VC, %	47,1(0,0; 53,8)	47,1(0,0; 58,9)			
p-value	0,000	0,000	0,020	0,230	p-value	0,020	0,230	p-value	0,251	0,021			
SEF	small diam., Hz	0,083(0,079; 0,114)	0,111(0,087; 0,129)	0,031(0,016; 0,031)	0,016(0,016; 0,047)	small diam., Hz	0,031(0,016; 0,031)	0,016(0,016; 0,039)	small diam., Hz	0,031(0,016; 0,031)	0,016(0,016; 0,039)		
	large diam., Hz	0,087(0,059; 0,103)	0,092(0,081; 0,128)	0,016(0,016; 0,016)	0,016(0,016; 0,023)	large diam., Hz	0,016(0,016; 0,016)	0,016(0,016; 0,023)	large diam., Hz	0,016(0,016; 0,031)	0,016(0,016; 0,023)		
	VC, %	24,6(12,6; 43,6)	21,7(16,3; 42,0)	47,1(23,5; 47,1)	23,5(0,0; 64,8)	VC, %	47,1(23,5; 47,1)	23,5(0,0; 64,8)	VC, %	47,1(0,0; 53,8)	47,1(0,0; 58,9)		
	p-value	0,125	0,882	0,012	0,122	p-value	0,012	0,122	p-value	0,251	0,021		
	small diam., Hz	0,099(0,084; 0,113)	0,089(0,071; 0,119)	0,031(0,016; 0,031)	0,016(0,016; 0,039)	small diam., Hz	0,031(0,016; 0,031)	0,016(0,016; 0,039)	small diam., Hz	0,031(0,016; 0,031)	0,016(0,016; 0,039)		
	large diam., Hz	0,093(0,063; 0,110)	0,097(0,081; 0,117)	0,016(0,016; 0,016)	0,016(0,016; 0,016)	large diam., Hz	0,016(0,016; 0,016)	0,016(0,016; 0,023)	large diam., Hz	0,016(0,016; 0,031)	0,016(0,016; 0,023)		
VC, %	15,9(6,8; 49,6)	14,0(6,7; 30,6)	47,1(0,0; 53,8)	47,1(0,0; 58,9)	VC, %	47,1(0,0; 53,8)	47,1(0,0; 58,9)	VC, %	47,1(0,0; 53,8)	47,1(0,0; 58,9)			
p-value	0,151	0,616	0,251	0,021	p-value	0,251	0,021	p-value	0,116	0,247			
small diam., Hz	0,115(0,097; 0,137)	0,099(0,083; 0,123)	0,031(0,016; 0,031)	0,016(0,016; 0,039)	small diam., Hz	0,031(0,016; 0,031)	0,016(0,016; 0,039)	small diam., Hz	0,031(0,016; 0,031)	0,016(0,016; 0,039)			
large diam., Hz	0,096(0,079; 0,111)	0,103(0,073; 0,134)	0,016(0,016; 0,016)	0,016(0,016; 0,023)	large diam., Hz	0,016(0,016; 0,016)	0,016(0,016; 0,023)	large diam., Hz	0,016(0,016; 0,031)	0,016(0,016; 0,023)			
VC, %	24,4(16,7; 41,5)	27,6(12,0; 41,5)	0,0(0,0; 47,1)	47,1(0,0; 47,1)	VC, %	0,0(0,0; 47,1)	47,1(0,0; 47,1)	VC, %	47,1(0,0; 47,1)	47,1(0,0; 47,1)			
p-value	0,118	0,841	0,116	0,247	p-value	0,116	0,247	p-value	0,116	0,247			

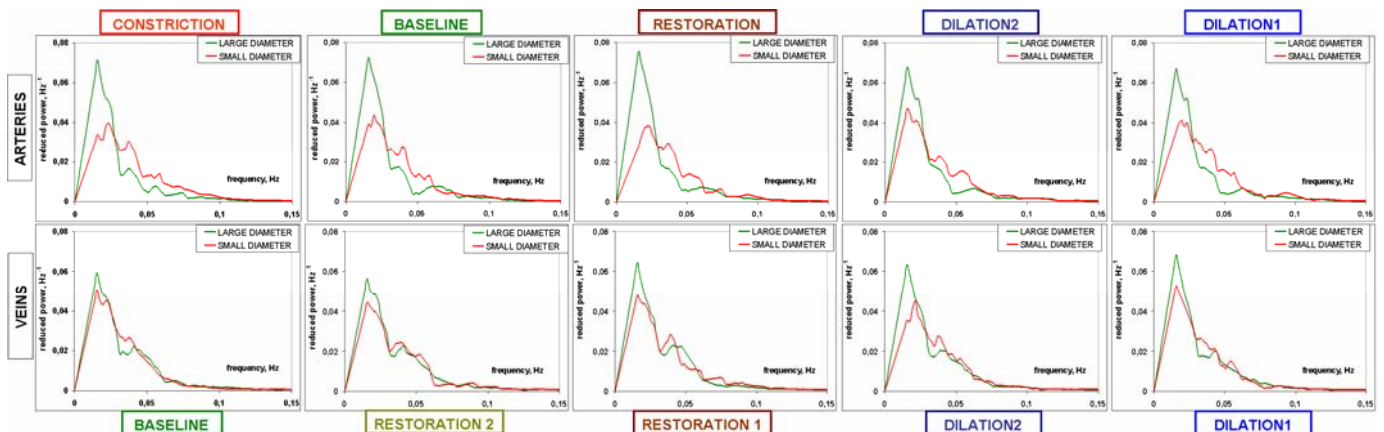


Fig. 57. Average reduced power spectra of spatial longitudinal arterial profiles for dimensional reproducibility pilot study at 5 phases of arterial (top) and venous (bottom) reaction during flicker stimulation assessment. 16 measured vessel segments in each compared group. The sequence of phases was chosen according to the increase in vessel diameter from the left to the right, similar to Fig. 43.

Spatial reproducibility

Differences between the right and the left eye

Table 13. Results of spatial reproducibility pilot-study. Differences between right and left eye (median (1. quartile; 3. quartile). BAS-baseline, DIL1-dilation1, CON-constriction; RES1-restoration1.

		ARTERIES	VEINS			ARTERIES	VEINS	
abs. diameter	right eye, RU	101,6(97,9; 109,4)	136,9(132,3; 153,6)	REL1	band sq.	right eye	0,434(0,217; 0,691)	0,432(0,347; 0,489)
	left eye, RU	100,7(87,7; 113,5)	121,7(106,5; 141,5)			left eye	0,473(0,283; 0,614)	0,428(0,164; 0,626)
	p-value	0,857	0,097			p-value	0,739	0,958
	right eye, RU	100,4(95,6; 106,0)	131,4(128,9; 148,1)			right eye	0,579(0,385; 0,722)	0,425(0,401; 0,574)
	left eye, RU	99,7(86,7; 112,9)	117,9(104,0; 140,8)			left eye	0,393(0,232; 0,542)	0,383(0,264; 0,556)
	p-value	0,964	0,197			p-value	0,159	0,412
SEF	right eye, RU	102,1(98,6; 110,2)	134,5(130,6; 150,8)	DIL1	pr. peak fr.	right eye	0,471(0,370; 0,702)	0,490(0,377; 0,600)
	left eye, RU	101,9(88,0; 114,2)	120,8(106,1; 141,7)			left eye	0,368(0,192; 0,522)	0,426(0,217; 0,563)
	p-value	0,910	0,208			p-value	0,203	0,261
	right eye, Hz	0,088(0,077; 0,100)	0,106(0,083; 0,152)			right eye, Hz	0,016(0,016; 0,031)	0,016(0,016; 0,016)
	left eye, Hz	0,085(0,074; 0,104)	0,102(0,077; 0,122)			left eye, Hz	0,016(0,016; 0,031)	0,016(0,016; 0,039)
	p-value	0,360	0,230			p-value	0,889	0,224
	right eye, Hz	0,084(0,068; 0,097)	0,097(0,078; 0,114)			right eye, Hz	0,016(0,016; 0,016)	0,016(0,016; 0,016)
	left eye, Hz	0,101(0,081; 0,120)	0,095(0,076; 0,120)			left eye, Hz	0,016(0,016; 0,031)	0,016(0,016; 0,031)
	p-value	0,158	0,977			p-value	0,909	0,010
	right eye, Hz	0,089(0,070; 0,101)	0,094(0,080; 0,129)			right eye, Hz	0,016(0,016; 0,027)	0,016(0,016; 0,016)
	left eye, Hz	0,112(0,096; 0,137)	0,103(0,080; 0,134)			left eye, Hz	0,031(0,016; 0,031)	0,016(0,016; 0,031)
	p-value	0,037	0,911			p-value	0,533	0,299

Basic parameters of the study and their p-values (non-parametric Dunn-Test) are represented in tabular form (Table 13). Significant differences were found for SEF of arterial profiles during dilation and for frequency of the primary peak in veins during baseline.

Location in the fundus

Table 14. Results of spatial reproducibility pilot-study. Differences in location in the fundus nasal/temporal inferior/superior (median (1. quartile; 3. quartile). BAS-baseline, DIL1-dilation1, CON-constriction; RES1-restoration1.

		ARTERIES	VEINS			ARTERIES	VEINS	
abs. diameter	nasal inf., RU	93,6(83,8; 100,8)	112,0(102,0; 114,6)	REL1	band sq.	nasal inf.	0,193(0,168; 0,246)	0,086(0,056; 0,149)
	temp. inf., RU	103,7(94,3; 117,6)	129,5(99,4; 152,6)			temp. inf.	0,260(0,171; 0,375)	0,113(0,083; 0,144)
	nasal sup., RU	91,4(86,1; 93,0)	122,6(113,0; 127,1)			nasal sup.	0,232(0,133; 0,234)	0,089(0,077; 0,182)
	temp. sup., RU	115,5(111,7; 131,3)	134,3(110,5; 157,7)			temp. sup.	0,312(0,097; 0,393)	0,109(0,088; 0,182)
	significance	n.s. (Dunn)	n.s. (Dunn)			significance	n.s. (Dunn)	n.s. (Dunn)
	nasal inf., RU	91,2(81,2; 98,8)	109,4(99,6; 112,0)			nasal inf.	0,147(0,124; 0,200)	0,182(0,092; 0,268)
	temp. inf., RU	103,8(94,7; 116,8)	124,8(96,9; 147,2)			temp. inf.	0,206(0,167; 0,282)	0,093(0,084; 0,109)
	nasal sup., RU	91,3(86,2; 91,4)	120,1(109,8; 126,1)			nasal sup.	0,393(0,329; 0,482)	0,121(0,064; 0,188)
	temp. sup., RU	115,4(109,9; 129,6)	133,3(109,1; 156,0)			temp. sup.	0,294(0,112; 0,403)	0,123(0,090; 0,234)
	significance	n.s. (Dunn)	n.s. (Dunn)			significance	n.s. (Dunn)	n.s. (Dunn)
	nasal inf., RU	94,5(84,3; 101,8)	111,3(101,4; 114,0)			nasal inf.	0,224(0,193; 0,250)	0,187(0,051; 0,332)
	temp. inf., RU	105,1(95,9; 118,7)	127,6(98,8; 150,1)			temp. inf.	0,129(0,106; 0,232)	0,077(0,050; 0,114)
nasal sup., RU	91,6(88,1; 93,0)	121,4(112,0; 129,3)	nasal sup.	0,371(0,311; 0,468)	0,095(0,088; 0,157)			
temp. sup., RU	118,3(112,0; 133,0)	134,7(110,6; 158,3)	temp. sup.	0,276(0,212; 0,376)	0,111(0,099; 0,189)			
significance	n.s. (Dunn)	n.s. (Dunn)	significance	n.s. (Dunn)	n.s. (Dunn)			
SEF	nasal inf. Hz	0,113(0,102; 0,124)	0,124(0,109; 0,143)	REL1	pr. peak fr.	nasal inf. Hz	0,023(0,015; 0,043)	0,023(0,015; 0,035)
	temp. inf., Hz	0,065(0,051; 0,084)	0,127(0,120; 0,138)			temp. inf., Hz	0,015(0,015; 0,019)	0,031(0,015; 0,046)
	nasal sup. Hz	0,081(0,075; 0,083)	0,077(0,069; 0,086)			nasal sup. Hz	0,015(0,015; 0,015)	0,015(0,015; 0,046)
	temp. sup., Hz	0,086(0,077; 0,104)	0,081(0,071; 0,097)			temp. sup., Hz	0,015(0,015; 0,031)	0,015(0,015; 0,027)
	significance	n.s. (Dunn)	n.s. (Dunn)			significance	n.s. (Dunn)	n.s. (Dunn)
	nasal inf. Hz	0,112(0,105; 0,148)	0,100(0,085; 0,118)			nasal inf. Hz	0,015(0,015; 0,031)	0,031(0,027; 0,035)
	temp. inf., Hz	0,064(0,057; 0,083)	0,116(0,096; 0,137)			temp. inf., Hz	0,015(0,015; 0,019)	0,031(0,015; 0,046)
	nasal sup. Hz	0,105(0,091; 0,106)	0,084(0,062; 0,098)			nasal sup. Hz	0,031(0,031; 0,031)	0,015(0,015; 0,031)
	temp. sup., Hz	0,095(0,083; 0,132)	0,085(0,076; 0,118)			temp. sup., Hz	0,015(0,015; 0,031)	0,015(0,015; 0,027)
	significance	n.s. (Dunn)	n.s. (Dunn)			significance	n.s. (Dunn)	n.s. (Dunn)
	nasal inf. Hz	0,131(0,131; 0,143)	0,117(0,092; 0,136)			nasal inf. Hz	0,023(0,015; 0,039)	0,031(0,027; 0,039)
	temp. inf., Hz	0,084(0,064; 0,105)	0,126(0,114; 0,139)			temp. inf., Hz	0,015(0,015; 0,019)	0,031(0,015; 0,046)
	nasal sup. Hz	0,103(0,098; 0,142)	0,082(0,070; 0,111)			nasal sup. Hz	0,031(0,031; 0,031)	0,015(0,015; 0,031)
	temp. sup., Hz	0,097(0,094; 0,144)	0,090(0,078; 0,098)			temp. sup., Hz	0,031(0,015; 0,031)	0,015(0,015; 0,027)
	significance	n.s. (Dunn)	n.s. (Dunn)			significance	n.s. (Dunn)	n.s. (Dunn)

Basic parameters of the study and their p-values (non-parametric Dunn-Test) are represented in tabular form (Table 14). No significant differences were found for the parameters in 4 quadrants of the fundus: nasal inferior, temporal inferior, nasal superior, temporal superior.

3.2 CFD simulation of the blood flow in retinal vessels with different internal microstructure

3.2.1 Newtonian approach

3.2.1.1 Color mapping of the results of CFD simulation

Color mapping of the results of CFD simulation is represented in Fig. 58.

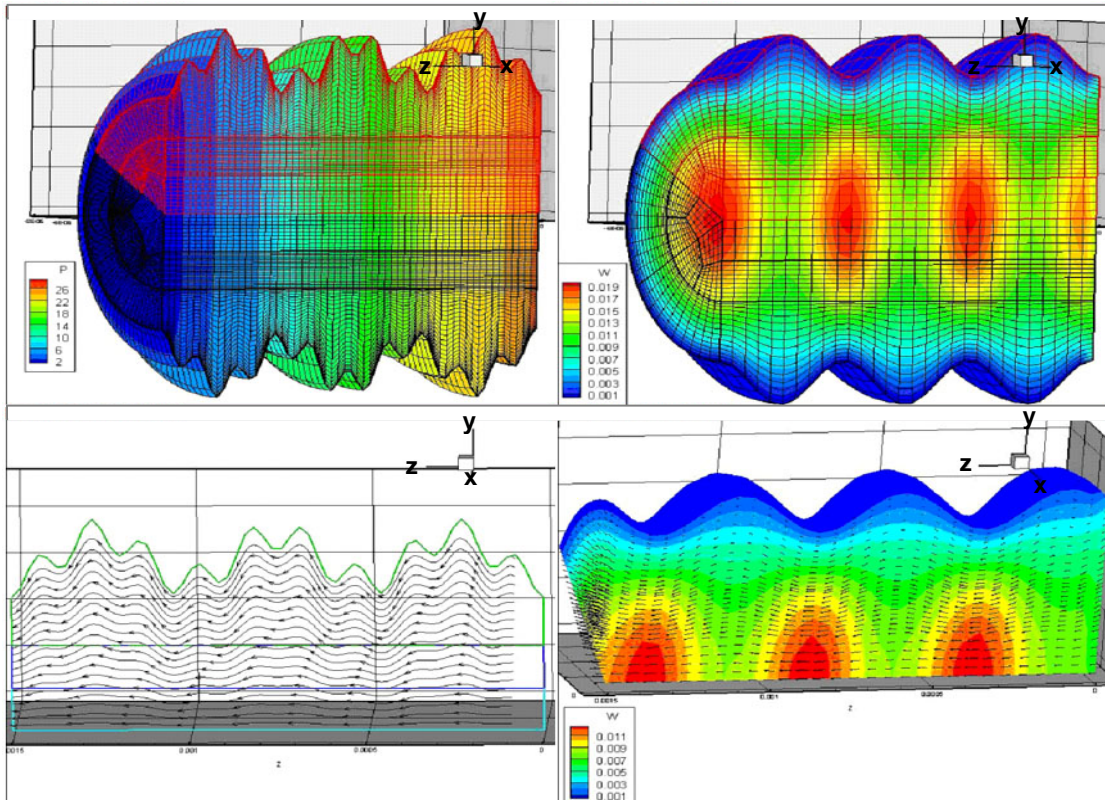


Fig. 58. Color mapping of the results of CFD simulation: **a:** pressure distribution in a simulated wavy vessel segment. **b:** values of the sum velocity vector in a less wavy vessel segment. **c:** streamlines along a wavy wall; **d:** velocity vectors in a wavy vessel segment. Real scales along x , y and z -axes were changed for better performance.

3.2.1.2 Increase of high frequency vessel profile microirregularity augments the vessel hydraulic resistance

The CFD simulations clearly showed that there is no significant difference between results prescribed a laminar and a turbulent flow model in the first numerical tests. Thus, further numerical calculations were performed only using the laminar model.

The results of CFD simulation with constant inflow velocity $\overline{c_{in}}$ are shown in Fig. 59 and Fig. 60.

Fig. 59 *b, c,* and *d* show the variations for one-component sinus-profiles, which are depicted in Fig. 59*a*. For all these charts the averaged velocity $\overline{c_{in}} = 5$ mm/s and the considered vessel length $l = 1,5$ mm have been kept constant. The dependence of the loss coefficient describing the hydraulic resistance

$$\zeta_v = f \{ L; \Lambda = const; A = const \} \quad (31)$$

represented in Fig. 59 is evident. The coefficient ζ_v of an investigated vessel segment increases as the dimensionless parameter vessel length L or the reciprocal diameter of the vessel segment increases, while A and Λ remain constant. Consequently, the longer the segment is, or the less the vessel diameter is, the higher is the hydraulic resistance, which coincides with the laminar tube flow (Hagen-Poiseuille's Law, 1.2.5.3). Changes in resistance with L are almost proportional to L . Indeed a variation of $L \sim l$ with "frozen" A and Λ means a simple change of the length of the tube l with certain parameters of the waviness. For each combination of parameters A and Λ a separate curve can be calculated; see Fig. 59b.

Fig. 59c represents the dependence of the resistance coefficient ζ_v on the waviness parameter Λ :

$$\zeta_v = f \{ \Lambda; L = const; A = const \}. \quad (32)$$

The coefficient of hydraulic resistance ζ_v of an investigated vessel segment decreases as dimensionless parameter Λ , describing the wavelength of the longitudinal profile, increases, while A and L remain constant. Consequently, the longer the waves of the longitudinal profile are, the less is its hydraulic resistance, which obviously tends to an asymptotical limit. The hydraulic resistance of the same segment with no waviness is equivalent with a straight tube with smooth parallel walls. The larger the diameter of the segment is in comparison to the magnitude of the waviness (the less is the dimensionless parameter A), the lesser is the influence of the waviness on the hydraulic resistance of the vessel segment. The corresponding curve $\zeta_v(\Lambda)$ is shifted towards lower ζ_v - values, see Fig. 59c.

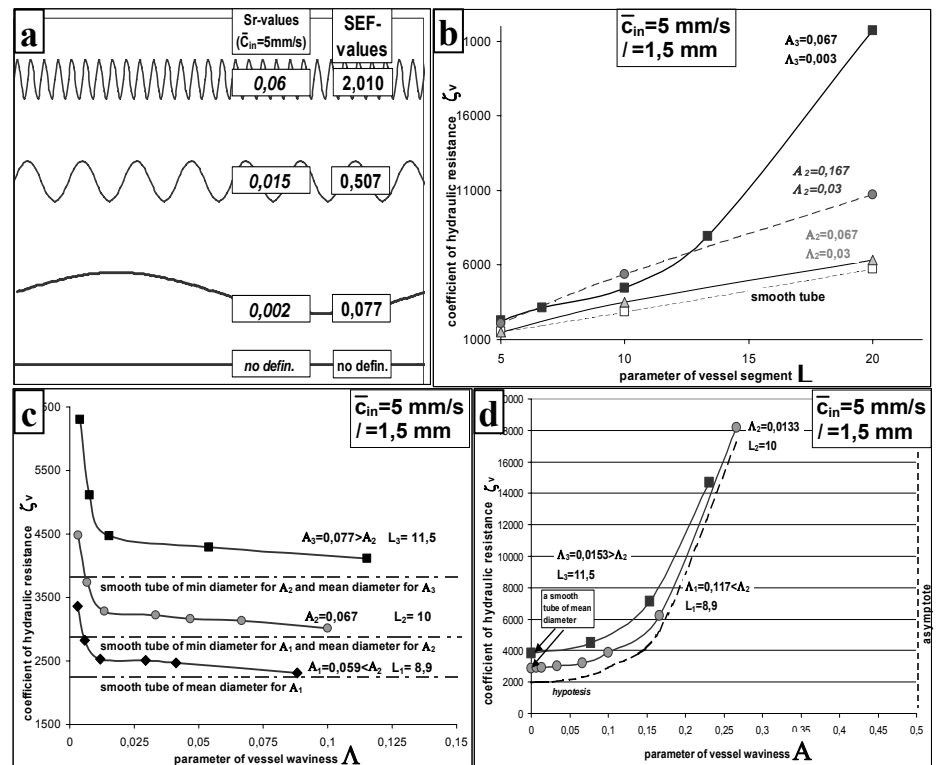


Fig. 59. Quantitative results of CFD simulation on plots. **b,c,d:** calculated dimensionless coefficient of hydraulic resistance in a vessel segment dependent on dimensionless parameters, $L=l/\bar{d}$, $\Lambda=\lambda/\bar{d}$ and $A=a/\bar{d}$ with sense of the segment diameter, the wavelength and the magnitude of vessel wall waviness correspondingly for vessel wall configurations represented on **a**. Inflow velocity $c_{in}=5\text{ mm/s}$ and the vessel length $l=1,5\text{ mm}$ in all numerical calculations here.

Obviously, the $\Lambda \rightarrow \infty$ tends to the resistance of the smooth straight non wavy tube with $A=0$ for the same L and diameter \bar{d} . For fixed parameters L and A , $\Lambda \rightarrow 0$ tends to the resistance of a smooth tube with a "minimal" diameter of $\bar{d} - 2a$. According to the numerical simulation, the resistance of a highly wavy vessel segment can overcross this level and become even higher. On the other hand at $\Lambda=0$ the amplitude $A=0$ and the resistance of the vessel segment equals rigorously to the resistance of a smooth tube of a "mean" diameter \bar{d} . Therefore the curves in Fig. 59c should have an inflection somewhere near $\Lambda=0$. From this inflection point the vessel resistance should

Obviously, the $\Lambda \rightarrow \infty$ tends to the resistance of the smooth straight non wavy tube with $A=0$ for the same L and diameter \bar{d} . For fixed parameters L and A , $\Lambda \rightarrow 0$ tends to the resistance of a smooth tube with a "minimal" diameter of $\bar{d} - 2a$. According to the numerical simulation, the resistance of a highly wavy vessel segment can overcross this level and become even higher. On the other hand at $\Lambda=0$ the amplitude $A=0$ and the resistance of the vessel segment equals rigorously to the resistance of a smooth tube of a "mean" diameter \bar{d} . Therefore the curves in Fig. 59c should have an inflection somewhere near $\Lambda=0$. From this inflection point the vessel resistance should

decrease at $\Lambda \rightarrow 0$. Nevertheless the vessel resistance at these small values of Λ is not applicable from the practical point of view.

Fig. 59d represents the dependence of the resistance coefficient ζ_v as a function of the amplitude A :

$$\zeta_v = f \{ A; L = const; \Lambda = const \}. \quad (33)$$

If wavelength λ of the longitudinal profile and the vessel diameter \bar{d} remain constant, and the magnitude a increases, the hydraulic resistance of the vessel segment ζ_v increases. It approaches the infinity if the magnitude a approaches half the diameter, since the waviness closes completely the vessel clearance. The higher the Λ value is, the higher is the appropriate curve shifted up in Fig. 59d.

The hydraulic resistance of the vessel segment ζ_v increases when SEF of the vessel longitudinal profile increases (Fig. 60b,d). At the lower end it tends to the resistance of a straight vessel (for a straight line SEF cannot be correctly calculated, and it was considered to be 0). Here, like the plot Fig. 59c, the larger is the diameter of the segment, while the magnitude of the waviness remains constant, the lesser is the influence of the waviness on the hydraulic resistance of the segment. The corresponding curves in Fig. 60b,d is shifted towards lower values of ζ_v .

3.2.1.3 Comparison of geometric parameter influence to the model. Sensitivity analysis

The sensitivity analysis was carried out with the goal to define the sensitivity of the model outcome measure (the coefficient of hydraulic resistance of the vessel segment) to variations in geometrical model inputs Λ , A and L . Comparative influence of each geometrical parameter of the wavy vessel

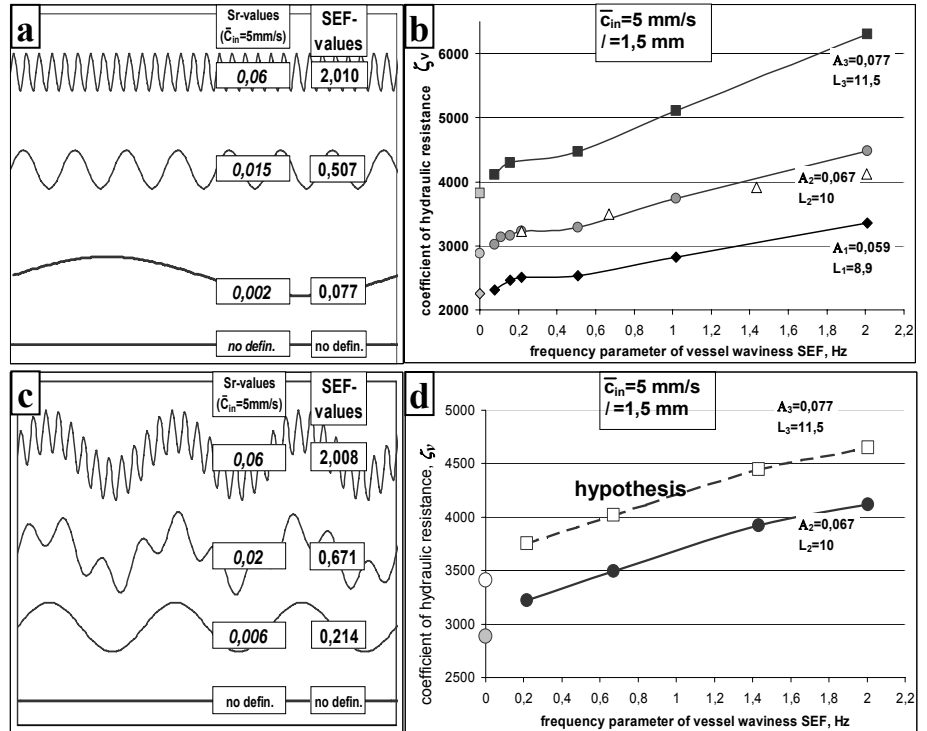


Fig. 60. Quantitative results of CFD simulation on plots **b, d**: dimensionless resistance coefficient ζ_v in a vessel segment dependent on SEF of vessel wall configurations represented on a and c correspondingly. SEF-values for each curve are shown on a and c as well. For comparison one of the curves from **d** is depicted in **b** with white triangles. The points corresponding to the smooth straight vessel wall are shown in **b** and **d** on the ordinate axis with no connection to the curves. Inflow velocity $\bar{c}_{in} = 5$ mm/s and the vessel length $l = 1,5$ mm in all numerical calculations here.

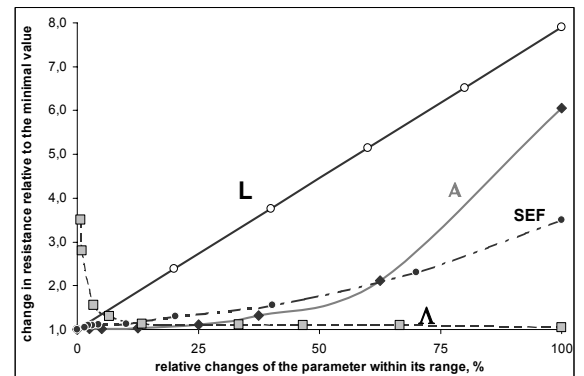


Fig. 61. Sensitivity analysis. Comparative influence of each geometrical parameter of the wavy vessel segment to the resistance of the segment.

segment on its hydraulic conductivity is studied numerically. The geometrical factors studied were varied independently over their ranges from their minimal (0%) to their maximal values (100%). The change of the outcome measure relative to its minimal calculated value is depicted in Fig. 61.

Though the relationship “vessel diameter – vessel length” caused most changes in hydraulic resistance, the parameters of the waviness do still considerably influence the resistance of the blood flow, see Fig. 61. Λ represents here the most interesting parameter, because it reflects changes of the frequency of the waviness, which reflects the changes in the vessel wall microstructure shown in the experimental studies of the present work. Note that Λ might cause up to 3 – 4 times change in hydraulic resistance of a vessel segment if period of the waviness λ is relatively low, i.e. SEF is relatively high and the vessel segment wall possesses microirregularities.

3.2.1.4 Pump head-capacity characteristic

It seems, that from the practical medical point of view another representation of numerically calculated data on vessel segment resistance can be more informative, namely the analogue of pump head-capacity characteristic, i.e. the pressure loss along a vessel segment dependent on volumetric flow rate. This seems to show comparatively, how much power should have the heart to pump the blood through the vessel system with certain parameters of waviness. These dependences for one-component sinus-profiles of the vessel wall and the inflow velocities ranged from 1 to 50 mm/s are shown in Fig. 62. From formula (2) it follows:

$$\Delta p \sim \zeta_v(Q)Q^2. \quad (34)$$

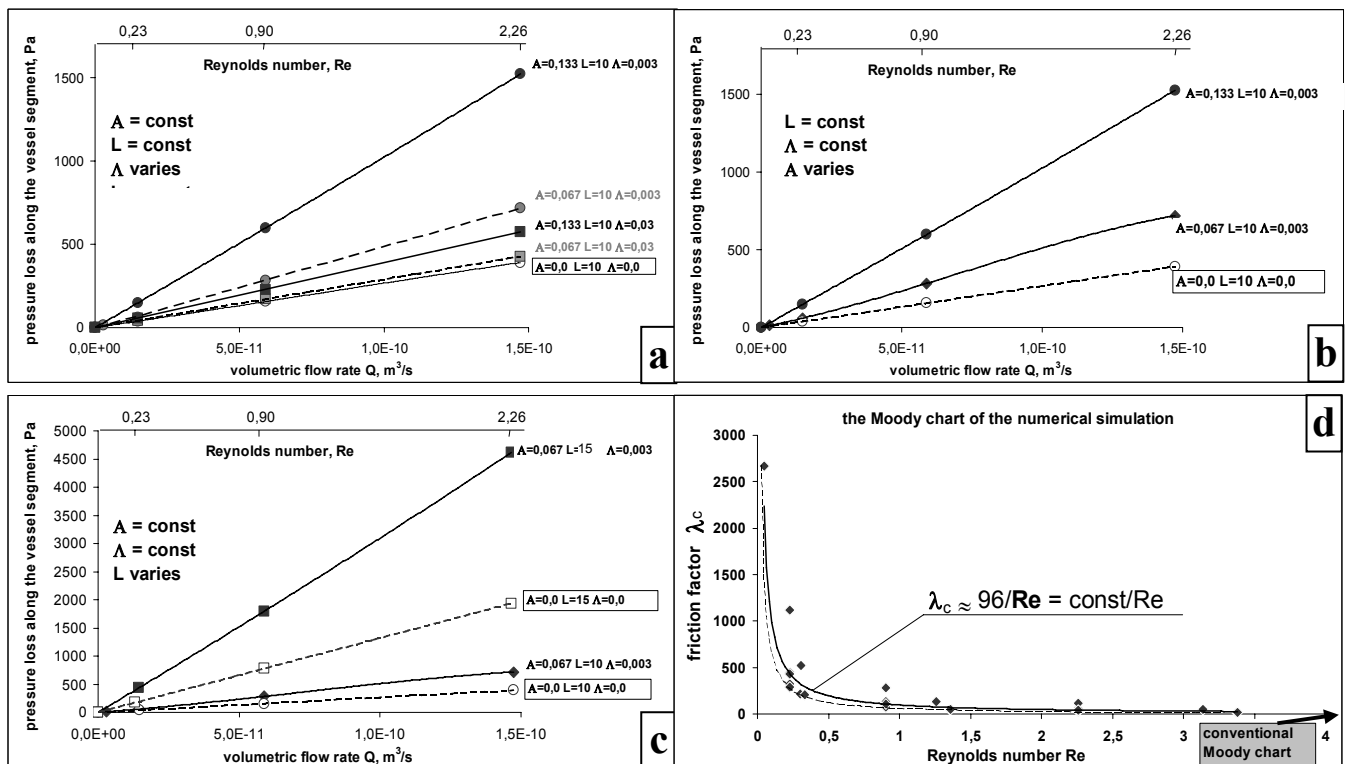


Fig. 62. Quantitative results of CFD simulation. **a,b,c:** analogue of pump head-capacity characteristic: pressure loss along a vessel segment dependent on volumetric flow rate for cases when two parameters of the waviness are constant and one parameter changes. White points correspond to the smooth straight vessel wall. Inflow velocity c_{in} varies from 1 to 50 mm/s. **d:** reality check of the model (Moody chart): calculated from ζ , friction factor λ_c is nearly proportional to the reciprocal of Reynolds number. Theoretically predicted dependence $\lambda_c = 64/Re$ is depicted with dashed line.

Replacing ζ_v by the friction coefficient λ_c from the equation (34) may be written as follows:

$$\Delta p = \lambda_c(Q) \frac{l}{d} Q^2 \quad (35)$$

In the model formulation used, the flow is laminar and the Reynolds numbers \mathbf{Re} are very small, see equation (28). It is known, that for small Reynolds numbers, $\lambda_c \sim 1/\mathbf{Re}$ that is $\lambda_c(\mathbf{Q}) \sim 1/\mathbf{Q}$. This leads to the fact that the pressure loss is proportional to the flow rate.

$$\Delta p \sim Q \quad (36)$$

Numerical modeling yields the same result, i.e. the pressure drop along the tested vessel segment is proportional to the flow rate, and the slope depends on geometric characteristics of the vessel wall (Fig. 62a,b,c). Each line in the Fig. 62a,b,c is calculated for a certain vessel wall configuration at different inflow velocities.

Per definitionem, the power needed to pump the blood through the vessel-tube equals to the area under the pump head-capacity characteristic. The more hydraulic resistance of the vessel is, the more is the corresponding needed pump power and the steeper is the straight line in Fig. 62a,b,c. From Fig. 62a,b it can be seen that changes in parameters \mathbf{A} and $\mathbf{\Lambda}$ lead to changes of the same order in the slope. However in the calculated examples a ten times decrease of the parameter $\mathbf{\Lambda}$, see Fig. 62a, leads almost to the similar changes in the slope as the two times increase of the parameter \mathbf{A} , see Fig. 62b. A variation of \mathbf{L} influences the slope much more than a variation of the other two geometric parameters (Fig. 62c).

Fig. 62d represents a so called “reality check” for the applied numerical method. The plot shows the Moody diagramm (Blevins 1984) for small Reynolds numbers. The friction factors λ_c are recalculated from ζ_v , which were obtained numerically during the simulation. The chart shows, that λ_c is nearly proportional to the reciprocal Reynolds number, as it was expected. The power trend line of depicted calculated points runs near to the theoretically predicted dependence for a round vessel cross-section with straight walls, $\lambda_c = 64/\mathbf{Re}$, which is depicted in Fig. 62d as a dashed line.

3.2.1.5 Influence of the blood viscosity

Rheological parameters of the blood are of paramount importance in the model, also in simplified Newtonian case. Since exact data on blood viscosity in retinal arteries are not available the averaged value of apparent dynamic blood viscosity $\eta=0,0035\text{Pa}\cdot\text{s}$ has been taken from the literature (Fung 1990; Andrews et al. 2000) ($\nu=3,317\cdot 10^{-6} \text{ m}^2/\text{s}$). Presumably this data should be corrected for the case of small blood vessels. Fahreaus-Lindquist effect on the one hand (decrease of blood viscosity when outflowing from a big vessel into a small one (Fung 1990; Samoilov 2004)) as well as increased blood concentration in small

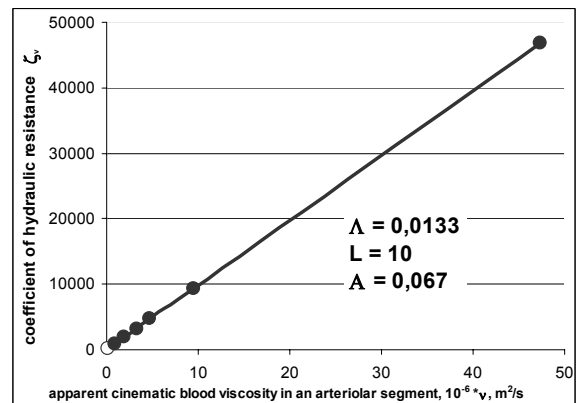


Fig. 63. Calculated influence of apparent cinematic viscosity ν in the model on the dimensionless resistance coefficient ζ_v in a vessel segment.

vessels on the other hand (Samoilov 2004) do play an important role here with vessels smaller than $500\mu\text{m}$ in diameter. However quantitative values of η and hematocrit in small vessels are controversial. For example, according to A. Samoilov (2004) the apparent dynamic blood viscosity in small arterioles and capillaries approaches the value of $0,8 \text{ Pa}\cdot\text{s}$ or $\nu=758\cdot 10^{-6} \text{ m}^2/\text{s}$. Fung affirms that the apparent dynamic viscosity in small vessels should be even less than $0,0035 \text{ Pa}\cdot\text{s}$ (Fung 1990).

Nevertheless, the tendency of the waviness influence on the resistance to flow obtained in the present study will not change if corrected data on apparent blood viscosity is prescribed, but the quantitative results will, since vessel segment resistance is strongly influenced by this parameter, see Fig. 63, to be compared with Fig. 59 and Fig. 60.

Conclusions: Results of Newtonian CFD simulation show that increasing high frequency waviness worsens hydraulic conductivity of the vessel segment hence increasing its resistance to flow. There was no significant difference between results calculated with laminar and turbulent model in this model formulation for the whole considered range of vessel segment waviness.

3.2.1.6 Color mapping and hydraulic resistance of real longitudinal vessel profiles. Examples.

Color mapping and quantitative results of Newtonian CFD simulation in real longitudinal retinal vessel profiles are shown in Fig. 65 - Fig. 67. The example longitudinal profiles are chosen from the glaucoma study 2. They correspond to the profiles shown in Fig. 39a,b. Note, that real relations vessel length - vessel diameter are not maintained here for the better performance. In order to analyse, how the real vessel lumen relations look like in reality, the examples of the inner structure of baseline vessel lumen recalculated from measured longitudinal vessel profiles with the assumption of axial symmetry *in the real scale* are depicted in Fig. 64.

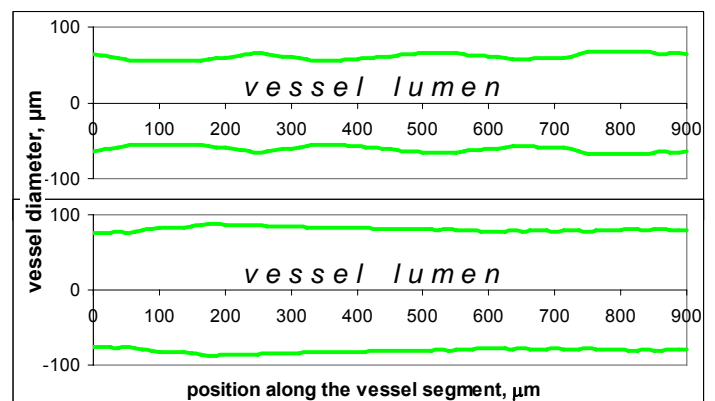


Fig. 64. Clinically measured baseline configurations of vessel lumen. Examples of a normal person (Top) and a glaucoma patient (Bottom) from glaucoma study 2, Fig. 39. Real scales along x and y -axes are maintained.

In Fig. 65 the examples of real longitudinal arterial profiles of a normal person and a glaucoma patient are redrawn in absolute scale for 4 phases of vessel reaction. The inner structure of vessel lumen recalculated from measured longitudinal vessel profiles with the assumption of axial symmetry for these vessel reaction phases is given underneath. Color mapping of axial and vertical velocities in Newtonian CFD simulation are shown below for these profiles at mentioned phases of vessel reaction ordered according to the vascular tone change from the constriction (maximal tone) to the dilation (minimal tone), see Fig. 40. Fig. 66 shows the pressure drop color mapping and the values of the main geometric and hemodynamic parameters in SI system of units with the presumption that the inflow velocity \bar{c}_{in} amounts to 5 mm/s in accordance with results in Fig. 59 and Fig. 60.

Since this velocity rate might be too low for real vessels, the color mapping of axial and vertical velocities in the baseline vessel lumen configuration and the values of the main geometric and hemodynamic parameters at

different inflow velocities \bar{c}_{in} are plotted in Fig. 67. Note that the pressure loss Δp increases when \bar{c}_{in} and the corresponding volumetric flow rate Q increase as it was predicted in Fig. 62. However, the coefficient of hydraulic resistance ζ , decreases with increasing \bar{c}_{in} . The last examples in both columns show the flow conditions with equal volumetric flow rates. The example vessel of a glaucoma patient has a larger lumen than the corresponding vessel of a healthy volunteer. As the vessel diameter has the major influence to its hydraulic resistance (Fig. 61), the quantitative results of a patient and a control person are not directly comparable with each other.

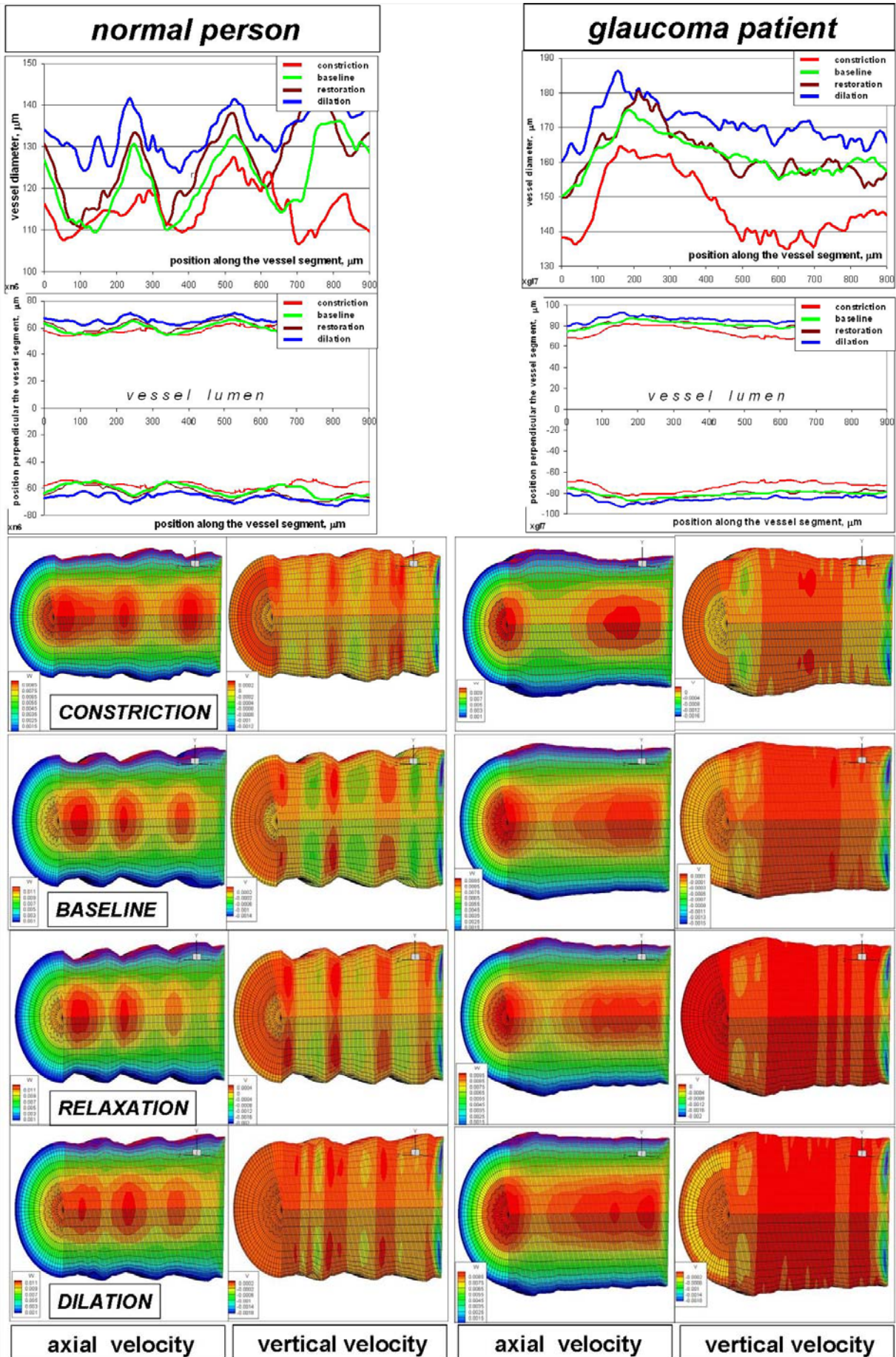


Fig. 65. CFD simulation for real retinal arterial profiles measured with RVA. Examples of a normal person and a glaucoma patient (glaucoma study 2, Fig. 39). **Top:** absolute values of longitudinal vessel profiles at different phases of vessel reaction from the constriction to the dilation. **Middle:** the inner structure of vessel lumina recalculated from measured longitudinal vessel profiles with the assumption of axial symmetry. **Bottom:** color mapping of axial and vertical velocities. Real scales along x , y and z -axes are modified for better performance. Color scales in maps differ from each other.

Fig. 66. CFD simulation for real arterial profiles measured with RVA: color mapping of pressure drop and values of main parameters. Examples of a normal person and a glaucoma patient (glaucoma study 2, Fig. 39). Real scales along x , y and z -axes are modified for better performance. \bar{c}_{in} - inflow velocity; \bar{d} - median vessel diameter; A_s - cross-sectional area of the vessel lumen at the inflow; Q - volumetric flow rate; Δp - pressure drop along the vessel segment; ξ_v - coefficient of hydraulic resistance; Re - Reynolds number; SEF - Spectral Edge Frequency; Sr - Strouhal number. Color scales in maps differ from each other.

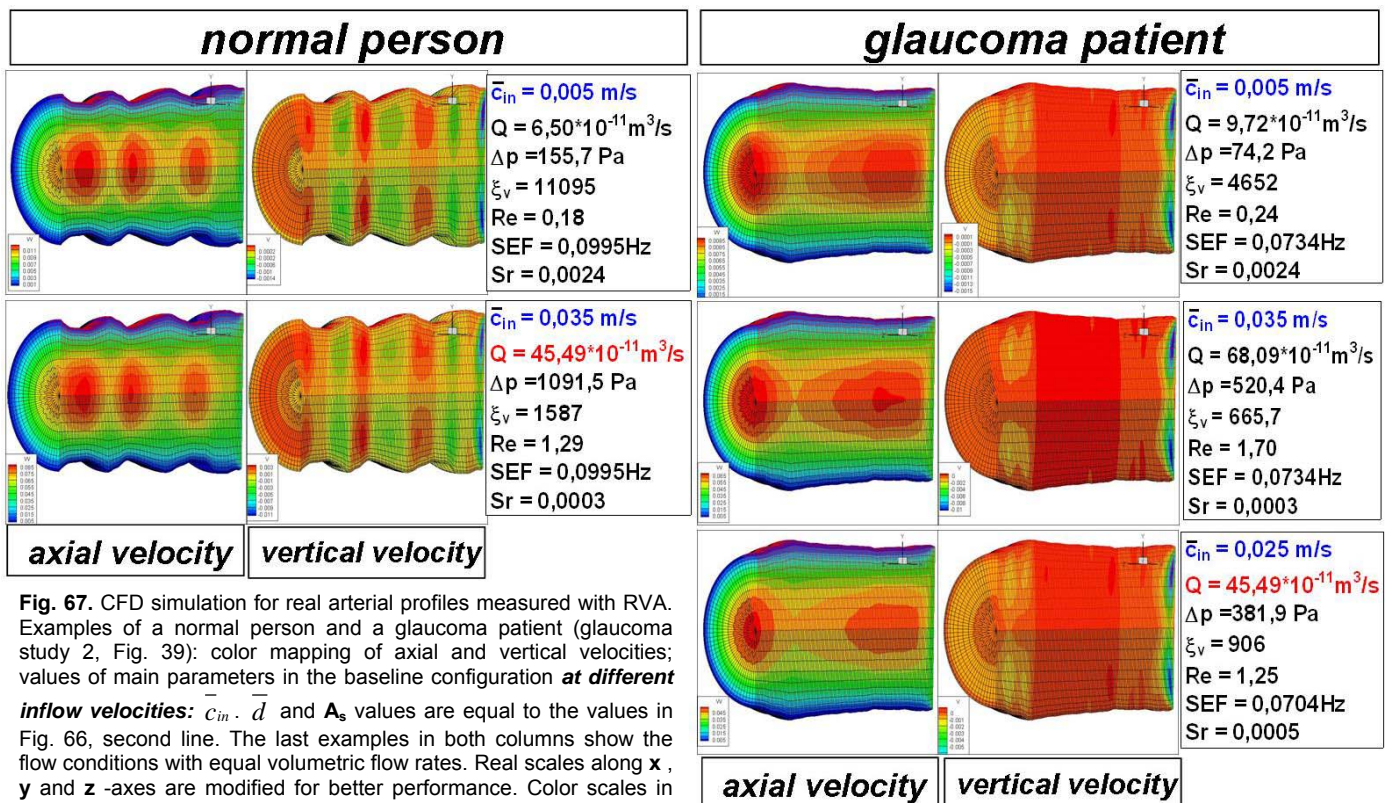
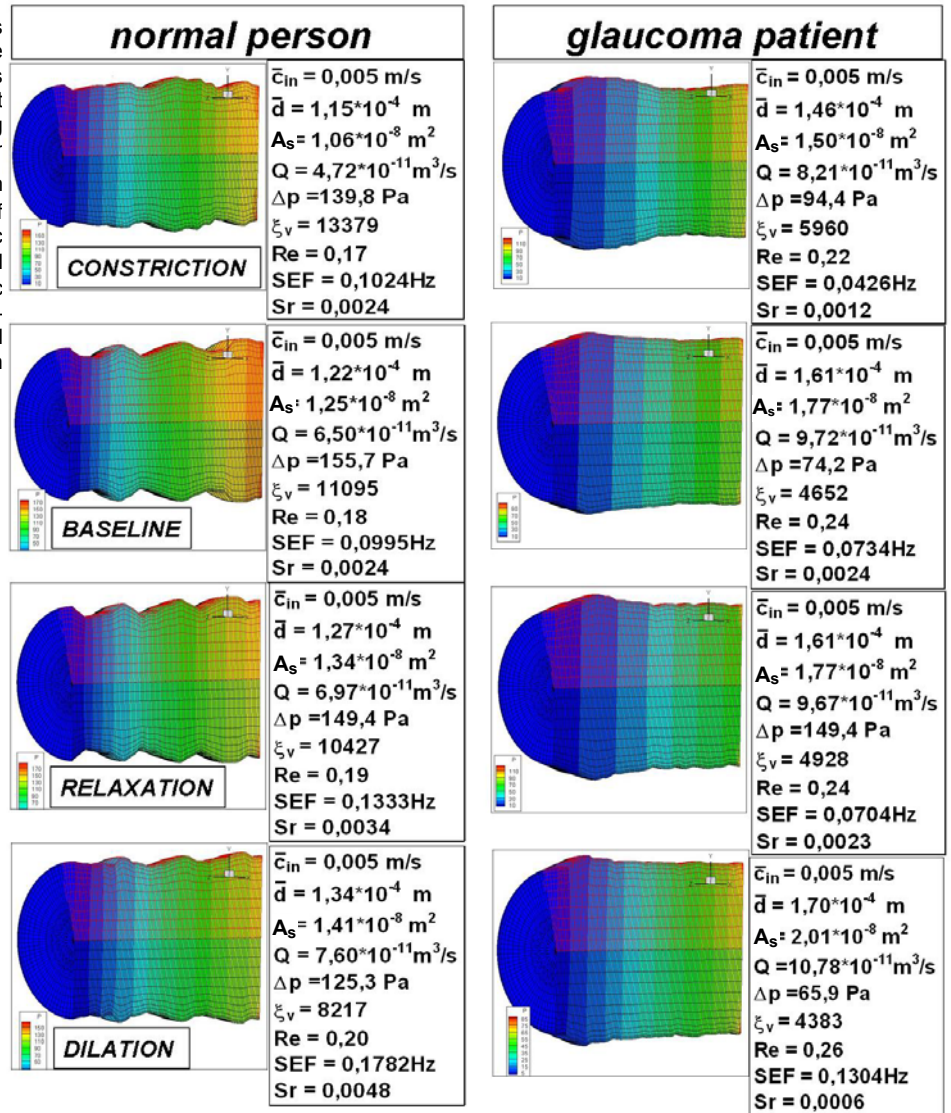


Fig. 67. CFD simulation for real arterial profiles measured with RVA. Examples of a normal person and a glaucoma patient (glaucoma study 2, Fig. 39): color mapping of axial and vertical velocities; values of main parameters in the baseline configuration **at different inflow velocities**: \bar{c}_{in} . \bar{d} and A_s values are equal to the values in Fig. 66, second line. The last examples in both columns show the flow conditions with equal volumetric flow rates. Real scales along x , y and z -axes are modified for better performance. Color scales in maps differ from each other.

3.2.2 Non-Newtonian approach

3.2.2.1 Color mapping and results of CFD simulation

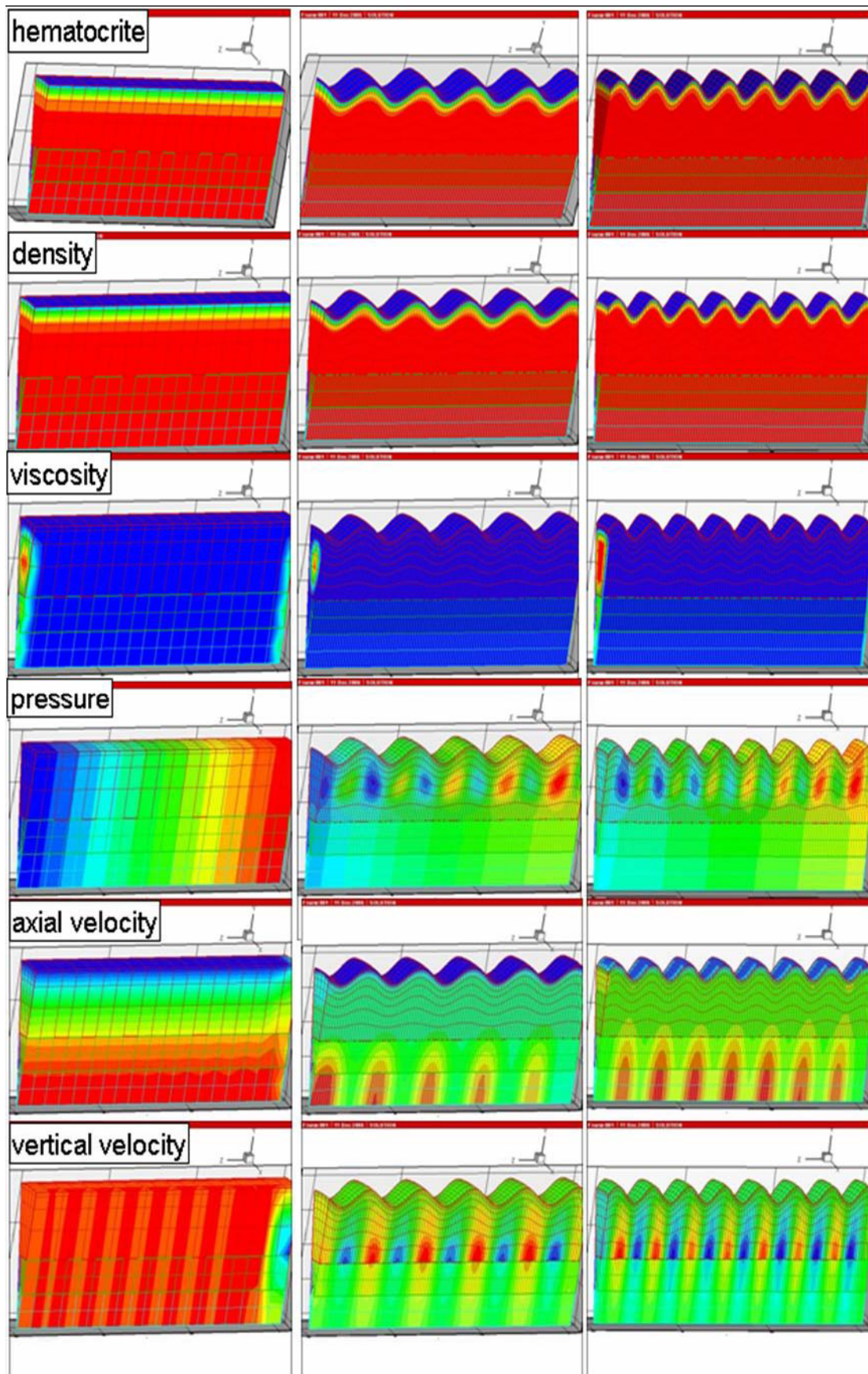


Fig. 68. Color mapping of the results of CFD simulation. An example.

3.2.2.2 Increase of high frequency vessel profile microirregularity augments the vessel hydraulic resistance

First results of CFD simulation are represented in Fig. 69 and Fig. 69a shows the dependence of the relative resistance coefficient ζ_v / ζ_{v0} as a function of the non-dimensional amplitude A :

$$\zeta_v / \zeta_{v0} = f \{ A; \Lambda = const; L = const \} . \quad (37)$$

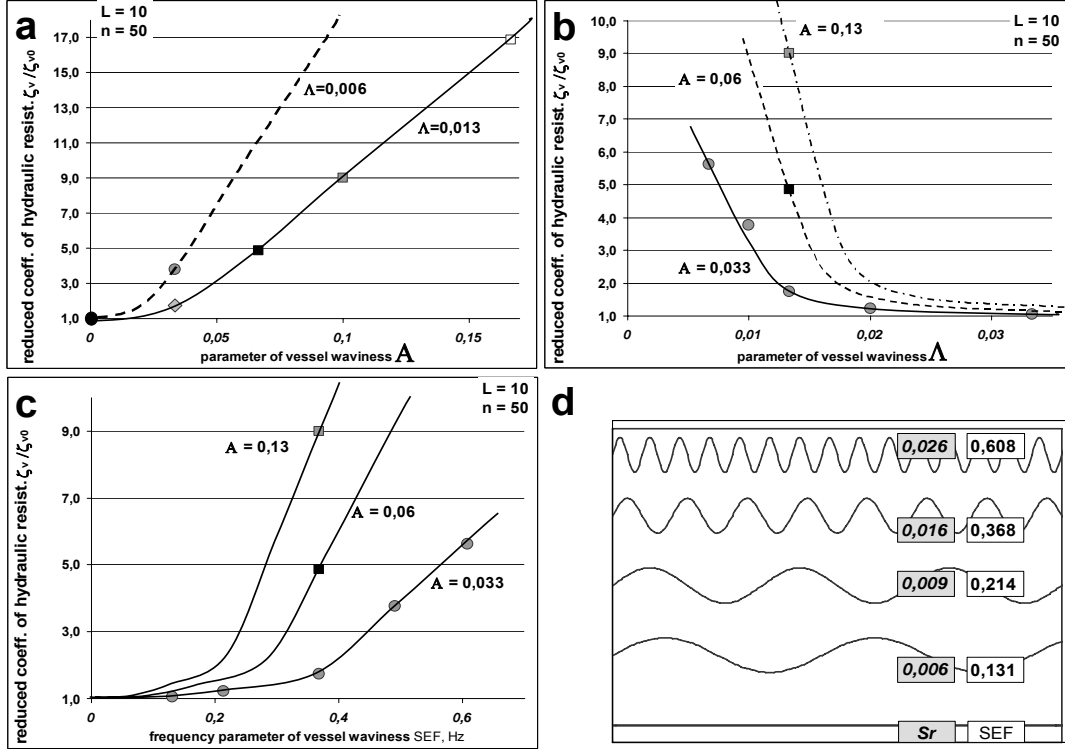


Fig. 69. First results of CFD simulation. **a,b:** calculated reduced coefficient of hydraulic resistance ζ_v / ζ_{v0} dependent on dimensionless fluidmechanical parameters A and L (Fig. 29, Fig. 30) with sense of magnitude and wavelength of longitudinal vessel wall configuration. **c:** reduced coefficient of hydraulic resistance ζ_v / ζ_{v0} dependent on SEF. Grey circlets in plots correspond to vessel wall configurations represented in **d**. **SEF**-values and **Sr** numbers for each curve are shown in **d** in small frames.

In the equation (37) ζ_{v0} is the hydraulic resistance of the same vessel segment with no waviness – a straight tube with smooth parallel walls. The ratio ζ_v / ζ_{v0} increases as the wavelength λ of the longitudinal profile and vessel diameter \bar{d} as well as the vessel length l remain constant, and the magnitude A increases for chosen parameter set. Obviously, ζ_v / ζ_{v0} approaches the infinity if A approaches half the diameter – the waviness closes vessel lumen completely.

Fig. 69b represents the dependence of ζ_v / ζ_{v0} as a function of Λ :

$$\zeta_v / \zeta_{v0} = f \{ \Lambda; L = const; A = const \} . \quad (38)$$

The ratio ζ_v / ζ_{v0} decreases as dimensionless parameter Λ with sense of wavelength of the longitudinal profile increases, while A and L remain constant. Consequently, the longer the waves in the profile are,

the less is its hydraulic resistance. It approaches to the hydraulic resistance of the same segment with no waviness. The straight-walls-tube-resistance is an asymptotical limit for all curves in Fig. 69b.

The ratio ζ_v/ζ_{v0} increases when SEF of the longitudinal profile rises, see Fig. 69c. In case of simple sinus profile SEF tends to be the frequency of the waviness. Consequently, this plot is only a reformulation of Fig. 69b, needed for the conclusions.

Conclusions: *Results of CFD simulation both in the Newtonian and in the Non-Newtonian case show that the increase of high frequency waviness increases the hydraulic resistance of the vessel segment.*

4 Discussion

4.1 Microstructural changes and increase of high frequency microirregularity of longitudinal vessel profile – clinical symptoms characterizing vascular dysfunction.

4.1.1 Age dependence study

Changes in intima media thickness with age in large vessels such as the carotid artery in healthy population have been well demonstrated (Schmidt-Trucksass et al. 2003). Michelson et al. (Michelson et al. 2007) showed age related changes in the wall thickness of small retinal arteries and veins. Since retinal vessels are easily observable and are part of the microvasculature they could be used as a substitute for assessment of small vessel disease.

The primary functional characteristic of vessels is their lumen diameter. The diameter determines their resistance. The diameter itself is determined by the active properties and structural properties of the vessel. The effectors for displaying active properties of a vessel are the smooth muscle cells, their number, their arrangement and their state of contraction. The latter is massively influenced by the endothelial cells and their mediators.

As it was already mentioned, endothelial changes are seen in atherosclerosis, arterial hypertension (Luscher et al. 1987; Luscher 1990; Forte et al. 1997), diabetes mellitus (Tesfamariam et al. 1989), ischemia (Ku 1982; Lesnefsky et al. 1987), and cardiovascular disease (Ku 1982). Several studies indicate that aging and endothelial dysfunction progress in parallel (Matz & Andrantsitohaina 2003; Brandes et al. 2005; Yildiz 2007). In neurovascular coupling vessel dilation is caused by local increase of endothelium-derived nitric oxide triggered by the application of light to the retina. The effect can be blocked by L-NMMA (Dorner et al. 2003), which highlights the importance of nitric oxide and regular endothelial function for a normal neurovascular coupling effect.

The structural properties of the vessel (lumen diameter, media thickness and wall thickness) should be determined with the smooth muscle cells relaxed and with the vessel exposed to a known intravascular pressure. A reduced lumen and increased media to lumen ratio was found with the size of the individual smooth muscle cells being normal and the functional responses of the smooth muscles cells being affected only on a small scale. Since there was no increase in media cross sectional area, the remodeling consisted of a rearrangement of normal cells around a smaller diameter.

In aging A. Ferrari et al. (2003) described migration or proliferation of vascular smooth muscle cells infiltrating the subendothelial space, increased deposition of collagen, elastin, and proteoglycans, in conjunction with an increase in blood cells. M. Lundberg and M. Crow (1999) showed impaired signal transduction pathways in vascular smooth muscle cells examining the ability of older cells to respond to inhibitors. Being non-uniformly

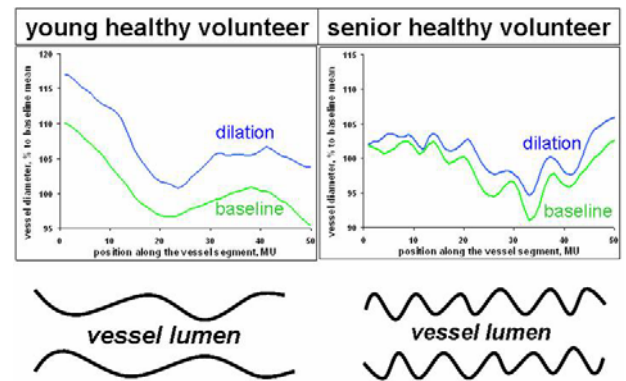


Fig. 70. Age dependence study. Schematic illustration of obtained results. **Top:** characteristic longitudinal arterial profiles in individual baseline and during dilation. **Bottom:** graphic interpretation.

distributed along an artery these pathologic processes might be a cause for microirregularities in the longitudinal vessel profile.

A statistically significant difference in the arteriolar longitudinal vessel profiles was found in the three different age groups (Fig. 37, right). In older healthy persons more small undulations were found. The younger group had more lower frequency diameter changes. Interestingly this pattern was undisturbed by application of the stimulus flickering light and was kept rather constant in the dilation and constriction states caused by neurovascular coupling. The middle age group also showed interesting findings. At baseline longitudinal vessel profile amounted to values inbetween the young and old age group without reaching statistical significance. However during all functional stimulated states the middle age group differed significantly from the young one and was almost identical to the old age group (Fig. 37, right). Although no significant differences in the arteriolar longitudinal vessel profiles were found during the stimulation in the middle age group, this means that in the unstimulated state the vessel wall in middle age is still similar to the one encountered in young persons. However when metabolic demand by stimulation via mediators causes a muscular reaction this pattern changes to the one encountered in older age. So in middle age there is already some functional impairment in vascular reaction following flicker light stimulation.

It is known that the relationship between arteriolar and venous diameter changes with age (Hubbard et al. 1999). In older age arteries possess a smaller diameter in relation to the retinal veins independently from any other arteriosclerotic risk factors. An explanation for the findings of the present work and the reduced arterio-venous relation in older age could be a functional one with smooth muscle cells exhibiting a more pronounced constriction during baseline. This might be due to endothelial dysfunction with may have several effects:

There is defective dilatation even though the endothelium is intact, which may contribute to increases in vasoconstrictor response; Vasodilatation is attenuated or reversed to vasoconstriction, in response to vasoactive products released by activated platelets; impaired endothelium dependent relaxation may contribute to augmented vasoconstriction by serotonin released by platelet aggregation; increased destruction of nitric oxide may play an important role in impairment of endothelium-dependent relaxation thus nitric oxide formation may be normal or even increased but increased degradation of nitric oxide may result in impaired vasodilatation.

Impaired production or impaired reaction to mediators could explain a more irregular appearance of the wall depending on local expression of the changes.

Another explanation for the findings of more high frequency and more irregular longitudinal vessel profiles could be a structural one implying that in older age, similar to the state in hypertension, a smaller lumen exists with normal sized and functioning smooth muscle cells. Since the diameter of the lumen is reduced even small irregularities in smooth muscle cell status are reflected in a more pronounced way. Research from gerontology by A. Ferrari et al (2003) demonstrated that although arteries of healthy elderly subjects have no endothelial lesions or discontinuities, endothelial cells can be irregular in shape and have increased height. This fact might also be part of the age-related retinal vessel irregularity that was found in the longitudinal arterial profile.

As it was mentioned above the pattern of wall irregularities did not change during stimulation. This is presumably an effect of the rather intact feed back mechanism: endothelial cell - smooth muscle cell, in a healthy population which is able to react to physiologic stimuli in an adequate way even in older age (Yildiz 2007).

In venous segments a significant difference in vascular inner wall irregularities between the age groups was found only at the baseline. This is consistent with less pronounced changes in arteriosclerosis in this vascular bed.

Assessment of microirregularities of the vessel lumen applying contemporary methods of image analysis is now widely performed in clinical medicine. Characterization of microirregularities of the arterial inner wall using mathematical methods including frequency analysis has been recently published by several groups analysing intima media configuration in the carotid artery (Espeland et al. 1994; Ishizu et al. 2002; Schmidt-Trucksass et al. 2003; Labropoulos et al. 2005). Labropoulos (2005) reported that “with increased age and number of risk factors present, the wall/blood interface in the carotid artery became more irregular”. The main results of this study are shown in Fig. 71. The strategy of the study and the method of mathematical data analysis are similar to the present work (compare with Fig. 36). However all mentioned attempts have been limited yet mostly to large vessels and have used parameters such as e.g. intima media thickness (IMT) or pulse wave velocity. The present age-dependence study claims to be the first detailed clinical report on age related changes of the longitudinal inner wall structure in large retinal arteries. These findings in retinal arteries complement the knowledge acquired for microirregularities in large vessels.

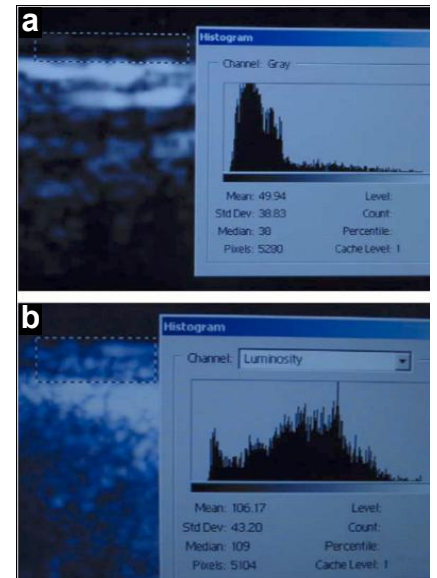


Fig. 71. Computer echo density analysis of the carotid IMT from (Labropoulos et al. 2005). The median distribution of grey values of pixels within the intima media of a healthy volunteer (a) has a much lower value than that from an older patient (b).

The question remains, whether more irregular and higher frequency of vessel wall diameter change have any implication. Since fluidmechanical simulations in the present study showed that irregular rough structure of the internal vessel wall lead to increased resistance to flow, the reported experimental findings might be an explanation for increase in blood pressure in older populations. Also the adherence of cellular blood components might be increased by more irregular structures.

Conclusions: *The blood column or lumen diameter of retinal arteries shows a significantly higher degree of irregularity in older subjects than in younger subjects at different phases of vessel reaction. The irregularities are likely due to microirregularities of the inner arterial wall. Such findings have been reported in larger conduit arteries but the technology to investigate this phenomenon in much smaller arteries in the microcirculation has not existed. Clinical implications of these findings remain to be evaluated.*

4.1.2 Glaucoma study

An appropriate parameter of vessel microirregularity was introduced in this study. It was used to demonstrate quantitative differences in longitudinal arterial profiles between healthy subjects and age matched glaucoma patients without treatment. Arteries of untreated POAG patients seem to possess more microirregularities in their walls than arteries of healthy persons of the same age (Fig. 72). This finding might correspond to the described corrugated arteries in vascular diseases (Foster et al. 1968; Alm 1992) and “sausage-string” patterns in microvascular

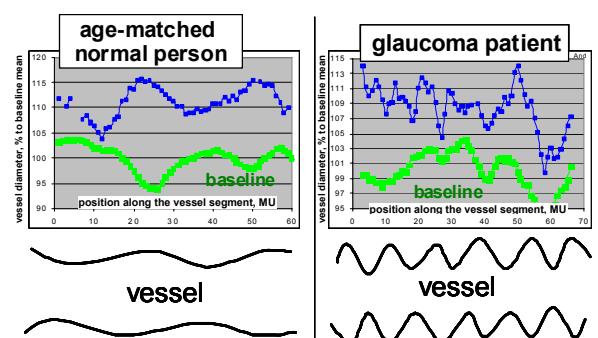


Fig. 72. Glaucoma study. Schematic illustration of obtained results. **Top:** characteristic longitudinal arterial profiles in individual baseline and during dilation. **Bottom:** graphic interpretation.

structures in systemic hypertension (Alstrøm et al. 1999; Jacobsen et al. 2002).

The question is whether the vessel microirregularities encountered in systemic diseases damaging the vascular endothelium might be similar to those found by us in glaucoma patients. A dominating view is that due to high blood pressure, the vascular endothelium undergoes alterations and local irregularities appear (New 1966; Jacobsen et al. 2002).

It could be argued that the periodic pattern reflects a possible pathologic spatial heterogeneity in the distribution of receptors on the vascular smooth muscle cells or a heterogeneity in the distribution of contractile filaments along the vessel. An uniform increase in the tone of the vascular smooth muscle cells along a homogeneous vessel can lead to the formation of a periodic pattern of constrictions and dilations (Alm 1992; Jacobsen et al. 2002). Jacobsen et al. (2002) suggested that under certain conditions the normal, cylindrical shape of a blood vessel may become unstable, and as a result the vessel exhibits a periodic pattern of constrictions and dilations. To the best of the author's knowledge no study has yet demonstrated evidence for increased muscle tone in retinal arteries or pathologic spatial heterogeneity in the distribution of receptors on the vascular smooth muscle cells in glaucoma.

The increased HFW of retinal arterial segments in glaucoma patients might be explained by local endothelial dysfunction in POAG and could be due to the following local cellular mechanisms (Brown & Jampol 1996; Buckley et al. 1997): endothelin activation of a membrane receptor such as acetylcholine, can lead to an increase in the concentration of intracellular calcium, which in turn activates NO-synthase and the production of nitric oxide. This leads to relaxation of the underlying smooth muscle cells and consequently to vasodilation. On the surface of smooth muscle cells acetylcholine may also interact with a receptor and in a similar manner, increase the intracellular concentration of calcium. This can lead to the contraction of smooth muscle cells. This vasoconstrictive effect is counterbalanced by the strong relaxing effect of NO under normal conditions. However in pathologic conditions as in endothelial dysfunction with a decrease in NO production such an agonist can cause local vasoconstriction instead of relaxation (Brown & Jampol 1996).

With increased high frequency waviness of longitudinal arterial profiles such local disturbances between vasoconstrictive and vasodilative actions in glaucoma are assumed to have observed. Consequently smooth muscle bundles in the vessel wall cannot relax to demand (Fig. 73, dark grey circles) despite autoregulative request. As retinal arteries still possess areas with intact endothelial lining, other muscle bundles (pale grey circlets) can still relax properly in response to such a demand. Thereby a wavy vessel wall profile is formed (Fig. 73).

Increased waviness of the vessel wall might represent transient vasospasms because of progressive endothelial dysfunction, thereby disturbing autoregulation of a whole vessel segment.

In order to assess the dependence of HFW on the underlying vascular tone the state of vessel tone against the HFW found during studies 1 and 2 (Fig. 40, Fig. 41) was plotted. The results in the control group confirm the results of the age-dependence study for healthy middle aged volunteers: the HFW of retinal arteries in healthy

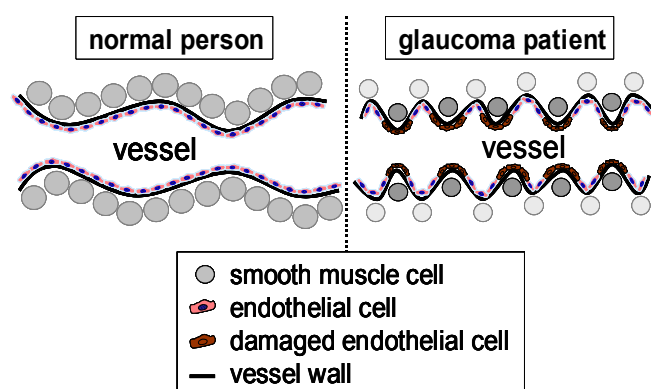


Fig. 73. Possible explanation for increased vessel thickness change frequency of arterial segments in glaucoma. Presumably some smooth muscle cells (dark grey painted circlets) do not react in glaucoma patients because of endothelial dysfunction.

subjects does not change considerably regardless of the underlying tone. As can be seen in Fig. 40 and Fig. 41 this is not the case in the POAG patients in either provocation study. One could argue that suprasystolic IOP increase does not reflect a natural insult as encountered in POAG. However the moderate IOP increase as performed in study 2 is quite likely occurring in normal persons rubbing their eyes and may be even in the course of POAG. From the results of the present work it seems that retinal vessels of POAG patients are not able to react even to moderate IOP increase in a healthy physiological manner. It was also found that the HFW at baseline does not differ between the groups. Treatment by dorzolamide shows a trend toward less HFW changes following IOP provocation. Whether this effect is real, needs further investigations and cannot be statistically proven from experiments of the present study with rather small numbers of subjects. The results of the present work together with the detected differences in micro parameters between groups at dilation phase demonstrates that autoregulation and its pathological changes needs to be evaluated in their dynamic circumstances (Nagel et al. 2001).

The observed difference in HFW between the control and untreated groups may be attributed not only to local endothelial dysfunction, but might be due to the difference in baseline IOP between the two groups and a different vessel status due to IOP level. It is impossible to differentiate between the underlying causes with experimental set up used in the present work.

If assuming that local endothelial dysfunction of retinal vessels is associated with POAG, the HFW obtained in the treated POAG group should have also shown a significant difference from that in the normal control group. HFW in the treated group was between the normal and POAG before treatment groups in the present study. However the sample size might have been too small to reach a level of significance. In order to investigate the probable effects of carboanhydrase inhibitors on endothelial function with the experimental set up of the present work larger numbers of patients need to be studied.

The structure of high frequency waviness of longitudinal vessel profiles changes significantly after the stimulus in POAG patients and differs from HFW of normal persons (Fig. 40). HFW as a manifestation of arterial microirregularity is an individual characteristic of an arterial segment which changes over time physiologically or following pathologies causing vascular dysfunction, like POAG and might be influenced by drugs. It also represents only a small component of the total regulatory action which occurs mainly in smaller precapillary retinal vessels (20 – 40 μm). HFW should be considered to be an integral part of the functional dynamic autoregulative response to increased metabolic demand after IOP provocation either in experiments or in nature by POAG.

The provocation for vessel reaction in both studies study was induced by artificial IOP increase by suction cup, which causes a decrease in perfusion pressure and a metabolic deficit. Microcirculation responded differently in patients with POAG and in healthy subjects. Whether that experimental IOP increase represents a stimulus similar to the one encountered in glaucoma remains to be proven. Suprasystolic IOP values are not usually encountered in POAG. However the stimulus in the study 1 might represent an exaggerated impact such as the one responsible for reperfusion injury in the disease. The stimulus in study 2 seems to be more resembling to the insult in POAG. The selected provocation time of 100 s proved to be too short to observe a new steady state of the vessels during the continuous perfusion pressure reduction (Nagel & Vilser 2004). However the oscillations in the temporal response curve (Fig. 25, bottom) during the provocation phase suggest that a new equilibrium was to be achieved under changed but constant perfusion conditions. Further studies of vessel reactivity are needed with different stimuli achieving a more appropriate IOP increase. IOP increase is however the most similar insult to glaucoma

disease among the stimuli used to date when employing RVA compared to oxygen breathing (Lanzl et al. 2000), use of Bayliss effect (Bayliss 1902; Blum et al. 1999) or retinal flicker (Lanzl et al. 2002; Polak et al. 2002; Kotliar et al. 2004).

Both glaucoma studies and the age-dependence study (3.1.1) are not directly comparable with each other, since they used different stimuli. Incidentally the old healthy volunteers in both glaucoma studies were of similar age as healthy volunteers of the senior group in the age-dependence study. Therefore one would expect the same SEF values of longitudinal vessel

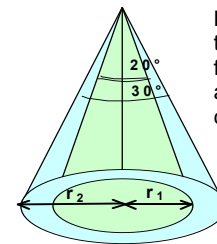


Fig. 74. Principles of the correction factor for linear dimensions at different fundus camera angles.

profiles. The results are similar indeed, when performing a correction of the observation angle of the fundus camera correcting for the field of view of the obtained image: it was 20° in the glaucoma study, while the age-dependence study uses a 30° field. The more is the observation angle of the fundus camera the more fundus field can be observed and the smaller are details of the image. Consequently all linear dimensions as well as the frequency on spatial longitudinal sections of measured vessels and SEF-value should be corrected with a factor (Fig. 74):

$$r_1/r_2 = \text{ctg}10^\circ/\text{ctg}20^\circ = 0,65. \quad (39)$$

Alterations of perfusion parameters in glaucoma patients have been described by numerous authors (e.g. (Martinez & Sanchez 2005; Michelson & Scibor 2006). Using SEF a significant difference between normals and untreated glaucoma patients was demonstrated. Additionally a trend of glaucoma patients treated with dorzolamide possessing less HFW than untreated patients during dilation was shown. Moreover the treated glaucoma patients were by trend similar to normal persons in this parameter. The linear slopes of treated POAG patients in both Fig. 40 and Fig. 41 (right panels) lay between the corresponding slopes of normals and untreated POAG patients. However in the presented experiments the findings between treated and untreated POAG patients were not statistically significant.

Since the fluidmechanical simulations of the present work showed that irregular rough structure of the internal vessel wall lead to increased resistance to flow, the experimental findings might give a possible explanation for ischemic processes in the glaucomatous retina: indeed, during vessel dilation the blood inflow should be increased in order to maintain a needed level of tissue metabolism. The results of CFD simulation predict that in this phase of retinal vessel reaction the glaucomatous retina would obtain less blood supply than the healthy retina. Further implications to blood flow are possible, since the wall shape of a vessel has an instrumental impact on the flow within its lumen.

Conclusions: Results of both glaucoma studies indicate a local vessel wall difference in glaucoma patients compared to age matched controls. Significant increase of arterial microirregularities in the POAG retina during vascular dilation might be an indication for vascular endothelial alterations in glaucoma, leading to impaired perfusion in response to IOP increase.

4.1.3 Ocular hypertension study

While the microstructure of longitudinal arterial profiles in healthy volunteers does not change for different phases of the vessel reaction, the longitudinal arterial profiles in systemic hypertension become less irregular during vessel dilation (Fig. 45, middle, bottom).

Additionally for further discussion the unpublished results by Fuhrmann, Vilser & Nagel on strong retinal arterial constriction during oxygen breathing and the paper by Vilser et al. (2002) were used. According to their data, strongly constricted retinal arteries and veins of a healthy volunteer become straighter and flatter, while the narrow segments along the vessel constrict less than the wide ones (Fig. 75). In contrast to a healthy person retinal vessels of a hypertensive patient lose their constriction ability. Some segments along a vessel can still react, while other segments do not react any more.

These results together with results of the present work might be explained by endothelial dysfunction in systemic hypertension, which presumably has focal distribution along the vessel in primary stages of the disease and would lead to non-uniform vessel reaction. A. Yamada (1995) described the irregularity of endothelial nuclei arrangement and their elongation in retinal arteries of renal hypertensive rats.

Irregularities in smooth muscle cell status and segmental smooth muscle loss in vessels in systemic hypertension can be another possible explanation, see (Vilser et al. 2002) and Vilser personal communication (Fig. 76, top). This hypothesis is supported with light and electron microscopic studies. T. Kimura et al (2005) reported that sclerotic blood vessels had walls in which the smooth muscle cells had been replaced by collagen fibers, proteoglycan filaments, and ruthenium red-positive materials. Such a pathologic effect was also described in human diabetic retina (Rungger-Brändle et al. 1997).

Well, vessel segments with loss of smooth muscles cannot constrict properly, but unaffected segments can. This forms an uneven longitudinal profile of a constricted hypertensive vessel (Fig. 76, bottom). When proceeding these considerations to the vessel dilation, the findings of the present study can also be explained: during vessel dilation in a patient with systemic hypertension unaffected smooth muscles relax more than neighboring segments with reduced smooth muscles. Consequently the vessel wall becomes more flat during its dilation (Fig. 45, bottom).

The reduction of normal segmental dilation behaviour because of the biomechanical alterations of the arterial wall status

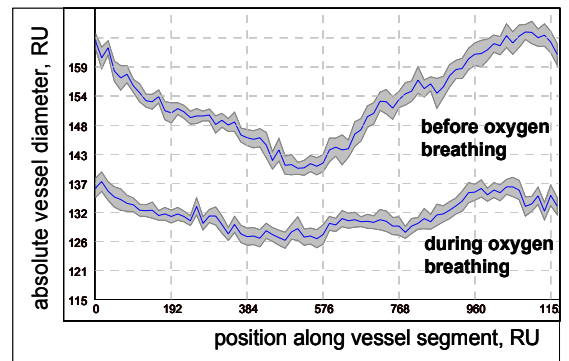


Fig. 75. Longitudinal arterial profiles of a normal subject, 100% oxygen breathing. Temporal mean and confidence interval. Strong arterial constriction up to 20%. Modified from (Vilser et al. 2002) and Fuhrmann, Vilser & Nagel, unpublished data.

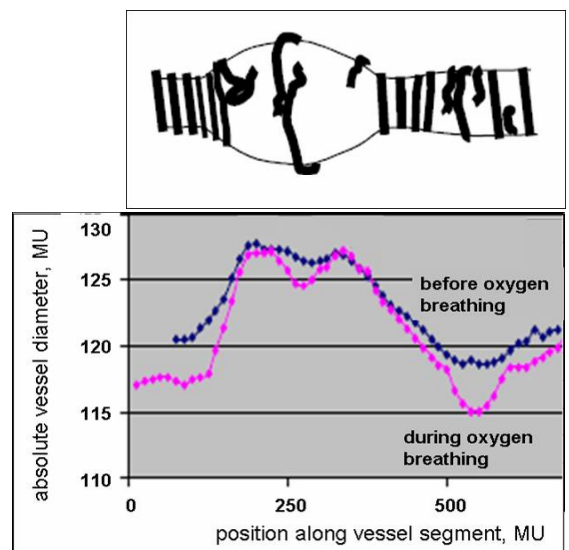


Fig. 76. Top: Segmental smooth muscle loss along a vessel. Bottom: longitudinal arterial profiles of a patient with systemic hypertension, 100% oxygen breathing. Temporal mean. Segmental vessel constriction. Modified and corrected from (Vilser et al. 2002). Top and bottom panels are adjusted to each other according to the position along the vessel.

like vessel narrowing or increase of vessel wall rigidity might represent an alternative reason for obtained results on smoothing of longitudinal arterial profiles in systemic hypertension during vessel dilation (Fig. 77). A completely relaxed or completely constricted (Fig. 75) normal retinal vessel would presumably represent a tube with straight parallel inner walls. An actual baseline longitudinal vessel configuration is between its maximal dilation and maximal constriction. Smooth muscles are partially relaxed, partially constricted in this stage, building an actual wavy vessel profile.

A normal healthy vessel has large dilation reserves. It never reaches its maximal dilation or constriction in the physiological blood flow regulation. Its walls in longitudinal section shift up (dilation) or down (constriction) almost parallel during vessel reaction (Fig. 77, top panel). In contrary dilation reserves of a pathologic vessel might be exhausted because of vessel narrowing or starting of vessel collagen frame. Such a vessel can reach its maximal dilation ability during its response to flicker stimulus. Consequently the wavy baseline longitudinal vessel profile becomes flatter (Fig. 77, bottom panel).

Let us consider this last sophisticated explanation in detail. Longitudinal vessel profiles of a normal subject are nearly harmonic (e.g. Fig. 39, Fig. 46). One could explain this finding with harmonic variation of smooth musculature density along the vessel. But to the best of the author's knowledge there is no evidence of this muscular irregularity in retinal vessels in the literature.

A normal retinal vessel would have densely and homogenously distributed smooth musculature (Rungger-Brändle et al. 1997) and presumably harmonically changed vessel wall stiffness along its longitudinal profiles. Hence, there should exist a physiological harmonic variation of vessel wall thickness along a normal retinal arterial segment (Fig. 78, left panel). During complete constriction smooth muscles are maximally stretched, which seems to be enough to contract the whole vessel homogeneously to the straight tube (Fig. 78, left panel top). During relaxation to an actual baseline vessel configuration less rigid segments of an artery get more dilated than more rigid ones. This forms a characteristic harmonic (almost sinusoidal) longitudinal vessel wall profile with narrow and wide segments along the vessel (Fig. 78, left panel, middle). Consequently the longitudinal vessel profile is formed, which usually can be seen in healthy subjects (e.g. Fig. 42, right panel, top). The normal vessel regulation happens near this baseline state, so that vessel walls in longitudinal section shift almost parallel during vessel reaction. During intense dilation the less rigid areas reach vessel dilation reserve limit (vessel collagenous frame), so that they cannot expand anymore with muscle relaxation. In the contrary less rigid segments go on with their dilation: vessel walls become straighter with less diameter variation along itself (Fig. 78, left panel, bottom). However the frequency distribution of a corresponding longitudinal vessel profile remains unchanged, confirming the results for healthy persons (Fig. 43, top panel)

In systemic hypertension there are plaque depositions in the vessel wall along the vessel. Areas with plaque become thicker and consequently stiffer. Although there is an evidence of the proliferation of synthetic smooth muscle cells in the intima around the plaque deposition, this proliferated muscle cells presumably cannot compensate the lost of mobility of the vessel wall in the plaque area. A completely constricted artery in systemic hypertension would represent a tube with straight parallel walls and small prominences inside the lumen in the

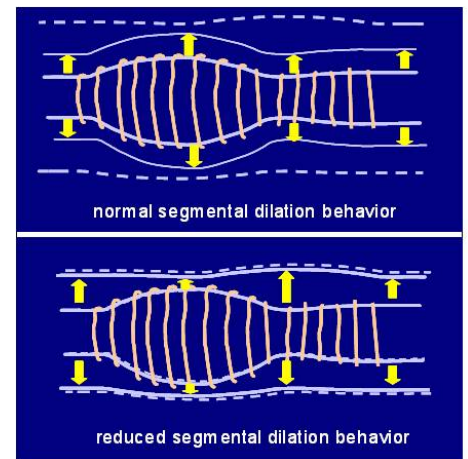


Fig. 77. Vessel dilation shown in its longitudinal section. Normal and reduced segmental dilation behaviour. Dilation reserves are depicted with dashed lines.

plaque areas (Fig. 78, right panel, above). In such a pathologic vessel wall there are more rigid segments, including plaque areas, and less rigid segments. The latter appear more rare than in normal persons and become more relaxed. Additionally the “natural” stiff areas and plaque areas have different rigidity and would react to different extent. Hence a quasi-harmonic mid frequency longitudinal vessel profile is formed during vessel relaxation to an actual baseline vessel configuration (Fig. 78, right panel, middle). Obviously this baseline configuration would differ from

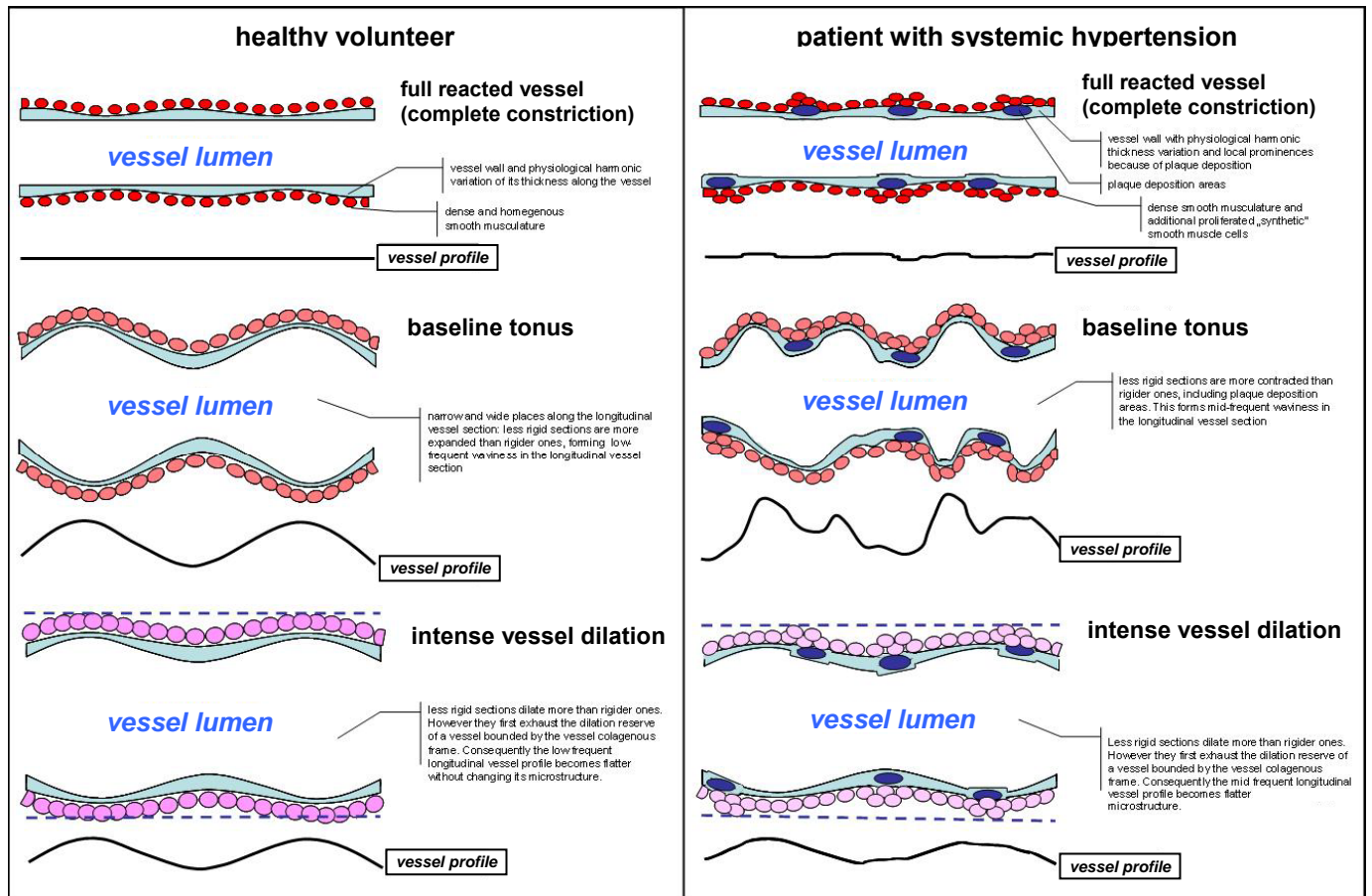


Fig. 78. Longitudinal sections and longitudinal profiles of normal retinal arteries (left panel) and retinal arteries in systemic hypertension at different phases of vessel reaction. See detailed explanation in text.

a normal one at the same phase of vessel reaction. During intense dilation most elastic areas would reach vessel dilation reserve limit bounded by the vessel collagenous frame, so that they cannot expand anymore with muscle relaxation. Corresponding local vessel expansions would partly or completely disappear with further dilation. In the contrary less rigid segments go on with their dilation. Consequently vessel walls become flatter with less diameter variation along itself (Fig. 78, right panel, bottom).

One can assess the amount and the density of the plaque in retinal arteries using RVA. The frequency of plaque area appearance in the longitudinal arterial profile is characterized by secondary peaks in the power spectrum of a corresponding arterial profile (Fig. 43, upper panels).

Assuming vascular musculature to be homogeneously distributed along the vessel segment, vascular endothelium to be intact and the induced muscular stress to be equal everywhere along the segment at a functional provocation, one can use RVA as a unique in-vivo stress-strain device to access local vessel wall stiffness at each point of the longitudinal vessel profile. One needs simply measure the displacement at a point along the vessel segment and recalculate it in sense of stiffness. In reality this suggestion meets a number of physiological limitations and cannot be directly introduced in the most cases. Although the idea to use RVA measurements to estimate local vessel wall stiffness has been already mentioned, for example, by K. Gugleta et al. (2006), and it needs to be elaborated in detail in future studies.

It was reported, that a uniform increase in vessel wall tension induces a pattern characterized by periodic constrictions and dilations along the vessel (Alstrøm et al. 1999; Jacobsen et al. 2002). Such pattern have been observed in large and small blood vessels (New 1966; Foster et al. 1968). It needs to be emphasized, that periodic constrictions and dilations along the vessel could be seen both in healthy volunteers and in patients with systemic hypertension. These patterns were able to be differentiated using functional provocation in the present study.

In severe hypertension a so-called “sausage-string pattern” might occur under certain conditions during vessel constriction, which is explained through the instability of the vessel wall (Alstrøm et al. 1999; Jacobsen et al. 2002). The phenomenon was shown in rats mostly in the large arterioles of 25÷50µm in diameter. The probability to observe the phenomenon in larger or smaller vessels was low (Jacobsen et al. 2002). The vessels in the present study ranged from 90 to 210 µm. According to J. Jacobsen et al., the length of a “sausage” can be estimated by multiplication of the diameter to a coefficient of 6,4. It would be ranged from 576 µm to 1344 µm (or 46,1÷107,5 MU) and would presumably occur during vessel constriction. Apparently such a pattern was not observed in the present study in systemic hypertension group for the following reasons: large vessel diameters, insufficiency of flicker induced vasoconstriction and not severe form of systemic hypertension in patient group. However I cannot exclude the mechanical instability of the vessel wall as a possible reason for the main phenomenon observed in present study: while a relaxed dilated artery in systemic hypertension has a relatively smooth profile, it might switch to the uneven form with periodic constrictions and dilations along the vessel when vessel wall tension increases uniformly (Fig. 42 left, bottom, Fig. 45 bottom) because of mentioned instability phenomenon.

Longitudinal retinal venous profile of systemic hypertension patients differed from those of normal persons. The veins of patients were wider and had higher caliber changes along themselves. The difference in these two parameters in both groups allows us to assume that in systemic hypertension group the veins are not only pre-dilated but might be even pre-stretched. Surprisingly this fact does not influence average temporal venous dilation in response to flicker in the hypertensive group, which remains similar to the dilation in the control group (Fig. 26, bottom).

Additionally the Fourier analysis shows, that the veins in systemic hypertension have smoother inner wall in all phases of physiological venous reaction in comparison to healthy veins. Significant differences in ARPS between both groups can be only partially explained with the difference of absolute venous diameter. The dimensional reproducibility study (3.1.5.3) showed a similar but only a small trend difference between ARPS of very small and very large veins (Fig. 57). The prevalence of power spectra of healthy volunteers within frequency band of 0,03÷0,065 Hz indicates, that systemic hypertension patients loose the mid frequency waves along their venous profiles (compare Fig. 46 left upper panel with right upper panel). This result can be explained with presumable thinning of venous wall or segmental alterations of venous vessel wall rigidity in systemic hypertension. Consequently the presumable physiological harmonic variations of vessel wall thickness along a normal retinal vessel segment (like Fig. 78, left panel) would change to larger segments with thin wall and smaller rarer segments with thicker wall along a vessel. This would lead to the vessel profiles like Fig. 46 left upper panel rather than to the profiles like Fig. 46 right panel.

Thus the arteries in systemic hypertension become smoother at the dilation. Since fluidmechanical simulations in Newtonian fluids in the present study showed that irregular rough structure of the internal vessel wall lead to increased resistance to flow, the reported morphological findings might represent a natural mechanism

regulating retinal blood flow in systemic hypertension. The mechanism would allow to increase the blood flow in dilated hypertensive vessels to the certain extent, while the vessels dilation is reduced: a smoothed low frequency longitudinal arterial profile provides more blood flow in comparison to a more wavy mid frequency profile even if the inflow vessel diameter remains constant.

Conclusions: *while the microstructure of longitudinal arterial profiles in healthy volunteers does not change for different phases of the vessel reaction, the longitudinal arterial profiles in systemic hypertension become less irregular during vessel dilation. The retinal veins in systemic hypertension are wider and have higher caliber changes along themselves. The veins of hypertensive patients possess smoother inner wall in all phases of physiological vessel reaction in comparison to healthy veins. Microstructural changes in longitudinal profiles of retinal vessels in systemic hypertension might be an indication for alterations in the vessel wall rigidity, vascular endothelium and smooth muscle cells in this disease, leading to impaired perfusion and regulation.*

4.1.4 Obesity study

The microstructure of longitudinal arterial profiles in obese persons does not change for different phases of the vessel reaction similar to the longitudinal arterial profiles of age-matched healthy volunteers.

Surprisingly, the longitudinal arterial profiles in obesity are even more regular than in healthy volunteers (Fig. 50). The prevalence of power spectra of healthy volunteers within frequency band of $0,055 \pm 0,095$ Hz indicates that obese persons lose the mid frequency waves along their arterial profiles (compare Fig. 49 left upper panel with right upper panel). Another possible implication is shown in Fig. 49 left bottom panel compared with right bottom panel: there can be regions along arteries with large vessel diameter increase, like aneurisms, in obese persons.

Although the temporal course of arterial reaction to flicker stimulation in obesity is similar to the reaction of healthy seniors 12,5 years older (Fig. 28), there is no such a similarity in longitudinal profiles. I do not have yet any satisfactory clinical explanation of these findings. Such systemic disorders as diabetes mellitus typ 2 and systemic hypertension (2.3.4) were not exclusion criteria for the study. These are so called accompanying diseases for the obesity. Apparently the separate influence of these severe pathologies on the longitudinal profiles of retinal arteries need to be thoroughly investigated before one can find clinical reasons for the described differences between obese persons and healthy volunteers of the same age. Anyway the difference between both groups is statistically significant and it has an influence on the hemodynamics of retinal arteries according to the results of CFD simulation (3.2).

Conclusions: *The microstructure of longitudinal arterial profiles in obese persons does not change for different phases of the vessel reaction. The longitudinal arterial profiles in obesity are even less irregular than in healthy volunteers. The author does not have yet any satisfactory clinical explanation of these findings. Microstructural abnormalities in longitudinal profiles of retinal vessels in obesity might be an indication for alterations in the vessel wall rigidity, vascular endothelium and smooth muscle cells in this pathology, leading to changed perfusion and regulation.*

4.1.5 Evaluation of retinal longitudinal vessel profiles. Accuracy, repeatability and reproducibility

In the present work the mathematical method was developed to describe the structure of longitudinal retinal vessel profiles in healthy subjects and patients using spectral analysis. Additionally to above mentioned remarks on the method itself and its limitations the following considerations on the accuracy, repeatability and reproducibility of the method need to be given.

4.1.5.1 Accuracy of longitudinal vessel profile analysis

It should be emphasized again that the accuracy of the whole longitudinal vessel profile assessment and analysis, including RVA-assessment is not the matter of the present work. It is impossible so far to validate that the true configuration of the inner wall of retinal vessels is assessed with RVA and analyzed with methods proposed in the present study. This is the matter of further histological studies, which will show this true configuration to be compared. However the accuracy of mathematical analysis is tested in the present study, i.e., how precise the parameters of a longitudinal vessel profile can be estimated.

The ideal assessed longitudinal vessel profile represents a “snapshot” of the longitudinal vessel configuration at certain phase of the vessel reaction. When assessing longitudinal vessel profiles the investigator needs to balance between chosen vessel segment length and the time interval of vessel diameter assessment. If the length of the vessel segment is too short – the segment is not representative enough for the vessel; the accuracy of spectral analysis is poor. If it is too large (or if the time interval is too small) – the accuracy of the assessment itself is not satisfactory: the assessed profiles might possess “holes” which need to be interpolated. Consequently some findings especially in high frequency region might be missed, some artifacts might appear. If the time interval is too large, one can miss the certain phase of vessel reaction because of quick vessel diameter changes. The averaged longitudinal vessel profile during the time interval, containing several vessel constrictions and dilation will smash the information on “snapshot” profile.

Additionally, the Fast Fourier Transform needs the data vectors of the length, which is a power of 2. All profiles in a evaluated study must have at least this length to be analyzed identically. Thus the analysis is limited to vessel segments of 32MU, 64MU or 128 MU in length.

Because of above mentioned considerations profiles of 32MU were analyzed in all the studies

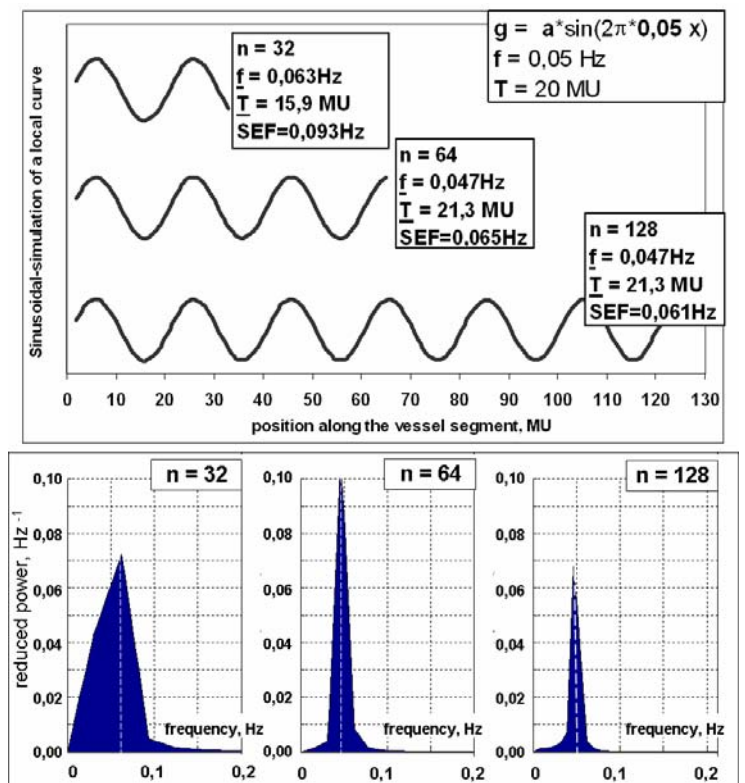


Fig. 79. Comparative analysis on how the vessel length can influence the accuracy of the spectral analysis. Vessel segments of different length are analyzed. f and T – true frequency and period of the waviness; n - number of analysed points, \hat{T} - estimated periods, \hat{f} – estimated frequencies of the waviness (peak frequencies in the power spectra in the low panel).

with previous RVA-version with the assessment accuracy of 25 measurements a second. The chosen time intervals were 30 s for quick changing phases or 60 s for slow changing phases of vessel reaction. The new DVA with the assessment accuracy of 25 measurements a second per a pixel allowed us to reduce the time interval to 3 – 5 s and to expand the vessel length to at least 64 MU. In the obesity study where no off-line re-measurement of data from video tape was possible still the minimal length of 32MU was taken.

Comparative analysis was performed on how the vessel length can influence the accuracy of the spectral analysis. A sinus-curve with a known eigenfrequency $f = 0,05\text{Hz}$, near to real peak frequencies measured in reported studies (e.g. Fig. 44, Fig. 47) modeled a longitudinal vessel profile. This was analyzed using the technique applied for the spectral analysis in the present work. Different vessel lengths were involved in the analysis. The results are shown in Fig. 79. The true power spectrum for this task represents the vertical line at frequency f . Because of peculiarities of Fourier analysis a kind of blur appears around the bar and the quality of the frequency estimation decreases with decreased number of points involved in the analysis. However the kind of frequency distribution and the scale along frequency axis almost do not change. For the chosen frequency rate the sampling of 64MU gives already a good estimation for the eigenfrequency, which is not getting improved when analyzed vessel length increases (Fig. 79).

Conclusions: *Better sampling rate and the increase of the analyzed vessel segment length improves the accuracy of the spectral analysis, provided precision of RVA measurements remains enough. Since in each study of the present work the patient group and the control group were examined and analyzed using equal methods, the results are well comparable intraindividually as well as interindividually within the certain study. However one needs to be careful when attempting to compare quantitative results of different studies. For future studies on longitudinal vessel profiles DVA vessel assessment of at least 64 MU long vessel segments is recommended.*

4.1.5.2 Repeatability and reproducibility of longitudinal vessel profile assessment and analysis

Short-term repeatability

The method used in the present work for the longitudinal vessel profile assessment and analysis is quite repeatable in short-term period, which is confirmed with the results of the corresponding study (3.1.5.1 and Table 10). Generally the preliminary results on short-term repeatability show that longitudinal arterial profiles are robust enough to allow a relatively repeatable assessment (Fig. 53, left panel). The results on venous longitudinal profiles scatter much more (Fig. 53, right panel). This might be an important reason for few statistically significant results in veins in all the clinical studies of the present work.

Results on absolute vessel diameter for arteries and veins correspond to the published results on the repeatability of RVA-measurements (Polak et al. 2000; Seifert & Vilser 2002). VC for SEF and **band sq.** at baseline amounts to ~10% and less and it is satisfactory. VC<3% for SEF at dilation and **band sq.** at baseline show a very good repeatability for arteries confirming their robustness regarding longitudinal profiles assessment. In contrary the veins show a poor repeatability for SEF and **band sq.** at dilation (~15%). A complex vascular regulatory process occurs between two dilations during the standard RVA-assessment. Apparently longitudinal profiles of retinal veins do not manage to come back to the initial baseline configuration before the second flicker-

stimulation. Consequently longitudinal configuration of a vein during evoked second dilation might not repeat its configuration at the first vessel dilation.

Thus, when assessing longitudinal venous profiles during vessel reaction attention should be paid to the interpretation of results. The frequency of the primary peak shows an excellent repeatability for arteries as well as for veins. This parameter were very good repeatable for the analysis of longitudinal vessel profiles. Unfortunately there were no significant differences in it between the groups in all the studies considered in the present work.

Long-term reproducibility

The method used in the present work for the longitudinal vessel profile assessment and analysis shows poor reproducibility in extended long term period of 6 month (3.1.5.2 and Table 11). Only results on absolute vessel diameter and the frequency of the primary peak at the baseline for arteries and veins show excellent reproducibility. Reproducibility of the absolute arterial and venous diameter is even better than the published results on the reproducibility of RVA-measurements (Polak et al. 2000; Seifert & Vilser 2002). The frequency of the primary peak at the baseline were well long-term reproducible for the analysis of longitudinal vessel profiles. However, there were no significant differences in it in all the studies considered in the present work.

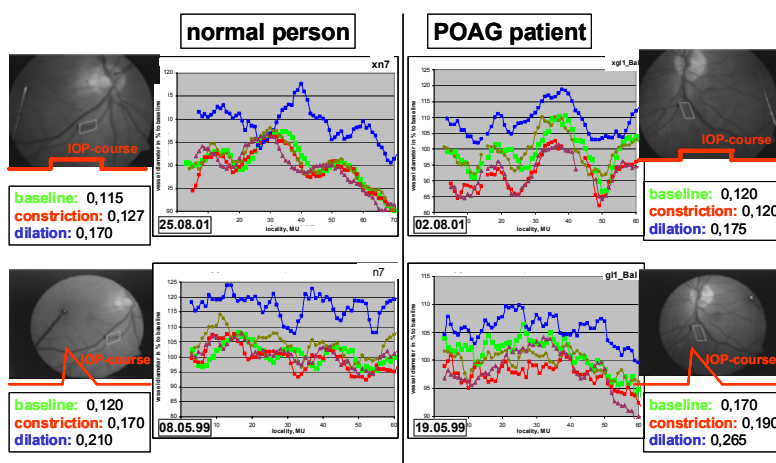


Fig. 80. Comparison of two glaucoma studies. One healthy person and one glaucoma patient participated in both studies. For each experiment the location of the **arterial** segment on the fundus, longitudinal arterial profiles, as well as SEF of most important profiles are depicted. Date of the measurement is shown in the left lower corner of each diagram.

Generally the preliminary results on long-term reproducibility show that the arterial and venous profiles could be considerably changed in extended long-term period of a half year and more. An example from the glaucoma study with two measurements performed with a time interval of two years show the similar tendency (Fig. 80): even baseline profiles are changed.

Presumably imperfection of the RVA repeated measurement system represents another possible issue of poor long-term reproducibility. The system gets hold of the characteristic cross or a bifurcation in the retinal vessel net. The measured vessel segment is recognized not by its peculiar longitudinal structure but by its coordinates relative to the location survey. Over time it might have been shifted along the vessel, conserving its absolute distance to the survey (e.g. Fig. 54, upper panel).

Veins seem to be more robust long-term. They show sometimes a relatively reproducible assessment of their longitudinal profiles (Fig. 54, bottom right panel compared with left panel). Basically, results on arterial longitudinal profile parameters scatter more, then the venous ones (Table 11).

Recently an evidence has appeared that temporal parameters of retinal vessel reaction to the flicker are rather unstable in mid-term periods and can vary dependent on the day-time (C. Erb, personal communication) and on the fasting/dehydration of a test person (Heitmar & Gherghel 2006). Sport exercises, smoking, coffee, tee short time before the examination can influence flicker induced vessel dilation as well (W. Vilser, personal communication). I believe that spatial parameter of longitudinal vessel profiles considered and discussed in the

present work might be more stable to these interfering factors in mid term period. This affirmation need to be examined in future reproducibility studies with RVA.

Dimensional reproducibility

ARPS of small retinal arteries differs from ARPS of large retinal arteries. From Fig. 57 it seems that mid frequency waves along small arteries have similar magnitudes as low frequency waves, while in large arteries the low frequency waves of a high magnitude dominate compared to waves of higher frequency (compare top left and top right panels in Fig. 56). Small vessels appear to represent proportionally reduced analogues of the large ones. Smaller magnitudes and periods of main waves along vessel wall characterize vessels of smaller diameters.

The significant difference in spectral parameters of small and large arteries in the presented reproducibility study shows the necessity to correct the data on longitudinal profiles to the absolute vessel diameter. This can be an important cue for future studies on longitudinal vessel profiles. At least it should be verified that vessel diameters are similar in compared groups and do not differ significantly between groups. In all studies of the present work this requirement was fulfilled (see 3.1.1, 3.1.2, 3.1.3, 3.1.4) for arteries. Thus the findings on differences in longitudinal vessel profiles cannot be due to presumably different absolute vessel diameters.

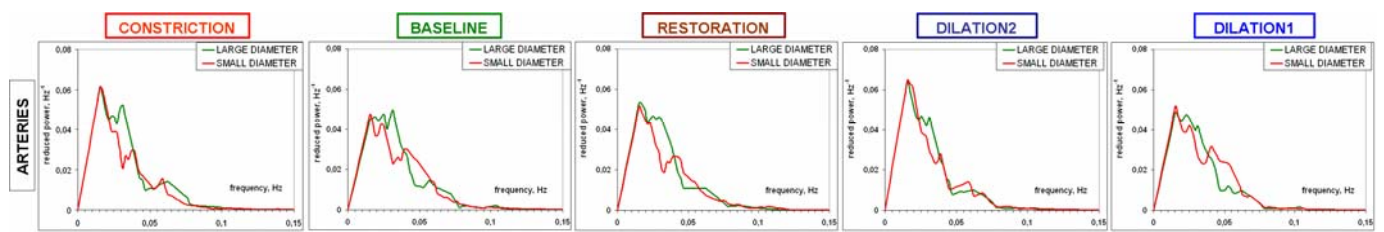


Fig. 81. Average reduced power spectra of spatial longitudinal arterial profiles of another healthy volunteer at 5 phases of arterial reaction (dimensional reproducibility study). To be compared with Fig. 57. 9 measured vessel segments in each compared group. The sequence of phases was chosen according to the increase in vessel diameter from the left to the right, similar to Fig. 57

Below some remarks are given concerning the nature of find differences between small and large vessels.

Since small retinal vessels of about 80 RU in diameter are on the borderline of the accuracy of RVA-measurements (Seifert & Vilser 2002; Vilser et al. 2002), there might be a systematic error, which results in obtained significant differences of longitudinal profiles of small and large retinal vessels. At least this issue cannot be excluded because the difference showed in arteries for dimensional reproducibility can be shown only for wide range of arterial diameters if smallest and largest arteries are included in compared groups. However the lack of measurement precision should relate to high frequencies rather than to low frequencies, where differences are seen in Fig. 57 (top).

Additionally retinal arterial profiles of another young healthy 25 years old volunteer were analyzed with the same protocol of dimensional reproducibility study, described in 2.2.5.3. The fundus of the volunteer had less measurable vessels and only 18 arterial segments ranged from 85RU to 144RU were measured (to be compared with 30 segments and range of 72÷153RU for the first volunteer). Consequently each compared group consisted only of 9 segments with smaller differences in average vessel diameter between groups. No expressed differences in ARPS of longitudinal arterial profiles were found in this case (Fig. 81 compared with Fig. 57). This can have at least two reasons: either arteries larger than 85RU can be measured more precisely or the small diameter range of compared arteries does not give significant differences in longitudinal vessel profiles of smallest and largest

arteries. Two considerations can reject the former reason: the remark in the end of the previous paragraph and the fact that ARPS of large vessels rather differ between Fig. 81 and Fig. 57 (top). Furthermore detailed dimensional reproducibility study is needed to clarify this question.

Spatial reproducibility

Differences between the right and the left eye

When comparing the structure of retinal vessels in the right and in the left eye no significant differences in the most parameters were found as it has been expected (Table 13). Surprisingly there was a difference in SEF during arterial dilation and in the frequency of the primary peak at venous baseline between the right and the left eye. In order to check whether these findings are not a chance only and to give a possible cue for future studies retinal arterial profiles of another young healthy 25 years old volunteer were analyzed additionally with the same

Table 15. Differences between the right and the left eye (median (1. quartile; 3. quartile) for longitudinal arterial profiles of another young healthy volunteer 25 y.o. BAS-baseline, DIL1-dilation1, CON-constriction; RES1-restoration1.

abs. diameter	right eye, MU	121,5(118,1; 131,3)	band sq.	right eye	0,429(0,198; 0,763)	CON
	left eye, MU	127,0(104,1; 133,4)		left eye	0,403(0,240; 0,498)	
	p-value	0,383		p-value	0,711	
	right eye, MU	120,8(116,8; 130,3)		right eye	0,482(0,394; 0,721)	BAS
	left eye, MU	125,3(103,4; 131,0)		left eye	0,394(0,193; 0,593)	
	p-value	0,356		p-value	0,352	
	right eye, MU	122,2(119,1; 131,9)		right eye	0,482(0,394; 0,721)	DIL1
	left eye, MU	127,8(104,6; 133,9)		left eye	0,394(0,193; 0,593)	
	p-value	0,360		p-value	0,352	
SEF	right eye, Hz	0,076(0,072; 0,077)	pr. peak fr.	right eye, Hz	0,016(0,016; 0,031)	CON
	left eye, Hz	0,082(0,046; 0,092)		left eye, Hz	0,031(0,016; 0,031)	
	p-value	0,794		p-value	0,520	
	right eye, Hz	0,083(0,071; 0,091)		right eye, Hz	0,016(0,016; 0,031)	BAS
	left eye, Hz	0,075(0,068; 0,096)		left eye, Hz	0,031(0,031; 0,031)	
	p-value	0,952		p-value	0,120	
	right eye, Hz	0,070(0,069; 0,071)		right eye, Hz	0,016(0,016; 0,016)	DIL1
	left eye, Hz	0,098(0,080; 0,107)		left eye, Hz	0,031(0,016; 0,031)	
	p-value	0,020		p-value	0,129	

protocol of spatial reproducibility study, described in 2.2.5.3. The fundus of the volunteer had less measurable vessels and only 18 arterial segments ranged from 85RU to 144RU were measured (to be compared with 30 segments and range of 72÷153RU for the first volunteer). Equal amount of arterial segments were measured in both eyes (9 in each eye). Basic parameters of the study were compared between both eyes. The results confirmed the previous findings of the present work: SEF during arterial dilation was significantly different between the right and the left eye (Table 15). Thus the effect was shown in two randomly chosen volunteers but as far as I know, there is no evidence in the literature for such a difference in young healthy subjects.

In relation to this finding the recent experience of two independent studies by the author and collaborators in anamnestic healthy volunteers can be mentioned:

- one study in 155 volunteers of 20 – 70 years old with one measured arterial segment for each eye (Lanzl et al. 2006) and
- another study with 11 participants of 20 – 30 years old, where a number of arterial segments was measured in each eye (Wirtz et al. 2007).

Temporal arterial reaction to flicker stimulation similar to Fig. 24 was assessed with RVA and analyzed. The maximal arterial dilation in response to the provocation was more in the right eye than in the left one in both studies. Apparently the mechanism of arterial dilation differs in the left and in the right eye, which can have a number of anatomical and physiological reasons. However the differences between the right and the left eye in the arterial and venous inner microstructure need to be verified in detail in future histological and clinical studies.

Location in the fundus

When comparing the structure of retinal vessels within the fundus no significant difference in the vessel wall structure was found either for arteries or for veins (Table 14). Partly this result can be explained with high stringency of Dunn test for 4 samples used in the statistical evaluation (Glantz 1999). However otherwise it would be impossible to consider all 4 full length samples and to use the non-parametric statistics. From the other side the explorative approach used for dimensional reproducibility study (see 2.2.5.3) would lead to runaway results here.

Additionally retinal arterial profiles in both eyes of mentioned above young healthy 25 years old volunteer were analyzed with the same protocol of spatial reproducibility study, described in 2.2.5.3. All arterial longitudinal profiles in both eyes were divided in four groups according to their location within the retina: temporal inferior (3 right, 2 left), temporal superior (6 right, 7 left). Nasal arteries were not well measurable. Non-parametric statistics with Dunn-Test for two samples of different size was applied for the analysis. Basic parameters of the study were compared between inferior and superior location independently in both eyes. The results confirmed the findings for arteries: no significant difference in the vessel wall structure in mentioned locations in the fundus was found either in the left eye or in the right one. When comparing this finding with results of dimensional reproducibility pilot study, it can be concluded, that the absolute vessel diameter rather than spatial location in the fundus might determine the longitudinal arterial profile structure. Structure of longitudinal venous profiles seems to be independent both of the location in the fundus and the absolute vessel diameter.

Conclusions: *The method of the longitudinal vessel profile assessment and analysis is quite repeatable in short-term period. The arterial profiles are robust and allow a relatively repeatable assessment of their longitudinal profiles. The results on longitudinal venous profiles scatter much more. The method is poor reproducible in extended long-term period, because the longitudinal vessel profiles change over long period of time. Veins are more robust long-term and show sometimes a relatively reproducible assessment of their longitudinal profiles. One need to be careful in the interpretation of the results, especially when assessing longitudinal vessel profiles in long-term period and longitudinal venous profiles during vessel reaction in short-term period.*

Dimensional reproducibility (absolute diameter) rather than spatial reproducibility (location of the vessel) is important in studies on longitudinal vessel profiles. When calculating ARPS the data on longitudinal arterial profiles need to be corrected to the absolute vessel diameter if vessel diameters differ significantly between compared groups. For longitudinal profiles of arteries of about 80 RU and smaller one need to be careful in the interpretation of results. Whether significant differences in ARPS can be shown only for smallest and largest arteries needs to be verified. More detailed reproducibility study need to be performed for groups of healthy volunteers of different age and for patients in order to confirm the preliminary results on repeatability and reproducibility of the pilot studies reported in the present work.

4.2 CFD simulation of the blood flow in retinal vessels – a powerful tool to assess the influence of internal vessel microstructure to the retinal blood flow

To the best of author's knowledge a new way to investigate dynamic functional retinal vessel behaviour was described in the present study. Vessels are not tubes with a constant lumen, but rather possess narrower and wider diameters in different areas.

Results of CFD simulation in the present work both in Newtonian and Non-Newtonian models show that increasing high frequency waviness of longitudinal vessel profiles worsens hydraulic conductivity of the vessel segment hence increasing its resistance to flow.

No significant difference in Newtonian model formulation between results calculated with laminar and turbulent model was found in the reported model formulation for the whole considered range of vessel segment waviness. This means that there are no turbulent effects in a wavy vessel segment, when the blood flow is calculated with the presented model.

Calculated values of ζ , which represents the relation of the static pressure loss to the dynamic pressure loss (Fig. 59 & Fig. 60), seem to be too high for those who are normally dealing with the technical tube flows. However in the model formulation of the study for retinal arterioles the linear dimensions are very small: in the order of $\sim 10^{-4}$ m and the volumetric flow is even smaller: in the order of $\sim 10^{-11}$ m³/s, so thoroughly estimated with the formula (4) the ζ -value gives us the order $\sim 10^3$.

The influence of each geometrical parameter of the wavy arterial segment on its hydraulic conductivity at constant inflow velocity c_{in} (Fig. 59) was investigated for a relatively low value of $c_{in}=5$ mm/s. The latest data on measured real maximal velocities in large retinal arteries are 0,5 – 1 order higher (Nagaoka et al. 2002; Ferguson et al. 2004). However the inflow velocity in the present work was constant and corresponded to the mean velocity of the profile, which is less than the maximal value. For example, for an ideal parabolic velocity distribution it is 1,6 times less than the maximum (Loytsyanskiy 1987; Fung 1990). Besides, the linear increase of the pressure loss with increased volumetric flow rate for each tested configuration of the vessel segment (Fig. 62) allows us to affirm, that the response of hydraulic resistance changes showed in Fig. 59 remains valid for higher inflow velocity rates as well.

The possibility to assess hemodynamic parameters and to obtain the color mapping of these parameters for real vessels gives a cue for the diagnosis of retinal microcirculation. This feature can be also adopted for other microcirculation systems and for the vessels of macrocirculation using the data on the vessel structure gathered from different medical imaging systems (e.g. like the ultrasound measurement of carotid artery (Labropoulos et al. 2005)), and corresponding geometric and rheological blood parameters. The corresponding methods for the evaluation and comparison of fluid mechanical data of such individual CFD simulations need to be elaborated.

I am aware that contemporary optical methods are so far very potent to elaborate the device, which can optically assess the detailed blood flow in big retinal vessels. Recently A. Bachman et al. (2007) proposed a method of optical "3D vivisection" of big retinal vessel improving the

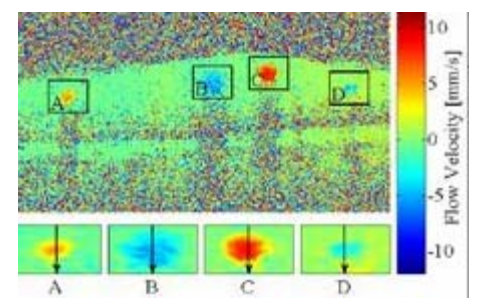


Fig. 82. First results on "optical vivisection" of big retinal vessels with Fourier Domain OCT. Cross-sectional velocity maps. Modified from (Bachmann et al. 2007).

conventional Fourier domain optical coherence tomography (Leitgeb et al. 2003) by phase-matching a reference signal to the sample motion. The unique modern method allows 3D color mapping of the real flow in retinal vessels (Fig. 82). Though it is currently in elaboration and for the time being detailed information neither on the inner vessel wall configuration nor on the flow and velocity profiles close to the vessel wall has been provided.

Individual vessels have different vessel diameters, length and structures. Thus their hemodynamic resistances cannot be directly compared with each others. Nevertheless the follow up intraindividual check of retinal microcirculation and earlier individual diagnosis is possible. It needs still to be elucidated, which parameter can adequately characterize the resistance of a real vessel to the blood flow and can be an indicator of pathological vascular changes: either Spectral Edge Frequency **SEF**, Strouhal number **Sr**, volumetric flow rate **Q**, pressure drop Δp or hydraulic resistance coefficient ξ_v .

There is one further point to consider in the interpretation of the obtained data: RVA data acquisition is performed by assessing grey values in an image. RVA therefore measures what it detects optically. This is not the inner diameter of a vessel but the thickness of the red blood cell column without the blood plasma layer. The irregularity of measured RBC-column profiles might be related to the microirregularities of the inner arterial wall as described above. The low frequency waviness of the vessel longitudinal profile is obviously a property of the vessel wall configuration. For high frequency waves a fluid mechanical effect might also be considered. A mathematical model for Non-Newtonian media published by T. Khantuleva (1999) recently describes self-organization and self-regulation effects in open systems. It explains systems adapting to varying conditions and models the changes during transitions due to the interacting underlying mechanisms. For blood flow in small vessels it includes the possibility of a random local formation of small vortex pulsations near the vessel wall (at the border of the plasma layer), dependent on flow parameters, rheological conditions and geometrical configuration of the vessel. Consequently the effects on microirregularities of the RBC- column found in the reported clinical experiments could also be due to these self-regulated Non-Newtonian hemodynamical effects in the blood flow, and not only due to changes in the vessel wall. This needs to be validated in further experimental and numerical studies.

Conclusions: *Increasing high frequency waviness of longitudinal vessel profiles increases the hemodynamic vessel resistance. The possibility to assess hemodynamic parameters and to obtain the color mapping of these parameters for real vessels gives a possible cue for the diagnosis of retinal microcirculation. The effects on microirregularities of the RBC- column found in the clinical experiments could also be due to self-regulated Non-Newtonian hemodynamical effects in the blood flow, not only due to changes in the vessel wall microstructure.*

5 Conclusions and Suggestions

5.1 General conclusions

To the best of author's knowledge a new way to investigate dynamic functional behaviour of large retinal vessels was described. A method to assess longitudinal structure of inner wall of retinal arteries and veins was developed. Parameters to quantify structural vascular changes were proposed and evaluated.

What determine retinal blood flow is the perfusion pressure and the retinal vascular resistance, the latter depending upon vessel wall viscoelasticity, vessel length, vessel inner wall structure and constantly changing vessel diameter. The present study shows that vessel inner wall structure might also alter as vessel diameter changes. Retinal vessels are not straight tubes with a constant lumen, but rather possess narrower and wider diameters in different segments which are changing in response to metabolic demand. The method of interpretation of local retinal vessel behaviour was developed, because, to the author's opinion, the valuable information regarding the autoregulatory potential is lost in common RVA-assessment when concentrating on a summation effect over time.

It is demonstrated that retinal vessels in the elderly, in systemic hypertension, obesity and in primary open angle glaucoma sustain significant microstructural changes in their longitudinal profiles, which might be an expression of

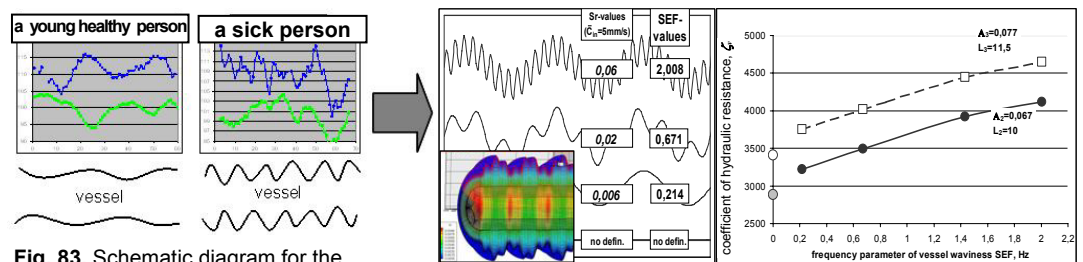


Fig. 83. Schematic diagram for the conclusions.

endothelial damage, the instability of vessel wall or partial degradation of smooth musculature of the vessel wall. Commonly pathological alterations in cardiovascular system begin in the vessels of microcirculation invading the big vessels afterwards. Hence, the microstructure of longitudinal retinal vessel profile can be an indicator determining true biological age of a person and representing an additional clinical symptom for early diagnosis of the examined systemic and ocular diseases, thus improving prophylaxis and individualized therapy for the benefit of patients.

The proposed method of investigation of functional reactive vessel behaviour opens up new possibilities of vessel analysis, highlighting the action of the vessel wall, a regulatory element of blood flow. The presented method allows an indirect insight into the physiological state of the brain microvasculature and into its alterations in vascular pathologies, since the retina is a part of the brain and retinal vessels akin to vessels of brain microcirculation in their structure and functioning

With CFD simulations it was shown that changes in microstructure of retinal vessels can alter hemodynamic parameters of a vessel and can be a reason for altered retinal perfusion in elderly, in obesity, in systemic hypertension and in glaucoma. The increase of vessel resistance to the blood flow with changing microstructure of the vessel inner wall might represent an additional fluid mechanical mechanism in the pathogenesis of aging and mentioned diseases.

5.2 **Suggestions for future studies**

The present work opens new ways in clinical vascular research as well as in CFD modeling of the blood flow. It brings forth novel ideas for future studies and projects, where the matter of the study can be investigated in detail and appropriately validated. Additionally the analytic methods and approaches, used in the study can be improved. The following directions of new projects on the topic can be suggested inter alia:

5.2.1 **Wavelet analysis of longitudinal vessel profiles.**

The frequency analysis with Fourier Transform used in the present work possesses a number of limitations mentioned above. The main disadvantage of this mathematical tool: the phase shift cannot be considered. Consequently there is no reciprocation between the analyzed curve and the corresponding power spectrum: one can build one power spectrum for a curve, but there is infinity of curves, which correspond to a power spectrum. Another mathematical tool – the wavelet analysis allows to obtain a two-dimensional frequency-phase representation map for a curve, which represents the unique “fingerprint” of the curve and contains the whole frequency-phase information about it (Schmidt 2000). The wavelet analysis has been already applied in the medicine, mainly for the analysis of temporal medical signals like electrocardiogram (Kantelhardt et al. 2007; Matsuyama et al. 2007) and electroencephalogram (Nayak et al. 1994; Browne & Cutmore 2000). This type analysis is also applicable for spatial curves and has been successfully used in geodesy (Schmidt 2000). The application of the wavelet analysis for the evaluation of longitudinal retinal vessel profiles in the future seems to be very promising.

5.2.2 **Histological analysis of longitudinal sections of retinal vessels.**

Clinical results on longitudinal vessel microstructure obtained with RVA need to be validated in histological studies or in studies with corrosion casts (El-Barghouty et al. 1996). The research project on histological evaluation of longitudinal sections of large retinal arteries and veins in enucleated eyes of healthy donors of different age and glaucomatous eyes can include:

- the literature research on histological evaluation of longitudinal sections of carotid artery or other large central and peripheral arteries of healthy donors of different age and in arteriosclerosis, see (Schmidt et al. 1983; El-Barghouty et al. 1996) for the example;
- acquiring of enucleated human eyes;
- histological preparation of enucleated human eyes;
- medical and mathematical analysis of the preparations;
- comparison of the experimental data (histology and corrosion casts) with clinical data on retinal arterial irregularities assessed previously with the Retinal Vessel Analyzer (Kotliar et al. 2002; Kotliar et al. 2005).

Alternatively the corrosion cast study on aging and glaucomatous mouse models can be performed and evaluated.

5.2.3 Experimental measurements of real flow of a synthetic fluid with blood properties in silicone casts

Numerical results on retinal blood flow in vessels with different microstructure obtained in the present work need to be validated in model experiments. The proposed research project can include:

- Preparation of anatomically realistic replica of retinal arteries from silicon rubber using prepared corrosion tube casts. This method is already elaborated for vessels with diameter of 5mm÷4cm (Liepsch & Zimmer 1978; Liepsch 1990; Botnar et al. 2000) in the working group by Prof. D. Liepsch (Munich University of Applied Science). The method should be applied for big retinal vessels of ~0,1 mm in diameter.
- Experimental measurements of the real flow of the technical fluid with blood properties in these true-to-scale elastic retinal artery models. The experimental design for the measurements of pulsatile flow in elastic silicon-rubber carotid artery models using a Non-Newtonian, blood-like fluid (for the instance, a water-glycerin mixture with a cinematic viscosity of $\nu=0,037 \text{ cm}^2/\text{s}$ (Botnar et al. 2000)) under physiological conditions (non-stationary flow conditions (Botnar et al. 2000) with a mid systolic flow rate of 8,8 $\mu\text{l}/\text{min}$ (Guan et al. 2003)) was developed previously (Botnar et al. 2000; Liepsch 2002) and needs to be approved for small tube casts, modeling large retinal vessels.

5.2.4 CFD simulation of Non-Newtonian pulsatile blood flow in real retinal vessels with structure interaction.

The CFD models developed in the present work possess a number of limitations mentioned above. More detailed model need to be developed. The project on the CFD simulation of Non-Newtonian pulsatile blood flow in retinal vessels will include:

- CFD simulation of non-stationary pulsatile blood flow on 2D-model of vessel segments with longitudinal profiles simulated with sinus curves with different combinations of parameters;
- analysis of parameter influence;
- evaluation of longitudinal profiles of manufactured corrosion tube casts of different donors and CFD calculation of the hydraulic conductivity of the casts.

5.2.5 CFD simulation of dynamic processes in retinal vessels during a functional provocation.

Non-stationary processes in the retinal blood flow during the vessel response to a functional provocation are going to be investigated. Temporal course of mean vessel diameter changes in a vessel segment during its dilation, following quick constriction and/or ensuing slow relaxation

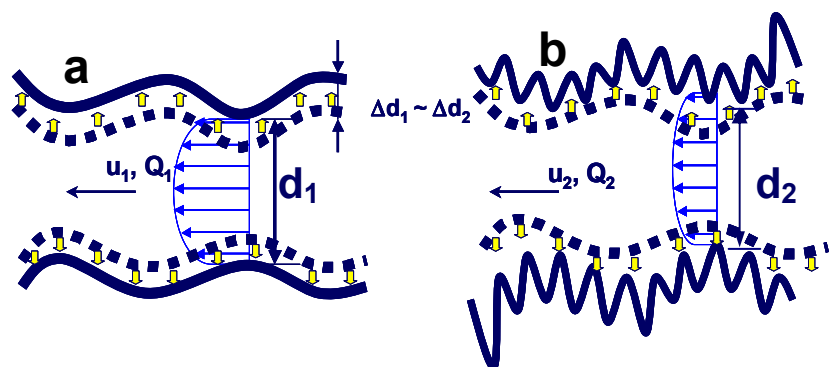


Fig. 84. Transient vessel reaction. Problem statement.

can be evaluated from real clinical studies with RVA reported above, e.g. Fig. 24, Fig. 26 and Fig. 27. The flow regimes in a vessel segment are studied in two cases:

- low frequency wavy walls of a segment move parallel during transient dilation and relaxation (Fig. 84a);
- low frequency wavy walls of a segment move parallel during transient dilation and acquire an additional high frequency component which increases in amplitude over time. During the transient relaxation phase the high frequency component changes (Fig. 84b).

Amplitude **a** of the high frequency waviness increases (decreases) gradually with increased (decreased) vessel dilation. Velocity profile **u** and volumetric flow rate **Q** need to be calculated in several cases with a fixed value of high frequency waviness in each case, considering the ranges of other parameters. Main aspects of the blood flow modeling in a vessel during transient vessel diameter changes in response to a functional provocation are considered in (Regirer & Shadrina 2002; Regirer & Shadrina 2005). Additional parameters of the model (according to Fig. 24, Fig. 26, Fig. 27):

- *Transient process (dilation) time (I): 10÷80 s.*
- *Time in dilated state (II): 5÷60 s.*
- *Slow transient reversal process (relaxation) time (III): 50÷400 s.*
- *Amplitude of dilation $\Delta d_1 \approx \Delta d_2$: 5 ÷ 20 μm*

5.2.6 CFD simulation of the blood flow in a vessel branching

The present work considers the blood flow in straight simple vessel segments. It is known that the blood flow regime might become very complicated when approaching a vessel bifurcation (Botnar et al. 2000; Liepsch 2002). Two different modes of blood flow can be compared and their parameters calculated in a future project: flow through the more wavy and less wavy branched segment of a vessel (Fig. 85). In detail velocity profile **u**

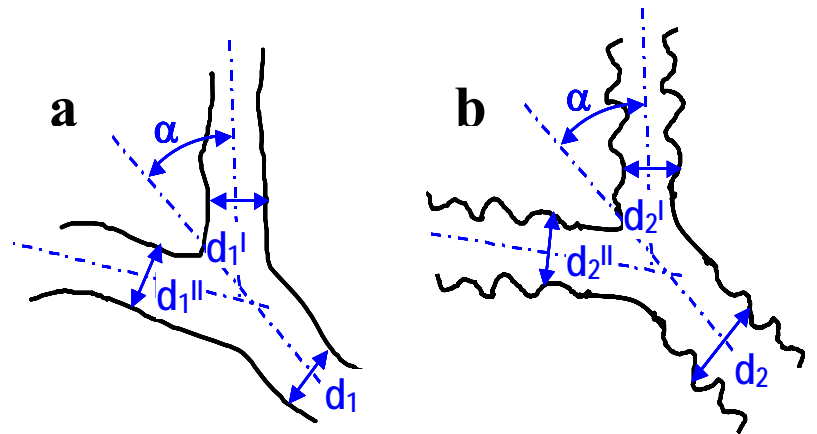


Fig. 85. Flow in a vessel bifurcation. Problem statement.

and volumetric flow rate **Q** need to be calculated, considering the ranges of other parameters, when high frequency waviness changes within its range. Additional parameters of the model (see Fig. 85):

- *Diameter of the main trunk $d_1 \approx d_2$: 60 ÷ 170 μm .*
- *Diameter of branches $d_1' \approx d_2'$; $d_1'' \approx d_2''$: 40 ÷ 100 μm .*
- *The angle of a branch attachment α : 10° ÷ 50° (according to (Bethe et al. 1927)): it depends on relative energy transferred through the main and branched trunks i.e. on relative diameters of the main and branched trunks: the less is a diameter of a branched artery relative to the main trunk diameter, the more is α .*
- *Amplitude of the waviness **a**: according to same issue, the arterial wall is thicker and stronger in the areas of bifurcation. Thus, it can be considered, that the waviness in this area is less, than in branches and in the main*

trunk. In the problem statement it can be considered, that the amplitude of the waviness α reduces in all branches, when approaching towards the place of bifurcation.

- *Flow direction: from the main trunk into branches (artery) or from branches into the main trunk.*

References

- Ahmetoglu A, Erdol H, Simsek A, Gokce M, Dinc H & Gumele HR (2003): Effect of hypertension and candesartan on the blood flow velocity of the extraocular vessels in hypertensive patients. *Eur J Ultrasound* 16: 177-182.
- Alberts B, Johnson A, Lewis J, Raff M, Roberts K & Walter P (2002): Leukocyte functions and percentage breakdown. In: *Molecular biology of the cell*. 4th ed. New York, London. Garland Publishing
- Alm A (1992): Ocular circulation. In: Hart WM(ed.) *Adler's physiology of the eye*. St. Louis, Baltimore: Mosby: 198-227.
- Alm A, Tornquist P & Maepea O (1981): The uptake index method applied to studies on the blood-retinal barrier. II. Transport of several hexoses by a common carrier. *Acta Physiol Scand* 113: 81-84.
- Alstrøm P, Equiluz VM, Colding - Jørgensen M, Gustafsson F & Holstein-Rathlou N-H (1999): Instability and "sausage-string" appearance in blood vessels during high blood pressure. *Phys. Rev. Lett.* 82: 1995-1998.
- Anderson DR (1999): Introductory comments on blood flow autoregulation in the optic nerve head and vascular risk factors in glaucoma. *Surv Ophthalmol* 43 Suppl 1: S5-9.
- Andrews J, Wood HG, Allaire PE & Olsen DB (2000): Numerical analysis of blood flow in the clearance region of a continuous flow artificial heart pump. *Artificial Organs* 24: 492-500.
- Antonov AS, Munn DH, Kolodgie FD, Virmani R & Gerrity RG (1997): Aortic endothelial cells regulate proliferation of human monocytes in vitro via a mechanism synergistic with macrophage colony-stimulating factor. Convergence at the cyclin E/p27(Kip1) regulatory checkpoint. *J Clin Invest* 99: 2867-2876.
- Artoli AMMAMH (2003): *Mesoscopic Computational Hemodynamics*. Amsterdam. University van Amsterdam: 142.
- Ashton N (1963): Studies of the Retinal Capillaries in Relation to Diabetic and Other Retinopathies. *Br J Ophthalmol* 47: 521-538.
- Astakhov YS & Dzhaliashvili OA (1990): Contemporary trends in study on ocular hemodynamics in glaucoma *Oftalmologicheskij Zhurnal* 3: 179-183.
- Baaijens JP, van Steenhoven AA & Janssen JD (1993): Numerical analysis of steady generalized Newtonian blood flow in a 2D model of the carotid artery bifurcation. *Biorheology* 30: 63-74.
- Bachmann AH, Villiger ML, Blatter C, Lasser T & Leitgeb RA (2007): Resonant Doppler flow imaging and optical vivisection of retinal blood vessels. *Opt. Express* 15: 408-422.
- Bayliss WM (1902): On the local reactions of the arterial wall to changes of internal pressure. *J Physiol* 28: 220-231.
- Beers AP & van der Heijde GL (1996): Age-related changes in the accommodation mechanism. *Optom Vis Sci* 73: 235-242.
- Benson K (1999): *MCAT Review Book MCAT Review*. City. Emory University: 155.
- Bethe A, v. Bergmann G, Embden G & Ellinger A (1927): *Handbuch der normalen und pathologischen Physiologie*. Berlin: Verlag von J. Springer: 866-872.
- Bill A, Sperber G & Ujji K (1983): Physiology of the choroidal vascular bed. *Int Ophthalmol* 6: 101-107.
- Bill A & Sperber GO (1990): Aspects of oxygen and glucose consumption in the retina: effects of high intraocular pressure and light. *Graefes Arch Clin Exp Ophthalmol* 228: 124-127.
- Bird RB, Armstrong RD & Hassager O (1987): *Dynamics of Polymeric Liquids*. John Wiley & Sons.
- Bitsch L (2002): *Blood Flow in Microchannels*. Technical University of Denmark: 111.
- Blevins RD (1984): *Applied fluid dynamics handbook*. New York. Van Nostrand Reinhold: 221.
- Blum M, Bachmann K, Wintzer D, Riemer T, Vilser W & Strobel J (1999): Non-invasive measurement of the Bayliss effect in retinal autoregulation. *Graefes Arch Clin Exp Ophthalmol* 237: 296-300.
- Böhm C (2004): *Numerische Simulation des Fischdurchgangs durch Wasserturbinen*. Munich, Germany. Munich University of Technology: 157.

- Botnar R, Rappitsch G, Scheidegger MB, Liepsch D, Perktold K & Boesiger P (2000): Hemodynamics in the carotid artery bifurcation: a comparison between numerical simulations and in vitro MRI measurements. *J Biomech* 33: 137-144.
- Brandes RF, Fleming I & Busse R (2005): Endothelial aging. *Cardiovasc Res* 66: 286-294.
- Bronzino JD, Siok CJ, Austin K, Austin-Lafrance RJ & Morgane PJ (1987): Spectral analysis of the electroencephalogram in the developing rat. *Brain Res* 432: 257-267.
- Brown SM & Jampol LM (1996): New concepts of regulation of retinal vessel tone. *Arch Ophthalmol* 114: 199-204.
- Browne M & Cutmore TR (2000): Adaptive wavelet filtering for analysis of event-related potentials from the electro-encephalogram. *Med Biol Eng Comput* 38: 645-652.
- Brubaker RF (1998): Clinical measurements of aqueous humor dynamics: Implications for addressing glaucoma. In: Civan MM(ed.) *The eye's aqueous humor: from secretion to glaucoma*. San Diego: Academic Press: 234-284.
- Büchi ER (1996): The blood supply to the optic nerve head. In: Kaiser H(ed.) *Ocular blood flow*. Basel: 1-8.
- Buckley CH, Hadoke PW & O'Brien CJ (1997): Use of isolated ocular arteries in vitro to define the pathology of vascular changes in glaucoma. *Br J Ophthalmol* 81: 599-607.
- Bühl A & Zöfel P (2002): *SPSS Version 10 Einführung in die moderne Datenanalyse unter Windows*. München, Boston, San-Francisco. Addison-Wesley: 323-346.
- Bunin AY (1971): Hemodynamics of the eye and methods of its investigation. Moscow. *Medicina*: 196
- Burt VL, Whelton P, Roccella EJ, Brown C, Cutler JA, Higgins M, Horan MJ & Labarthe D (1995): Prevalence of hypertension in the US adult population. Results from the Third National Health and Nutrition Examination Survey, 1988-1991. *Hypertension* 25: 305-313.
- Caro CG, Pedley TJ, Schroter RC & Seed WA (1978): *The mechanics of the circulation*. Oxford University Press.
- Casson M (1959): A flow equation for pigment-oil suspensions of the printing ink type. In: Mills CC(ed.) *Rheology of Disperse Systems*. Oxford: Pergamon: 84-104.
- Charm SE & Kurland GS (1974): *Blood Flow and Microcirculation*. New York. John Wiley & Sons: 79.
- Cheung N, Saw SM, Islam FM, Rogers SL, Shankar A, de Haseth K, Mitchell P & Wong TY (2007): BMI and retinal vascular caliber in children. *Obesity (Silver Spring)* 15: 209-215.
- Chien S, Luse SA & Bryant CA (1971): Hemolysis during filtration through micropores: a scanning electron microscopic and hemorheologic correlation. *Microvasc Res* 3: 183-203.
- Chobanian AV, Bakris GL, Black HR, Cushman WC, Green LA, Izzo JL, Jr., Jones DW, Materson BJ, Oparil S, Wright JT, Jr. & Roccella EJ (2003): The Seventh Report of the Joint National Committee on Prevention, Detection, Evaluation, and Treatment of High Blood Pressure: the JNC 7 report. *Jama* 289: 2560-2572.
- Cines DB, Pollak ES, Buck CA, Loscalzo J, Zimmerman GA, McEver RP, Pober JS, Wick TM, Konkle BA, Schwartz BS, Barnathan ES, McCrae KR, Hug BA, Schmidt AM & Stern DM (1998): Endothelial cells in physiology and in the pathophysiology of vascular disorders. *Blood* 91: 3527-3561.
- Cioffi GA, Granstam E & Alm A (2003): Ocular circulation. In: Kaufmann PL and Alm A(eds.) *Adler's physiology of the eye*. St. Louis, London: Mosby: 747-784.
- Cocklet GR (1986): The rheology and tube flow of blood. In: Skalak R and Chien S(eds.) *Handbook of Bioengineering*. New York, St. Luis, San Francisco: McGraw-Hill Book Company: 14.11-14.17.
- Criqui MH, Browner D, Fronck A, Klauber MR, Coughlin SS, Barrett-Connor E & Gabriel S (1989): Peripheral arterial disease in large vessels is epidemiologically distinct from small vessel disease. An analysis of risk factors. *Am J Epidemiol* 129: 1110-1119.
- Cross MM (1965): Rheology of Non-Newtonian fluids: a new flow equation for pseudoplastic system. *Journal of Colloid Science* 20: 417-437.
- Cunha-Vaz JG, Shakib M & Ashton N (1966): Studies on the permeability of the blood-retinal barrier. I. On the existence, development, and site of a blood-retinal barrier. *Br J Ophthalmol* 50: 441-453.
- DaSilva FA, Kriegelstein GK & von Collani E (1979): [Measurement of arterial tension at the eye with the Stepanik arteriotonomograph (author's transl)]. *Klin Monatsbl Augenheilkd* 174: 706-714.

- Davies MG & Hagen PO (1993): The vascular endothelium. A new horizon. *Ann Surg* 218: 593-609.
- Dawber TR & Kannel WB (1961): Susceptibility to coronary heart disease. *Mod Concepts Cardiovasc Dis* 30: 671-676.
- Delles C, Michelson G, Harazny J, Oehmer S, Hilgers KF & Schmieder RE (2004): Impaired endothelial function of the retinal vasculature in hypertensive patients. *Stroke* 35: 1289-1293.
- Dohi Y, Kojima M, Sato K & Luscher TF (1995): Age-related changes in vascular smooth muscle and endothelium. *Drugs Aging* 7: 278-291.
- Dollery CT (1968): Dynamic aspects of the retinal microcirculation. *Arch Ophthalmol* 79: 536-539.
- Dorner GT, Garhofer G, Kiss B, Polska E, Polak K, Riva CE & Schmetterer L (2003): Nitric oxide regulates retinal vascular tone in humans. *Am J Physiol Heart Circ Physiol* 285: H631-636.
- Dorner GT, Polska E, Garhofer G, Zawinka C, Frank B & Schmetterer L (2002): Calculation of the diameter of the central retinal artery from noninvasive measurements in humans. *Curr Eye Res* 25: 341-345.
- Drance SM, Douglas GR, Wijsman K, Schulzer M & Britton RJ (1988): Response of blood flow to warm and cold in normal and low-tension glaucoma patients. *Am J Ophthalmol* 105: 35-39.
- Dufax J, Quemada D & Mills P (1980): Determination of rheological properties of red blood cells by Couette viscometry. *Rev Phys Appl* 15: 1367.
- Duker JS & Brown GC (1989): Anterior location of the crossing artery in branch retinal vein obstruction. *Arch Ophthalmol* 107: 998-1000.
- Durbin PA (1995): Separated flow computations with the $k-\epsilon-v^2$ model. *AIAA Journal* 33: 659-664.
- Durbin PA (1996): On the $k-\epsilon$ stagnation point anomaly *International Journal of Heat and Fluid Flow* 17: 89-90.
- Eastoppe PL & Brooks DE (1980): A comparison of rheological constitutive functions for whole human blood. *Biorheology* 17: 235-247.
- Eichhorn M (2001): Morphologische Grundlagen der Mikrozirkulation von Retina und Chorioidea. In: Mutschler E, Wiederholt M and Upmeyer HJ(eds.) *Regulationsdynamik by Glaukom*. Stuttgart: Wiss. Verlagsgesellschaft mbH: 6-16.
- El-Barghouty NM, Levine T, Ladva S, Flanagan A & Nicolaides A (1996): Histological verification of computerised carotid plaque characterisation. *Eur J Vasc Endovasc Surg* 11: 414-416.
- Embleton SJ, Hosking SL, Roff Hilton EJ & Cunliffe IA (2002): Effect of senescence on ocular blood flow in the retina, neuroretinal rim and lamina cribrosa, using scanning laser Doppler flowmetry. *Eye* 16: 156-162.
- Ernest JT (1977): The effect of systolic hypertension on rhesus monkey eyes after ocular sympathectomy. *Am J Ophthalmol* 84: 341-344.
- Ernest JT (1989): Macrocirculation and microcirculation of the retina. In: Ryan SJ and Ogden TE(eds.) *Retina*. St. Louis: CV Mosby: 65-66.
- Espeland MA, Hoen H, Byington R, Howard G, Riley WA & Furberg CD (1994): Spatial distribution of carotid intimal-medial thickness as measured by B-mode ultrasonography. *Stroke* 25: 1812-1819.
- Falk E, Shah PK & Fuster V (1995): Coronary plaque disruption. *Circulation* 92: 657-671.
- Feke GT, Tagawa H, Deupree DM, Goger DG, Sebag J & Weiter JJ (1989): Blood flow in the normal human retina. *Invest Ophthalmol Vis Sci* 30: 58-65.
- Ferguson RD, Hammer DX, Elsner AE, Webb RH & Burns SA (2004): Wide-Field Retinal Hemodynamic Imaging with the Tracking Scanning Laser Ophthalmoscope. *Optics Express* 21: 5198-5208.
- Ferrari-Dileo G, Davis EB & Anderson DR (1990): Response of retinal vasculature to phenylephrine. *Invest Ophthalmol Vis Sci* 31: 1181-1182.
- Ferrari AU, Radaelli A & Centola M (2003): Invited review: aging and the cardiovascular system. *J Appl Physiol* 95: 2591-2597.
- Flammer J, Haefliger IO, Orgul S & Resink T (1999): Vascular dysregulation: a principal risk factor for glaucomatous damage? *J Glaucoma* 8: 212-219.
- Flammer J, Orgul S, Costa VP, Orzalesi N, Krieglstein GK, Serra LM, Renard JP & Stefansson E (2002): The impact of ocular blood flow in glaucoma. *Prog Retin Eye Res* 21: 359-393.
- Forrester JV, Dick AD, McMenemy PG & Lee WR (2002): *The Eye. Basic science in practice*. WB Saunders: 48-52.

- Forster BA, Ferrari-Dileo G & Anderson DR (1987): Adrenergic alpha 1 and alpha 2 binding sites are present in bovine retinal blood vessels. *Invest Ophthalmol Vis Sci* 28: 1741-1746.
- Forte P, Copland M, Smith LM, Milne E, Sutherland J & Benjamin N (1997): Basal nitric oxide synthesis in essential hypertension. *Lancet* 349: 837-842.
- Foster JH, Killen DA & Klatt E (1968): Corrugated arteries--an enigma. *Am Surg* 34: 398-412.
- Frank RN, Turczyn TJ & Das A (1990): Pericyte coverage of retinal and cerebral capillaries. *Invest Ophthalmol Vis Sci* 31: 999.
- Fuchsjager-Mayrl G, Wally B, Georgopoulos M, Rainer G, Kircher K, Buehl W, Amoako-Mensah T, Eichler HG, Vass C & Schmetterer L (2004): Ocular blood flow and systemic blood pressure in patients with primary open-angle glaucoma and ocular hypertension. *Invest Ophthalmol Vis Sci* 45: 834-839.
- Fujino T & Hamasaki DI (1967): Effect of intraocular pressure on the electroretinogram. *Arch Ophthalmol* 78: 757.
- Fung YC (1990): *Biomechanics. Mechanical Properties of Living Tissues*. 2. ed. New York. Springer-Verlag: 66-105.
- Gaethgens P (1980): Flow of blood through narrow capillaries: Rheological mechanism determining capillary hema-tocrit and apparent viscosity. *Biorheology* 17: 183-189.
- Garhofer G, Zawinka C, Resch H, Huemer KH, Schmetterer L & Dorner GT (2004): Response of retinal vessel diameters to flicker stimulation in patients with early open angle glaucoma. *J Glaucoma* 13: 340-344.
- Gasser P & Flammer J (1991): Blood-cell velocity in the nailfold capillaries of patients with normal-tension and high-tension glaucoma. *Am J Ophthalmol* 111: 585-588.
- Giese J (1964): *Acute Hypertensive Vascular Disease. 2. Studies on Vascular Reaction Patterns and Permeability Changes by Means of Vital Microscopy and Colloidal Tracer Technique*. *Acta Pathol Microbiol Scand* 62: 497-515.
- Gilmore ED, Hudson C, Preiss D & Fisher J (2005): Retinal arteriolar diameter, blood velocity, and blood flow response to an isocapnic hyperoxic provocation. *Am J Physiol Heart Circ Physiol* 288: H2912-2917.
- Glagov S, Weisenberg E, Zarins CK, Stankunavicius R & Kolettis GJ (1987): Compensatory enlargement of human atherosclerotic coronary arteries. *N Engl J Med* 316: 1371-1375.
- Glantz SA (1999): *Primer of biostatistics*. New York, St. Louis, San Francisco. McGraw-Hill: 460.
- Goldblatt HJ (1938): Studies on experimental hypertension. VII. The production of the malignant phase of hypertension. *Exp Med* 67: 809-826.
- Goldmann H (1962): [On rheology of the episcleral venous system and the corneoscleral trabecula.]. *Doc Ophthalmol* 16: 128-149.
- Goldsmith HL (1972): The microrheology of human erythrocyte suspensions. In: Becker E and Mikhailov GK(eds.) *Theoretical and Applied Mechanics*. 13th IUTAM Congress. New York: Springer.
- Graham SL & Drance SM (1999): Nocturnal hypotension: role in glaucoma progression. *Surv Ophthalmol* 43 Suppl 1: S10-16.
- Grayson MC & Laties AM (1971): Ocular localization of sodium fluorescein. Effects of administration in rabbit and monkey. *Arch Ophthalmol* 85: 600-603 passim.
- Gregersen MI, Bryant CA, Hammerle WE, Usami S & Chien S (1967): Flow Characteristics of Human Erythrocytes through Polycarbonate Sieves. *Science* 157: 825-827.
- Grunwald JE, Hariprasad SM & DuPont J (1998): Effect of aging on foveolar choroidal circulation. *Arch Ophthalmol* 116: 150-154.
- Grunwald JE, Maguire AM & Dupont J (1996): Retinal hemodynamics in retinitis pigmentosa. *Am J Ophthalmol* 122: 502-508.
- Grunwald JE, Riva CE, Stone RA, Keates EU & Petrig BL (1984): Retinal autoregulation in open-angle glaucoma. *Ophthalmology* 91: 1690-1694.
- Guan K, Hudson C & Flanagan JG (2003): Variability and repeatability of retinal blood flow measurements using the Canon Laser Blood Flowmeter. *Microvasc Res* 65: 145-151.
- Gugleta K, Kochkorov A, Katamay R, Zawinka C, Flammer J & Orgul S (2006): On pulse-wave propagation in the ocular circulation. *Invest Ophthalmol Vis Sci* 47: 4019-4025.

- Gugleta K, Zawinka C, Rickenbacher I, Kochkorov A, Katamay R, Flammer J & Orgul S (2006): Analysis of retinal vasodilation after flicker light stimulation in relation to vasospastic propensity. *Invest Ophthalmol Vis Sci* 47: 4034-4041.
- Guyton AC (1977): An overall analysis of cardiovascular regulation: fifteenth annual Baxter-Travenol lecture. *Anesth Analg* 56: 761-768.
- Haefliger IO, Meyer P, Flammer J & Luscher TF (1994): The vascular endothelium as a regulator of the ocular circulation: a new concept in ophthalmology? *Surv Ophthalmol* 39: 123-132.
- Harkness J (1971): The viscosity of human blood plasma: its measurements in health and disease. *Biorheology* 8: 171-193.
- Harris A, Dinn RB, Kagemann L & Rechtman E (2003): A review of methods for human retinal oximetry. *Ophthalmic Surg Lasers Imaging* 34: 152-164.
- Harris A, Jonescu-Cuypers C, Martin B, Kagemann L, Zalish M & Garzosi HJ (2001): Simultaneous management of blood flow and IOP in glaucoma. *Acta Ophthalmol Scand* 79: 336-341.
- Harris A, Swartz D, Engen D, Beck D, Evans D, Caldemeyer K & Martin B (1996): Ocular hemodynamic effects of acute ethanol ingestion. *Ophthalmic Res* 28: 193-200.
- Hayreh SS (1975): Segmental nature of choroidal vasculature. *Br J Ophthalmol* 59: 631.
- Hayreh SS (1996): Duke-elder lecture. Systemic arterial blood pressure and the eye. *Eye* 10 (Pt 1): 5-28.
- Hayreh SS (1999): The role of age and cardiovascular disease in glaucomatous optic neuropathy. *Surv Ophthalmol* 43 Suppl 1: S27-42.
- Hayreh SS, Podhajsky P & Zimmerman MB (1999): Role of nocturnal arterial hypotension in optic nerve head ischemic disorders. *Ophthalmologica* 213: 76-96.
- Heitmar R & Gherghel D (2006): The effects of voluntary fasting on retinal and peripheral vessel reactivity – a case study. *Acta Ophthalmol Scand* 84 (Suppl 239): 63.
- Helbig H, Kornacker S, Berweck S, Stahl F, Lepple-Wienhues A & Wiederholt M (1992): Membrane potentials in retinal capillary pericytes: excitability and effect of vasoactive substances. *Invest Ophthalmol Vis Sci* 33: 2105-2112.
- Henderson AH (1991): St Cyres lecture. Endothelium in control. *Br Heart J* 65: 116-125.
- Hoffman R, Benz Jr EJ, Shattil SJ, Furie B, Cohen HJ, Silberstein LE & McGlave P (2000): *Hematology - Basic Principles and Practice*. 3 ed. New York, NY. Churchill Livingstone.
- Hogan MJ, Alvarado JA & Weddell JE (eds.) (1971): *Histology of the Human Eye. An Atlas and Textbook*. Philadelphia. WB Saunders: 687.
- Hubbard LD, Brothers RJ, King WN, Clegg LX, Klein R, Cooper LS, Sharrett AR, Davis MD & Cai J (1999): Methods for evaluation of retinal microvascular abnormalities associated with hypertension/sclerosis in the Atherosclerosis Risk in Communities Study. *Ophthalmology* 106: 2269-2280.
- Hussain MA, Puniyani HR & Kar S (1994): Quantification of blood viscosity using power Law model in cerebrovascular accidents and high-risk controls. *Clinical Hemorheology* 14: 685-701.
- Ishizu T, Ishimitsu T, Kamiya H, Seo Y, Moriyama N, Obara K, Watanabe S & Yamaguchi I (2002): The correlation of irregularities in carotid arterial intima-media thickness with coronary artery disease. *Heart Vessels* 17: 1-6.
- Jacobsen JC, Beierholm U, Mikkelsen R, Gustafsson F, Alstrom P & Holstein-Rathlou NH (2002): "Sausage-string" appearance of arteries and arterioles can be caused by an instability of the blood vessel wall. *Am J Physiol Regul Integr Comp Physiol* 283: 1118-1130.
- Janssen I, Katzmarzyk PT & Ross R (2004): Waist circumference and not body mass index explains obesity-related health risk. *Am J Clin Nutr* 79: 379-384.
- JNC (1993): The fifth report of the Joint National Committee on Detection, Evaluation, and Treatment of High Blood Pressure (JNC V). *Arch Intern Med* 153: 154-183.
- Jonas JB (2003): Central retinal artery and vein collapse pressure in eyes with chronic open angle glaucoma. *Br J Ophthalmol* 87: 949-951.
- Kador PF (2007): Pathology of the Eye. Chapter 18. Ocular Pathology of Diabetes Mellitus. In: Tasman W and Jaeger EA(eds.) *Duane's Foundations of Clinical Ophthalmology*. Hagerstown: Lippincott Williams & Wilkins.

- Kagemann L, Harris A, Chung HS, Costa VP & Garzosi HJ (1999): Basics and limitations of color doppler imaging. In: Pillunat LE, Harris A, Anderson DR and Greve EL(eds.) Current concepts on ocular blood flow in glaucoma. The Hague, The Netherlands: Kugler Publ: 103-110.
- Kaiser HJ, Schotzau A & Flammer J (1996): Blood-flow velocities in the extraocular vessels in normal volunteers. *Am J Ophthalmol* 122: 364-370.
- Kanngiesser HE, Kniestedt C & Robert YC (2005): Dynamic contour tonometry: presentation of a new tonometer. *J Glaucoma* 14: 344-350.
- Kantelhardt JW, Bauer A, Schumann AY, Barthel P, Schneider R, Malik M & Schmidt G (2007): Phase-rectified signal averaging for the detection of quasi-periodicities and the prediction of cardiovascular risk. *Chaos* 17: 015112.
- Kastrup J, Bulow J & Lassen NA (1989): Vasomotion in human skin before and after local heating recorded with laser Doppler flowmetry. A method for induction of vasomotion. *Int J Microcirc Clin Exp* 8: 205-215.
- Kaufmann PL & Alm A (eds.) (2003): Adler's physiology of the eye. St. Louis, London. Mosby: 876.
- Khantuleva TA & Mescheryakov YI (1999): Nonlocal theory of the high-strain-rate processes in a structured media. *Intern. J. of Solids and Structures* 36: 3105-3129.
- Kimura T, Mizota A, Fujimoto N & Tsuyama Y (2005): Light and electron microscopic studies on human retinal blood vessels of patients with sclerosis and hypertension. *Int Ophthalmol* 26: 151-158.
- Köhler W, Schachtel G & Voleske P (1995): Biostatistik. Einführung in die Biometrie für Biologen und Agrarwissenschaftler. Berlin, Heidelberg, New York. Springer: 285.
- Kotliar KE, Mücke B, Vilser W & Lanzl IM (2005): Aging Effects Measured by Retinal Vessel Analyzer. *Invest Ophthalmol Vis Sci* 46 (Suppl): E:3916.
- Kotliar KE, Nagel E, Schilling R, Vilser W & Lanzl IM (2006): Functional in-vivo assessment and fluidmechanical analysis of microstructural changes in retinal arteries in glaucoma. XXX International Congress of Ophthalmology. Sao Paulo, Brasil: 86.
- Kotliar KE, Nagel E, Vilser W & Lanzl IM (2002): Assessment of local behaviour of retinal arteries in response to intraocular pressure increase in normals and glaucoma patients. *Ophthalmic Research* 34(Suppl.1): 159.
- Kotliar KE, Nagel E, Vilser W & Lanzl IM (2007): Functional in-vivo assessment of retinal artery microirregularities in glaucoma *Acta Ophthalmol Scand* (E-pub ahead of print).
- Kotliar KE, Schilling R, Einzinger J, Anciger D & Lanzl IM (2005): First results of biofluidmechanical simulation for age-dependent microirregularities in retinal arteries. 5-th International Conference on eye biomechanics. Moscow Helmholtz Institute for Eye Diseases, Moscow: 55-64.
- Kotliar KE, Schilling R, Einzinger J & Lanzl IM (2006): Retinal blood flow is influenced by age-dependent microirregularities in retinal arterial walls. Biofluidmechanical simulation. *Invest Ophthalmol Vis Sci* 47 (Suppl1): E:469.
- Kotliar KE, Vilser W & Lanzl IM (2000): Beeinflusst Neosynephrin 10% die retinalen Gefäße? . *Klin Monatsbl Augenheilkd* 217: 5.
- Kotliar KE, Vilser W & Lanzl IM (2007): Unterschiede der retinalen Vasomotorik und Venenpulsation bei Gesunden und Glaukompatienten. German Ophthalmological Society (DOG). Berlin, Germany: 47(Do1405).
- Kotliar KE, Vilser W, Nagel E & Lanzl IM (2004): Retinal vessel reaction in response to chromatic flickering light. *Graefes Arch Clin Exp Ophthalmol* 242: 377-392.
- Krupatkin AI (2003): Klinische Neuro-Angiophysiologie der Extremitäten. Perivaskuläre Innervation und nervale Trophik. Moskau. Nautschy Mir.
- Krupatkin AI (2003): Clinical neuroangiophysiology of extremities. (Perivascular innervation and neural throphism) Moscow. Nauchnyi Mir.
- Ku DD (1982): Coronary vascular reactivity after acute myocardial ischemia. *Science* 218: 576-578.
- Kvermo HD, Stefanovska A, Kirkeboen KA & Kvernebo K (1999): Oscillations in the human cutaneous blood perfusion signal modified by endothelium-dependent and endothelium-independent vasodilators. *Microvasc Res* 57: 298-309.
- Kwon YH & Caprioli J (2007): Chapter 52. Primary Open-Angle Glaucoma. In: Tasman W and Jaeger EA(eds.) Duane's Clinical Ophthalmology. Hagerstown: Lippincott Williams & Wilkins.
- Labropoulos N, Leon LR, Jr., Brewster LP, Pryor L, Tionson J, Kang SS, Mansour MA & Kalman P (2005): Are your arteries older than your age? *Eur J Vasc Endovasc Surg* 30: 588-596.

- Lanzl IM, Kotliar KE, Bock A, Vilser W, Halle M & Schmidt-Trucksäß A (2006): Wie altern gesunde retinale Gefäße? Deutsche Medizinische Wochenschrift 131(Supp.6): 180-181.
- Lanzl IM, Vilser W & Kotliar K (2002): Retinal artery dilation in response to different colors in chromatic flickering light. *Ophthalmic Res* 34: 115.
- Lanzl IM, Witta B, Kotliar K & Vilser W (2000): [Retinal vessel reaction to 100% O₂-breathing--functional imaging using the retinal vessel analyzer with 10 volunteers]. *Klin Monatsbl Augenheilkd* 217: 231-235.
- Laties AM (1967): Central retinal artery innervation. Absence of adrenergic innervation to the intraocular branches. *Arch Ophthalmol* 77: 405-409.
- Leitgeb R, Hitzenberger C & Fercher A (2003): Performance of fourier domain vs. time domain optical coherence tomography. *Opt. Express* 11: 889-894.
- Lerche D & Oelke R (1990): Theoretical model of blood flow through hollow fibres considering hematocrit-dependent, non-Newtonian blood properties. *Int J Artif Organs* 13: 742-746.
- Lesnefsky EJ, Pacheco J, Adcock K, Buckner JK & Van Benthuyzen KM (1987): Thallium scintigraphic evidence of reversible myocardial ischemia caused by anomalous origin of the left main coronary artery from the anterior sinus of Valsalva. *Am Heart J* 114: 896-897.
- Lien FS, Chen WL & Leschziner MA (1996): Low-Reynolds number eddy-viscosity modelling based on non-linear stress-strain / vorticity relations. In: Rodi W and Bergeles E (eds.) 3-rd International Symposium on Engineering Turbulence Modelling and Experiments. Crete, Greece: 91-100.
- Liesch D (2002): An introduction to biofluid mechanics--basic models and applications. *J Biomech* 35: 415-435.
- Liesch D, Thurston G & Lee M (1991): Studies of fluids simulating blood-like rheological properties and applications in models of arterial branches. *Biorheology* 28: 39-52.
- Liesch D & Zimmer R (1978): [A method for the preparation of true-to-scale inflexible and natural elastic human arteries (author's transl)]. *Biomed Tech (Berl)* 23: 227-230.
- Liesch DW (1990): Effect of blood flow parameters on flow patterns at arterial bifurcations--studies in models. *Monogr Atheroscler* 15: 63-76.
- Liu CJ, Chiou HJ, Chiang SC, Chou JC, Chou YH & Liu JH (1999): Variations in ocular hemodynamics in patients with early and late glaucoma. *Acta Ophthalmol Scand* 77: 658-662.
- Liu X, Ge J, Zhou W, Lin Y & Cai X (1998): Hemodynamics of ophthalmic artery and central retinal artery and correlation with other factors in patients with primary open angle glaucoma. *Yan Ke Xue Bao* 14: 138-144.
- Logean E, Falsini B & Riva CE (2001): [Effect of chromatic flicker on circulation of the optic nerve]. *Klin Monatsbl Augenheilkd* 218: 345-347.
- Logean E, Schmetterer LF & Riva CE (2003): Velocity Profile of Red Blood Cells in Human Retinal Vessels using Confocal Scanning Laser Doppler Velocimetry. *Laser Physics* 13: 45-51.
- Loytsyanskiy LG (1987): Fluid mechanics. Moscow: Nauka: 45-315.
- Lundberg MS & Crow MT (1999): Age-related changes in the signaling and function of vascular smooth muscle cells. *Exp Gerontol* 34: 549-557.
- Luo XY & Kuang ZB (1992): A study on the constitutive equation of blood. *J Biomech* 25: 929-934.
- Luscher TF (1990): The endothelium. Target and promoter of hypertension? *Hypertension* 15: 482-485.
- Luscher TF, Cooke JP, Houston DS, Neves RJ & Vanhoutte PM (1987): Endothelium-dependent relaxations in human arteries. *Mayo Clin Proc* 62: 601-606.
- Malek AM & Izumo S (1995): Control of endothelial cell gene expression by flow. *J Biomech* 28: 1515-1528.
- Martin JA & Roorda A (2005): Direct and noninvasive assessment of parafoveal capillary leukocyte velocity. *Ophthalmology* 112: 2219-2224.
- Martinez A & Sanchez M (2005): Predictive value of colour Doppler imaging in a prospective study of visual field progression in primary open-angle glaucoma. *Acta Ophthalmol Scand* 83: 716-722.

- Matsuyama A, Jonkman M & de Boer F (2007): Improved ECG signal analysis using wavelet and feature extraction. *Methods Inf Med* 46: 227-230.
- Matz RL & Andrantsitohaina R (2003): Age-related endothelial dysfunction. *DrugsAging* 20: 527-550.
- McLenachan JM, Vita J, Fish DR, Treasure CB, Cox DA, Ganz P & Selwyn AP (1990): Early evidence of endothelial vasodilator dysfunction at coronary branch points. *Circulation* 82: 1169-1173.
- Merrill EW, Benis AM, Gilliland ER, Sherwood TK & Salzman EW (1965): Pressure-flow relations of human blood in hollow fibers at low flow rates. *J Appl Physiol* 20: 954-967.
- Metaea MR & Newman EA (2006): Glial cells dilate and constrict blood vessels: a mechanism of neurovascular coupling. *J Neurosci* 26: 2862-2870.
- Michelson G, Groh MJ & Langhans M (1996): Perfusion of the juxtapapillary retina and optic nerve head in acute ocular hypertension. *Ger J Ophthalmol* 5: 315-321.
- Michelson G, Patzelt A & Harazny J (2002): Flickering light increases retinal blood flow. *Retina* 22: 336-343.
- Michelson G & Schuierer G (1991): [Absolute blood flow in the ophthalmic artery]. *Fortschr Ophthalmol* 88: 687-689.
- Michelson G & Scibor M (2006): Intravascular oxygen saturation in retinal vessels in normal subjects and open-angle glaucoma subjects. *Acta Ophthalmol Scand* 84: 289-295.
- Michelson G, Warntges S, Baleanu D, Welzenbach J, Ohno-Jinno A, Pogorelov P & Harazny J (2007): Morphometric age-related evaluation of small retinal vessels by scanning laser Doppler flowmetry: determination of a vessel wall index. *Retina* 27: 490-498.
- Michelson G, Warntges S, Harazny J, Oehmer S, Delles C & Schmieder RE (2006): Effect of NOS inhibition on retinal arterial and capillary circulation in early arterial hypertension. *Retina* 26: 437-444.
- Michelson G, Welzenbach J, Pal I & Harazny J (2001): Functional imaging of the retinal microvasculature by scanning laser Doppler flowmetry. *Int Ophthalmol* 23: 327-335.
- Miyazoe Y, Sawairi T, Ito K, Konishi Y, Yamane T, Nishida M, Asztalos B, Masuzawa T, Tsukiya T, S. E & Taenaka Y (1999): Computational Fluid Dynamic Analysis to establish the design process of a centrifugal B.P: Second report. *Artificial Organs* 23: 762-768.
- Moses RA (1972): A graphic analysis of aqueous humor dynamics. *Am J Ophthalmol* 73: 665-669.
- Nagaoka T, Mori F & Yoshida A (2002): Retinal artery response to acute systemic blood pressure increase during cold pressor test in humans. *Invest Ophthalmol Vis Sci* 43: 1941-1945.
- Nagel E, Vilser D, Fuhrmann G, Vilser W & Lang GE (2000): [Dilatation of large retinal vessels after increased intraocular pressure]. *Ophthalmologie* 97: 742-747.
- Nagel E & Vilser W (2004): Autoregulative behavior of retinal arteries and veins during changes of perfusion pressure: a clinical study. *Graefes Arch Clin Exp Ophthalmol* 242: 13-17.
- Nagel E & Vilser W (2004): Flicker observation light induces diameter response in retinal arterioles: a clinical methodological study. *Br J Ophthalmol* 88: 54-56.
- Nagel E, Vilser W & Lanzl I (2002): Functional analysis of retinal vessel diameter reaction to artificially raised intraocular pressure in glaucoma patients with and without dorzolamide therapy. *Vasa* 31: 230-234.
- Nagel E, Vilser W & Lanzl I (2004): Age, blood pressure, and vessel diameter as factors influencing the arterial retinal flicker response. *Invest Ophthalmol Vis Sci* 45: 1486-1492.
- Nagel E, Vilser W & Lanzl I (2005): Dorzolamide influences the autoregulation of major retinal vessels caused by artificial intraocular pressure elevation in patients with POAG: a clinical study. *Curr Eye Res* 30: 129-137.
- Nagel E, Vilser W & Lanzl IM (2001): Retinal vessel reaction to short-term IOP elevation in ocular hypertensive and glaucoma patients. *Eur J Ophthalmol* 11: 338-344.
- Nayak A, Roy RJ & Sharma A (1994): Time-frequency spectral representation of the EEG as an aid in the detection of depth of anesthesia. *Ann Biomed Eng* 22: 501-513.
- Nesterov AP (1967): Hydrodynamics of the eye. *Moscow. Medicina*: 235.
- New PF (1966): Arterial stationary waves. *Am J Roentgenol Radium Ther Nucl Med* 97: 488-499.

- Nguyen TT & Wong TY (2006): Retinal vascular manifestations of metabolic disorders. *Trends Endocrinol Metab* 17: 262-268.
- Nieuwenhuijs D, Coleman EL, Douglas NJ, Drummond GB & Dahan A (2002): Bispectral index values and spectral edge frequency at different stages of physiologic sleep. *Anesth Analg* 94: 125-129.
- NIH (2000): Clinical Guidelines on the Identification, Evaluation, and Treatment of Overweight and Obesity in Adults: The Evidence Report. National Institutes of Health. U.S. Dept. of Health and Human Services. NHLBI document 98-4083.
- Nyborg NC & Nielsen PJ (1990): The level of spontaneous myogenic tone in isolated human posterior ciliary arteries decreases with age. *Exp Eye Res* 51: 711-715.
- Ogden CL, Carroll MD, Curtin LR, McDowell MA, Tabak CJ & Flegal KM (2006): Prevalence of overweight and obesity in the United States, 1999-2004. *Jama* 295: 1549-1555.
- Ohashi K, Miyazaki S & Yamada H (1958): Test for retinal function and glaucoma by measuring macular capillary blood pressure. *Am J Ophthalmol* 45: 71-80.
- Oldroyd JJ (1958): Non-Newtonian effects in steady motion of some idealised elastico-viscous liquids. *Proceedings of the Royal Society of London: A245: 278-297.*
- Orge F, Harris A, Kagemann L, Kopecky K, Sheets CW, Rechtman E & Zalish M (2002): The first technique for non-invasive measurements of volumetric ophthalmic artery blood flow in humans. *Br J Ophthalmol* 86: 1216-1219.
- Park DJJ & Karesh JW (2007): Chapter 1. Topographic Anatomy of the Eye: An Overview. In: Tasman W and Jaeger EA(eds.) *Duane's Foundations of Clinical Ophthalmology*. Hagerstown: Lippincott Williams & Wilkins.
- Park SS (2007): Chapter 19. The Anatomy and Cell Biology of the Retina. In: Tasman W and Jaeger EA(eds.) *Duane's Foundations of Clinical Ophthalmology*. Hagerstown: Lippincott Williams & Wilkins.
- Parver LM, Auker C & Carpenter DO (1980): Choroidal blood flow as a heat dissipating mechanism in the macula. *Am J Ophthalmol* 89: 641.
- Pearson JD (1991): Endothelial cell biology. *Radiology* 179: 9-14.
- Pillunat LE, Anderson DR, Knighton RW, Joos KM & Feuer WJ (1997): Autoregulation of human optic nerve head circulation in response to increased intraocular pressure. *Exp Eye Res* 64: 737-744.
- Plange N, Kaup M, Weber A, Arend KO & Remky A (2006): Retrobulbar haemodynamics and morphometric optic disc analysis in primary open-angle glaucoma. *Br J Ophthalmol* 90: 1501-1504.
- Polak K, Dallinger S, Polska E, Findl O, Eichler HG, Wolzt M & Schmetterer L (2000): Effects of insulin on retinal and pulsatile choroidal blood flow in humans. *Arch Ophthalmol* 118: 55-59.
- Polak K, Dorner G, Kiss B, Polska E, Findl O, Rainer G, Eichler HG & Schmetterer L (2000): Evaluation of the Zeiss retinal vessel analyser. *Br J Ophthalmol* 84: 1285-1290.
- Polak K, Schmetterer L & Riva CE (2002): Influence of flicker frequency on flicker-induced changes of retinal vessel diameter. *Invest Ophthalmol Vis Sci* 43: 2721-2726.
- Polak K, Wimpfissinger B, Berisha F, Georgopoulos M & Schmetterer L (2003): Effects of sildenafil on retinal blood flow and flicker-induced retinal vasodilatation in healthy subjects. *Invest Ophthalmol Vis Sci* 44: 4872-4876.
- Pontrelli G (1997): Mathematical modelling for viscoelastic fluids. *Nonlinear Analysis* 30: 349-357.
- Pontrelli G (2001): Modeling the Fluid-Wall Interaction in a Blood Vessel. *Progress in Biomedical Research*: 330-338.
- Pontrelli G & Rossoni E (2003): Numerical modelling of the pressure wave propagation in the arterial flow. *Int. J. Numer. Meth. Fluids* 43: 651-671.
- Quemada D (1978): Rheology of concentrated disperse systems: III. General features of the proposed non-Newtonian model: comparison with experimental data. *Rheol Acta* 17: 643-653.
- Quemada D (1981): A rheological model for studying the hematocrit dependence of red cell-red cell and red cell-protein interactions in blood. *Biorheology* 18: 501-516.
- Quetelet LAJ (1871): *Antropométrie ou Mesure des Différences Faculté de l'Homme*. Brussels. Musquardt.
- Rassam SM, Patel V, Chen HC & Kohner EM (1996): Regional retinal blood flow and vascular autoregulation. *Eye* 10 (Pt 3): 331-337.

- Regirer SA & Shadrina N (2002): [A simple model of a vessel with a wall sensitive to mechanical stimuli]. *Biofizika* 47: 908-913.
- Regirer SA & Shadrina N (2005): [Mathematical models of nitric oxide transport in a blood vessel]. *Biofizika* 50: 515-536.
- Rethy I (1963): [the Significance of Blood Pressure Determination in the Ciliary Arteries in the Preparation for Eye Operations in Hypertensive Persons. (Preliminary Report)]. *Klin Monatsbl Augenheilkd* 143: 710-717.
- Rhie CM & Chow WL (1983): A numerical study of the turbulent flow past an isolated airfoil with trailing edge separation. *AIAA Journal* 21: 1525 - 1532.
- Richards LO (1989): *It Couldn't Just Happen*. Thomas Nelson, Inc: 139-140.
- Riva CE, Falsini B & Logean E (2001): Flicker-evoked responses of human optic nerve head blood flow: luminance versus chromatic modulation. *Invest Ophthalmol Vis Sci* 42: 756-762.
- Riva CE, Grunwald JE & Petrig BL (1986): Autoregulation of human retinal blood flow. An investigation with laser Doppler velocimetry. *Invest Ophthalmol Vis Sci* 27: 1706-1712.
- Riva CE, Grunwald JE, Sinclair SH & Petrig BL (1985): Blood velocity and volumetric flow rate in human retinal vessels. *Invest Ophthalmol Vis Sci* 26: 1124-1132.
- Riva CE, Sinclair SH & Grunwald JE (1981): Autoregulation of retinal circulation in response to decrease of perfusion pressure. *Invest Ophthalmol Vis Sci* 21: 34-38.
- Robinson F, Riva CE, Grunwald JE, Petrig BL & Sinclair SH (1986): Retinal blood flow autoregulation in response to an acute increase in blood pressure. *Invest Ophthalmol Vis Sci* 27: 722-726.
- Roh S, Weiter JJ & Duker JS (2007): Chapter 5. Ocular Circulation. In: Tasman W and Jaeger EA(eds.) *Duane's Clinical Ophthalmology*. Hagerstown: Lippincott Williams & Wilkins.
- Rosengarten B, Aldinger C, Spiller A & Kaps M (2003): Neurovascular coupling remains unaffected during normal aging. *J Neuroimaging* 13: 43-47.
- Ross R (1999): Atherosclerosis--an inflammatory disease. *N Engl J Med* 340: 115-126.
- Roy CS & Sherington CS (1890): On the regulation of the blood supply of the brain. *J Physiol* 11: 85-108.
- Rungger-Brändle E, Dosso AA, Alliod C & Leuenberger PM (1997): Smooth muscle lesions in large caliber arteries and veins of the human diabetic retina. *Invest Ophthalmol Vis Sci* 38 (Suppl.): S770.
- Samoilov VO (2004): *Medical biophysics*. St.Petersburg: Spets. Lit: 392-393.
- Sassani JW (2007): Chapter 19. Glaucoma. In: Tasman W and Jaeger EA(eds.) *Duane's Foundations of Clinical Ophthalmology*. Hagerstown: Lippincott Williams & Wilkins.
- Schafer AI (1997): Vascular endothelium: in defense of blood fluidity. *J Clin Invest* 99: 1143-1144.
- Schiebler TH, Schmidt W & Zilles K (1999): *Sehorgan, Hör- und Gleichgewichtsorgan*. Anatomie. Berlin: Springer Verlag: 685-703.
- Schiffrin EL & Hayoz D (1997): How to assess vascular remodelling in small and medium-sized muscular arteries in humans. *J Hypertens* 15: 571-584.
- Schilling R (2003): Application of CFD-techniques in fluid machinery. Conference of Modeling Fluid Flow (CMFF'03). Budapest, Hungary: 3-6.
- Schmetterer L, Garhofer G & Dorner GT (2001): Mediators of the neuro-vascular coupling in the human retina. Short-time effect of intravenously administrated sodium-lactate on flicker light induced vasodilation. *Ophthalmic Res* 33 (Suppl1): 188.
- Schmidt-Trucksass A, Sandrock M, Cheng DC, Muller HM, Baumstark MW, Rauramaa R, Berg A & Huonker M (2003): Quantitative measurement of carotid intima-media roughness--effect of age and manifest coronary artery disease. *Atherosclerosis* 166: 57-65.
- Schmidt EE, MacDonald IC & Groom AC (1983): Luminal morphology of small arterial vessels in the contracted spleen, studied by scanning electron microscopy of microcorrosion casts. *Cell Tissue Res* 228: 33-41.
- Schmidt M (2000): *Grundprinzipien der Wavelet-Analyse und Anwendungen in der Geodäsie*. München. Technische Universität München: 196.

- Schwender D, Daunderer M, Mulzer S, Klasing S, Finsterer U & Peter K (1996): Spectral edge frequency of the electroencephalogram to monitor "depth" of anaesthesia with isoflurane or propofol. *Br J Anaesth* 77: 179-184.
- Seidova S-F, Kotliar KE, von Düring C & Lanzl IM (2007): Dynamic retinal vessel reaction in patients with primary open angle glaucoma. *Acta Ophthalmol Scand.* 85 (Suppl 239): 55.
- Seifert BU & Vilser W (2002): Retinal Vessel Analyzer (RVA)--design and function. *Biomed Tech (Berl)* 47 Suppl 1 Pt 2: 678-681.
- Seitz R (1964): *The Retinal Vessels. Comparative Ophthalmoscopic and Histologic Studies on Healthy and Diseased Eyes.* St. Louis. CV Mosby.
- Shamshinova AM & Volkov VV (1998): Functional methods of investigation in ophthalmology Moscow, Russia. *Medicina:* 415
- Sharpa MK, Thurston GB & Moore JE (1996): The effect of blood viscoelasticity on pulsatile flow in stationary and axially moving tubes. *Biorheology* 33: 185-208.
- Sidorov VV, Cheremis NK & Krasnikov GV (2001): Laser Doppler Flowmetry for the estimation of hemodynamic rhythms of microcirculatory blood flow oscillations. . International Congress: "Laser and informational technologies in the medicine of XXI century" St. Petersburg, Russia: 500-501.
- Silver DM, Farrell RA, Langham ME, O'Brien V & Schilder P (1989): Estimation of pulsatile ocular blood flow from intraocular pressure. *Acta Ophthalmol Suppl* 191: 25-29.
- Skoda R (2003): Numerische Simulation abgelöster und transitionaler Strömungen in Turbomaschinen. Munich, Germany. Munich University of Technology: 150.
- Skoda R, Schilling R & Schoebei MT (2007): Numerical Simulation of the Transitional and Unsteady Flow through a Low Pressure Turbine. *International Journal of Rotating Machinery* 2007: 1-11.
- Stary HC, Blankenhorn DH, Chandler AB, Glagov S, Insull W, Jr., Richardson M, Rosenfeld ME, Schaffer SA, Schwartz CJ, Wagner WD & et al. (1992): A definition of the intima of human arteries and of its atherosclerosis-prone regions. A report from the Committee on Vascular Lesions of the Council on Arteriosclerosis, American Heart Association. *Arterioscler Thromb* 12: 120-134.
- Stevens RJ, Douglas KM, Saratzis AN & Kitas GD (2005): Inflammation and atherosclerosis in rheumatoid arthritis. *Expert Rev Mol Med* 7: 1-24.
- Stodtmeister R & Pillunat LE (1991): Das primäre Offenwinkelglaukom - eine Mikrozirkulationsstörung. In: Stodtmeister R and Pillunat LE(eds.) *Mikrozirkulation in Gehirn und Sinnesorganen.* Stuttgart: Enke Verlag 114-123.
- Stork S, Feelders RA, van den Beld AW, Steyerberg EW, Savelkoul HF, Lamberts SW, Grobbee DE & Bots ML (2006): Prediction of mortality risk in the elderly. *Am J Med* 119: 519-525.
- Strouhal V (1878): IV. Ueber eine besondere Art der Tonerregung. *Annalen der Physik und Chemie (Leipzig).* Neue Folge Leipzig: Verlag von Johann Ambrosius Barth: 216-251.
- Sugrue MF (1996): The preclinical pharmacology of dorzolamide hydrochloride, a topical carbonic anhydrase inhibitor. *J Ocul Pharmacol Ther* 12: 363-376.
- Tamm E, Flugel C, Stefani FH & Rohen JW (1992): Contractile cells in the human scleral spur. *Exp Eye Res* 54: 531-543.
- Tesfamariam B, Jakubowski JA & Cohen RA (1989): Contraction of diabetic rabbit aorta caused by endothelium-derived PGH₂-TxA₂. *Am J Physiol* 257: H1327-1333.
- Theander G (1960): Arteriographic demonstration of stationary arterial waves. *Acta radiol* 53: 417-425.
- Thurston GB (1972): The viscoelasticity of human blood. *Biophysical Journal* 12: 1205-1217.
- Topol EJ & Yadav JS (2000): Recognition of the importance of embolization in atherosclerotic vascular disease. *Circulation* 101: 570-580.
- Tso MO & Jampol LM (1982): Pathophysiology of hypertensive retinopathy. *Ophthalmology* 89: 1132-1145.
- Tuzcu EM, Kapadia SR, Tutar E, Ziada KM, Hobbs RE, McCarthy PM, Young JB & Nissen SE (2001): High prevalence of coronary atherosclerosis in asymptomatic teenagers and young adults: evidence from intravascular ultrasound. *Circulation* 103: 2705-2710.
- Ulrich WD & Ulrich C (1985): Oculo-oscillo-dynamography: a diagnostic procedure for recording ocular pulses and measuring retinal and ciliary arterial blood pressures. *Ophthalmic Res* 17: 308-317.

- Ulrich WD & Ulrich C (1985): Okulo-oszillodynamographie, ein neues Verfahren zur Bestimmung des Ophthalmikablutdruckes und zur okulären Perfusionsanalyse. *Klin Monatsbl Augenheilkd* 186: 385-388.
- Ustymowicz A, Mariak Z, Weigle J, Lyson T, Kochanowicz J & Krejza J (2005): Normal reference intervals and ranges of side-to-side and day-to-day variability of ocular blood flow Doppler parameters. *Ultrasound Med Biol* 31: 895-903.
- Vilser W, Klein S, Wulff P, Siegel C & Fuchs G (1991): [Automated measurement of retinal vascular diameter]. *Fortschr Ophthalmol* 88: 482-486.
- Vilser W, Nagel E & Lanzl I (2002): Retinal Vessel Analysis--new possibilities. *Biomed Tech (Berl)* 47 Suppl 1 Pt 2: 682-685.
- Virmani R, Avolio AP, Mergner WJ, Robinowitz M, Herderick EE, Cornhill JF, Guo SY, Liu TH, Ou DY & O'Rourke M (1991): Effect of aging on aortic morphology in populations with high and low prevalence of hypertension and atherosclerosis. Comparison between occidental and Chinese communities. *Am J Pathol* 139: 1119-1129.
- Volkov VV (2001): Pseudo-normal tension glaucoma. *Moscow. Medicina*: 310.
- Walburn FJ & Schneck DJ (1976): A constitutive equation for whole human blood. *Biorheology* 13: 201-210.
- Walsh JB, Rosen RB & Berinstein DM (2007): Diseases of the Retina. Chapter 13. Systemic Hypertension and the Eye. In: Tasman W and Jaeger EA(eds.) *Duane's Clinical Ophthalmology*. Hagerstown: Lippincott Williams & Wilkins.
- Wang JJ, Taylor B, Wong TY, Chua B, Rochtchina E, Klein R & Mitchell P (2006): Retinal vessel diameters and obesity: a population-based study in older persons. *Obesity (Silver Spring)* 14: 206-214.
- Wang X & Stoltz JF (1994): Characterisation of pathological blood with a new rheological relationship. *Clinical Hemorheology* 14: 237-245.
- Weaver JP, Evans A & Walder DN (1969): The effect of increased fibrinogen content on the viscosity of blood. *Clin Sci* 36: 1-10.
- Weigert G, Findl O, Luksch A, Rainer G, Kiss B, Vass C & Schmetterer L (2005): Effects of moderate changes in intraocular pressure on ocular hemodynamics in patients with primary open-angle glaucoma and healthy controls. *Ophthalmology* 112: 1337-1342.
- Weiter JJ & Ernest JT (1974): Anatomy of the choroidal vasculature. *Am J Ophthalmol* 78: 583.
- WHO (2000): Obesity: preventing and managing the global epidemic. Technical report series 894. Geneva. World Health Organization.
- Wirtz C, Lanzl IM & Kotliar KE (2007): Which vessel segments are suited for measurements with the RVA? Symposium "Basics and Methods for Microvascular Diagnosis of the Retina (sympMDR). Ilmenau, Germany: 12.
- Wise GN, Dollery CT & Henkind P (1971): *Retinal Circulation*. New York. Harper & Row.
- Wolf S, Arend O, Schulte K, Ittel TH & Reim M (1994): Quantification of retinal capillary density and flow velocity in patients with essential hypertension. *Hypertension* 23: 464-467.
- Yamada A (1995): [Observation of retinal vasculature in experimental renal hypertension rat using bis-benzimide]. *Nippon Ganka Gakkai Zasshi* 99: 154-160.
- Yao Y, Ma Z & Zhao J (2002): Luminal characteristics of central retinal vessels in the anterior optic nerve of the young human. *Retina* 22: 449-454.
- Yeleswarapu KK (1996): Evaluation of continuum model for characterising the constitutive behaviour of blood. Pittsburg. University of Pittsburg.
- Yildiz O (2007): Vascular smooth muscle and endothelial functions in aging. *Ann N Y Acad Sci* 1100: 353-360.
- Yu DY, Cringle SJ, Su EN & Yu PK (2005): Sphincter activity in retinal arterioles feeding the deeper capillary layer in pig. *Curr Eye Res* 30: 781-787.
- Zaluczowska-Marcela K, Rusek P, Dudzinski A & Filipecka I (2000): [Assessment of the retinal blood flow by DRG retina Doppler in primary open angle glaucoma and normal tension glaucoma]. *Klin Oczna* 102: 115-118.
- Zetlan SR, Sponsel WE & Stodtmeister R (1992): Retinal capillary hemodynamics, visual-evoked potentials, and pressure tolerance in normal human eyes. *Invest Ophthalmol Vis Sci* 33: 1857-1863.
- Zhang JB & Kuang ZB (2000): Study on blood constitutive parameters in different blood constitutive equations. *J Biomech* 33: 355-360.

List of Illustrations

Fig. 1. Top: Detailed diagram of the human eye. Modified from http://www.phys.ufl.edu/~avery/course/3400/gallery/gallery_vision.html. Bottom: Morphological organisation of the retina. Scaled up detailed presentation of the area within the red rectangle in the upper panel. Modified from www.dma.ufg.ac.at/assets/16457/intern/retina.jpg.

Fig. 2. Macroscopic anatomy of the ocular circulation. Top: blood supply to the eye (arterial system). Bottom: blood drainage (venous system). Modified from www.missionforvisionusa.org/anatomy/uploaded_images by B. Glasgow, M.D. Los Angeles, CA, USA

Fig. 3. Blood supply of the human eye. Modified from Schiebler (Schiebler et al. 1999)

Fig. 4. Blood supply of the retina. Retinal capillaries are densely distributed within inner layers of the retina, ~260 μm thick. The outer layer, ~130 μm thick, has no blood vessels and nourished from the choroid. a: Scheme modified from (Alm 1992). b: Modified scheme by Bergmann 1962 cited from (Eichhorn 2001)

Fig. 5. Normal human retina. A 50° fundus photograph, right eye. The optic nerve: a circular white area ~ 2 x 1.5 mm across. From the center of the optic nerve radiate the major retinal blood vessels. 4,5-5 mm (2,5 half disc diameters) to the left of the disc: slightly oval-shaped, blood vessel-free spot, the fovea, which is at the center of the area known as the macula by ophthalmologists. Modified from: <http://webvision.med.utah.edu /imageswv/huretina.jpeg>

Fig. 6. Structural cross-sectional organisation of capillaries. Top: closed or continuous capillary. Bottom: fenestrated capillary. Modified drawing by Caceci from: <http://education.vetmed.vt.edu/ Curriculum/VM8054/Labs/Lab12b/Lab12b.htm>

Fig. 7. Structural cross-sectional organisation of a small artery. Modified from: www.vascularsurgeon.co.uk/anatomy.htm

Fig. 8. Human retinal vasculature, including arteries (A), veins (V), arterioles, venules and capillaries. Note capillary free zone around arteries. Modified data by Henking cited from (Park 2007)

Fig. 9. Temporal changes of the blood flow velocity in a short posterior ciliary artery and in a vortex vein. Color Doppler imaging. Modified from (Kagemann et al. 1999)

Fig. 10. Measured velocity values across a retinal arterial segment during systolic and diastolic phases of cardiac cycle and corresponding parabolic fits. Modified from (Logean et al. 2003)

Fig. 11. Histologic scheme of a large retinal artery and definitions of different vessel diameters. Modified from (Michelson et al. 2007)

Fig. 12. Process of atherosclerotic lesion formation. See explanation in the text. Modified from (Falk et al. 1995; Ross 1999; Topol & Yadav 2000)

Fig. 13. Longitudinal section of arteriole in the contracted spleen of a cat. Vessel lumen (L); within pleated wall: internal elastic lamina, smooth muscle layer, darkly staining collagen (C), and trabecular smooth muscle (T). Short bar: 10 μm . Amplification x 500. Modified from Schmidt et al. (1983).

Fig. 14. Arteriolar cast from the contracted spleen of a cat. Note sharp ridges due to pleated vessel wall, and fine surface detail. Dramatic narrowing of luminal diameter (black arrows) is apparently caused by contraction of vascular smooth muscle. Short bars: 10 μm . Amplification x 360.

Fig. 15. Diagrammatic logarithmic representation of the effects of red cell aggregation and red cell deformation on the shear dependence of blood viscosity. Modified from (Chien et al. 1971).

Fig. 16. Parameters of the Non-Newtonian Quemada model derived from (Dufax et al. 1980; Quemada 1981; Cockett 1986)): Top: the low and the high shear rate intrinsic viscosities k_0 (blue line) and k_∞ (red line) depicted recalculated and fitted from experimental data by Quemada (1981). Grey lines represent the data on Quemada model for blood at 37°C from (Dufax et al. 1980) reported by Cockett (1986). Bottom: critical shear rate γ_c for blood at 23°C and 37°C. Distributions were modified from the data by Cockett (1986)

Fig. 17. Retinal Vessel Analyzer

Fig. 18. Principles of the Retinal Vessel Analyzer measurements

Fig. 19. Left: Oculooscillograms of paired eyes of a healthy volunteer 32 years old. PPsret – systolic perfusion pressure in the retina; PPscl – systolic perfusion pressure in the ciliary body; PPOc – diastolic perfusion pressure. Right: OODG-provocation and measurements. Modified from (Volkov 2001)

Fig. 20. Data representation in the RVA. 3D –time-space matrix

Fig. 21. Definition of longitudinal vessel profile

Fig. 22. Assessment of longitudinal vessel profiles. Longitudinal vessel profiles during baseline (green), constriction (red), dilation (blue) and relaxation (grey and brown) as displayed. Top: in RVA-system in glaucoma study. Bottom: in DVA-system in systemic hypertension study. Assessed temporal cycle is marked within the whole temporal vessel diameter course.

Fig. 23. Characteristic parameter of the high frequency waviness of arterial segments: spectral edge frequency (SEF). Examples of harmonic functions on the right show the range of calculated SEF-values. a, λ – corresponding parameters of the formula (10).

Fig. 24. Temporal arterial (top) and venous (bottom) vessel reaction to flicker provocation and explanation of time intervals of local vessel reaction assessment.

Fig. 25. Temporal arterial reaction to pressure provocation (graphs are modified from (Nagel et al. 2001; Nagel et al. 2002)) and definition of time intervals for local vessel reaction assessment. Top: study 1 (suprasystolic IOP provocation): summary of temporal reaction of all normal persons and glaucoma patients; Bottom: study 2 (moderate 100 s IOP provocation): individual temporal vessel reaction of a healthy subject.

Fig. 26. Systemic hypertension study. Summary temporal arterial (top) and venous (bottom) reaction to flicker in the examined groups (N=15)

Fig. 27. Examples of temporal arterial (top) and venous (bottom) vessel reaction to flicker provocation and explanation of time intervals of local vessel reaction assessment.

Fig. 28. Obesity study. Summary of temporal arterial reaction to flicker in examined groups (N=16)

Fig. 29. Problem statement and parameters for the CFD-model. a: general problem statement. b: geometrical parameters of a wavy vessel segment. c: 3-dimensional grid generation for CFD simulation.

Fig. 30. Examples of the dimensionless profiles and corresponding Sr-values by analogy with denominate profiles in Fig. 23 right panel. L, A, Λ , – parameters of the formula (20).

Fig. 31. 3-D geometry of Finite Volume Model of a wavy vessel segment. (compare with real vessels in Fig. 14). A 60° “piece of pie” sector of the whole model.

Fig. 32. Parameters of Non-Newtonian Quemada model (derived from (Quemada 1981; Lerche & Oelke 1990)): a: radial hematocrit profiles, normalized by mean capillary hematocrit; b: radial γ_c profiles; c: radial k_0 profiles; d: radial k_∞ profiles.

Fig. 33. Adaptive remeshing of a fluid element near the vessel wall.

Fig. 34. 3-D geometry of Finite Volume Model of a real vessel segment (compare with Fig. 31). A 180° sector of the whole model. An example.

Fig. 35. Typical longitudinal vessel profiles in the age dependence study. Upper row shows longitudinal arterial profiles, the lower one – longitudinal venous profiles. On the left: vessel profiles of a young subject, on the right: vessel profiles of a senior volunteer.

Fig. 36. Average reduced power spectra of spatial longitudinal vessel profiles for the three age groups at the 4 phases of vessel reaction during flicker stimulation assessment. Upper group: arteries; lower group: veins. The sequence of phases was chosen according to increase in diameter of the vessel from left to right. Small vertical black lines show median SEF-values for corresponding summarised longitudinal vessel profiles.

Fig. 37. High frequency waviness of longitudinal vessel profiles, expressed by SEF dependent on vascular tone. Left: arteries; Right: veins. Cartoons along the axes illustrate “waviness” and “tone”. Vascular tone is represented in arbitrary units, which are ranged from -10 to 10, where -10 corresponds to the complete constriction, 0 – the baseline tonus, 10 – full vessel dilation.

Fig. 38. High frequency waviness of longitudinal vessel profiles expressed by SEF dependent on age at the 4 phases of vessel reaction during flicker stimulation assessment. Each subject is represented by a diamond (◆). Top: arteries; Bottom: veins. Corresponding correlation coefficients and their significance (*) are represented.

Fig. 39. High frequency waviness of longitudinal vessel profiles expressed by SEF dependent on age at the 4 phases of vessel reaction during flicker stimulation assessment. Each subject is represented by a diamond (◆). Top: arteries; Bottom: veins. Corresponding correlation coefficients and their significance (*) are represented.

Fig. 40. Individual longitudinal vessel profiles in the glaucoma study 2. The profiles are derived from RVA data at one time point as described in Fig. 22 top, lower right insert. a: healthy age matched person; b: glaucoma patient; c: glaucoma patient after 4 week treatment with three times daily dorzolamide.

Fig. 41. High frequency waviness of arterial segments, expressed by SEF dependent on vascular tone. Left: results of study 1. Right: regression analysis of study 1. The chart on the right demonstrate lesser change in HFW after IOP provocation in healthy age matched normals shown by flatter incline of the grey linear regression slope.

Fig. 42. High frequency waviness of arterial segments, expressed by SEF dependent on vascular tone. Left: results of study 2. Right: regression analysis of study 2. The chart on the right demonstrate lesser change in HFW after IOP provocation in healthy age matched normals shown by flatter incline of the grey linear regression slope.

Fig. 43. Typical longitudinal arterial profiles in the examined groups. Systemic hypertension study. Arteries.

Fig. 44. Average reduced power spectra of spatial longitudinal vessel profiles for systemic hypertension study at the 5 phases of vessel reaction during flicker stimulation assessment. The sequence of phases was chosen according to the increase in vessel diameter from the left to the right. Upper group: arteries; lower group: veins.

Fig. 45. Mathematical analysis on ARPS of arterial profiles. Different peaks correspond to dominating frequencies in spatial longitudinal arterial profiles. In syst. hypertension group the area under the power spectrum within the black frame differs significantly at baseline and dilation.

Fig. 46. Mathematical reconstruction of a characteristic spatial longitudinal arterial profile from power spectra in Fig. 43. Top: set of harmonic functions. Examples of representative longitudinal arterial profiles. Middle: vessel segment analyzed with RVA Bottom: retinal arterial segment of 2 mm length and graphic interpretation of obtained results

Fig. 47. Typical longitudinal venous profiles in the examined groups. Systemic hypertension study. Veins.

Fig. 48. Mathematical analysis on ARPS of venous profiles. Baseline. Peaks correspond to dominating frequencies in spatial longitudinal venous profiles. The area under the power spectrum within the black frame differs significantly at baseline, restoration 1,2 and dilation 1 between the examined groups.

Fig. 48. Mathematical reconstruction of a characteristic spatial longitudinal venous profile from power spectra in Fig. 43. Top: retinal venous segment of 2 mm length. Bottom: graphic interpretation of the obtained results

Fig. 49. Typical longitudinal arterial profiles in the examined groups. Obesity study. Arteries

Fig. 50. Average reduced power spectra of spatial longitudinal arterial profiles for obesity study at the 5 phases of arterial reaction during flicker stimulation assessment. The sequence of phases was chosen according to the increase in vessel diameter from the left to the right, similar to Fig. 43.

Fig. 51. Mathematical analysis on ARPS of arterial profiles. Restoration. Peaks correspond to dominating frequencies in spatial longitudinal arterial profiles. The areas under the power spectrum within black frames differ significantly at dilation 1, dilation 2 (for 0,055-0,095Hz only) and restoration between examined groups.

Fig. 52. Typical longitudinal arterial profiles of the examined volunteers. Short-term repeatability pilot-study. Medically healthy volunteers.

Fig. 53. Average reduced power spectra of spatial longitudinal arterial profiles for short-term repeatability pilot study at 2 phases of vessel reaction.

Fig. 54. Typical longitudinal arterial profiles of the examined patients. Long-term reproducibility pilot study. Patients with metabolic syndrome

Fig. 55. Average reduced power spectra of spatial longitudinal arterial profiles for long-term reproducibility pilot study at 2 phases of vessel reaction.

Fig. 56. Typical longitudinal arterial profiles of the examined vessels. Dimensional reproducibility pilot study. Young healthy volunteers.

Fig. 57. Average reduced power spectra of spatial longitudinal arterial profiles for dimensional reproducibility pilot study at 5 phases of arterial (top) and venous (bottom) reaction during flicker stimulation assessment. 16 measured vessel segments in each compared group. The sequence of phases was chosen according to the increase in vessel diameter from the left to the right, similar to Fig. 43.

Fig. 58. Color mapping of the results of CFD simulation: a: pressure distribution in a simulated wavy vessel segment. b: values of the sum velocity vector in a less wavy vessel segment. c: streamlines along a wavy wall; d: velocity vectors in a wavy vessel segment. Real scales along x, y and z -axes were changed for better performance.

Fig. 59. Quantitative results of CFD simulation on plots. b,c,d: calculated dimensionless coefficient of hydraulic resistance in a vessel segment dependent on dimensionless parameters, $L=l/\bar{d}$, $\Lambda = \lambda/\bar{d}$ and $A=a/\bar{d}$ with sense of the segment diameter, the wavelength and the magnitude of vessel wall waviness correspondingly for vessel wall configurations represented on a. Inflow velocity $c_{in} = 5$ mm/s and the vessel length $l = 1,5$ mm in all numerical calculations here.

Fig. 60. Quantitative results of CFD simulation on plots. b, d: dimensionless resistance coefficient ζ_v in a vessel segment dependent on SEF of vessel wall configurations represented on a and c correspondingly. SEF-values for each curve are shown on a and c as well. For comparison one of the curves from d is depicted in b with white triangles. The points corresponding to the smooth straight vessel wall are shown in b and d on the ordinate axis with no connection to the curves. Inflow velocity $c_{in} = 5$ mm/s and the vessel length $l = 1,5$ mm in all numerical calculations here.

Fig. 61. Sensitivity analysis. Comparative influence of each geometrical parameter of the wavy vessel segment to the resistance of the segment.

Fig. 62. Quantitative results of CFD simulation. a,b,c: analogue of pump head-capacity characteristic: pressure loss along a vessel segment dependent on volumetric flow rate for cases when two parameters of the waviness are constant and one parameter changes. White points correspond to the smooth straight vessel wall. Inflow velocity c_{in} varies from 1 to 50 mm/s. d: reality check of the model (Moody chart): calculated from ζ_v friction factor λ_χ is nearly proportional to the reciprocal of Reynolds number. Theoretically predicted dependence $\lambda_\chi = 64/Re$ is depicted with dashed line.

Fig. 63. Calculated influence of apparent cinematic viscosity ν in the model on the dimensionless resistance coefficient ζ_v in a vessel segment.

Fig. 64. Clinically measured baseline configurations of vessel lumen. Examples of a normal person (Top) and a glaucoma patient (Bottom) from glaucoma study 2, Fig. 39. Real scales along x and y-axes are maintained.

Fig. 65. CFD simulation for real retinal arterial profiles measured with RVA. Examples of a normal person and a glaucoma patient (glaucoma study 2, Fig. 39). Top: absolute values of longitudinal vessel profiles at different phases of vessel reaction from the constriction to the dilation. Middle: the inner structure of vessel lumina recalculated from measured longitudinal vessel profiles with the assumption of axial symmetry. Bottom: color mapping of axial and vertical velocities. Real scales along x, y and z -axes are modified for better performance. Color scales in maps differ from each other.

Fig. 66. CFD simulation for real arterial profiles measured with RVA: color mapping of pressure drop and values of main parameters. Examples of a normal person and a glaucoma patient (glaucoma study 2, Fig. 39). Real scales along x, y and z -axes are modified for better performance. \bar{c}_{in} - inflow velocity; \bar{d} - median vessel diameter; A_s - cross-sectional area of the vessel lumen at the inflow; Q - volumetric flow rate; $\Delta\pi$ - pressure drop along the vessel segment; ζ_v - coefficient of hydraulic resistance; Re - Reynolds number; SEF - Spectral Edge Frequency; S_r - Strouhal number. Color scales in maps differ from each other.

Fig. 67. CFD simulation for real arterial profiles measured with RVA. Examples of a normal person and a glaucoma patient (glaucoma study 2, Fig. 39): color mapping of axial and vertical velocities; values of main parameters in the baseline configuration at different inflow velocities: \bar{c}_{in} .

\bar{d} and A_s values are equal to the values in Fig. 66, second line. The last examples in both columns show the flow conditions with equal volumetric flow rates. Real scales along x , y and z -axes are modified for better performance. Color scales in maps differ from each other.

Fig. 68. Color mapping of the results of CFD simulation

Fig. 69. First results of CFD simulation. a,b: calculated reduced coefficient of hydraulic resistance ζ_v/ζ_{v0} dependent on dimensionless fluidmechanical parameters A and L (Fig. 29, Fig. 30) with sense of magnitude and wavelength of longitudinal vessel wall configuration. c: reduced coefficient of hydraulic resistance ζ_v/ζ_{v0} dependent on SEF. Grey circlets in plots correspond to vessel wall configurations represented in d. SEF-values and S_r numbers for each curve are shown in d in small frames.

Fig. 70. Age dependence study. Schematic illustration of obtained results. Top: characteristic longitudinal arterial profiles in individual baseline and during dilation. Bottom: graphic interpretation.

Fig. 71. Computer echo density analysis of the carotid IMT from (Labropoulos et al. 2005). The median distribution of grey values of pixels within the intima media of a healthy volunteer (a) has a much lower value than that from an older patient (b).

Fig. 72. Glaucoma study. Schematic illustration of obtained results. Top: characteristic longitudinal arterial profiles in individual baseline and during dilation. Bottom: graphic interpretation.

Fig. 73. Possible explanation for increased vessel thickness change frequency of arterial segments in glaucoma. Presumably some smooth muscle cells (dark grey painted circlets) do not react in glaucoma patients because of endothelial dysfunction.

Fig. 74. Principles of the correction factor for linear dimensions at different fundus camera angles

Fig. 75. Longitudinal arterial profiles of a normal subject, 100% oxygen breathing. Temporal mean and confidence interval. Strong arterial constriction up to 20%. Modified from (Vilser et al. 2002) and Fuhrmann, Vilser & Nagel, unpublished data.

Fig. 76. Top: Segmental smooth muscle loss along a vessel. Bottom: longitudinal arterial profiles of a patient with systemic hypertension, 100% oxygen breathing. Temporal mean. Segmental vessel constriction. Modified and corrected from (Vilser et al. 2002). Top and bottom panels are adjusted to each other according to the position along the vessel.

Fig. 77. Vessel dilation shown in its longitudinal section. Normal and reduced segmental dilation behaviour. Dilation reserves are depicted with dashed lines.

Fig. 78. Longitudinal sections and longitudinal profiles of normal retinal arteries (left panel) and retinal arteries in systemic hypertension at different phases of vessel reaction. See detailed explanation in text

Fig. 79. Comparative analysis on how the vessel length can influence the accuracy of the spectral analysis. Vessel segments of different length are analyzed. f and T – true frequency and period of the waviness; n - number of analysed points, \underline{T} - estimated periods, \underline{f} – estimated frequencies of the waviness (peak frequencies in the power spectra in the low panel).

Fig. 80. Comparison of two glaucoma studies. One healthy person and one glaucoma patient participated in both studies. For each experiment the location of the arterial segment on the fundus, longitudinal arterial profiles, as well as SEF of most important profiles are depicted. Date of the measurement is shown in the left lower corner of each diagram.

Fig. 81. Average reduced power spectra of spatial longitudinal arterial profiles of another healthy volunteer at 5 phases of arterial reaction (dimensional reproducibility study). To be compared with Fig. 57. 9 measured vessel segments in each compared group. The sequence of phases was chosen according to the increase in vessel diameter from the left to the right, similar to Fig. 57

Fig. 82. First results on “optical vivisection” of big retinal vessels with Fourier Domain OCT. Cross-sectional velocity maps. Modified from (Bachmann et al. 2007)

Fig. 83. Schematic diagram for the conclusions.

Fig. 84. Transient vessel reaction. Problem statement.

Fig. 85. Flow in a vessel bifurcation. Problem statement.

List of Tables

Table 1. Physiological blood flow velocities in different vascular beds of the eye.

Table 2. Mean vessel diameters in healthy volunteers in different vascular beds of the eye. μm ($\text{m} \times 10^{-6}$)

Table 3. Frequency ranges of temporal vessel wall modulation of

Table 4. Mean blood flow in healthy volunteers in different vascular beds of the eye. [$\mu\text{l}/\text{min}$ ($\text{m}^3/\text{s} \times 1,67 \times 10^{-10}$)]. (CDI – color Doppler Imaging, DSA – digitised subtraction angiography; LDV – Laser Doppler velocimetry, CLDF – Canon laser Doppler flowmetry; HLDF - Heidelberg laser Doppler flowmetry).

Table 5. Mean blood pressure in healthy volunteers in different vascular beds of the eye. [mmHg ($\text{Pa} \times 133,32$)]

Table 6. Activities of vascular endothelium and synthesized vasoactive substances. Modified from

Table 7. Various blood constitutive equations and their parameters. Review from (Fung 1990; Luo & Kuang 1992; Zhang & Kuang 2000; Bitsch 2002; Artoli 2003) and sources mentioned in the table.

Table 8. Input parameters for 3D-geometry program. The content of the file *settings.dat*

Table 9. Parameters of the Newtonian model

Table 10. Results of short-term repeatability pilot-study (median (1. quartile; 3. quartile)

Table 11. Results of long-term reproducibility pilot-study (median (1. quartile; 3. quartile)

Table 12. Results of dimensional reproducibility pilot-study (median (1. quartile; 3. quartile). BAS-baseline, DIL1-dilation1, CON-constriction; RES1-restoration1

Table 13. Results of spatial reproducibility pilot-study. Differences between right and left eye (median (1. quartile; 3. quartile). BAS-baseline, DIL1-dilation1, CON-constriction; RES1-restoration1.

Table 14. Results of spatial reproducibility pilot-study. Differences in location in the fundus nasal/temporal inferior/superior (median (1. quartile; 3. quartile). BAS-baseline, DIL1-dilation1, CON-constriction; RES1-restoration1.

Table 15. Differences between the right and the left eye (median (1. quartile; 3. quartile) for longitudinal arterial profiles of another young healthy volunteer 25 y.o. BAS-baseline, DIL1-dilation1, CON-constriction; RES1-restoration1.

List of own publications on the topic

(published per-reviewed papers are accentuated)

1. K.E. Kotliar, E. Nagel, S.-F. Seidova, I.M. Lanzl, Microstrukturelle Veränderungen in den arteriellen Gefäßlängsschnittprofilen bei systemischem Bluthochdruck // Deutsche Medizinische Wochenschrift, 2007; 132 (Suppl.1); p. 23-24.
2. **K.E. Kotliar, E. Nagel, W. Vilser, I.M. Lanzl. Functional in-vivo assessment of retinal artery microirregularities in glaucoma // Acta Ophthalmol Scand 2008; 86: 424-433.**
3. K.E. Kotliar, I.M. Lanzl, J. Einzinger, D. Anzinger, R. Schilling. First results of biofluidmechanical simulation for age-dependent microirregularities in retinal arteries // Ann Biom Eng 2007 (in review)
4. **Kotliar KE, Mücke B, Vilser W, Schilling R, Lanzl IM. Effect of aging on retinal artery blood column diameter measured along the vessel axis // Invest Ophthalmol Vis Sci 2008; 49(5): 2094-2102.**
5. K.E. Kotliar, E. Nagel, S.-F. Seidova, I.M. Lanzl, Microstructural changes of longitudinal retinal venous profiles measured by retinal vessel analyser in systemic hypertension. // Acta Ophthalmol Scand 2007; 85 (Suppl 239): 124.
6. K.E. Kotliar, E. Nagel, S.-F. Seidova, I.M. Lanzl. Microstructural changes of longitudinal retinal arterial profiles in systemic hypertension. Proceedings of Symposium "Basics and Methods for Microvascular Diagnosis of the Retina (sympMDR). September 10-11, 2007, Ilmenau, Germany: 11.
7. **K.E. Kotliar, G.A. Drozdova, A.M. Shamshinova. Ocular hemodinamics and contemporary methods of its assessment. Part III. Non-invasive methods of assessment of ocular blood flow. 2. Static and dynamic assessment of retinal vessel reaction to stimuli. // Glaukoma 2007; 2: 64-71 (in Russian).**
8. K.E. Kotliar, S-F. Seidova, E. Nagel, I.M. Lanzl. Microstructural changes of longitudinal retinal arterial profiles measured by Retinal Vessel Analyser in systemic hypertension. // ARVO-Abstract on CD-ROM, 2007, N1438
9. K.E. Kotliar, R. Schilling, J. Einzinger, I.M. Lanzl. Does the roughness of retinal arterial vessel walls induced by glaucoma influence the retinal blood flow? // Abstr. of papers, 6-th International Glaucoma symposium, Athens, Greece. Mar. 28-31, 2007: A09.
10. **K.E. Kotliar, G.A. Drozdova, A.M. Shamshinova. Ocular hemodinamics and contemporary methods of its assessment. Part III. Non-invasive methods of assessment of ocular blood flow. 2. Assessment of blood cell velocities and flow rates in intraocular vessels and vascular beds // Glaukoma 2007; 1: 61-68 (in Russian).**
11. K.E. Kotliar, R. Schilling, I.M. Lanzl. Non-Newtonian model of the blood flow in big retinal arteries in open-angle glaucoma. // Proceedings of the 6-th International Conference on eye biomechanics, Moscow Helmholtz Institute for Eye Diseases, Moscow, March, 14-16, 2007: 120-129.
12. **K.E. Kotliar, G.A. Drozdova, A.M. Shamshinova. Ocular hemodinamics and contemporary methods of its assessment. Part II. Invasive methods of assessment of ocular blood flow // Glaukoma, 2006; 4: 37-49. (in Russian).**
13. K.E. Kotliar. Methods of assessment of ocular hemodynamics. In: A.M. Shamshinova (ed.). Clinical physiology of Vision. Moscow: MBN-Press, 2006: 639-740 (in Russian).
14. **K.E. Kotliar, G.A. Drozdova, A.M. Shamshinova. Ocular hemodinamics and contemporary methods of its assessment. Part I. Ocular blood circulation and its quantitative estimation // Glaukoma 2006; 3: 62-73 (in Russian).**
15. K.E. Kotliar, R. Schilling, W. Vilser, I.M. Lanzl. Fluidmechanical analysis of microstructural changes in retinal arteries in glaucoma // Acta Ophthalmol Scand 2006; 84 (Suppl 239): 90.
16. K.E. Kotliar, R. Schilling, J. Einzinger, I.M. Lanzl. Beeinflusst die altersabhängige oder glaukombedingte Zunahme der Gefäßinnenwandrauigkeit den retinalen Blutfluß? // Abstr. of papers on CD-ROM, 104 Congress of the German Ophthalmological Society (DOG), Sep. 21-25, 2006, Sa1102: 123.
17. K.E. Kotliar, B. Mücke, W. Vilser, I.M. Lanzl. Mikroirregularitäten gesunder retinaler Gefäße bei unterschiedlichen Altersgruppen // Klin Monatsbl Augenheilkd 2006; 223 (Suppl 2): 6.
18. K.E. Kotliar, R. Schilling, J. Einzinger, I.M. Lanzl. Retinal Blood Flow Is Influenced by Age-Dependent Microirregularities in Retinal Arterial Walls. Biofluidmechanical Simulation // ARVO-Abstract on CD-ROM, 2006, N469.

19. K.E. Kotliar, E. Nagel, R. Schilling, W. Vilser, I. M. Lanzl. Functional in-vivo assessment and fluidmechanical analysis of microstructural changes in retinal arteries in glaucoma // Proceedings of the XXX International Congress of Ophthalmology, Sao Paulo, Brasil, February, 19-23, 2006: 86.
20. K.E. Kotliar, R. Schilling, D. Anciger, J. Einzinger, I.M. Lanzl. First results of biofluidmechanical simulation for age-dependent microirregularities in retinal arteries // Proceedings of the 5-th International Conference on eye biomechanics, Moscow Helmholtz Institute for Eye Diseases, Moscow, November, 16-18, 2005: 55-64.
21. K.E. Kotliar, R. Schilling, D. Anciger, J. Einzinger, I.M. Lanzl. Altersabhängige lokale retinale arterielle Gefäßreaktion auf Flickerlicht. Klinische Untersuchung und biofluidmechanische Simulation // Deutsche Medizinische Wochenschrift, 2005; 130 (Supp.4): 165.
22. K.E. Kotliar, R. Schilling, D. Anciger, J. Einzinger, W. Vilser, I.M. Lanzl. Biofluidmechanische Simulation der altersabhängigen lokalen retinalen arteriellen Gefäßreaktion auf monochromatisches Flickerlicht. // Klin Monatsbl Augenheilkd 2005; 222 (Suppl 3): 10.
23. K.E. Kotliar, R. Schilling, D. Anciger, J. Einzinger, W. Vilser, I.M. Lanzl. Biofluidmechanical simulation for age-dependent local retinal arterial reaction.// Ophthalmic research 2005; 37 (Suppl.1): 197.
24. K.E. Kotliar, W. Vilser, B.Mücke, I.M. Lanzl. Local retinal venous reaction to monochromatic flickering light in normal volunteers of different age.// Ophthalmic research 2005; 37 (Suppl.1): 102.
25. K.E. Kotliar, B. Mücke, W. Vilser, I.M. Lanzl. Age dependence of local retinal arterial reaction to monochromatic flicker light application. // Abstr. of papers on CD-ROM, 103 Congress of the German Ophthalmological Society (DOG), and 15. SOE Congress, Berlin, Germany, Sep. 25-29, 2005: 2509-10.06S.
26. I.M. Lanzl, E. Nagel, W. Vilser, K.E. Kotliar. Local retinal arterial reaction to moderate artificial reduction of perfusion pressure in glaucoma patients before and after treatment with dorzolamide. // Abstr. of papers on CD-ROM, 103 Congress of the German Ophthalmological Society (DOG), and 15. SOE Congress, Berlin, Germany, Sep. 25-29, 2005. 2509-6.13S.
27. K.E. Kotliar, B.Mücke, W. Vilser, I.M. Lanzl. Aging Effects Measured by Retinal Vessel Analyser. // ARVO-Abstract on CD-ROM, 2005: N3916.
28. I.M. Lanzl, E. Nagel, W. Vilser, K.E. Kotliar. Does vessel diameter profile of retinal arteries alter with IOP-increase in healthy volunteers and glaucoma patients? // Abstr. of papers, 5-th International Glaucoma symposium, Cape Town, South Africa. Mar. 30- Apr. 2, 2005: A40.
29. K.E. Kotliar, B.Mücke, W. Vilser, I.M. Lanzl. Lokale retinale arterielle Gefäßreaktion auf monochromatisches Flickerlicht bei normalen Probanden unterschiedlicher Altersgruppen. // Abstr. of papers, XIV Workshop zur okulären Mikro- und Makrozirkulation, Weimar, Germany, Feb. 26-27, 2005: 18.
30. K.E. Kotliar, E. Nagel, W. Vilser, I.M. Lanzl. Does therapy with dorzolamide eye drops affect vessel diameter profile of retinal arteries in glaucoma patients? // Abstr. of papers, 7-th International Scientific Meeting, Association for Ocular Pharmacology and Therapeutics, Catania, Italy. Feb 3-5, 2005: 63.
31. K.E. Kotliar, B. Mücke, W. Vilser, I.M. Lanzl. Endothelial damage caused by ageing measured by Retinal Vessel Analyser (Retinale Gefäßdarstellung mittels Retinal Vessel Analyser zur Charakterisierung des Endothelschadens durch Altern). // Deutsche Medizinische Wochenschrift 2004; 129 (Supp.3): 155.
32. K.E. Kotliar, E. Nagel, W. Vilser, A. Pichler, I.M. Lanzl. Lokale retinale arterielle Gefäßreaktion auf mäßige artifizielle Augeninnendruckerhöhung bei Glaukompatienten und Normalpersonen // Klin Monatsbl Augenheilkd 2004; 221 (Suppl 3): 8.
33. K.E. Kotliar, E. Nagel, W. Vilser, I.M. Lanzl. Local retinal arterial reaction to moderate artificial IOP increase in normals and glaucoma patients. // Abstr. of papers, Congress of Alpe Adria Community, Munich, Germany, Oct. 8-10, 2004: 67.
34. K.E. Kotliar, E. Nagel, W. Vilser, I.M. Lanzl. Local retinal venous reaction to moderate artificial IOP increase in normals and glaucoma patients. // Ophthalmic research, 2004; 36 (Suppl.1): 89.
35. K.E. Kotliar, E. Nagel, W. Vilser, I.M. Lanzl. Local retinal arterial reaction to moderate artificial reduction of perfusion pressure in normals and glaucoma patients. // Abstr. of papers, 102 Congress of the German Ophthalmological Society (DOG), Berlin, Germany, Sep. 23-26, 2004: 356.
36. K.E. Kotliar, E. Nagel, W. Vilser, I.M. Lanzl. Functional assessment of vessel width in normals, untreated and treated glaucoma patients following IOP provocation. // Abstr. of papers, 7-th Congress of the European Glaucoma Society, Florence, Italy, May 30 -Jun. 26, 2004: 146.

37. K.E. Kotliar, E. Nagel, W. Vilser, I.M. Lanzl. Vessel thickness change frequency in healthy persons, untreated and treated glaucoma patients – a functional analysis of microcirculation. // ARVO-Abstract on CD-ROM, 2004: N2407.
38. K.E. Kotliar, E. Nagel, W. Vilser, I.M. Lanzl. Comparative functional assessment of changes in local configuration of retinal vessels under considerable short-term intraocular pressure increase in healthy persons and glaucoma patients // Proceed. of the 2nd International Conference “Pathophysiology and Contemporary Medicine”, Moscow, Russia, April 22-24, 2004: 33 (in Russian).
39. I.M. Lanzl, K.E. Kotliar, E. Nagel, W. Vilser. Lokale retinale arterielle Gefäßreaktion auf mäßige artifizielle Augeninnendruckerhöhung bei Glaukompatienten und normalen Probanden. // Abstr. of papers, XIII Workshop zur okulären Mikro- und Makrozirkulation, München, Germany, Feb. 27-29, 2004: 28.
40. K.E. Kotliar, E. Nagel, W. Vilser, I.M. Lanzl. Does therapy with dorzolamide eye drops affect retinal vessel thickness change frequency in glaucoma patients? // Proceedings of the 5th International Symposium on Ocular Pharmacology and Therapeutics, Monte Carlo, Monaco, Mar. 11-14, 2004: 12.
41. K.E. Kotliar, E. Nagel, W. Vilser, I.M. Lanzl. Lokale retinale arterielle Gefäßreaktion auf Augeninnendruckprovokation bei Glaukompatienten und Normalprobanden.//Abstr. of papers, XII Workshop zur okulären Mikro- und Makrozirkulation, Dresden, Germany, Mar. 1, 2003: 22.
42. I.M. Lanzl, E. Nagel, W. Vilser, K.E. Kotliar. Comparison of local reactions of retinal arteries and veins in response to intraocular pressure increase in normals and glaucoma patients. // Abstr. of papers, 4-th International Glaucoma symposium, Barcelona, Spain, Mar. 19-22, 2003: 36.
43. I.M. Lanzl, K.E. Kotliar, E. Nagel, W. Vilser, Functional assessment of vessel width in normals, untreated and treated glaucoma patients following IOP provocation. // Der Ophthalmologe 2003; 100 (Suppl1): 25.
44. K.E. Kotliar, E. Nagel, W. Vilser, I.M. Lanzl. Local retinal vein reaction to increased intraocular pressure in normals and glaucoma patients. // ARVO-Abstract on CD-ROM, 2002, N320.
45. K.E. Kotliar, E. Nagel, W. Vilser, I.M. Lanzl. Assessment of local behaviour of retinal arteries in response to intraocular pressure increase in normals and glaucoma patients. // Ophthalmic research 2002; 34 (Suppl.1): 159.